Hybrid Thermophotovoltaic Power Systems

CALIFORNIA ENERGY COMMISSION

CONSULTANT REPORT

APRIL 2002
P500-02-048F

Gray Davis, *Governor*

CALIFORNIA ENERGY COMMISSION

Prepared By:

EDTEK, Inc.
7082 South 220th Street
Kent, WA 98032

Ed Horne,
Principal Investigator

Contract No. 500-97- 048

Prepared For

Prab Sethi,
Contract Manager

Elaine Sison-Lebrilla,
Project Manager

George Simon,
Program Area Lead

Terry Surles,
PIER Program Manager

Robert L. Therkelsen,
Executive Director

Legal Notice

Table of Contents

Preface xii
Executive Summary 1
Abstract 5
1.0 Introduction 6
1.1. Purpose of this PIER Project Report 6
1.2. Summary of Project Expenditures 7
1.3. Background 7
1.3.1. Project Technical and Economical Objectives 12
1.3.2. Project Approach 12
1.4. Report Organization 14
2.0 Project Objectives And Achievements 16
2.1. Technical Goals And Achievements 19
2.2. Project Economic Goals And Achievements 20
3.0 SGTPV Design 23
3.1. SGTPV Solar Concentrator Design 23
3.2. SGTPV Solar Receiver Design 26
3.2.1. Solar Entrance Window 26
3.2.2. SGTPV Absorber/Emitter Sizing 26
3.3. Burner / Recuperator Design 27
3.4. Thermal Containment Package 31
3.5. TPV Electrical Converter Design 32
3.6. Thermal Control System 36
4.0 Critical Component Development 36
4.1. Resonant Mesh IR Bandpass Filter Development 37
4.1.1. Filter Description 41
4.1.2. IR Band-pass Filter Fabrication 43
4.1.3. Masked Ion Beam Lithography 43
4.1.4. Performance of Filters Produced for Previous Testbed Demo 46
4.1.5. Performance of Filters Produced for Advanced Design Demo 49
4.2. Optical Coupler Development 53
4.3. GaSb PV Cell Development 53
4.3.1. Photovoltaic Cell Fabrication and Process Development 54
4.3.2. Device Electrical Performance 56
4.3.3. Cell Manufacturing Cost Evaluation 59
4.3.4. Process Reproducibility 60

4.4. Photovoltaic Array Development 62
4.5. Solar Concentrator Dish Development 64
4.5.1. Substrate Forming Process & Tempering (Process Steps 1 & 2) 66
4.5.2. Substrate Smoothing (Process Step 3) 67
4.5.3. Vacuum Deposition of Reflective Coating (Step 4 of Process) 67
4.5.4. Vacuum Deposition of Dielectric (glass) Protective Coating (Step 5 of Process) 68
4.5.5. Removal and Storage of Completed Dish Reflector 69
4.6. Fossil Fueled Tpv Generator Development 69
4.6.1. Fossil Fueled TPV Radiant Energy Source Development 69
4.6.2. TPV Electrical Converter Development 76
5.0 System level Test and Evaluation of Fossil Fueled TPV 81
5.1. Test-Bed Unit Description 81
5.2. TPV system Tests and measurements 83
5.3. System Level Test Evaluation 90
5.4. Advanced Test-Bed Fabrication, Test, and Evaluation 96
6.0 Solar Tpv Generator Development 98
6.1. Solar TPV Proof-of-Concept Experiment 98
6.1.1. Solar Concentrator 98
6.1.2. TPV Proof-of-Concept Receiver 100
6.2. Fabrication and Assembly of Test-Bed Solar TPV 104
6.3. Experimental Testing of GaSb Based Solar TPV System 107
6.4. ANALYSIS OF GaSb TPV RESULTS 110
6.5. Solar TPV Receiver Development 111
6.6. Advanced Solar Aperture and STPV Receiver 116
7.0 Hybrid SGTPV System Development And Fabrication 118
7.1. Solar Concentrator Fabrication 118
7.2. Tracking Sensor and Drive System 119
7.2.1. Tracking Drive System Development and Fabrication 119
7.2.2. Tracking Sensor and Control System 120
7.2.3. Micro-Computer Control System and Software Development 120
7.2.4. Concentrator Base and Mechanical Drive Assembly 120
7.3. SGTPV Converter Development and Fabrication 121
7.3.1. SGTPV Solar Aperture Development 121
7.3.2. SGTPV Emitter Development 121
7.3.3. Burner/recuperator Development 122
7.3.4. Evacuated Thermal Control Sleeve 124

7.3.5. SGTPV Filter Development and Fabrication 125
7.3.6. SGTPV Photovoltaic Cell Development and Fabrication 126
7.3.7. Electrical Converter 127
7.3.8. Converter Thermal Control System 128
7.3.9. SGTPV Control System 130
7.3.10. Summary and Status of SGTPV Development 131
8.0 Test And Evaluation Of SGTPV 135
9.0 Conclusions and Recommendations 149
9.1. Conclusions 149
9.1.1. Project Objectives and Achievements 149
9.2. Commercialization Potential 152
9.3. Recommendations 159
9.4. Benefits to California 159
10.0 References 161
11.0 GLOSSARY 1

Table of Figures

Figure 1. Illustration of Basic TPV Conversion Process 8
Figure 2. Conceptual Design of SGTPV Receiver 10
Figure 3. Assembled TPV Cavity Mounted to Back of Primary Reflector 11
Figure 4. Photograph of Two Concentrator Modules Mounted On a Pedestal with Tracking System 11
Figure 5. Illustration of the Versatility of Modular System Approach 24
Figure 6. Illustration of Energy Path Through Solar Concentrator 25
Figure 7. Perspective View of Solar Concentrator Dish Design 26
Figure 8. Effect of Internal Power Use on Natural Gas TPV System Performance 28
Figure 9. Impact of Internal Power Consumption on Net Fuel to Electric Power Efficiency 29
Figure 10. Illustration of Relative Thermal Resistances in Recuperator 30
Figure 11. Conceptual Design of the Emitter/Burner for the SGTPV Module 31
Figure 12. Measured Dependence of PC Cell Voltage on Current 32
Figure 13. Current-Voltage and Quantum Efficiency of GaSb PV Cells 33
Figure 14. Photograph of the Filters That Reject Out-Of-Band Energy Back to the Emitter 34
Figure 15. Measured TPV Power Out versus Emitter Temperature for Diesel TPV Testbed 35
Figure 16. Measured Diesel TPV Testbed Efficiency Compared to Calculated Predictions 36
Figure 17. Schematic Showing Overlap of GaSb PV Cell Response and 1200°C Blackbody Emission Spectrum 38
Figure 18. Schematic of IR Micromesh Response Compared to GaSb PV Response and 1200°C Blackbody Emission Spectrum 39
Figure 19. Transmittance and Reflectance of IR Micromesh Filter 40
Figure 20. Long Wavelength Reflectance of IR Micromesh Filter Compared to a Solid Gold Film 40
Figure 21. Filter Transmittance Performance Versus Angle of Incidence 41
Figure 22. (Left) Photomicrograph of the IR Micromesh Filter, (Right) Photograph of Filter at Oblique Angle, (Bottom) Schematic of Filter Structure 42
Figure 23. Photo of a 6 mm x 6 mm Silicon Membrane (note that one can read through the membrane due to its thin structure, the thick frame is ~1.5 mm x 1.5 mm) 44
Figure 24. Two Scans of Better (right) and Poorer (left) Performing Filters Fabricated for the Testbed Demonstration 47
Figure 25. Peak Transmittance Values Versus the Number of Fabricated Filters 47

Figure 26. Wavelength of Peak Transmission Versus the Number of Fabricated Filters 48
Figure 27. Schematic Diagram of Testbed Demo Unit Filter Layout 49
Figure 28. Photos of the Filters When Gluing into Outer Sleeve is Partially Completed and After Sleeve is Fully Populated 49
Figure 29. Transmittance of Prototype Improved Filter Compared to Best Dipole Filters 50
Figure 30. Peak Transmittance Value versus Number of Filters Fabricated (a), Wavelength of Peak Transmission versus Number of Filters Fabricated (b) 51
Figure 31. Schematic of Filter Layout in Advance Design Outer Sleeve Showing Relation Between Column Number and Position in Sleeve (Top Row = A, Bottom Row = B) 52
Figure 32. Filter Performance Top Row (A) and Bottom Row (B) of the Assembled Advanced Design Sleeve 52
Figure 33. Coupler Array for a 500 Watt TPV Electrical Converter Developed for the US Army 53
Figure 34. Schematic of TPV PV Cell Fabrication Process 55
Figure 35. Quantum Efficiency Variation as a Function of Wavelength for GaSb Devices Using Old and New Passivation Techniques 56
Figure 36. I-V Curves Under Different Light Intensities 57
Figure 37. Variation of Open Circuit Voltage with Temperature 58
Figure 38. Variation of Fill Factor with Temperature 58
Figure 39. Dependence of Power at the Maximum Power Point on Temperature 58
Figure 40. Photographs of Processed D Shaped and Circular Wafers 60
Figure 41. Open Circuit Voltage (Voc) and Fill Factor (FF) Values for Devices from a D Shaped Wafer 61
Figure 42. Frequency Distribution of Short Circuit Current of Devices Fabricated in Several Batches 61
Figure 43. Frequency Distribution of Open Circuit Voltage of Devices Fabricated in Several Batches 62
Figure 44. Frequency Distribution of Fill Factor of Devices Fabricated in Several Batches 62
Figure 45. Frequency of P_{max} for Devices Fabricated in Several Batches 62
Figure 46. Schematic of TPV Converter Photovoltaic Cell Arrays (a) and Photograph of a single TPV Cell Array from a Previous Study[6] (b) 63
Figure 47. Typical Current Voltage Characteristic Measured for a Six Series-Connected PV Cell String in the Testbed TPV 64

Figure 48. Photographs of the SGTPV 2x9 Array Showing 1) the Ceramic Board Before Cells are Bonded in place and 2) Complete Array with Board and Cells. 64
Figure 49. EDTEK Plans to Manufacture a 56-inch Diameter Concentrator Dish to Support Two Solar-to-Electric Converters, COGEN-1 and COGEN-2 65
Figure 50. Side and Top View Photos of Forming Machine Design 67
Figure 51. Cross Sectional Drawing of Reflective Metal and Dielectric Coating Machine 68
Figure 52. TPV Combustion Chamber and Emitter Configuration 70
Figure 53. Analysis of Thermal Profile on Emitter Surface 70
Figure 54. Measured Emitter Temperature and Photographs of Emitter Glowing Through a Screen and of the Inside of Combustion Chamber After One-Hour Burn 71
Figure 55. Measured Recuperator Performance Parameters 72
Figure 56. Recuperator Performance Parameters 73
Figure 57. Thermal Isolation Package Version 1 74
Figure 58. Photograph of Metal Sleeve and Filters Under Test in EDTEK TPV Testbed 75
Figure 59. Emitter and Recuperator Operating Temperature Versus Time for the Improved Evacuated Thermal Control Sleeve. 76
Figure 60. Full TPV Heat Source, Thermal and Spectral Control, and Converter Assembly 77
Figure 61. Photograph Showing the IR Filters after Bonding Into TPV Housing. 78
Figure 62. Photograph Showing a Prism Array Bonded to 18 PV Cells which were Previously Bonded to the Ceramic Board 78
Figure 63. Photograph of the TPV Converter just after the Cell-Ceramic Board Sub-Assemblies are Bonded in Place 79
Figure 64. Photograph of the 12 Water-Cooled Jackets Prior to Bonding to Ceramic Boards 79
Figure 65. Full TPV Heat Source, Thermal and Spectral Control, and Converter Assembly for PIER SGTPV Project 80
Figure 66. View into Center of TPV Converter Showing the IR Filter in Place. 80
Figure 67. Photograph of Filters Installed in Evacuated Quartz Sleeve 82
Figure 68. Photograph of TPV Converter During Assembly 82
Figure 69. Illustration of Important Physical Mechanisms That Must be Evaluated in the TPV System 83
Figure 70. Typical Fuel Burn Rate During System Level Tests 84
Figure 71. Comparison of Measured Generator Cooldown Data and Model Calculations 85

Figure 72. Illustration of Resultant Blackbody Spectrum After Being Transmitted Through the IR Filter 86
Figure 73. Summary of Energy Transmitted Through Filters From Blackbody Spectra at Various Emitter Temperatures 86
Figure 74. Summary of Transmitted Power Results Obtained From Integrating the Spectral Transmittance with the Blackbody Spectrum 87
Figure 75. Typical Current Voltage Characteristic Measured for a Six Series-Connected PV Cell String in the Testbed TPV 87
Figure 76. Comparison of Experimental Versus Theoretical TPV Power Performance 88
Figure 77. Calibration Curves for Exhaust Gas Mass Flow Rate Determination 89
Figure 78. Unexpected Non-Cavity Related Parasitic Losses Versus Improvement Steps 91
Figure 79. Spectral Characteristics of Filters Before and After Burner Tests 93
Figure 80. Illustration of the Effect of Resonant Frequency Shift on Thermal Energy Transmitted 94
Figure 81. Illustration of the Effect of Resonant Frequency Shift on PV Cell 94
Figure 82. Advanced TPV Testbed Unit Assembled for Calorimeter Testbed Testing 96
Figure 83. Electrical Power Out of Advanced TPV Versus Emitter Temperature 97
Figure 84. Photograph of Cassegrainian Concentrator Used in STPV Proof-of-Concept Evaluation 98
Figure 85. Calorimeter Measurement of Solar Energy Input to the TPV Cavity 99
Figure 86. TPV Cavity Geometry Used in Three-Dimensional Modeling 101
Figure 87. Spatial Distribution of Rays Striking Surface of the TPV Filter 101
Figure 88. Spectral Reflectance of Dendritic Tungsten Surface as a Function of Angle 102
Figure 89. Measured Performance of GaSb PV Cells With and Without Concentrating Elements 103
Figure 90. Photograph of TPV Cavity Showing Solar Entrance Window and the Dendritic Tungsten Emitter Illuminated by a HeNe Laser Beam 104
Figure 91. Photograph of TPV Cavity Showing the Dendritic Tungsten Emitter/Absorber, Tungsten Suspension Wires, Tungsten/Rhenium Thermocouple, and the Reflective Walls of the Elliptical Cavity 105
Figure 92. Photograph of GaSb PV Cell Array on Ceramic Printed Circuit Board 106
Figure 93. Measured Emitter Temperature as a Function of Time and Solar Input Energy With Gold Reflective Base Only and With Filter/PV Cell in Place 108
Figure 94. Comparison of Measured and Theoretical TPV Power Out Versus Emitter Temperature 109

Figure 95. PV Cell QE Filter Transmittance Data 110
Figure 96. Solar Aperture Ready for Installation in the Solar Receiver Test Unit 112
Figure 97. Solar Receiver Preliminary Design Test Unit 113
Figure 98. Solar Aperture Installed in the STPV Receiver 114
Figure 99. Complete STPV Receiver and Solar Aperture Installed in Calorimeter Bath 114
Figure 100. Experimental Measurement of Solar Aperture Efficiency 116
Figure 101. Full STPV Converter Ready for Aperture installation 117
Figure 102. Photograph of Pilot Production Dish Concentrator Production Forming Machine 118
Figure 103. Photograph of Pilot Production Dish Concentrator Coating Machine 118
Figure 104. Photograph of Finished Pilot Production Concentrator Dish 119
Figure 105. Photograph of Mounting, Tracking, and Sensor Assembly 120
Figure 106. Photograph of the Single Board Micro Computer Selected to Control the SGTP System 120
Figure 107. Tracking Drive System Mechanical Assembly 121
Figure 108. Photograph of Fabricated Silicon Carbide Emitter Parts 122
Figure 109. Photograph of Fabricated Burner/Recuperator Parts 123
Figure 110. Illustration of Windows in Evacuated Sleeve Outer Wall 124
Figure 111. Pilot Production Masked Ion Beam Lithography Equipment for Resonant Mesh IR Band Pass Filters 125
Figure 112. Production Run of Resonant Mesh IR Band Pass TPV Filters fabricated for The PIER Project Prototype Generator Demonstration 125
Figure 113. Pilot Line Production Equipment for GaSb TPV Cells 126
Figure 114. Production Batch of TPV Cells Fabricated for the PIER Prototype SGTPV 126
Figure 115. Completed Electrical Converter Module for the SGTPV 127
Figure 116. Photograph of Fabricated TPV Converter Substrates and Prisms 127
Figure 117. Photograph of the 12 Water-Cooled Back Plates Prior to Bonding to Ceramic Boards 128
Figure 118. Photograph of the TPV Converter just after the Prism-Cell-Ceramic Board Sub-Assemblies Prior to Bonding of Water-Cooled Back Plates 129
Figure 119. Photograph of the TPV Converter with the Water-Cooled Back Plates Bonded in Place and Interconnected. 129
Figure 120. Photograph of Prototype SGTPV Generator Fabricated for Testing and PIER Project Demonstration 132
Figure 121. Photograph of Complete SGTPV Module 133

Figure 122. Photograph of Back Side of SGTPV Module Showing Mounted TPV Converter 133
Figure 123. Rotameter Calibration Versus a) Mass flow Rate and b) Watts 136
Figure 124. Photograph of the TPV Burner Test Set-up 136
Figure 125. TPV Cell Short Circuit Current Versus Emitter Temperature During Gas Burner Test Run 140
Figure 126. Power out versus Emitter Temperature for Previous Oil Fired TPV Testbed 142
Figure 127. Percentage Excess Air versus Percentage Oxygen In Exhaust 142
Figure 128. Assembly of a Solar Dish Mounting and Tracking Hardware 143
Figure 129. Assembly of a Solar Concentrator Dish and the Dish Mounting and Tracking Hardware 144
Figure 130. TPV Converter Module Shown Prior to Insertion of Burner and Solar Collector Subassemblies 145
Figure 131. Evacuation of the SGTPV Converter Subsystem after Mounting on Solar Concentrator Flange 145
Figure 132. Photograph of Complete SGTPV System as Demonstrated to the CEC on 3/28/02 146
Figure 133. Photograph of Solar Concentrator Aligned On-Sun 147
Figure 134. Historical Trends For Energy Production In State Of California 155
Figure 135. Regional Solar Radiation And Electric Rate Data For The United States 156
Figure 136. Favorable Regions For EDTEK Systems In The United States Population Density: 157

Table of Tables

Table 1. Summary of Project Goals and Achievements 17
Table 2. "Hybrid Thermophotovoltaic Power Systems" Project Components 37
Table 3. Key Process Monitors Used In Tpv Cell Optimization 57
Table 4. Data For Wafer And Processed Unit Cell Cost 59
Table 5. Dependence Of Tpv System Efficiency On Recuperator Performance 72
Table 6. Energy Balance For Three Tpv Testbed Run Conditions 91
Table 7. Typical Thermal Balance Results 92
Table 8. Summary Of The Demonstration Testbed Performance And Analysis 95
Table 9. Summary of Gas Burner Fuel Supply System 135
Table 10. Summary of Gas Supply versus Air Supply Calibration Results 138
Table 11. Pressure Measurement Comparisons Between Previous[6] and New SGTPV Recuperator Design 138
Table 12. Summary of Potential Market 153
Table 13. Summary of Total Market Size Analysis 158

Preface

The Public Interest Energy Research (PIER) Program supports public interest energy research and development that will help improve the quality of life in California by bringing environmentally safe, affordable, and reliable energy services and products to the marketplace.

The PIER Program, managed by the California Energy Commission (Commission), annually awards up to $62 million to conduct the most promising public interest energy research by partnering with Research, Development, and Demonstration (RD&D) organizations, including individuals, businesses, utilities, and public or private research institutions.

PIER funding efforts are focused on the following six RD&D program areas:

- Buildings End-Use Energy Efficiency
- Industrial/Agricultural/Water End-Use Energy Efficiency
- Renewable Energy
- Environmentally-Preferred Advanced Generation
- Energy-Related Environmental Research
- Energy Systems Integration.

What follows is the final report for the Hybrid Thermophotovoltaic Power Systems project, Contract Number 500-97-048, conducted by EDTEK, Inc. The report is entitled Hybrid Thermophotovoltaic Power Systems. This project contributes to the PIER Renewable Energy program.

For more information on the PIER Program, please visit the Commission's Web site at: http://www.energy.ca.gov/research/index.html or contact the Commission's Publications Unit at 916-654-5200.

Executive Summary

The overall purpose of this Public Interest Energy Research (PIER) project was to design, develop, fabricate, test and demonstrate a prototype hybrid solar/gas fueled co-generating system for distributed, point-of-use power generation in California and elsewhere. The hybrid generating system is based on the thermophotovoltaic (TPV) conversion process. The work was performed by EDTEK, Inc. between 1999 and 2002. EDTEK is dedicated to the commercialization of TPV technology. Our patented resonant mesh infrared (IR) band-pass filter is the absolute linchpin to TPV spectral control, which is essential if high TPV efficiency is to be attained. With pilot production capability for the unique and enabling spectral control technology and commercially licensed GaSb low-band gap photovoltaic (PV) cells in place, we are committed to the commercialization of both civilian and military applications of TPV technology. This PIER project was a cost-shared program as follows: The California Energy Commission (CEC) provided $864,000 for the hybrid design and development, the U. S. Department of Defense (1) provided $1,515,603 for TPV technology development, and the U. S. Department of Energy (2) provided $204,944 for TPV technology development, and EDTEK provided $365,454 in internal research funds for process and pilot production equipment development. Since the work on these cost shared programs was concurrent and integral to the success of this PIER project much of its results are described in this report.

The TPV uses PV cells similar to the better-known silicon and gallium arsenide solar cell except that TPV cells respond to radiant energy in the infrared rather than to the visible spectrum typical of sunlight. This allows the TPV cell to convert energy from sources much lower in temperature than the sun. The second difference between TPV and conventional PV is that in TPV systems the radiant energy that is outside the response range of the TPV cells is recycled back to the radiant source so that higher efficiencies can be obtained. The EDTEK hybrid TPV design demonstrated by this project uses concentrated sunlight and/or a natural gas burner as a heat source. The concentrated sunlight or natural gas burner heats an absorber/emitter to incandescence. The radiant infrared energy from the incandescent emitter is filtered by a unique EDTEK IR band-pass filter that transmits a selected wavelength band and reflects 98% of all out-of-band energy back to the emitter. The transmitted energy impinges onto high performance, low-band gap GaSb PV cells in a TPV cavity where it is converted directly to electricity. The residual thermal energy is collected in process-grade hot water. In the TPV cavity, the electrical conversion efficiency can approach 30% for solar conversion and 15% to 20% for natural gas. Residual thermal energy recovery efficiency is on the order of 83%. The ability to operate on natural gas and/or solar energy permits 24-hour operation so that the PV array works continuously yielding a better return-on-investment than ordinary solar PV systems that only operate when the sun is available.

Objectives

The overall project objective was to demonstrate the performance of a hybrid solar-fossil thermophotovoltaic system that can operate on solar energy when the sun is available and switch to fossil fuel such as natural gas or oil when there is no sun.

Specific Technical Objectives:

1. To demonstrate a pre-production prototype hybrid solar/natural gas thermophotovoltaic system that can convert sunlight to electricity with ~25% overall efficiency and natural gas to electricity at an overall efficiency of 20% while producing process grade hot water at a recovery efficiency of ~83%.
2. To develop an absorber/emitter for the TPV system that can operate at 1600°C to increase energy densities on the PV array by a factor of 2.6:1 over the current design operating at 1400°C in order to lower materials and PV cell costs.

Specific Economical Objectives:

1. To develop an infrared concentrating component with a concentration ratio of 7:1 that can reduce overall cell active area requirements and, hence, reduce system cell cost, which the dominant obstacle to commercialization, by a factor of 7 compared to current systems operating with little or no concentration.
2. To develop and demonstrate a vertically integrated manufacturing process for producing low-cost high performance concentrator dishes (CR>1000:1) at low cost ($3.40/sq. ft.) which is comparable to the adhesive backed, reflective coated films currently used by most systems before substrate and film application labor costs are considered.
3. To develop a business plan and financial strategy for commercialization.

Outcomes

During the development effort of this project some of the major accomplishments achieved were concerned with the improvement of key technologies and processes for their production. These key technologies included the EDTEK TPV band-pass filters, gallium arsenide low band-gap infrared responsive TPV cells, concentrating transmitted infrared energy onto the TPV cells, and a low-cost, high performance parabolic solar concentrator dish. The masked ion beam lithography process used for making the IR filters has been greatly improved and matured toward production readiness. A pilot production capability with about 0.25 Mw/yr capacity is in place. The TPV GaSb cell fabrication process has been matured and the yield has been increased from about 33% to 95%. A pilot production capability with about 0.25 Mw/yr capacity is now in place. The concentrating components have been developed into a eighteen unit array integrated into a single unit that is manufactured in large volume by a outside glass-forming vendor. An important accomplishment of this program was the successful development and demonstration of the processes for forming, smoothing, and conformal coating solar concentrator dishes. Further, pilot production equipment for dish manufacture are in-place with a capacity to produce up to 2 Mw/yr in solar/gas thermophotovoltaic (SGTPV) modules. In addition to these key technologies, all the materials, subsystems and techniques for fabricating SGTPV modules have been explored and tested.

Additional important accomplishments centered on the development of the SGTPV co-generation system. These system developmental accomplishments included a successful conversion of the TPV burner to utilize propane fuel, coupling the solar input from a concentrating dish into the TPV module, and the development of a solar tracking system. During this program EDTEK successfully demonstrated ignition and efficient burning of propane fuel to heat the emitter along with the construction of a fully sealed burner / recuperator which demonstrated design parasitic losses. The coupling of the solar dish to the TPV emitter was demonstrated concurrently with heating by the propane burner. For the first time the EDTEK development group utilized a on-board micro-computer-on-a-board to control all housekeeping and power management functions as well as driving the flawlessly performing solar tracking system. The on-board computer demonstrated its versatility and its ability to be reprogrammed to compensate and conform the system to various existing conditions.

The experience and capabilities discussed above were used to construct a prototype SGTPV module that was demonstrated to the California Energy Commission in Sacramento. Our goals for the project were for the prototype to demonstrate conversion efficiencies of 25% to 30% for concentrated sunlight to electricity and 15% to 20% for gas to electricity. Unfortunately, an early failure of a vacuum seal between the IR filters and the thermal control jacket prevented our achieving full operating conditions to demonstrate the above efficiency goals. However, extrapolations of the lower temperature results we obtained indicated that a gas-to-electric efficiency of about 15.6% would be achieved at 1400°C. Our goals for reducing system costs included raising the emitter operating temperature to 1600°C in order to reduce the PV cell required (and hence the cost) by a factor of about 2.6. For materials and reliability reasons we abandoned the idea of a 1600°C operating temperature; however, we were able to reduce the cost of PV cells in the system by almost a factor of 5 by improving cell fabrication yield and by reducing cell starting material costs. We also had a goal to develop low-cost high-performance concentrator dishes ($3.21/sq. ft.); we achieved a process that promises $4.09/sq. ft. Thus, while all of the ultimate goals were not fully achieved, we came close on most of them and did move TPV to a competitive plane by demonstrating efficiencies about 3 to 4 times higher than any TPV work reported to date.

Conclusions

The experience gained with the equipment, processes, and prototype fabrication and performance was utilized to form a commercialization plan and a production readiness plan. These plans project that the SGTPV modules can provide a source of economical, on site and locally owned distributed power generation for customers who have a combined need for electricity and hot water.

Benefits to California

The potential benefits of the SGTPV to the State of California are summarized below. The on-site distributed power can save money for individual, light-industrial, and commercial users in California. The local on-site power generation using cost effective sun-power can substantially reduce the peak demands on central power generation stations and provide stability for the using customers. EDTEK has calculated that the SGTPV can generate electricity at a cost of about $0.035 per kilowatt-hour at the point of use. With current point of use (retail) rates

running around $0.16 per kilowatt-hour in California, this represents a substantial cost savings to the California users. These distributed power systems can also reduce the peak power demands and hence reduce capital investments in "over capacity" equipment by central power generators. It is estimated that by the year 2004 SGTPV systems will generate 17.5 million kW-hrs/year and by 2006 the numbers will be approximately 175 million kW-hrs/year. In addition to the benefits to immediate users and the power industry, the establishment of an infra structure for selling, installing, and servicing these new power systems will create many high quality jobs throughout the State of California. For example, with a small capital investment, our pilot production equipment can be expanded to produce about 2 Mw of product per year. Our estimate is that for each 2 Mw installed would employ 20 workers in high quality jobs. Our commercialization plan calls for production to expand tenfold in the fifth year so that 200 new workers would be added per year thereafter.

Environmentally, each co-generating SGTPV unit will displace natural gas consumption when the sun is available. When we combine the solar contribution with the natural gas generation and consider that the thermal residue also displaces natural gas, our net efficiency (defined as useful energy produced/natural gas burned) 72.8% which is about a factor of two higher than that of central power generating stations which have higher electrical conversion efficiencies but cannot use the solar heat nor can they retrieve and use the thermal residue. Thus, each Mw of SGTPV production reduces pollutant emissions by one-half what they would be for the central generation plant. Another benefit that is hard to quantify is satisfaction and the piece of mind of users being insulated from price fluctuations and brown outs that are beyond their control.

Recommendations

The developed SGTPV components are fully functional with the exception of the aforementioned vacuum seal problem in the TPV converter unit. The recommendations for further development center around this problematic seal.

It is further recommended that the SGTPV system fabricated under this PIER program be refurbished with the new converter design and tested. Ultimately, the goal will be to demonstrate and confirm the overall system efficiency with the desired sunlight-to-electric efficiency of 25% and gas-to-electric conversion at 20%.

Abstract

The overall objective of this PIER project is to develop, fabricate, test, and demonstrate both the technical and economical viability of an SGTPV module that can run alternately, or simultaneously, on solar heat input and/or natural gas. In order to achieve this overall goal, a set of specific goals was established for both technical and economical performance. These goals and the degree to which they were achieved are described in the following sections. Also described are the technical achievements realized as a result of the developmental program. Table 1 is a summary of the program objectives and achievements.

1.0 Introduction

1.1. Purpose of this PIER Project Report

The purpose of this document is to report on the findings of the development work accomplished under the PIER project number 500-97-048.

If the sun is to be a viable alternative source of electricity it must be able to compete directly with existing fuels such as hydro, fossil and nuclear fuels. Solar energy has a limited number of ways in which it can compete: 1) as a pure thermal source, i.e., industrial process heat; 2) as a source of electricity by means of electric generators driven by steam turbines or Stirling engines, or 3) as a direct source of electricity (photovoltaics). To date, solar has not been able to compete economically in any of these three modes. In each example the dilemma is the same: initial costs are sufficiently high that the electricity produced costs more than can be recovered by its sale. A PV cell cannot deliver enough electricity over its lifetime to repay its initial cost. This is due to three factors: 1) high efficiency, single crystal cells are still too expensive to fabricate ($3 to $4 per peak watt), 2) low-cost, one-sun PV cell panels are relatively inefficient (6% to 8%), 3) solar concentrators produce higher field intensities that replaces expensive cells with lower cost reflective surfaces; however, the reflective surfaces are still too expensive and the higher field intensity heats the PV cells thereby degrading cell performance which offsets the lower cost of the concentrator, and 4) sunlight is available for power generation only about one-third of the time resulting in poor capital utilization. Thus, stand-alone solar power systems are not commercially competitive.

Our overall purpose of this work plan is to bridge the cost and technology risk gaps necessary to lay the foundation for subsequent commercialization and full production of a distributed photovoltaic power generation technology that exceeds the "stretch goals" of the PIER general solicitation for renewables. By combining the use of solar energy and fossil fuels to excite the same photovoltaic array, we remove the barrier of poor capital utilization for the solar PV array; and we reduce the fuel costs for the natural-gas-generation of power by augmenting it with solar power and by utilizing waste heat to offset natural gas use in other processes within the customer's establishment. In this way, we utilize photovoltaics to produce electric and thermal energy.

This PIER project advanced the TPV converter technology toward commercialization for private use. These advances were made in two areas, both aimed at lowering system costs and reducing investment risk by a system level demonstration of the SFTPV. These areas include lowering overall PV cell costs in the system and lowering the solar concentrator cost. Advances in technology include: 1) streamlining the PV cell processing procedure to lower fabrication costs, 2) developing a secondary concentrator to reduce the requirement for costly GaSb PV cells in the system, and 3) optimizing the converter package configuration for performance, durability, safety, and reliability.

The project advanced the solar concentrator technology by developing the materials science to cost-effectively smooth high quality reflectors with superior performance. The new tracking system resulted in a low-cost, low parasitic loss tracking system to use with the SFTPV and with other solar based renewable energy concepts. The modular concentrator/receiver approach allows "one size to fit all" customers which will permit automation of the manufacturing

processes. The computerized system management advances the art of interfacing hybrid systems with user's applications and with the local utility grid. The modularized approach to manufacturing minimizes system costs, increases reliability through redundancy, and maximizes the range of customers that can be serviced by the technology.

1.2. Summary of Project Expenditures

This PIER project was a cost-shared program. The break-down of the cost-share is as follows: The California Energy Commission (CEC) provided $864,000 for the hybrid design and development, the U. S. Department of Defense (1) provided $1,515,603 for TPV technology development, and the U. S. Department of Energy (2) provided $204,944 for TPV technology development, and EDTEK provided $365,454 in internal research funds for process and pilot production equipment development. Since the work on these cost shared programs was concurrent and integral to the success of this PIER project much of its results are described in this report.

1.3. Background

Technology Concept

This PIER project centers around thermophotovoltaic (TPV) technology using concentrated sunlight as a renewable energy source. It differs from commercially available solar photovoltaic systems in that it is a hybrid, cogenerating system that can switch from sunlight to fossil fuel to supply electrical power and hot water 24 hours per day. In this way it can be very economically advantageous. The concept of TPV is an old concept that has been researched since about 1965; however, there are no commercially viable systems available at this time. The concept and its potential advantages are described below.

A photovoltaic (PV) cell illuminated by terrestrial sunlight cannot repay its initial investment because it cannot deliver enough electricity over its lifetime to pay for itself. This is due to two factors: 1) PV cells are relatively inefficient (6%-8 %) at converting sunlight to electricity, and 2) there is simply not enough energy in a square centimeter of sunlight to generate sufficient electricity to pay for the cost of the cell, particularly at low conversion efficiency. EDTEK addresses these two barriers by using a hybrid system that uses concentrated sunlight and/or a natural gas burner to heat an emitter to incandescence. The radiant infrared energy from the incandescent emitter is filtered by a unique EDTEK infrared (IR) band-pass filter that transmits a selected wavelength band of the radiant energy and reflects 98% of all out-of-band energy back to the emitter. The transmitted energy impinges onto high performance, low-bandgap GaSb PV cells in a thermophotovoltaic (TPV) cavity thereby producing much higher quantities of electricity per cell. In the TPV cavity the conversion efficiency can approach 30% for solar conversion and 15% to 20% for natural gas. The ability to operate on natural gas and/or solar energy permits 24-hour operation so that the PV array works continuously and hence yields a better return on investment.

This project focuses on developing the TPV technology. TPV is a basic process for directly converting heat to electricity Figure 1 illustrates the TPV conversion process. From left to right in Figure 1, energy from a heat source is absorbed by a thermal absorber/emitter that is heated to incandescence. After being heated to incandescence, the absorber/emitter then radiates

infrared energy. The broadband spectral distribution of this radiated blackbody energy is shown by the shaded area in the graph below the radiator. The blackbody radiation impinges onto a band-pass filter located between the emitter/absorber and a low-band gap PV cell.

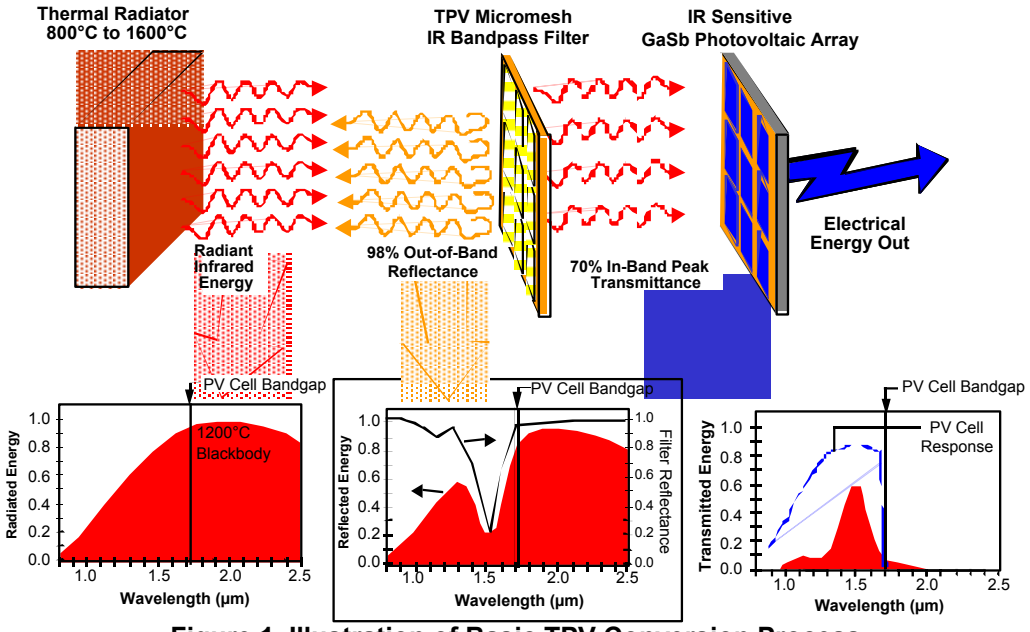

Figure 1. Illustration of Basic TPV Conversion Process

The band-pass filter transmits the radiant infrared energy that is in-band to the PV cell (i.e., 1.7 μm to ~0.65 μm) and reflects the remaining out-of-band energy back to the absorber/emitter which re-absorbs it. The spectral distribution of energy reflected back to the radiator is shown by the shaded area in the graph below the filter. The spectral distribution of the energy transmitted to the PV cell is shown by the shaded area in the right hand graph. By limiting the energy absorbed in the PV cell to a relatively narrow wavelength range which is centered about the PV cell's peak response wavelength, the cell can convert the transmitted energy with a theoretical efficiency up to ~48%. Thus, by limiting the transmitted energy to the cell's most efficient wavelength regime and recycling the energy which the cell cannot convert back to the absorber emitter, the TPV can achieve overall system efficiencies on the order of 30%. Key to achieving this high system efficiency is how well the design can suppress parasitic energy losses throughout the system.

Prior to this Public Interest Energy Research (PIER) project, the concept of TPV conversion had been studied by EDTEK, and many others, for years. EDTEK personnel have participated in four test bed demonstrations of TPV conversion. The first demonstration was a solar TPV generator intended for space power applications[1]. This solar demonstration was based on non-optimized silicon photovoltaic cells. An overall efficiency of 13.8% was demonstrated using these un-optimized parts. The main drawback observed was that silicon cells required emitter temperatures in excess of 1800°C which presented materials problems for long term space applications. Therefore, an effort was undertaken to develop a low band gap gallium antimonide (GaSb) photovoltaic cell to lower the emitter temperature requirements. Concurrently, a unique resonant, metal mesh infrared band-pass filter was developed for use

with the GaSb photovoltaic cell. A preliminary test bed experiment was conducted to assess the feasibility of these new components[2]. In this preliminary experiment, an array conversion efficiency of 13.3% was demonstrated using the first GaSb PV cells and non-optimized filters that were then available. Analytical models of both experiments indicated that the TPV conversion process behaved exactly as predicted and that, with optimized components, efficiencies on the order of 30% could be obtained with solar or radioisotope heat sources, which do not suffer parasitic losses from exhaust gases, and efficiencies up to 20% could be obtained with fossil fuel sources, which do have parasitic heat losses in their exhaust gases. Thus, all of these past studies concluded that the TPV concept had lots of potential; however, lack of appropriate technology precluded the realization of that potential. Enabling technology is now available in the form of two key TPV components, i. e., GaSb PV cells and resonant micromesh IR filters[3,4]. Using these newly available technologies, EDTEK has recently fabricated and tested a solar concentrator fueled TPV test bed[5] and a diesel fueled TPV testbed[6] where 21.4% and 7.4% respectively were measured. The details of these recent developments have been discussed in detail in earlier reports delivered to the California Energy Commission (CEC) as part of this PIER project. Some of the results are also discussed in 4.0 of this report.

While this approach promises to eliminate the barriers that have prevented photovoltaic devices from competing in mainstream energy markets, it produces other barriers of its own:

1. Gallium antimonide PV cells are more expensive than their direct-sun competitors. This disparity is eventually outweighed by the substantially higher performance of the GaSb cells in the TPV system (25%-30%) and the 24-hour continuous operation enabled by hybrid solar/gas operation. The EDTEK design also uses optical components to provide secondary concentration of the IR energy onto the GaSb PV cells to further reduce the area of expensive cells required.
2. The thermal residue from waste heat not converted to electricity must be captured in the form of process grade hot water. This, however, can provide a secondary revenue stream that further makes the system cost effective.
3. Solar concentrators have historically not achieved the economics desired for commercially competitive operation. EDTEK has developed a low-cost manufacturing process to address the problem and produce a low-cost, high-performance concentrator.

In order to address and overcome these obstacles EDTEK has developed, fabricated, and tested a pre-production prototype hybrid TPV system. An overview of how the individual components and subsystems of the solar/gas thermophotovoltaic (SGTPV) are finally assembled into a complete generator module is illustrated in Figure 2.

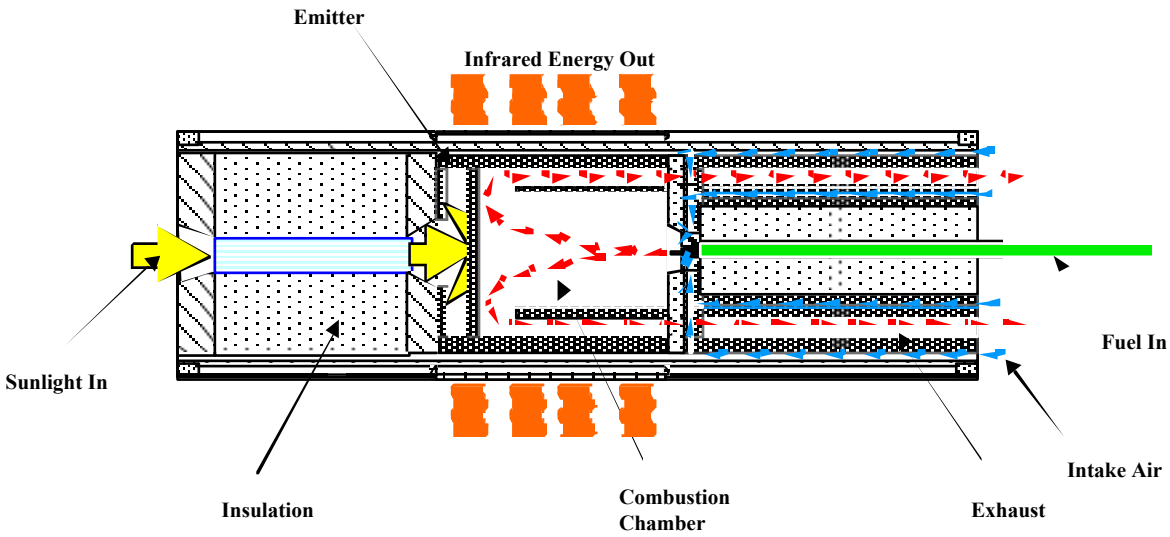

Figure 2. Conceptual Design of SGTPV Receiver

The fully assembled TPV cavity is mounted to the back of the primary reflector in the cassegrainian type solar concentrator as shown in Figure 3. The primary concentrator dish is 1.42 meters in diameter and has a 2-axis tracking system. Its electrical output will be about 500 watts. When the sun is out it will generate electricity with between 28% and 30% efficiency. When the sun is not shining, the generator will switch to natural gas fuel and generate electricity with efficiencies of ~20%. In both cases, hot water will be co-generated with a recovery efficiency of ~84%. The TPV converter is cooled by a two stage process; first cool water passes behind the cells (keeping them at optimum operating temperature), next the water continues on through a heat exchanger which transfers heat from the burner exhaust boosting the water temperature to values as high as 165°C. This temperature is within the range required of industrial process heat. The overall system becomes a co-generator, simultaneously providing electricity and process heat, both of which can be sold at market rates to repay the initial capital costs. These combined products render the EDTEK system very efficient. Over 80% of the energy entering the system can be captured and sold as either electricity or thermal energy. The combination of the two products provides the highest possible monetary return to amortize the capital costs. In this way, solar energy can finally break through the economic barriers that have prevented it from competing directly with mainstream energy sources.

Figure 3. Assembled TPV Cavity Mounted to Back of Primary Reflector

Figure 4 shows a photograph of two concentrator modules mounted onto a single pedestal and tracking system. Up to six SGTPV modules can be assembled onto a single mount and tracking system.

Figure 4. Photograph of Two Concentrator Modules Mounted On a Pedestal with Tracking System

In summary, the parametric performance of the hybrid solar/fossil TPV system is as follows:

1. Output electrical power: 500 watts electric per module.
2. Input hybrid solar/fossil fuel operation: 1211 watts thermal (solar), 683 watts thermal (fossil),
3. Input fossil fuel only operation: 2500 watts thermal,
4. Emitter operating temperature: 1400°C.
5. PV cell operating temperature: 40°C

1.3.1. Project Technical and Economical Objectives

The overall goal of this project is to lay the foundation for commercialization and full production of a distributed photovoltaic power generation technology that exceeds the "stretch goals" of the PIER general solicitation for renewables. To accomplish this we designed a project to overcome economic and technology obstacles that currently discourage private investment for commercialization. Our objective was to develop a hybrid system that utilizes the PV array 24-hours a day to give a better return on investment and to perform research and development on techniques for lower system initial costs. By combining the use of solar energy and fossil fuels to excite the same photovoltaic array, we remove the barrier of poor capital utilization for the solar PV array and we reduce the fuel costs for the natural gas generation of power by augmenting it with solar power. In addition, system waste heat is utilized to produce process-grade hot water thereby offsetting natural gas use in other processes within the customer's establishment. In this way we utilize photovoltaics to produce electric and thermal energy economically.

The overall project objective was to demonstrate the performance of a hybrid solar-fossil fueled thermophotovoltaic system that can operate on solar energy when the sun is available and switch to fossil-fuel, such as natural gas or oil, when there is insufficient sunlight. The specific technical objectives were two-fold. The first technical objective is to develop a pre-production prototype hybrid solar/natural gas thermophotovoltaic system that can convert sunlight to electricity with ~25% overall efficiency and natural gas to electricity at an overall efficiency of 20% while producing process-grade hot-water at a recovery efficiency of ~83%. The second technical objective is to develop an absorber/emitter for the TPV system that can operate at 1600°C. This will increase the energy densities on the PV array by a factor of 2.6:1 over the current design, which operates at 1400°C emitter temperature. The higher emitter temperature will lower materials and PV cells costs to the system.

The economic objectives centered around reducing the cost of the TPV system by a reduction in the photovoltaic cell costs and by developing an economical manufacturing process for the fabrication of the high-performance concentrating dishes. The cell-cost reduction approach was to reduce the number of cells required in the system and reduce the cost of fabricating the required PV cells. The specific objective was to develop an infrared concentrating optical component with a concentration ratio of 4:1. The use of this optical component will reduce the system cell costs, which is the dominant obstacle to commercialization, by a factor of four compared to current systems operating with little or no concentration. The second objective was to develop and demonstrate a vertically-integrated manufacturing process for producing high-performance concentrator dishes (CR>1000:1) at low cost ($3.40/sq. ft.). As a comparison, the stated objective is comparable to the just the materials cost of current concentrators that employ adhesive-backed reflective-coated films, these current systems then require the added cost of substrate and film application labor.

1.3.2. Project Approach

It was the goal of this project to develop a distributed photovoltaic power system that is efficient, reliable, and economically competitive with other more established generating systems. Our approach was to develop a hybrid, solar/fossil thermophotovoltaic (SFTPV) converter that can operate either individually or simultaneously on solar energy and fossil fuels

such as diesel, natural gas, and propane. This hybrid system removes the obstacle of poor capital utilization since the converter can be operated 24 hours a day utilizing sunlight as a free, renewable source of energy when it is available and then continue on with fossil fuel when the sun is not available. When operating on fossil fuel the system can be varied by varying the burn-rate without sacrificing efficiency. This variability allows power peaking of the system by operating on both solar energy and fossil fuel simultaneously to produce from one up to two times (depending on the fossil fuel burn-rate) the power that can be produced on either fuel alone. A modular design will maximize its market breadth and versatility.

Most of the issues regarding increasing TPV efficiency were addressed in our concurrent cost-share programs with the federal government. This TPV technology was transferred directly to the PIER project. Our specific approach for the PIER project centered on the development of two key issues of the TPV technology. First, the system must be efficient and it must be cost competitive. Second, the concept must be demonstrated as a pre-production prototype working system to reduce risk to an acceptable level for private investment capital.

Our approach for making the SFTPV system cost effective was two-fold; lower the cost of the required GaSb PV cells and lower the cost of the solar concentrator. The cost of the PV cells were lowered by reducing the cost of the cell starting materials, improving PV cell fabrication yield, reducing the number of PV cells required for each system, and increasing the energy density impinging on the PV cells by increasing the source temperature of the TPV system. The second group of key cost reducing technical issues are those to reduce the cost of the dish concentrator. Our approach was to focus on a key dish fabrication step; that of smoothing the formed substrate from as-received aluminum to an optically-specular surface which can be coated with reflective metal and dielectric protective layers.

A barrier to commercialization is the lack of a full system level demonstration of the hybrid SFTPV concept. Our approach to this barrier was to conduct such a system level demonstration. A pre-production prototype of the SFTPV was fabricated, evaluated and tested at the EDTEK facilities and then demonstrated at a site near the CEC. As further clarification of the approach we used to accomplish the objectives of this project, a brief summery of the statement of work is presented below.

Task 1 Establish Design Requirements and Philosophy - System requirements were developed around the needs of a midsize (~50,000 square feet) grocery supermarket. The design philosophy will be to maximize performance to the extent possible commensurate with providing for the customer's needs cost competitively. The advanced hybrid TPV system will be sized and designed to provide electricity and hot water in the grades necessary to meet the needs of the user, i. e., stored hot water for heating, low grade hot water for cleaning of the meat cutting facilities, or medium grade hot water for adsorption air conditioning.

Task 2 Define Conceptual SFTPV System Design - Taking into account above considerations, a conceptual design will be generated for the distributed utility and its integration into the customer’s building.

Task 3 Develop Key Technologies
Task 3.1 - Develop Infrared Secondary Concentrating Optical component
Task 3.2 - Develop Reflector Fabrication Process - . All the steps of the dish fabrication process have been previously demonstrated except the substrate-smoothing step which is required in order to provide a specular surface on which to deposit the reflective coating. Smoothing techniques will be explored with the optimum process implemented.

Task 4 Develop Hybrid Solar/Gas TPV Pre-Production Prototype - Based on the requirements dictated by the overall hybrid TPV system design discussed under task 1, and the conceptual design defined in task 2, a pre-production prototype hybrid solar/gas/thermal TPV module will be developed.

Task 5 Test and Evaluate SFTPV Prototype - Each component of the SFTPV will be fully instrumented and tested during its development and fabrication to confirm its performance according to the design function.

Task 6 Demonstration of the SFTPV System - When the initial evaluation tests of the pre-production prototype SFTPV are completed, the entire unit will be mounted on a mobile trailer test platform. The unit will then be transported to Sacramento for an on-sun demonstration to CEC personnel.

Task 7 Manufacturing and Production Planning - Estimation of near and mid-term manufacturing costs based in the materials and processes identified during design, fabrication and testing stages. Further estimates of production reliability, replace-ability, and manufacture-ability of critical components. Evaluation of product-level cost/performance trade-offs.

Task 8 Market Assessment

Task 9 Commercialization Planning

Task 10 Reporting

1.4. Report Organization

The remainder of this report is organized into eight sections. Each section describes a portion of the work accomplished in this PIER project. Section, 2.0, gives a general discussion of the technical and economic goals for the project and our achievements directed toward accomplishing those goals. Section 3.0 discusses the SGTPV design as achieved through the completion of tasks 1 and 2. Section 4.0 discusses the development work and accomplishments associated with the critical component develop achieved by task 3. System level development of the fossil-fueled TPV (results of task 4) is discussed in Section 4.0. Section 5.0 contains results of the solar TPV generator development. This includes discussion of the solar aperture and receiver portion of the SGTPV system (more results of task 4). Results from the development of the hybrid solar/gas TPV system are presented in Section 6.0. This section contains discussions of the solar concentrator development, the solar tracking system development, and the fabrication of the complete SGTPV system (task 4). Section 7.0 is a discussion of the results of the testing and evaluation of the hybrid solar/gas TPV system (results of tasks 5 and 6). Section

9.0 is a discussion of the conclusions and recommendations derived from this development program. Included in this section are some brief paragraphs regarding the commercialization of the SGTPV system and its benefits to the State of California. The final section, 10.0, is a list of the references. It should be noted that the results of tasks 7, 8, and 9 (Manufacturing and production planning, Market assessment, and Commercialization Plan, respectively) have been previously reported and approved by CEC in a separate document.

2.0 Project Objectives And Achievements

The overall objective of this PIER project is to develop, fabricate, test, and demonstrate both the technical and economical viability of an SGTPV module that can run alternately, or simultaneously, on solar heat input and/or natural gas. In order to achieve this overall goal, a set of specific goals was established for both technical and economical performance. These goals and the degree to which they were achieved are described in the following sections. Also described are the technical achievements realized as a result of the developmental program. Table 1 is a summary of the program objectives and achievements.

Table 1. Summary of Project Goals and Achievements

Summary of Project Goals and Achievements	
Overall Project Objective	Degree of goal fulfillment
To demonstrate the performance of a hybrid solar-fossil thermophotovoltaic system that can operate on solar energy when the sun is available and switch to fossil fuel such as natural gas or oil when there is no sun.	Fabricated and Demonstrated a pre-production prototype hybrid solar/natural gas commercial SGTPV system that meets most of our technical objectives. It features 1) a unique modular design such that customer power needs can be easily accommodated by adjusting the number of modules to be delivered, 2) a solar aperture for admitting sunlight into the SGTPV and an emitter design for running simultaneously on sunlight and gas, 3) an improved high throughput IR band-pass filter for increased power density, 4) a high concentration unit for reducing PV cell requirements, and 5) a modular, low-cost, high-performance parabolic concentrator system.
Technical Objectives	
1. To demonstrate a pre-production prototype hybrid solar/natural gas thermophotovoltaic system that can convert sunlight to electricity with ~25% overall efficiency and natural gas to electricity at an overall efficiency of 20% while producing process grade hot water at a recovery efficiency of ~83%.	Electrical energy production by the SGTPV module was demonstrated in the laboratory at low power levels; however, an early failure of a vacuum seal in the converter thermal control package precluded actual performance evaluation at full operating power. Extrapolation from the low power levels achieved indicted that, at full operating power, a gas-to-electric efficiency of 15.6% and 22.3% solar to electric would be achieved. We have measured 83% thermal residue recovery in our TPV systems.
2. To develop an absorber/emitter for the TPV system that can operate at 1600°C to increase energy densities on the PV array by a factor of 2.6:1 over the current design operating at 1400°C in order to lower materials and PV cell costs.	Because of material reliability considerations, the 1600°C operating temperature goal was abandoned as a means of lowering cell area, and hence, costs. Similar cell area savings were realized by increasing the throughput of in-band energy a factor of 1.36 by the development of improved IR filters.
Specific Economical Objectives	
1. To develop an infrared concentrating component with a concentration ratio of 7:1 that can reduce overall cell active area requirements and, hence, reduce system cell cost, which the dominant obstacle to commercialization, by a factor of 7 compared to current systems operating with little or no concentration.	A component with 4:1 concentration ratio was developed. The remaining cost reduction was achieved by increasing GaSb TPV cell production yields from 60% to 95% and by working with the vendor to lower GaSb material costs we reduced our starting wafer costs from $240 each to $110 each. These achievements with the filter discussed above reduced our cell costs by a factor of 12 exceeding our original goal.
2. To develop and demonstrate a vertically integrated manufacturing process for producing low-cost high performance concentrator dishes (CR>1000:1) at low cost ($3.40/sq. ft.) which is comparable to the adhesive backed, reflective coated films currently used by most systems before substrate and film application labor	A pilot production process that can produce field ready concentrator dishes in small volume at a price of $6.96/sq. ft. was developed. With further automation enabled by large volume, the price will drop to $4.06/sq. ft with the conformal reflecting finish coating costing about $1.74 and $1.01 respectively in low and high volume production.

costs are considered.	
3. To develop a business plan and financial strategy for commercialization.	Commercialization and production readiness plans for the SGTPV were developed.

2.1. Technical Goals And Achievements

The technical performance goals for the project are:

> To demonstrate a pre-production prototype hybrid solar/natural gas TPV system that can convert sunlight to electricity with ~25% overall efficiency and natural gas to electricity at an overall efficiency of 20% while producing process grade hot water at a recovery efficiency of ~83%. Unfortunately, an early failure of a vacuum seal between the IR filters and the thermal control jacket prevented our achieving full operating conditions to demonstrate the above efficiency goals. However, extrapolations of the lower temperature results we obtained indicated that a gas-to-electric efficiency of about 15.6% and a solar-to-electric efficiency of 22.3% would be achieved at 1400C.
>
> To develop an absorber/emitter for the TPV system that can operate at 1600°C to increase energy densities on the PV array by a factor of 2.6:1 over the current design operating at 1400°C in order to lower materials and PV cell costs. During the course of the project we abandoned the 1600°C emitter temperature objective but achieved the objective of lowering cell cost by two different approaches. First we increased the energy density on the PV cells by a factor of 1.36:1 by increasing the transmittance of the IR band-pass filters. Secondly, we improved the yield of our cell production process from 60% to 95% in addition to working with GaSb wafer vendors to lower the cost of wafers from $240 to $110 each. These two approaches lowered the PV cell cost by a factor 4.6 exceeding our original goal.

In the course of achieving these PIER project goals, we have accomplished the following technical developments:

1. A pre-production prototype hybrid solar/natural gas commercial TPV system that meets most of our technical objectives.
2. A unique modular design that can operate either from concentrated solar energy or a natural gas burner or operates from both of these power sources simultaneously.
3. A solar aperture for admitting sunlight into the SGTPV system.
4. An emitter design for running simultaneously on sunlight and gas.
5. A gas burner/recuperator subsystem.
6. An improved vacuum thermal control package for the SGTPV converter.
7. An improved high throughput IR bandpass filter for the SGTPV.
8. An improved vacuum tight seal for bonding filter substrates to the thermal control package.
9. A eighteen unit array design for concentrating the transmitted thermal energy onto the PV cells.
10. Thermal control and heat recovery system for PV cell arrays and recuperator exhaust system.

11. Developed a low-cost, high performance concentrator for supplying the solar energy to the TPV system.
12. A conformal reflective coating process for a 1.6 square meter aperture parabolic concentrator dish.
13. A uniquely actuated solar tracking system that is integrated with the mounting pedestal for the concentrator.
14. Microcomputer based electronic/software control system for the entire SGTPV system.

During the test and evaluation program, the following functions were demonstrated:

1. A complete solar/gas TPV prototype has been designed, developed, fabricated, and tested.
2. Heating of the emitter by a gas burner has been demonstrated.
3. Production of electricity by gas burner heating has been demonstrated.
4. Heating of the emitter by concentrated solar energy has been demonstrated.
5. Heating of the emitter by a gas burner and concentrated solar energy simultaneously has been demonstrated.
6. With the above accomplishments, the feasibility of the hybrid solar/gas TPV concept has been demonstrated.
7. Computer control of the air and fuel mixture to the gas burner has been demonstrated.
8. The computer-controlled, < 0.1°-accurate sun tracking system has been demonstrated.
9. Control of local "house keeping" functions such as night-time stowage has been demonstrated.
10. Solar concentration by the EDTEK fabricated parabolic dishes has been demonstrated.
11. A commercialization plan for the SGTPV has been compiled.
12. A production readiness plan for the SGTPV has been compiled.

The entire unit was transported and set up on a property in Roseville, California for demonstration of the above functions to CEC personnel. This demonstration also generated considerable interest among the local Roseville citizenry. The site was visited by about 22 interested persons; several of whom expressed a desire to purchasing our solar concentrator systems.

2.2. Project Economic Goals And Achievements

In addition to achieving the technical goals for the system, it is recognized that several cost and economic goals must be achieved in order for the system to be commercial viable. In the final analysis, the hybrid, co-generation techniques used in this project will only constitute a true breakthrough for distributed photovoltaic power if the entire system can be manufactured within market driven cost goals. The formula for determining this can be stated simply: The

cost of the system (including debt service) plus the cost of its operation and maintenance must be less than the after-tax income it accumulates over its operational life. To address these issues a commercialization plan and a manufacturing/production plan has been developed as part of this project. These plans address the following questions:

1. What are the projected costs of the system in large-scale manufacturing?
2. What are the projected maintenance and operation costs?
3. What is the value of the energy the system delivers over its life?

Three additional considerations significantly impact this issue:

4. What is the competing rate of interest available to potential investors; i.e., the U.S. 30-year bond?
5. What tax regulations apply; i.e., what are the applicable depreciation rates; what investment credits are available; and what rate of income and property taxes apply to the income flow and the installation itself?
6. What is the projected increase in the value of the energy produced over the life of the system (i.e., what is the likely increase in the cost of the fuel source being displaced)?

The overall intent of this project was to provide valid input data for determining the answers to the above questions through design, fabrication, and demonstration of a prototype system. To this end, we have identified the following economical/cost goals:

1. To develop an infrared concentrating unit with a concentration ratio of 7:1 that can reduce overall cell active area requirements and, hence, reduce system cell cost, which is the dominant obstacle to commercialization, by a factor of 7 compared to current systems operating with little or no concentration. We achieved 4:1 concentration with a secondary unit and realized system cost savings in other areas, i.e. PV cell cost and requirements reductions, that meet the goals for system cost reduction.
2. To develop and demonstrate a vertically integrated manufacturing process for producing low-cost high performance concentrator dishes (CR>1000:1) at low cost ($3.40/sq. ft.) which is comparable to the adhesive backed, reflective coated films currently used by most systems before substrate and film application labor costs are considered. We have developed a pilot production process that can produce field ready concentrator dishes in small volume at a price of $6.96/sq. ft. With further automation enabled by large volume, the price drops to $4.06/sq. ft with the conformal reflecting finish coating costing about $1.74 and $1.01 respectively in low and high volume production.
3. To develop a business plan and financial strategy for the commercialization of the SGTPV. We have developed both a commercialization plan and a manufacturing/production readiness plan that shows the SGTPV to be a very competitive product for point of use power generation.

In addition to the above achievements directed toward promoting economic viability for the SGTPV system we have also accomplished the following items:

1. An improved high yield process (~95%) for producing lower cost and higher performance GaSb PV cells with pilot production equipment that can produce cells capable of ~ 0.25 Mw/yr in SGTPV modules.
2. An improved pilot filter production process and equipment that can produce filters capable of ~ 0.25Mw/yr in SGTPV modules.
3. Deployed pilot production equipment for fabricating 1.6 square meter parabolic concentrator dishes capable of producing ~ 2Mw/yr in SGTPV modules.
4. Developed an alliance with a GaSb PV cell vendor that promises to reduce the cost of GaSb wafers by about a factor of 5 below current best prices.

3.0 SGTPV Design

Conceptual drawings of the SGTPV design and all its major subsystems were presented in Figure 2 and Figure 3. The system is based on a 56-inch diameter parabolic solar concentrator dish. A secondary mirror intercepts energy from the primary parabola and directs it into a optical-coupler which delivers it into the TPV absorber/emitter. The absorber/emitter is also heated by a gas burner. Waste heat in the exhaust of the gas burner is recovered by means of a recuperator heat exchanger which preheats the combustion air to the gas burner. Thermal losses by conduction and convection from the burner, recuperator and emitter are minimized by an evacuated shell that surrounds them. When the emitter is heated to incandescence, it radiates a blackbody spectrum of energy to an array of IR band pass filters surrounding it. These filters reflect most of the blackbody energy back to the emitter where it is reabsorbed and transmit a band of energy that is useful to the TPV cells through it. An array of optical elements located immediately behind the filters intercept the transmitted energy and concentrate it onto an array of TPV cells that convert a portion of it to electricity. The residual heat from that portion of energy in the TPV cells not converted to electricity is removed by a liquid coolant and is then available for delivery to a user or can be exchanged to the surrounding atmosphere by means of a secondary heat exchanger (not shown in the figures). Each of these subsystems, their functions, and designs are discussed in detail in the following sections.

The fully assembled TPV cavity is mounted to the back of the primary reflector in the cassegrainian type solar concentrator which as shown in Figure 3. The primary concentrator dish is 1.42 meters in diameter and has a 2-axis tracking system. Its electrical output will be 500 watts. When the sun is out, it will generate electricity with between 28% and 30% efficiency. When the sun is not shining, the generator will switch to natural gas fuel and generate electricity with efficiencies of 15% to 20%. In both cases, hot water will be co-generated with a recovery efficiency for the residual thermal energy of ~84%. For further customer flexibility the SGTPV receiver is designed to be interchangeable with the EDTEK Cogen-1 photovoltaic receiver. This interchangeability can make the entire system more economical for customers who do not require 24-hour generation.

In summary, the parametric performance of the hybrid solar/fossil TPV system is as follows:

1. Output electrical power: 500 watts electric per module.
2. Input hybrid solar/fossil fuel operation: 1211 watts thermal (solar), 683 watts thermal (fossil),
3. Input fossil fuel only operation: 2500 watts thermal,
4. Emitter operating temperature: 1400°C.
5. PV cell operating temperature: 40°C
6. Hot water recovery temperature: 65°C

3.1. SGTPV Solar Concentrator Design

It is desired that the solar concentrator be modular so that multiple small dishes can be arrayed together on a single tracking and power conditioning system. Figure 5 illustrates the approach. Such modularity is desirable because 1) it minimizes the cost of production equipment, 2) it

allows high volume production of a single element which lowers production cost, and 3) it permits the system to be custom sized to meet the needs of individual customers. After performing trade-off studies between cost, size, array profile etc. a diameter of 1.42 meters was selected for the primary collector dish.

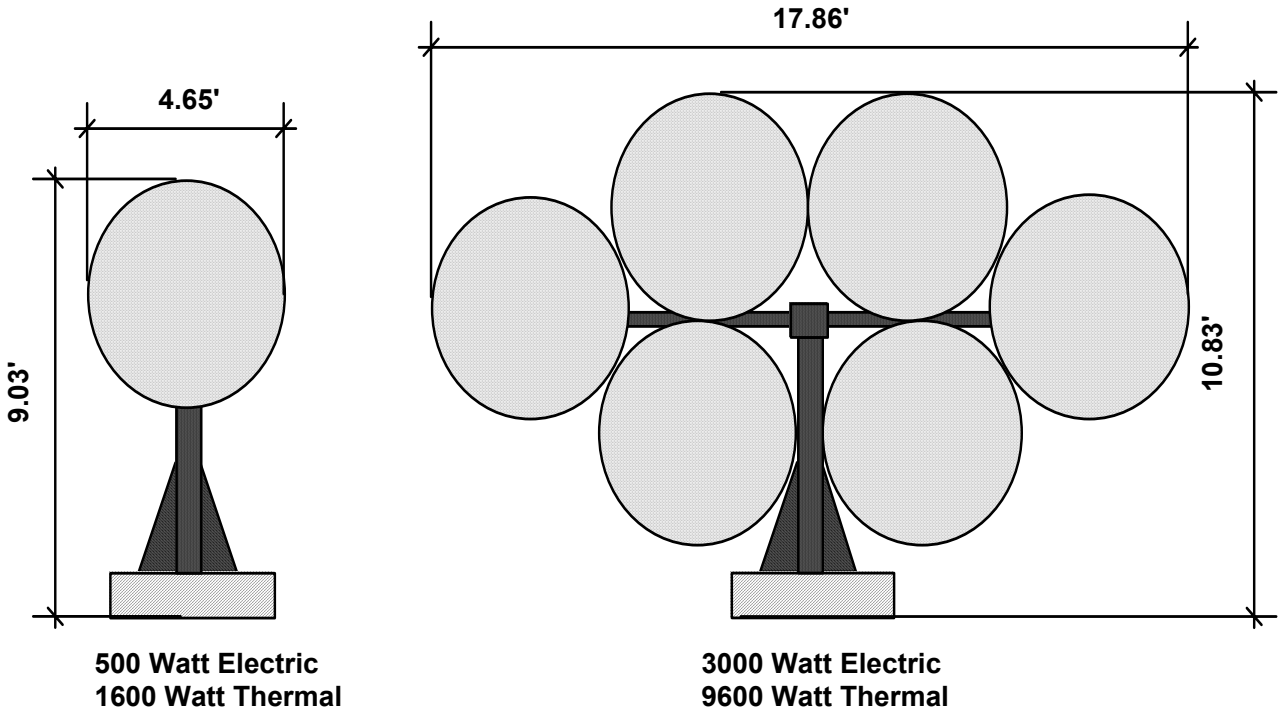

Figure 5. Illustration of the Versatility of Modular System Approach

The design of the concentrator for the SGTPV module is based primarily on experience gained in a small test bed solar concentrator cost-sharing program [5]. The new concentrator module is basically a scaled up design based on this experience.

Based on the successful results with the small test bed unit, a cassegrainian concentrator configuration is selected for the hybrid solar/gas modular TPV system. Both the pointing and tracking system and the calibration techniques developed with the test bed unit will be used to evaluate the concentrator for the SGTPV modules. The primary reflector for the SGTPV module is a parabolic dish with "fast" optics which focuses the incident solar energy to a point in the plane of the rim of the primary dish. Located at the focal point of the primary dish is a secondary reflector that intercepts and re-directs the energy to a new focal point at the center of the surface, or base, of the primary dish. Such a configuration, known as a cassegrainian design, suffers some loss due to the reflectance of the secondary reflector; however, the advantage of the receiver and all the receiver hardware being located behind the dish which obviates shadow losses, offsets the disadvantage of the reflective loss. Figure 6 illustrates the configuration and traces the energy through the concentrator system as outlined in the following steps.

1. The diameter of the primary concentrator is 1.42 meters (56 inches) which results in solar interception aperture of 1.59 m^2 (17.1 ft^2).

2. The peak solar intensity is assumed to be 900 W/m^2.

3. The reflectance of the primary is 0.92 therefore the energy directed to the secondary lens is
   Esecondary = 1.59 m^2 x 900 W/m^2 x 0.92 = 1,317 W.

4. The reflectance of the secondary is 0.92 so that the solar energy directed to the receiver is
   Ereceiver = 1,317 W x 0.92 = 1,211 W.

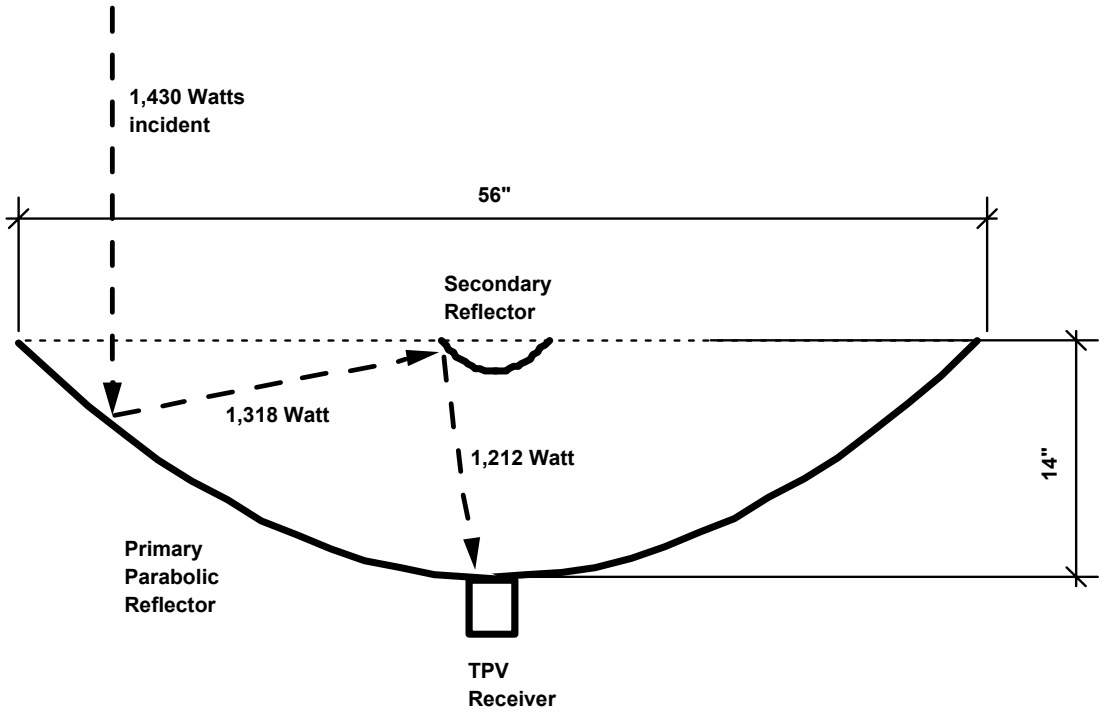

Figure 6. Illustration of Energy Path Through Solar Concentrator

A perspective view of the concentrator dish is shown in Figure 7. The concentrator dish will be fabricated by a seven step process which was developed on a prior EDTEK program[7]. A key step in this process is being optimized in a separate task under this PIER project. The dish manufacturing process will be discussed in detail in the technology development section of this report.

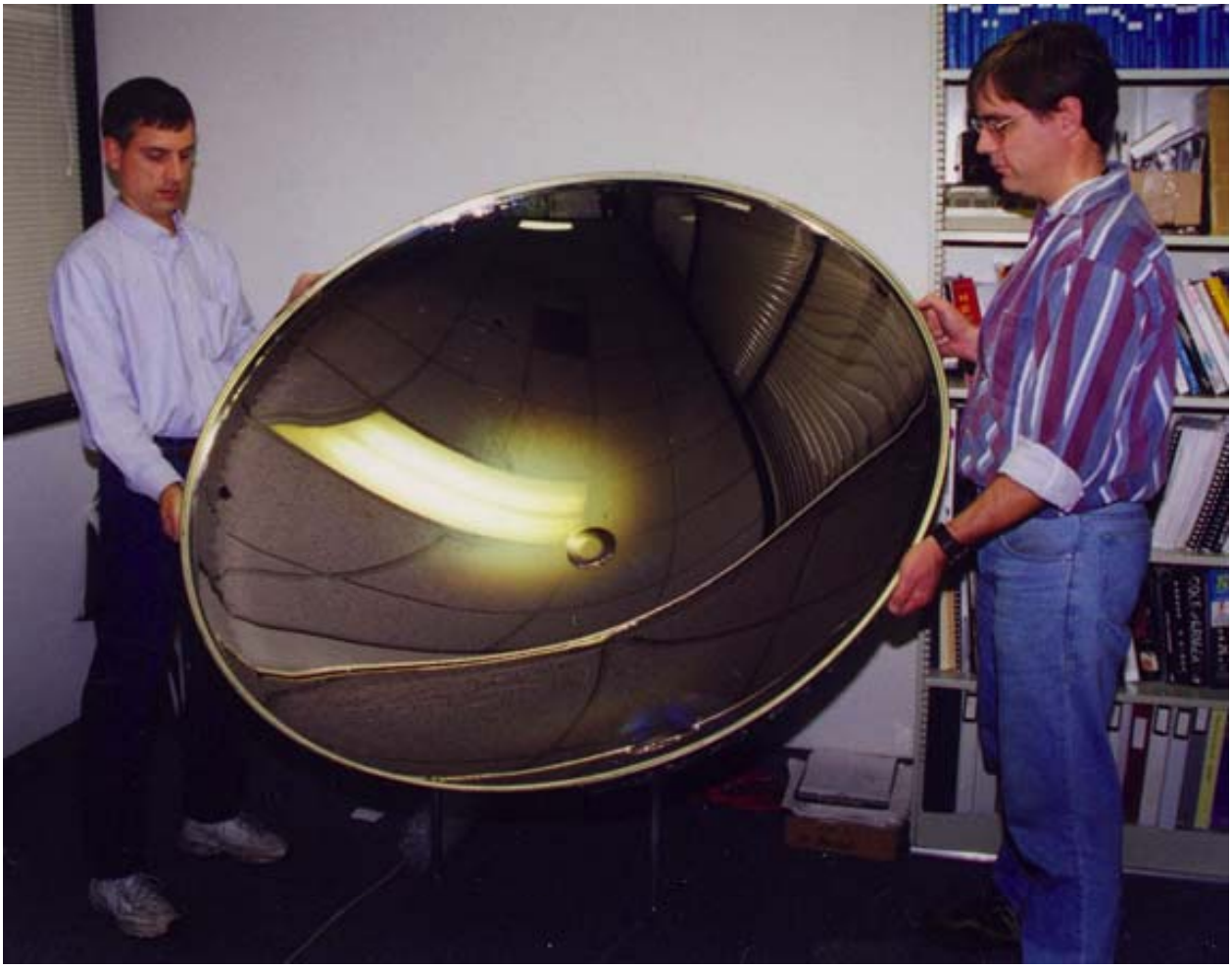

Figure 7. Perspective View of Solar Concentrator Dish Design

3.2. SGTPV Solar Receiver Design

3.2.1. Solar Entrance Window

There are two primary considerations in designing the solar entrance window. First, it must admit the sunlight to the TPV cavity efficiently, and second, it must prevent undue leakage of infrared energy back out of the cavity. The concentrated solar energy from the secondary reflector is intercepted an conducted into the entrance to the TPV cavity. The design allows for sufficient insulation between the emitter and the outside of the converter to minimize thermal losses out of the cavity and limits the amount of IR energy that can be transmitted back out of the cavity to a small percentage of the total energy in the cavity. The size of the window constitutes less than 1% of the area of the cavity walls.

3.2.2. SGTPV Absorber/Emitter Sizing

The emitter is the heart of the SGTPV receiver. It intercepts heat energy from both the solar concentrator and the natural gas burner and radiates infrared energy to the TPV cells for electrical conversion. Our goal is to achieve an emitter operating temperature of 1400°C. In

order to meet this requirement, the emitter must be sized to achieve the operating temperature with the solar energy input which is fixed by the solar concentrator. Another requirement which derives from our business plan is that the TPV receiver needs to generate at least 500W to make the system economically feasible. Since the concentrator will not supply enough energy to generate this much electricity, the natural gas burner can then be designed to deliver some amount of energy to the emitter to augment the solar energy and then sufficient energy to generate the full 500W when the sun is not available. In order to size the emitter for the SGTPV, we have again drawn upon experience from the small solar TPV and the diesel TPV testbed units to determine the emitter size to generate 500W. Using this experience and emitter size, the relative amounts of energy required from the solar concentrator and the gas burner was determined. To achieve the appropriately balance between solar and gas energy one must begin from solar concentrator energy delivered to the receiver. The sizing is then an iterative process. First, an approximate emitter size is obtained by neglecting losses. Then using the approximation, a more realistic size can be obtained by inserting realistic values for filter transmittance, cavity wall absorptance, and solar entrance window losses. From an energy balance the emitter temperature can be calculated and the size can be adjusted. After evaluating the results of the balance, the emitter size can be refined and the balance repeated until the desired operating parameters are achieved. From these calculations and the conversion efficiency of the GaSb photovoltaic, it was determined that the power generated by solar input to the SGTPV is 281 watts. This yields a solar-to-electric conversion efficiency of about 24.5%.

When the energy lost to the cavity walls and transmitted to the cells is accounted for in the calculation, the emitter temperature will not reach 1400°C unless the gas burner supplies some additional energy to the system.

From iterative calculations of this kind, it was found there is a trade-off between emitter temperature and cavity efficiency. There is also a trade-off between emitter efficiency and cost. In order to keep the overall power out of the system to at least 500W, for economic considerations, it is assumed that the natural gas burner will be used to supplement the solar energy to maintain 1400°C operation.

3.3. Burner / Recuperator Design

Sizing the burner requires a balance between the fuel burned in the TPV combustion chamber. The energy transmitted from the emitter to the TPV cells, parasitic losses in the TPV cavity, energy recovered and returned to the combustion chamber via preheated air from the exhaust by the recuperator heat exchanger, and energy recovered in hot water from the gases finally exhausted from the system. A computer code for the analysis of the overall heat balance on the TPV co-generation system from the gas burner-only viewpoint has been prepared. The purpose of the code is to allow analysis of the effects which design parameters have on overall performance as well as to get information on system flows and temperatures. These will then be employed as input for more detailed design work as the work progress beyond the conceptual stage.

The code input parameters include: fuel firing rate; gas temperature leaving the combustion chamber/emitter section (entering the recuperator); recuperator effectiveness; parasitic thermal losses from the emitter section; system internal electric power use; excess air; and the

temperature of the exhaust gas leaving the system. Incoming ambient air is fixed, and the TPV cell conversion efficiency is assumed to be 34%. Code output includes: air, fuel, and exhaust gas mass flows, recuperator air preheat temperature; exhaust gas temperature at the recuperator outlet [entering the waste heat recovery heat exchanger (hot water)]; total recuperator heat transfer; gross and net electric power produced from the gas fuel input (no consideration of solar); energy recovered from cell cooling; heat transfer in the waste heat recover exchanger; and the output distribution of input energy.

From exercising this computer code, it was found that a fuel firing rate of 1800 W produces approximately the same net electric power out as did the solar concentrator input energy of 1222 W with a particular recuperator effectiveness. Such a recuperator effectiveness results in an air preheat temperature of 1285°C which is close to the allowable temperatures for the best available metal alloys (about 1250°C). Based on availability of materials and this code, an optimum recuperator effectiveness was determined for our design.

Another interesting point to make from the results of this heat balance analysis is the impact the internal electric power use has on the overall performance. Figure 8 and Figure 9 show the results of a study of sensitivity to internal power use for the case of 1800 W fuel input energy and 1400°C emitter temperature. Clearly, one important design goal is to minimize the internal power use by fans etc.

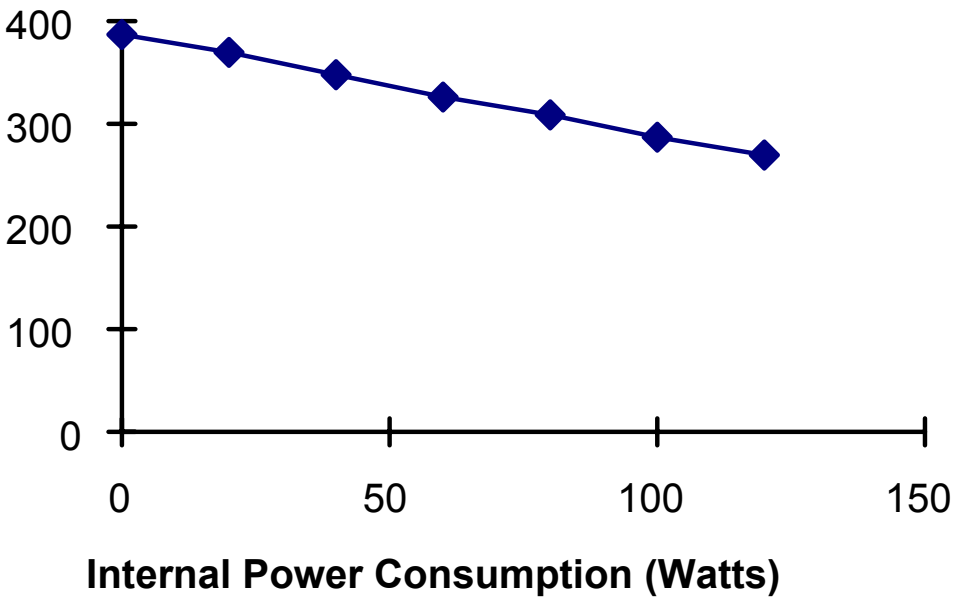

Figure 8. Effect of Internal Power Use on Natural Gas TPV System Performance

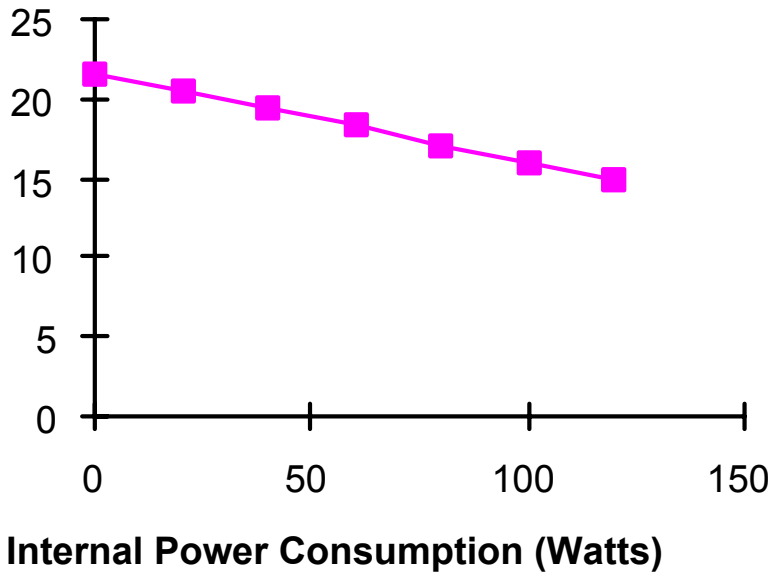

Figure 9. Impact of Internal Power Consumption on Net Fuel to Electric Power Efficiency

It appears that if the internal power consumption can be minimized, then the overall gas to electric efficiency goal of >15% can be met. Higher efficiencies could be obtained if the recuperator could be made more effective; however, a ceramic recuperator would be required to do so. Another method of minimizing the consumption of individual burners is to use a single fan to supply combustion air to an array of burners. This method will be explored in the overall design. There are also other methods for improving overall efficiency, i. e., better IR filters and/or TPV cells than those used in this model.

One concern that needs to be addressed before progressing further with the conceptual design of the 1400°C hybrid system is whether a ceramic recuperator is feasible from a thermal heat exchanger standpoint. In order to address this issue, a simple recuperator design program was completed to allow the initial evaluation of a ceramic such as silicon carbide, SiC, as a recuperator material. It has the desirable properties of survivability in air to temperatures up to 1750°C so that it is more than adequate from that respect. For manufacturing reasons, the walls of a SiC heat exchanger must be at least one-eighth inch thick for mechanical strength. Our first consideration was whether or not the conductivity of the thick SiC walls would be an issue. Figure 10 shows the relative contributions of air-side convection resistance, SiC wall conductivity, and gas side convection resistance to the total heat transfer resistance in the recuperator assuming a single sided recuperator.

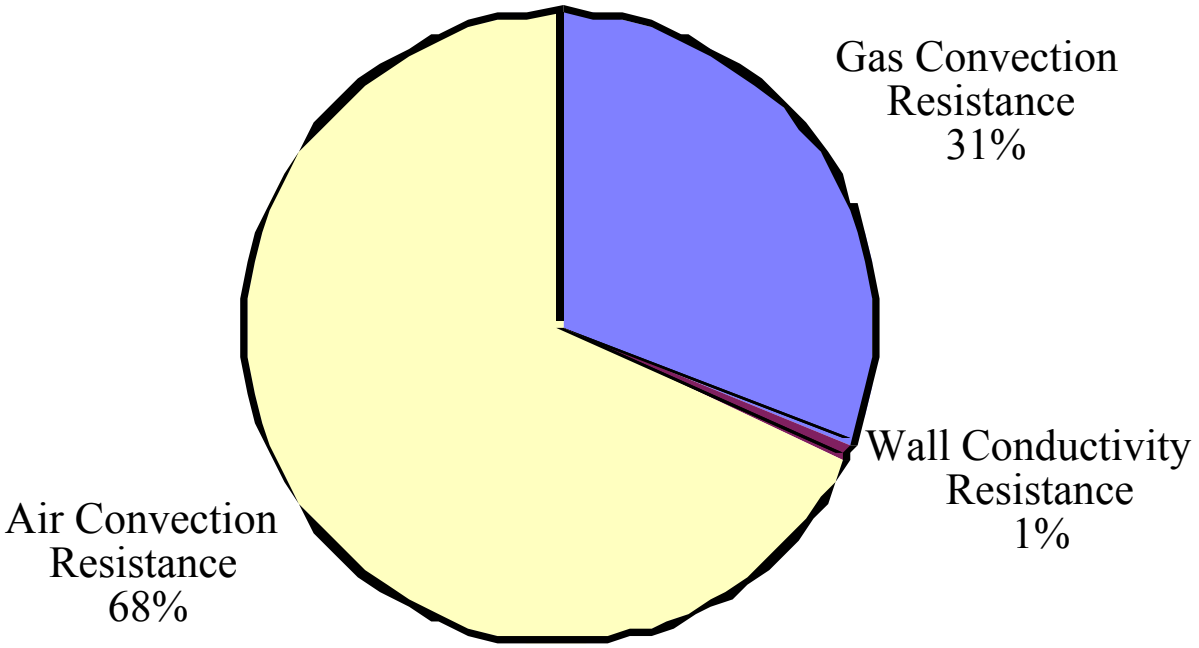

Figure 10. Illustration of Relative Thermal Resistances in Recuperator

As is evident in Figure 10, the thermal resistance of the SiC walls is negligible compared to the convective resistances presented by the gas and air interfaces. Thus, the ceramic materials seem viable as a candidate for the high temperature recuperator heat exchanger design.

The next consideration of importance is the air pressure drop required in the recuperator in order to get good heat transfer and acceptable recuperator effectiveness. In order to investigate this, the recuperator computer-coded-model was used to determine the effect of recuperator wall-gap size on the heat transfer performance and pressure drop within the recuperator. It was found that a pressure drop on the order of 0.2 inches of water is required. Based on this conclusion, a fan will be required to achieve the required pressure drop. It will be extremely important to use as small a fan as practical since it contributes to the internal power use of the system which degrades efficiency as illustrated in Figure 9. One approach that is being considered is the use of a single fan to supply the forced air for an array of modules in order to minimize the average internal power use of each module.

Based on the considerations discussed above, a conceptual design for the SGTPV emitter/burner/recuperator module has been synthesized. To the degree practical, it is a scaled version of the diesel burner/recuperator system developed on a cost share program [6]. The conceptual design of the SGTPV emitter/burner design is presented in Figure 11.

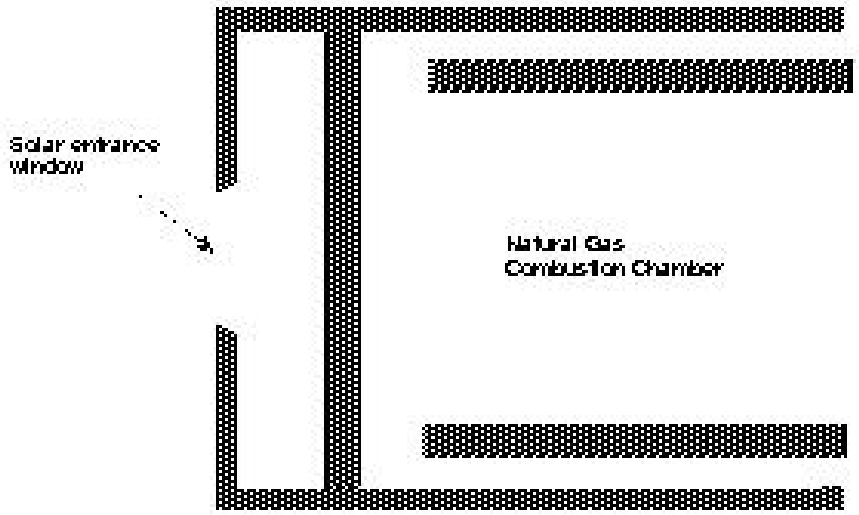

Figure 11. Conceptual Design of the Emitter/Burner for the SGTPV Module

3.4. Thermal Containment Package

For the design of the thermal containment package we draw primarily on the experience gained with the diesel TPV system developed as a cost-shared effort. The package is essentially a quartz "thermos bottle". It consists of a double walled quartz structure with a vacuum in the gap between the walls. A gold infrared reflecting film is vapor deposited on the inside of the outer wall of the assembly everywhere except the surface immediately adjacent to the emitter. The surface adjacent to the emitter is covered with resonant micromesh IR bandpass filters which were bonded to it with Dow Corning DC-93 500 silicone adhesive. This configuration proved to be a weak point in the design of the diesel testbed system limiting the emitter operating temperature of the system to about 1150°C instead of the 1400°C for it was designed to operate.

For our commercial SGTPV module, we desire to operate the emitter at a temperature of 1400°C. Thus the thermal package design must be improved. In addition to eliminating the potential for adhesive damage, the IR wavelength-selective filters located on the inner surface of the outer converter sleeve must be maintained at a temperature such that filter damage is avoided. Since the majority of the heat absorbed in the filter must be rejected through the PV cell stack, sufficient thermal conductivity of these layers must be maintained. It is also critical that the operating temperature of the PV cells be maintained in the face of the increased operating temperature of the emitter. Thermal analyses of the system have been performed to ensure sufficient cooling for the entire converter stack consisting of the IR filters, PV cells, and substrates and cell interconnects. These analyses will be discussed later in the 3.5); however, they have guided us in synthesizing a conceptual design for an improved vacuum thermal containment package. The primary change is that the quartz outer wall of the vacuum package used in the previous program is replaced. Windows are cut into the wall and the filter substrates soldered around their periphery into the frames surrounding the windows in the wall. In this way, organic adhesives are eliminated and even the solder bonding agent is not exposed to the full intensity of the graybody spectrum. In order to ascertain the viability of this

configuration, physical testing of components and subsystems will be performed as needed during the development and fabrication phase of the project to establish thermal, optical and mechanical properties.

3.5. TPV Electrical Converter Design

As described in References 5 and 6, two testbed TPV converters, one solar fueled and one diesel fueled, have been developed on cost-sharing efforts. This conceptual design for the hybrid solar/gas TPV converter incorporates the lessons learned from the two prior projects in order to develop an advanced conceptual design. Although the PV cell array for the advanced SGTPV will be similar in geometry to the diesel fueled unit the lay-up of the array and the function of the filters can be more clearly illustrated using the geometry of the solar fueled design. The basic technology is the same for the two arrays. The circuit board is a ceramic, thermally conducting board with laminated copper layers into which the interconnect-circuit for the array is etched. Contact is made from the top of the PV cells to the circuit board by means of conductors that provide a continuous conduction path around the entire periphery of the PV cell active area. This continuous interconnect is important in order for the cells to handle the high currents generated by the TPV conversion. Each of the cells see the same flux so that they can be arranged in series connected strings of cells. Optical elements couple the IR energy onto the TPV cells. Increasing the IR intensity on the cells increases the voltage as shown by the measured data presented in Figure 12. This increased voltage increases the conversion efficiency of the cells by about 10% overall.

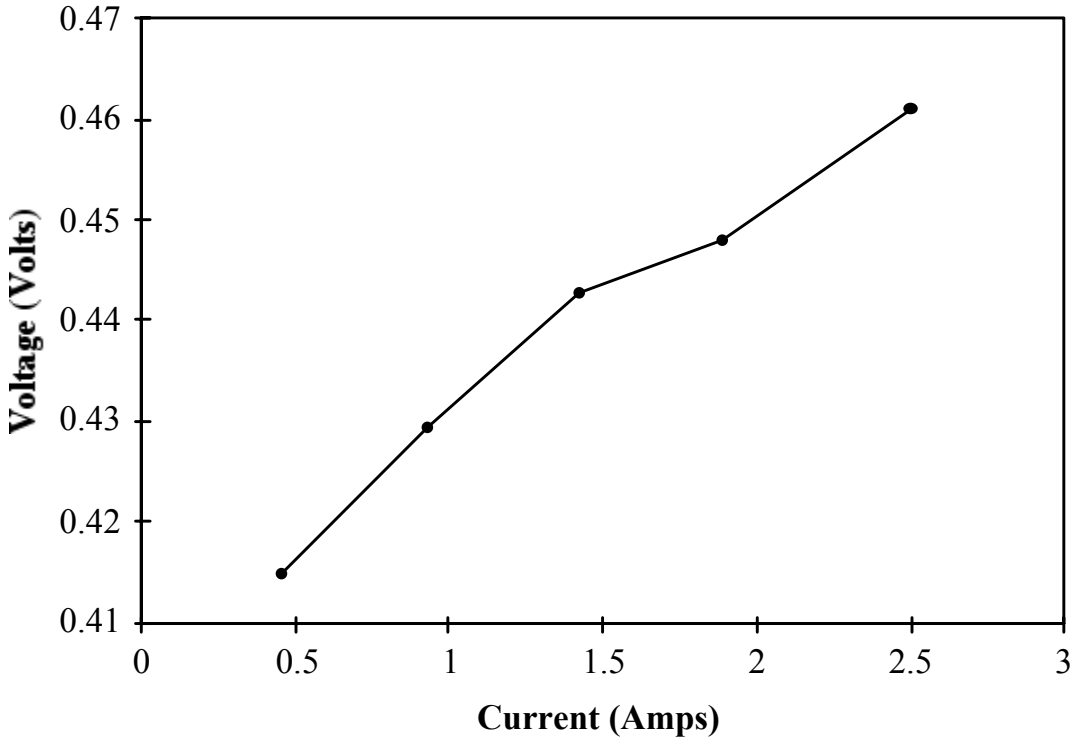

Figure 12. Measured Dependence of PC Cell Voltage on Current

Diffused junction GaSb PV cells are used for the electrical conversion of the concentrated light exiting emitter cavity. Typical electrical and spectral response characteristics of these cells are shown in Figure 13. In the small solar TPV testbed described above the current density incident on the TPV cells was fairly low; however, the current density in the diesel testbed and the current solar/hybrid unit is much higher. For the current advanced hybrid design, because of component and design improvements, the current density will be at least a factor of 3 times higher than in the diesel unit. Thus, the electrical current carrying capability of the PV cells must also be taken under consideration. Cells and interconnects with deficient current capability will result in high series resistance which could significantly degrade system performance. Given the infrared flux through the wavelength-selective filter and the quantum efficiency of the GaSb PV cell, the current generated can be calculated and proper cell grid design and interconnect design were established. Due to the experience on cost-share programs, EDTEK understands every aspect of the delicate balance needed to integrate and accomplish this design.

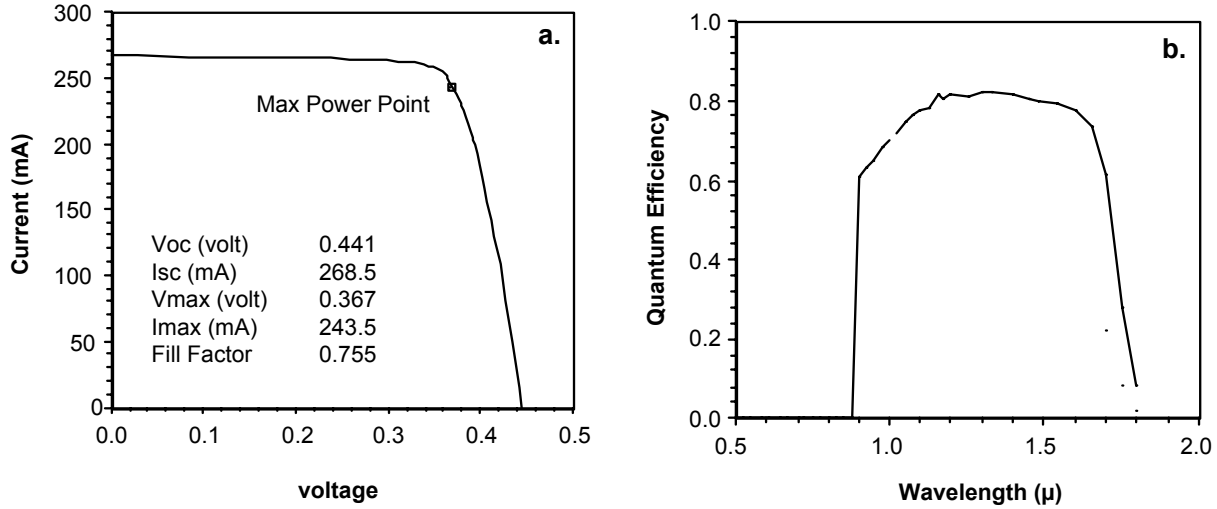

Figure 13. Current-Voltage and Quantum Efficiency of GaSb PV Cells

Figure 14 shows the filter that is bonded to the front of the PV cell stack to reject out-of-band energy and let only useful energy into the PV cells. The active region of the filter can be distinguished from the surrounding gold film by the reflection created by a grating effect from the etched pattern at visible wavelengths. This patented EDTEK TPV filter is the key to efficient TPV conversion. The resonant mesh filter transmits a band of energy centered around its resonant frequency. By tuning the transmitted band of energy to the wavelengths that can be most efficiently converted to electricity by the PV cells the power out of the system can be maximized for the amount of energy absorbed by the cells. The unique feature of the EDTEK TPV filter is that all energy that is not transmitted to the PV cells is reflected back to the emitter for re-absorption with an efficiency of >98%. Thus, the main energy escaping form the system

is confined to those wavelengths most efficiently converted by the TPV cells.

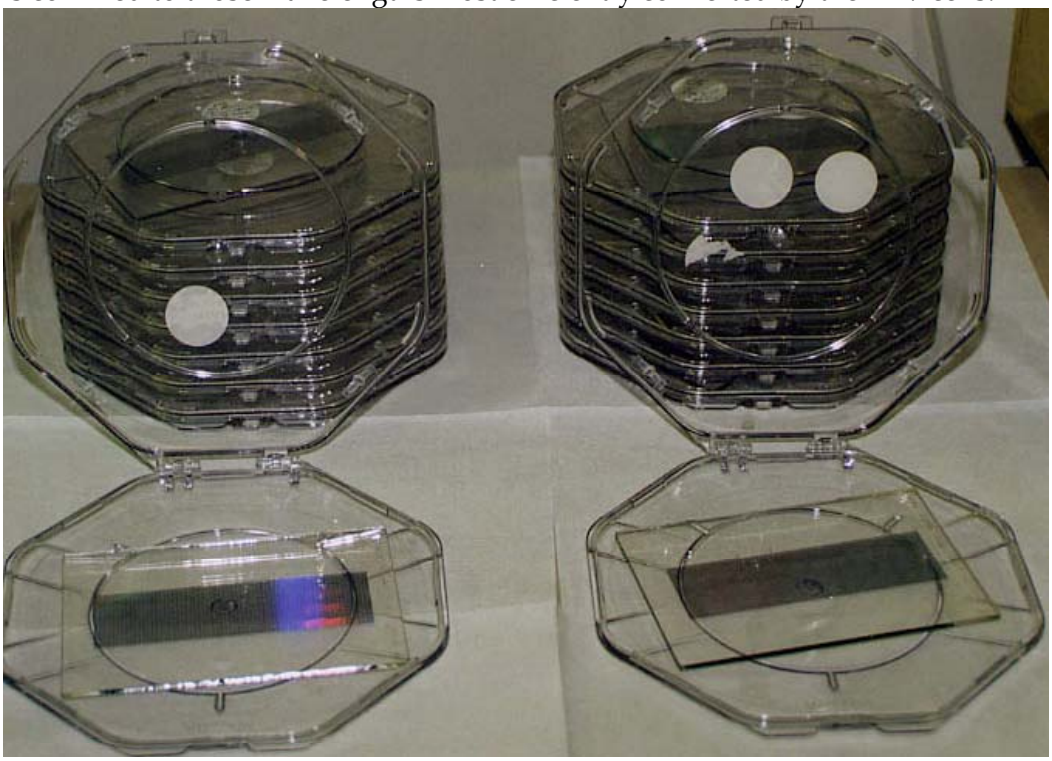

Figure 14. Photograph of the Filters That Reject Out-Of-Band Energy Back to the Emitter

As in most designs, the SGTPV requires a tradeoff between efficiency, emitter temperature, and cost. The higher energy density generated by a higher emitter temperature results in less cell area being required for a given electric power out. The lower cell area requirement translates into lower cost since the PV cells are the most expensive components in the system. However, lower efficiency requires more cells; therefore we require a trade-off study to see which effect results in the best cost compromise in terms of dollars per watt. As a potential solution that will not require such a compromise for the advanced SGTPV, we propose a new filter design to replace the dipole cross patterns that were used in the diesel testbed system. The transmittance characteristic for an improved pattern is wider bandwidth than the transmittance of the dipoles used in the two prior testbed units. The improved filter promises to improve the transmittance of energy into the cell by as much as 36%. This means that instead of transmitting approximately 15% of the total blackbody radiated energy to the cell, the new design will transmit approximately 20% of the total energy. This increased transmittance will increase the electrical power output relative to the loss terms in the cavity and hence increase overall efficiency.

The converter module designed for the SGTPV is an improvement over its predecessors in several ways. First, it eliminates adhesives in the vacuum gap between the walls of the thermal containment jacket. Second, it permits all assembly to be performed on flat surfaces external to the actual generator. This external assembly will permit automation of the fabrication when large volume production is required. Thirdly, the advanced module will permit removal and repair of converter elements that do not meet specifications.

All of the basic TPV converter technology used in the SGTPV design was tested in both the diesel fueled test bed and the solar concentrator fueled test beds. Figure 15 and Figure 16 present test results from the diesel testbed configuration. The model predicted curve used for comparison in the figure is based on calculations made using the measured response of the IR filter and PV cells with the theoretical temperature dependence and spectrum for blackbody radiant energy. A three-dimensional ray tracing code traced the omni-directional blackbody radiant spectrum through the TPV system to generate the predicted curve of Figure 16. Power-out-values as a function of temperature were measured for series connected PV cell arrays in the testbed system at the emitter temperatures indicated. These tests showed that the testbed converter operated exactly as predicted in our design model. Thus, the complete three-dimensional analytical model of the TPV system has been experimentally confirmed to be accurate. This model was employed to optimize our advanced design using the detailed data for each component.

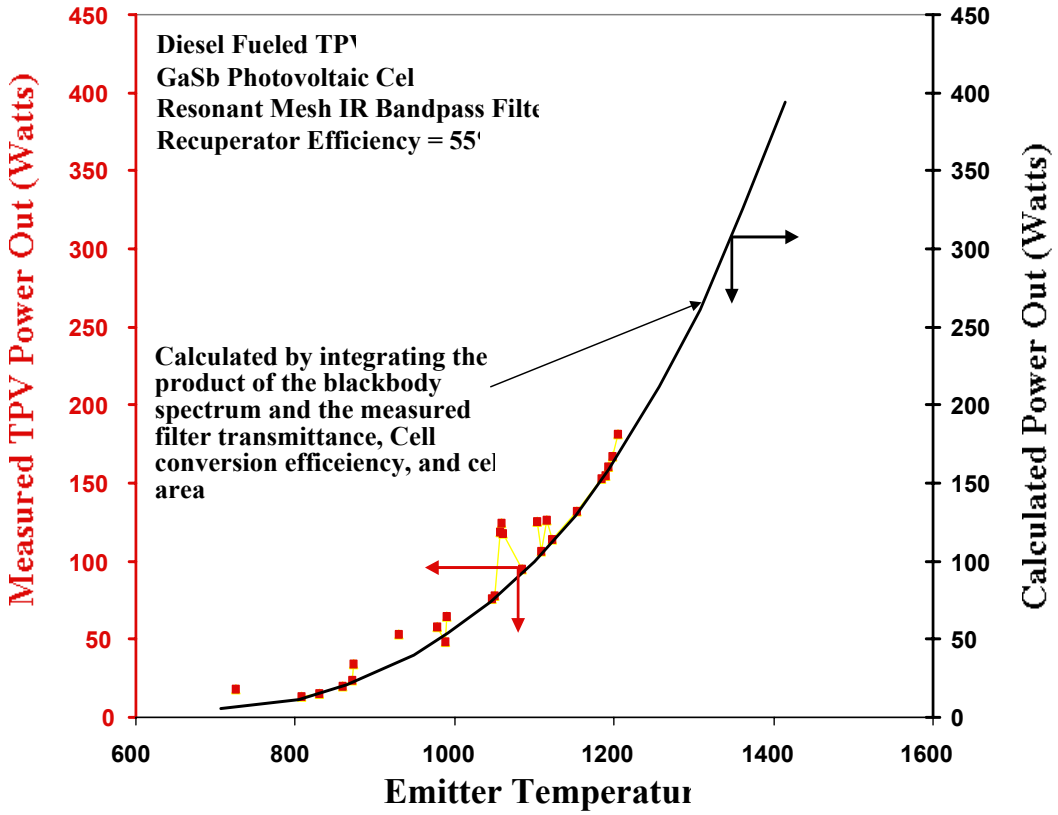

Figure 15. Measured TPV Power Out versus Emitter Temperature for Diesel TPV Testbed

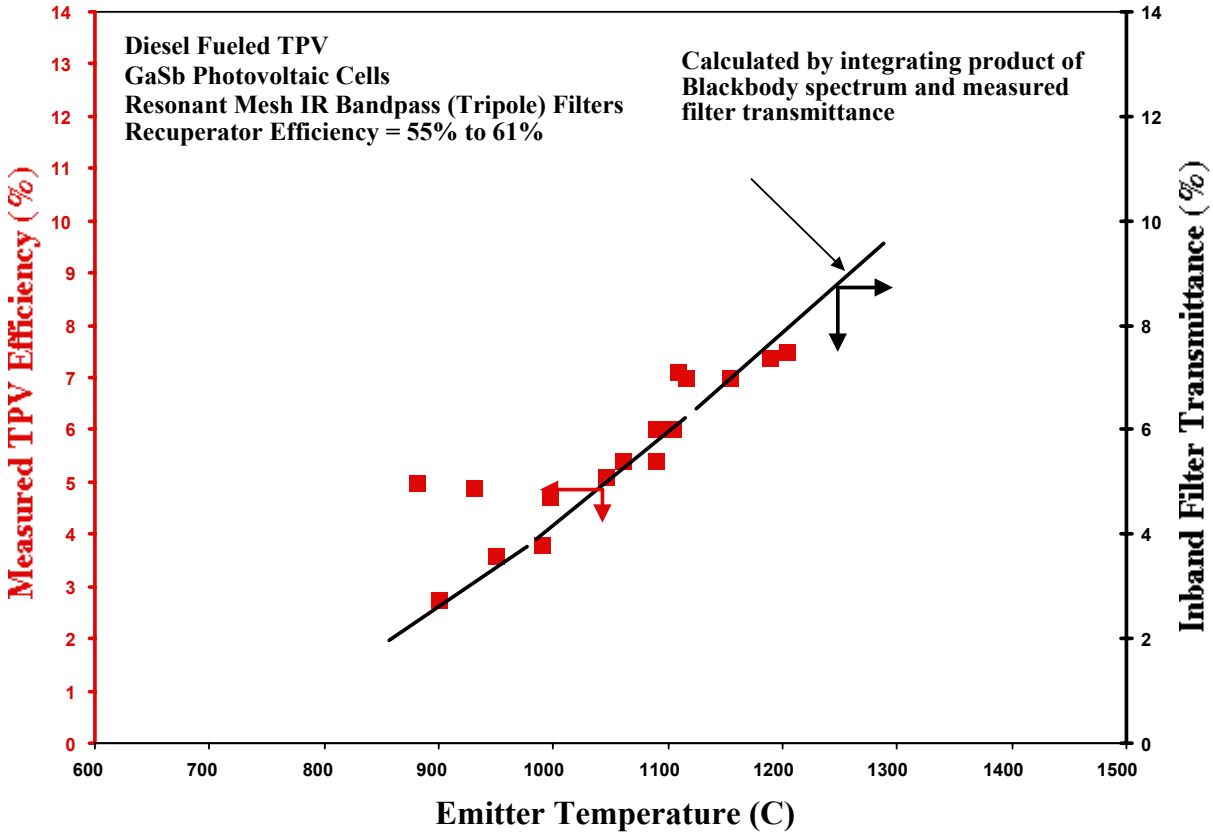

Figure 16. Measured Diesel TPV Testbed Efficiency Compared to Calculated Predictions

3.6. Thermal Control System

Due to the high energy density on the TPV photovoltaic cells in the SGTPV, thermal control is a challenge. In the DARPA/CECOM and the solar testbed designs cooling of the cells was achieved by forced air supplied by a low speed fans through finned heat exchangers. The energy from the cells was first spread over a larger area using water/copper heat pipes. From this base area, the heat was then conducted into an array of fins through which the forced air was passed. However, we desire the SGTPV to be co-generating in that the waste heat is recovered in the form of hot water. For this reason, in the advanced SGTPV design, we will use circulated water as a coolant to remove waste heat from the PV cells. After picking up the waste heat from the PV cells the water will be about 40°C in temperature. It will then be passed through a heat exchanger in the gas burner exhaust system to boost its temperature to the range of 60°C to 70°C.

4.0 Critical Component Development

4.0 contains a discussion of the development of critical components of the SGTPV system employed during this PIER project. Some of this component development occurred during previous programs and will be presented here for informational and background purposes. Table 2 contains a summary of the SGTPV component development.

Table 2. "Hybrid Thermophotovoltaic Power Systems" Project Components

Component	Problem	Approach	Solution	Discussed in Section
IR Filters	To achieve high efficiency TPV conversion, photons not converted by PV cells must be returned to emitter to help maintain emitter temperature.	Place band-pass filter between emitter and PV cell array to allow transmittance of only in-band photons to PV cell; reflecting out-of-band photons back to emitter.	EDTEK's Resonant Mesh IR Band-pass Filter. This filter successfully transmits 70% of in-band photons through to the PV cell array while reflecting 98% of out-of-band photons back to emitter.	4.1, 4.6, 5.0, 6.0, 7.0
Concentrator Prisms	Minimize area of PV cells to reduce cost of system. Allow space for PV cell array interconnection without losing incident energy.	Employ a total internally reflecting optical device to collect incident energy and direct it to a reduced area of PV cells.	EDTEK's 2x9 array of prisms is a single glass molded device that successfully concentrates (4x) the incident energy (transmitted by the IR filter) onto the individual PV cells. The prisms allow room for cell-to-cell and power bus electrical interconnections	4.2, 4.6, 5.0, 6.0, 7.0
GaSb PV Cells	Reduce cost of PV cell fabrication.	Improve fabrication process yield while reducing starting material costs.	Successfully worked with wafer suppliers to decrease the wafer cost. Modified two critical cell fabrication process steps to increase cell performance by 15% and batch yield to over 80%.	4.3, 4.6, 6.0
PV Arrays	Cell arrays must show performance comparable to that of individual cells.	Bond individual PV cells to a metallized ceramic board and interconnect using solder.	The PV cell arrays fabricated by EDTEK for the PIER project maintained 97% of the performance of the individual PV cells.	4.4, 5.0, 6.0, 7.0
TPV Converter Module	Assemble filter, prism, and PV cell arrays while maintaining vacuum gap and thermal control.	Seal IR filters using glass frit; seal inner quartz sleeve using high-temperature adhesive.	Frit bonding failed resulting in necessity to use lesser qualified high temperature adhesive as back-up. Vacuum gap, necessary for thermal isolation, degraded due to partial failure of high temperature adhesive. We are working two approaches to fixing this problem.	4.6
Fossil-Fueled TPV Burner	Convert TPV burner to utilize propane fuel. Minimize air leaks in burner/ recuperator.	Modify burner and igniter. Seal burner recuperator via all continuous weld construction.	Successfully demonstrated ignition and efficient burning of propane fuel to heat emitter. Successfully constructed fully sealed burner / recuperator and demonstrated design parasitic losses.	4.6, 4.0, 5.0, 7.0
Solar Concentrator Dish	Fabricated low cost, high concentration solar dish.	Utilize one piece aluminum-forming technique and innovative smoothing process.	Demonstrated a highly successful fabrication process by forming, smoothing, reflective coating, and protective layer deposition a fully functional solar concentrator dish.	4.5, 5.0, 6.0, 7.0
TPV Solar Collector	Collect solar energy to heat TPV emitter while simultaneously heating emitter with fossil-fueled burner.	Employ solar concentrating dish coupled to quartz light-pipe to trap solar energy and direct it into emitter cavity.	EDTEK successfully demonstrated solar dish and quartz light-pipe coupling to heat the TPV emitter while heating by propane burner was taking place.	4.6, 5.0, 6.0, 7.0
Dish Support and Solar Tracker	Support solar dish without detrimental vibration, track sun to ±0.1 degree.	Utilize an on-board micro-computer-on-a-board to control all housekeeping functions as well as drive the solar tracker.	EDTEK demonstrated the flawless performance of the hydraulic driven solar tracker. The on-board computer demonstrated its versatility and its ability to be reprogrammed to compensate and conform the system various existing conditions.	4.6, 5.0, 6.0, 7.0

4.1. Resonant Mesh IR Bandpass Filter Development

In order for the TPV conversion efficiency to be maximized an approach must be realized that will allow some spectral control of the blackbody spectrum radiated from the heated emitter of the system. The challenge of efficient TPV conversion is illustrated in Figure 17 which shows that a great deal of the energy contained in a high temperature blackbody spectrum is not responsive to the GaSb PV cell. This potentially wasted energy must be captured and returned to the blackbody if conversion efficiencies greater than 2-3% are to be achieved. The spectral

control can take the form of one of two basic approaches; 1) it can somehow prevent the emission of those wavelengths not efficiently converted by the PV cell or 2) it may be a device separate from the emitter and reflect certain wavelengths back to the heat source to help maintain its operating temperature. EDTEK has chosen an IR band-pass filter (approach 2 of above) which is placed between the heat source and the PV cell array. The filter must transmit blackbody photons whose wavelengths allow them to be convertible by the GaSb cell and reflect photons whose wavelengths make the PV cell unresponsive to them. An ideal TPV filter would transmit all wavelengths less than the bandgap of GaSb (~1.7 microns) and totally reflects (R = 100%) those wavelengths greater than the bandgap of GaSb. Ideals are rarely realized, however, EDTEK's micromesh IR filter, when coupled to a TPV generator, has sufficient transmittance and reflectance performance to make the system commercially viable (typical EDTEK filter in-band transmittance is 60 - 70% and out-of-band reflectance is 98%). An illustration of how the transmittance and reflectance perform in relation to the blackbody emission spectrum and the GaSb response spectrum is shown in Figure 18.

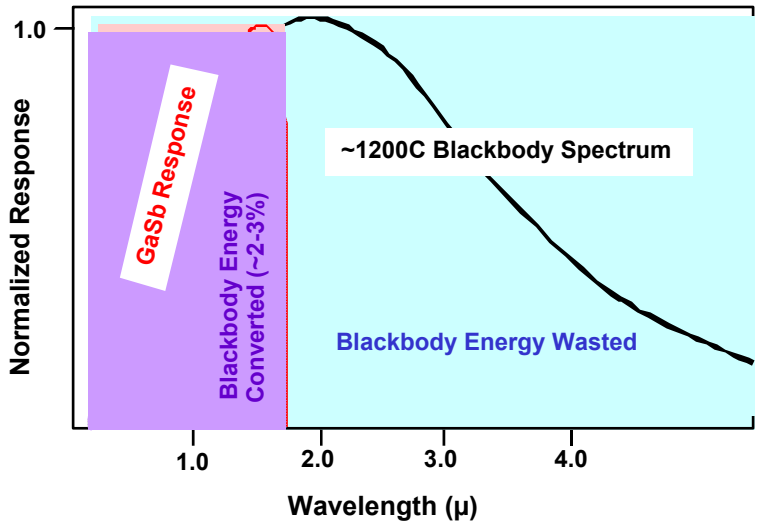

Figure 17. Schematic Showing Overlap of GaSb PV Cell Response and 1200°C Blackbody Emission Spectrum

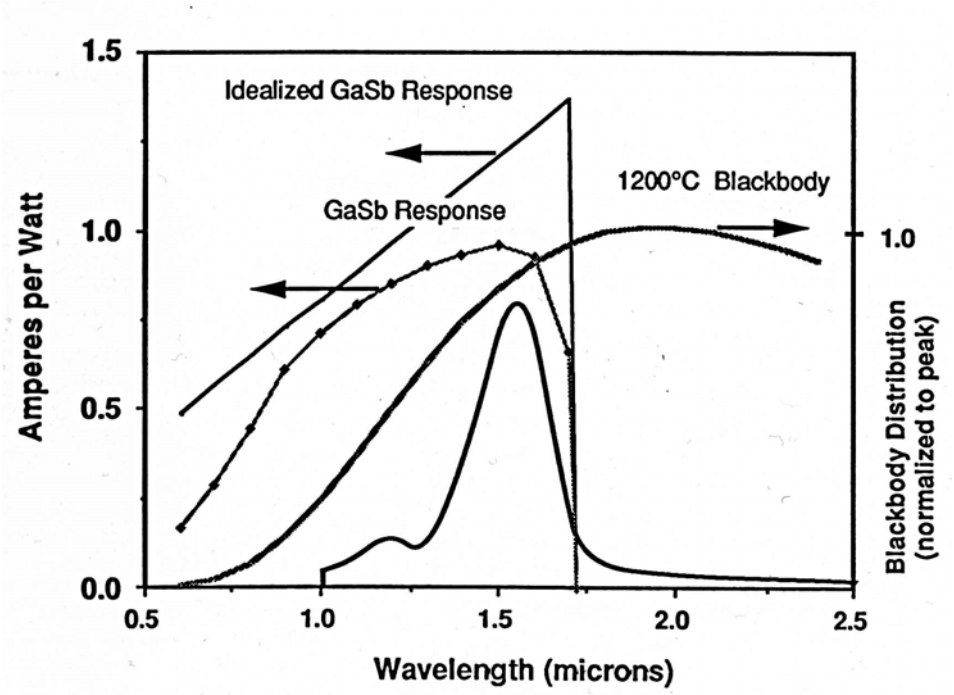

Figure 18. Schematic of IR Micromesh Response Compared to GaSb PV Response and 1200°C Blackbody Emission Spectrum

The key performance parameters of the micromesh IR filters are its broadband transmittance and reflectance (both on-axis and off-axis). The transmittance must be as high as possible within the wavelength response window of the GaSb PV cell. Outside of this bandpass region, reflectance must be maximized while throughout the spectrum the absorptance must be minimized. Figure 19 shows transmittance and reflectance of a small test filter of an EDTEK micromesh filter. This device was fabricated to test the filter design and is not suitable for TPV conversion since peak transmittance wavelength is too long for GaSb, however; it readily demonstrates the proof of concept. Figure 20 shows the long wavelength reflectance performance of the filter as compared to a vapor deposited gold film standard. This figure demonstrates the excellent reflectance characteristics of this filter design achieving ~98% total reflectance at wavelengths beyond the peak transmittance band. Another important consideration of this filter design is its off-axis performance. Blackbody emitters are omni-directional so that the filter must accept incident radiation at all incident angles without performance degradation. Figure 21 demonstrates the filter performance to off-axis radiation. The key result here is that the peak transmission wavelength is not affected by the angle of incidence. While there is a reduction in overall transmittance at incident angles greater than 30 degrees, it is important to note that as the transmittance decreases the reflectance increases so that the energy is not lost but rather just reflected back to the heat source to be reabsorbed and re-emitted. The resonant wavelength is independent of incident angle with the off-normal transmittance dropping of as the cosine of the angle of incidence.

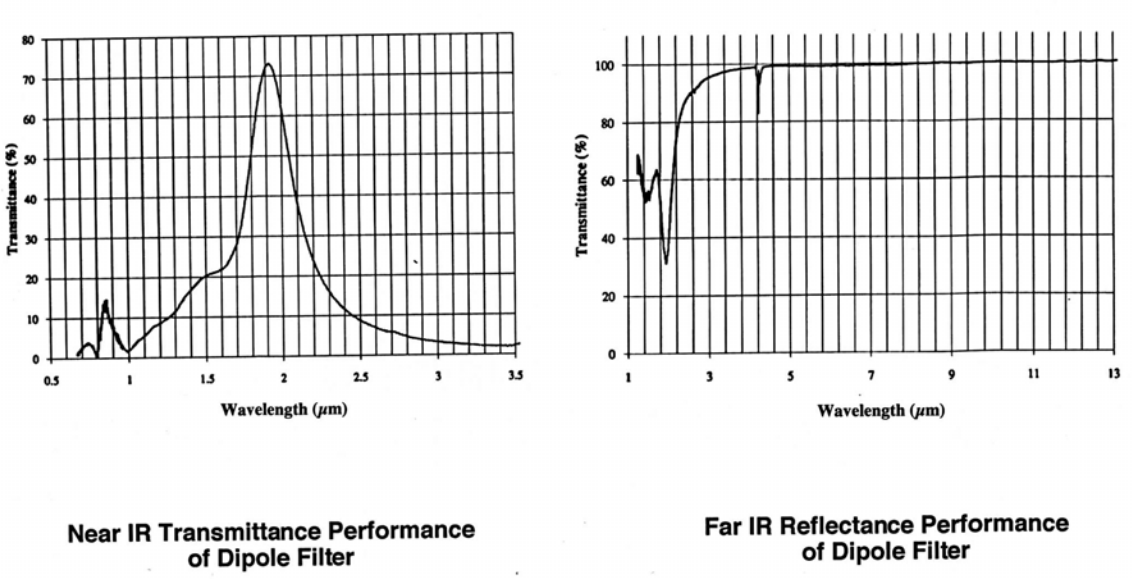

Figure 19. Transmittance and Reflectance of IR Micromesh Filter

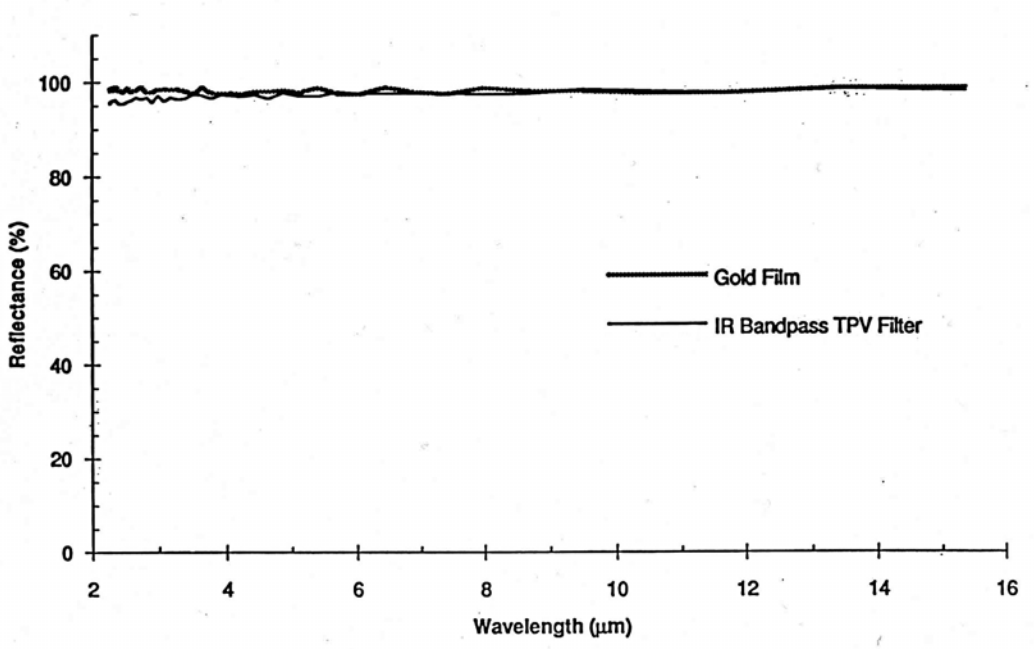

Figure 20. Long Wavelength Reflectance of IR Micromesh Filter Compared to a Solid Gold Film

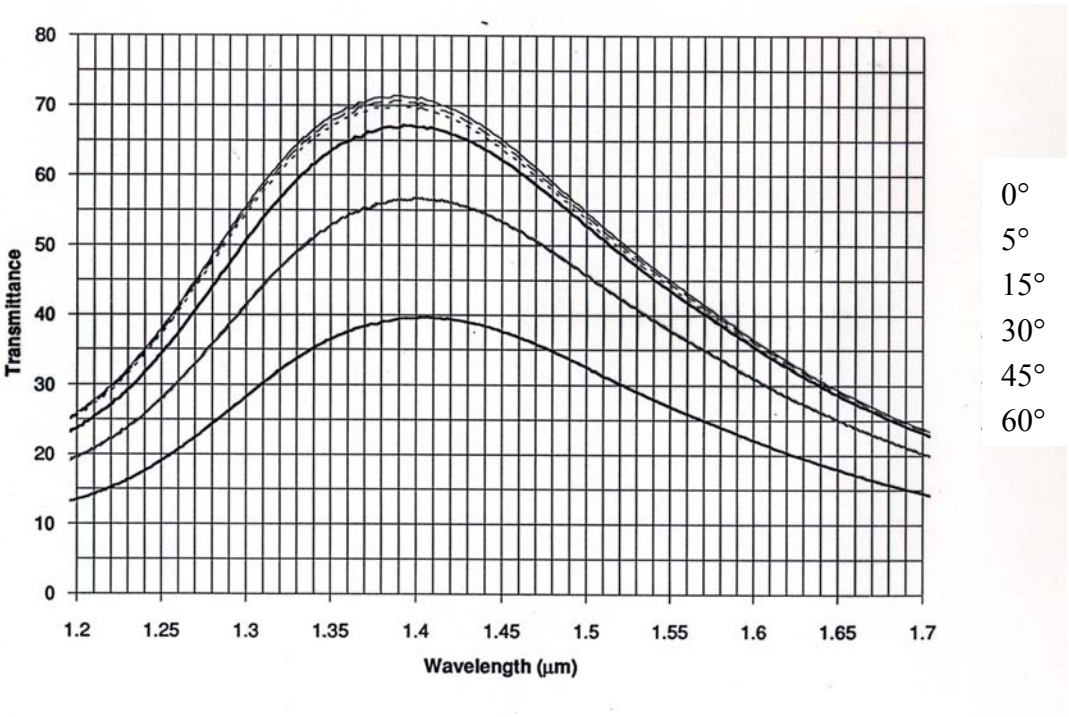

Figure 21. Filter Transmittance Performance Versus Angle of Incidence

4.1.1. Filter Description

The EDTEK micromesh IR bandpass filters are unique. These filters function as an array of antenna elements which are tuned to resonant (or transmit) at near-infrared wavelengths. In order to achieve resonance at these wavelengths the antenna elements must have physical dimensions on the order of this wavelength. This requirement makes the fabrication of a low cost filter a challenge. Figure 22 shows two photomicrographs of the micromesh filter along with a schematic showing the basic structure of the filter. It is a quite simple structure comprised of a thin gold film on a glass or quartz substrate. The actual antenna elements are the plus-sign shaped slots cut through the gold film. Typical gold film thickness is 200-250 nanometers (nm). Typical slot length is 400- 450 nm with the slot width being 60-120 nm; element to element dimension is about 650-800 nm. For the pictured filter, which resonants at 1.50 microns, the length of the antenna slots is about 460 nm and the width about 80 nm.

The operation of the filters depends on the interaction of electric and magnetic fields with the submicron conductive elements of the mesh and the dielectric properties of the surrounding media. A primarily inductive mesh is formed if the field-induced currents can flow between filter elements, such as the array of crossed slots patterned in a continuous metal film. If the dimensions of the elements are comparable to the wavelength of the interacting electromagnetic field, then resonant conditions can be set up. The inductive resonant mesh configuration produces a bandpass filter. At the resonant wavelength, the interacting electromagnetic field induces currents in the gold film and electric and magnetic fields in the slots such that identical currents and fields are excited on the far side of the film. These currents and fields cause the emission of an electromagnetic wave on the side of the gold away from the source; i.e., the transmitted light is emitted. So at resonance the filter can be thought to absorb the IR energy on one side and re-emit it on the opposite side of the gold film.

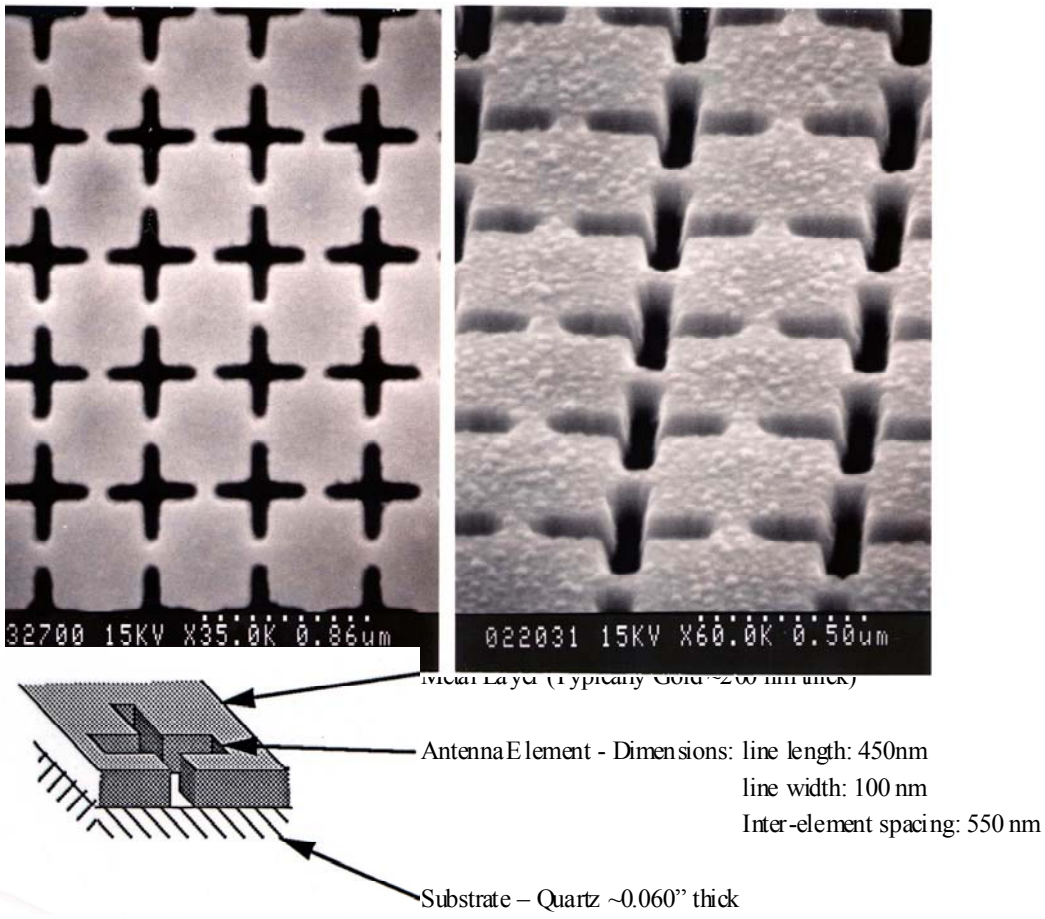

Figure 22. (Left) Photomicrograph of the IR Micromesh Filter, (Right) Photograph of Filter at Oblique Angle, (Bottom) Schematic of Filter Structure

The degree of transmittance and reflectance of the filter is a function of the size and shape of the elements, the resistivity of the metal film, and the dielectric and optical properties of the substrate and the media surrounding the film. The so-called square crossed dipole array is the pattern that was utilized during the testbed demo. The entire IR filter area of the testbed demo was populated using filters fabricated into this geometry. The square crossed dipole pattern produces filters with narrow bandpass and moderate peak transmittance (~60%).

Another parameter that allows us to affect the filter performance is the dielectric and optical properties of the substrate and the media surrounding the gold film. During design of the filter, element geometry and substrate dielectric constant are considered.

Peak transmittance is determined primarily by the density of filter elements etched into the metal film, i.e., higher densities yield higher peak transmittance. There is a similar relationship between element density and bandwidth. Given a PV cell quantum efficiency performance, the filter performance can be adjusted via element length, density and linewidth to maximize conversion efficiency. To the first order, filter peak transmission wavelength is determined by

the length of the element and the refractive index on either side of the metal film. This is expressed below:

$$\lambda = 2L\sqrt{\frac{\left(n_1^2 + n_2^2\right)}{2}}$$

where:

λ is the wavelength at peak transmittance.

n_1 and n_2 are refractive indices of the medium above (air) and below (substrate) the film, respectively.

L is the filter element length.

This calculates the resonant wavelength for a single isolated dipole. As an array is built of many dipoles the near neighbors couple with each other and this above expression is no longer accurate. From this simplified expression however, it can be seen that dielectric of the substrate must be considered during design of the filter antenna elements to achieve a particular performance.

As the infrared wavelength moves away from the resonance band, the filter behaves optically like the parent metal film. Thus the filter exhibits efficient broadband, angular insensitive reflectance to out of band energy. For a gold film, the out of band reflectance is 98% to 99%.

Thus the filters are excellent candidates for the TPV application for the following reasons:

- The resonance can be tuned to the specific TPV emitter/cell combination.
- They accept in-band energy useful to the PV cells and transmit it into the PV cells.
- The in-band energy not transmitted to the cells is reflected back to the source.
- The filters exhibit the broadband reflective properties of gold film (>98.5%) in the out-of-band regions of the spectrum.
- The resonant frequency of the filters is independent of angle of incidence and the transmittance falls off only as the cosine of the angle of incidence of the light.

The EDTEK TPV filter can be tuned to the photovoltaic cell type most suitable to the particular application. Overall transmittance and bandwidth are adjustable by antenna element geometries and annealing. Fine-tuning of the resonant wavelength is accomplished by varying the refractive index of the surrounding media. Thus, there is considerable latitude for tailoring the filters to particular cell types or TPV applications.

4.1.2. IR Band-pass Filter Fabrication

4.1.3. Masked Ion Beam Lithography

The challenge of these IR filters is in their fabrication, more specifically; it's making low-cost filters. The small physical dimension of the antenna elements of the filters means that fabrication techniques such as photolithography, which is the usual method for making microcircuit elements, are unavailable because of its insufficient resolution capabilities. Typical photolithography is able to achieve minimum feature sizes of about 200 nm. The next step is electron beam lithography (EBL). This technique is able to produce more than adequate

resolution; typical minimum feature size is five nanometers. However, all this resolution comes at a very high monetary cost. The EBL machines are very complex and prohibitively expensive. This forced EDTEK to explore alternative lithography techniques that lead us to masked ion beam lithography (MIBL). EDTEK now has the capability to produce a 70 cm^2 area of nanoscaled features (typically 300 nm line-length and 60 nm line-width) in a 0.5-hour exposure time. This is compared to using EBL that would require about 35 days of exposure time to achieve this same area. The drawback to MIBL is that a stencil is required to print with ions. Fabrication of the ion stencil, or mask, is fairly costly; a typical daughter stencil is about $5000. However, once the mask is completed, it can be used through many exposures cycles. At EDTEK, a single daughter ion-stencil survived about 8500 exposures, which is about 1,320 in^2 of nanoscaled features.

Ion beam lithography begins with the fabrication of a stencil. The stencil is made from a thin silicon membrane (see Figure 23), which were originally purchased from an outside vendor. Most recently, EDTEK has been developing the capability to fabricate our own membranes. This has been a collaborated effort involving EDTEK and the University of Washington. We have found that EDTEK produced membranes have less problems during the etching step described below. Our plan is to phase-in the locally fabricated membranes while using up our stock of outside-vendor membranes. The completed stencil may now be used to print the filter pattern on a glass substrate thus making an IR filter or the pattern may be printed on another silicon membrane thus producing a daughter mask.

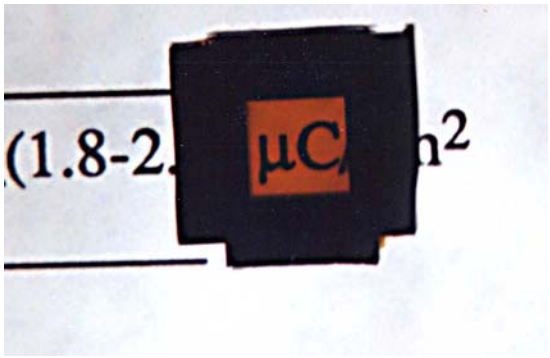

Figure 23. Photo of a 6 mm x 6 mm Silicon Membrane (note that one can read through the membrane due to its thin structure, the thick frame is ~1.5 mm x 1.5 mm)

Our desire is to have MIBL stencils that are able to print 1 cm^2 per exposure. To achieve this goal, 1 cm^2 of printed area must first be patterned onto a silicon membrane (which, when processed, will become a daughter stencil). The patterning of this large area cannot be economically done by EBL. Our alternative is to write the pattern for a large area stencil (1 cm^2) by MIBL and to do this we need a stencil. However, to write only 1 cm^2 requires a fairly small area stencil (typically 1-4 mm^2) and this area may be written economically by EBL. So attaining a large area stencil (1 cm^2) is a two step process: 1) a small area membrane is pattern using EBL and then processed resulting in a MIBL stencil which prints about 4 mm^2 per exposure, 2) this small area stencil is employed to pattern a large area membrane using step-and-repeat MIBL. The large area membrane will require 25 exposures (using the small area stencil) to step out a 1 x 1 cm printed area. The small area stencil, which was printed using EBL, is referred to as the

'master stencil' and the large area stencil, printed by MIBL, is referred to as the 'daughter stencil'. The daughter stencil is then used to print large areas of infrared filters onto glass substrates. The Master/Daughter idea offers an advantage other then greatly reducing the cost of making a large area stencil: when a master stencil is available it is a relatively easy process to print and process many daughters from one master. This means that if a daughter stencil is somehow made to print poorly, another daughter can be fabricated easily and quickly without a costly trip to an e-beam facility. Four master stencils have been fabricated. Two for fabricating dipole daughter stencils and two others for the improved daughter stencils. The daughter stencils were used to print the IR filters used on the advanced design demonstration.

4.1.3.1. Filter Fabrication Process

The micromesh IR filters are fairly simple structures, dipoles shaped slots, cut into a thin film of gold that is supported on a glass substrate. Fabrication of the micromesh IR filters is made difficult by the physical size of the dipole shape. The size of the elements is dictated by which wavelengths of IR light we wish to pass through the filter. For a resonance, peak transmittance, to occur at the near IR wavelength of 1.50 microns the dipole dimension must be about 450 nm with the dipole linewidth of ~100 nm. To achieve dimensions of this order, techniques and equipment employed for the fabrication of nanoscaled features area required. This includes such processes as masked ion beam lithography, reactive ion etch (RIE), vacuum vapor deposition, and the application and dissolution of thin layers of polymer films.

A multiple-step process has been developed to fabricate the filters. The steps begin with a glass or fused silica substrate having a typical thickness of 0.060". The substrate is cleaned using solvents and a plasma process followed immediately by the application of two polymer layers. Both polymers are applied by spin coating techniques.

Step 2 is the actual writing of the pattern into the resist. This is done using MIBL techniques; the ions that pass through the holes in the stencil expose the first polymer layer and thus define the desired pattern on the filter to be. During the exposure, the polymer is weakened due to energetic charged particles that break some of the polymer cross-linking. This makes the exposed polymer soluble to a particular solvent while the unexposed polymer remains insoluble. The development, step 3, of the exposed polymer consists of dissolving away only exposed polymer

The next few steps involve reactive ion etching and subsequent deposition of thin metal films to transfer the written pattern from the ion sensitive resist to the final metal layer. This final layer will be a gold film with appropriate shaped slots etched through its thickness down to the glass substrate. A final etch is employed to clean the final gold layer and remove any polymer masking material remaining so that all that remains is gold on glass substrate. Figure 22 is a photo of the results of these final steps.

Filter fabrication is kept on track with some key process monitors used during a filter production run. The steps that are closely monitored during fabrication are: polymer spinning, ion exposure, etching, and gold deposition.

The monitoring of the polymer spinning step confirming that the polymers are applied evenly and without particle contamination. This is readily done by observing the substrates after spinning. Any variations in polymer layer thickness can be visualized by color changes of the

films. This is due to the optical interference of the thin transparent films with light reflected off the substrate. Using the color changes as a variation as small as one hundred angstroms are detectable. Substrates with thickness variations on this order are stripped and re-coated.

Print quality can be observed using a high quality light microscope whereby the general pattern of printed features can be monitored. While individual elements remain unresolved, the overall pattern is clear and from that print quality can be inferred. Electron microscopy at this stage is not possible. If the substrate does not pass this visual inspection it is stripped, re-coated, and exposed again.

During the etch step, it is important to etch the down to the substrate and to clear all the appropriate material away from the substrate surface. This etch is carefully monitored for etch rate and clearing by using a very sensitive profilometer which measures thin film thickness to within 10Å. Once the material is cleared it is also important not to over-etch since this will weaken the structures above the substrate. End-point detection is achieved using the profilometer. The final monitor is achieved by a visual inspection of the substrate after the gold deposition followed by a electron microscope analysis of the completed filter. Final inspection with our Scanning Electron Microscope (SEM) verifies that the filter patterning was successful.

The next section sets the stage for development of the advanced TPV design through discussions of the problems we encountered during the fabrication of a test-bed unit constructed on a previous program.

4.1.4. Performance of Filters Produced for Previous Testbed Demo

In an earlier test-bed design, forty-eight individual filters, measuring 0.62" x 2.50", were required to populate the testbed demonstration unit. The filters were fabricated, using the crossed dipole pattern, on 0.006" thick glass substrates with two filters per substrate. After fabrication, each filter was annealed to maximize transmittance performance and then fine tuned to ensure that the wavelength of peak transmittance corresponded with the peak conversion efficiency of the GaSb PV cell. Before assembly into the testbed unit, filters were tested for transmittance and reflectance performance and then diced from the glass substrate to their final dimensions.

The filters showed a range of transmittance performance, better performing filters peaked at about 55% transmission, some of the poorer performing filters showed about 40%. Figure 24 shows two transmittance scans, one for better performing filter and one for poorer performers. The wavelength of peak transmission for all the filters occurred at wavelengths between 1350 microns and 1450 microns. Figure 25 shows the number of fabricated filters that achieved a particular peak transmittance. The majority of the filters produced had transmission values of 50-55%. Figure 26 shows the number of fabricated filter verses the wavelength of peak transmission. The target wavelength was 1400 nm and the majority of the produced filters showed peak wavelength from 1360 – 1400 nm.

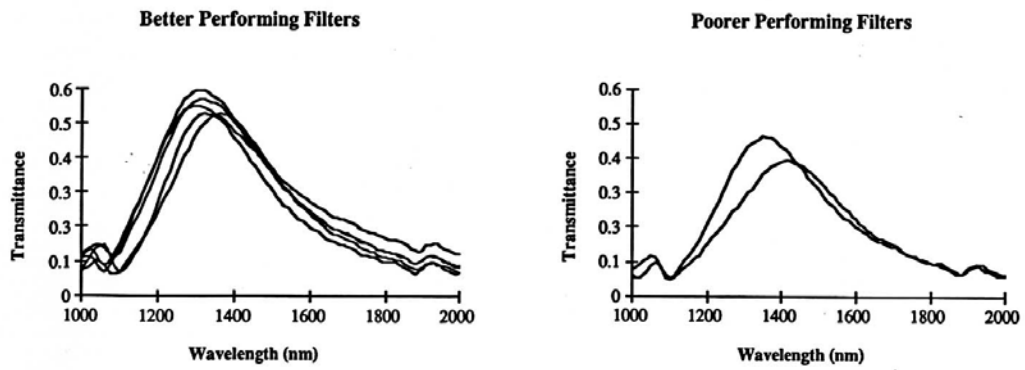

Figure 24. Two Scans of Better (right) and Poorer (left) Performing Filters Fabricated for the Testbed Demonstration

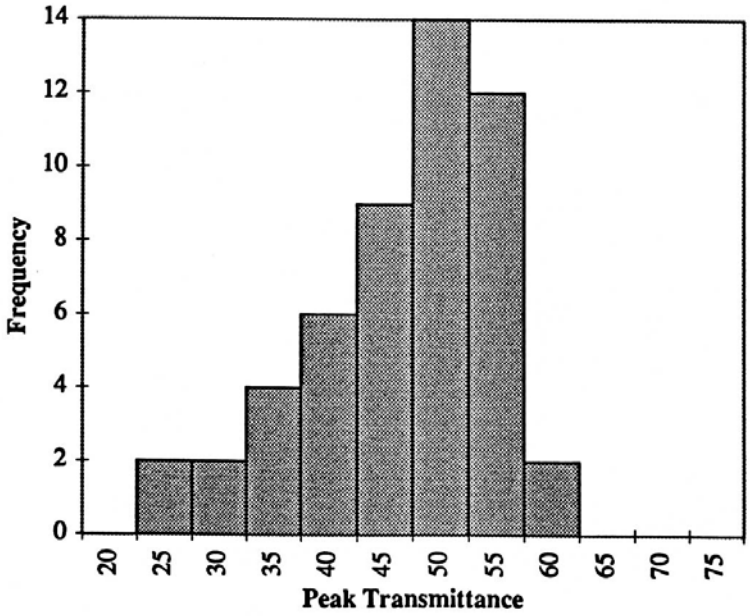

Figure 25. Peak Transmittance Values Versus the Number of Fabricated Filters

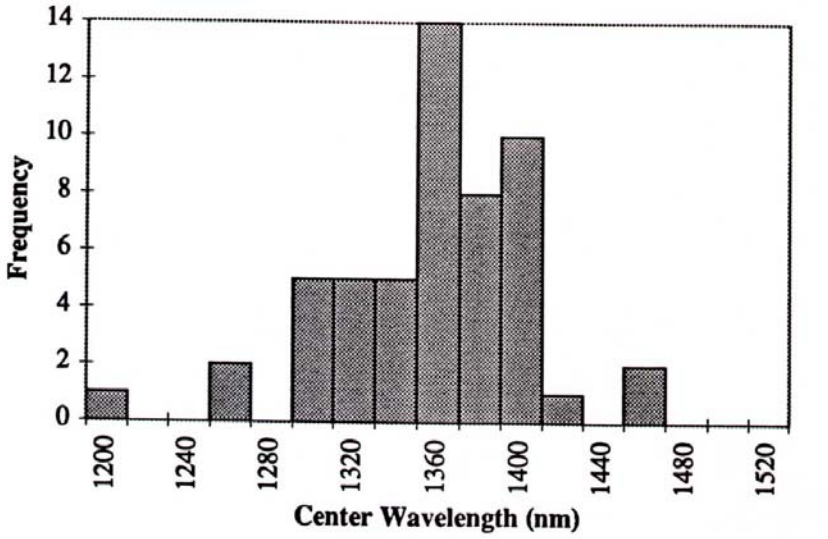

Figure 26. Wavelength of Peak Transmission Versus the Number of Fabricated Filters

After being diced to their final dimensions, the filters were glued onto the inner wall of the outer quartz sleeve of the testbed unit. During the gluing, careful attention was paid to the filter location to minimize cracks that occur between the filters. Our concern was twofold: 1) cracks would be a source of parasitic heat loss during testing and 2) cracks would allow the adhesive, used to affix the filters, to be damaged by IR spectrum exposure. Unfortunately, even the small cracks that existed were enough to result in glue damage and subsequent filter failure. This failure was one of the motivations to create an advanced sleeve design. Figure 27 is a schematic showing the filter layout in the testbed demo unit. Photographs of the filters bonded into the outer quartz sleeve are shown in Figure 28.

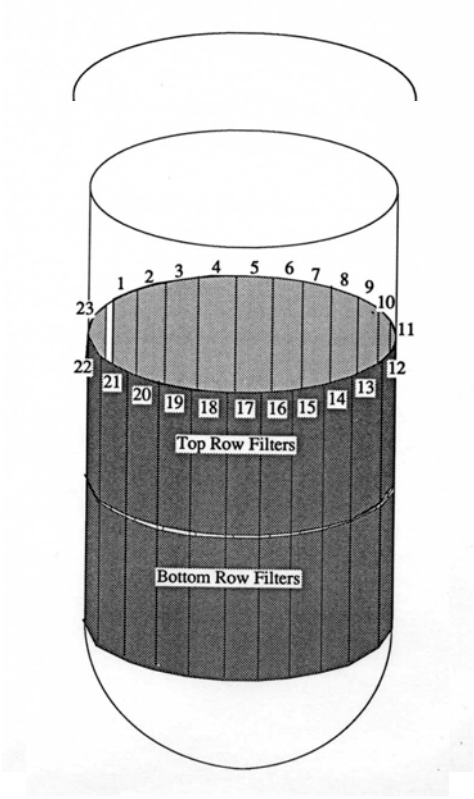

Figure 27. Schematic Diagram of Testbed Demo Unit Filter Layout

Figure 28. Photos of the Filters When Gluing into Outer Sleeve is Partially Completed and After Sleeve is Fully Populated

4.1.5. Performance of Filters Produced for Advanced Design Demo

The following is a discussion of an advanced design demonstration unit fabricated and demonstrated under an U.S. Army program[6] that utilized improved filters. The new pattern allows for large antenna element density and thus higher peak transmittance. This design is successful for achieving peak transmittances as high as 90%. However, the high transmittance comes at the cost of a large long-wavelength transmittance tail that allows photons beyond the GaSb response zone to be lost from the system as waste heat. We found that a balance could be

struck which allowed the use of this pattern for transmittances of ~70% while still maintaining adequate long-wavelength cutoff for high efficiency. Figure 29 shows the performance of prototype filter compared to the performance of the best dipole filters fabricated for the earlier testbed demo. This figure clearly shows the potential of the improved design for increasing filter throughput and thus overall system power.

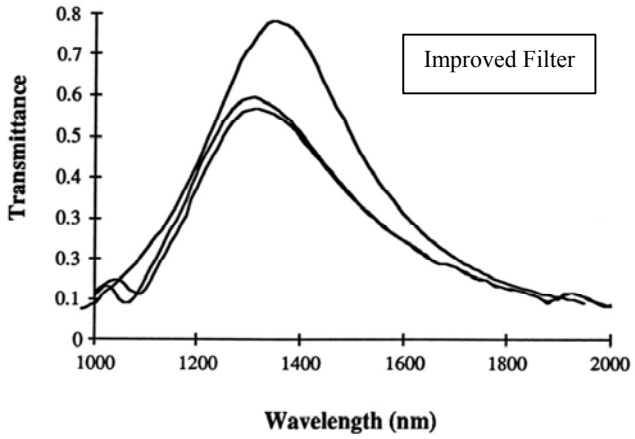

Figure 29. Transmittance of Prototype Improved Filter Compared to Best Dipole Filters

The master stencils were fabricated with an active area of 4 mm^2. From this stencil, a daughter stencil was written that had an active area of 1 cm^2. The large area daughter stencil allowed us to print 70 cm^2 of filter area on 0.065" thick quartz substrates. The quartz substrate was chosen because of its thermal properties. For the advanced design demo unit 13 substrates were printed and processed. After processing, all the filters were subjected to spectral measurements to determine transmittance and reflectance characteristics. Each of these substrates could yield six filters. However, of the 13 substrates fabricated, five substrates yielded their full complement of six filters, five of the substrates produced five filters each, one substrate produced four filters, and the last two only produce two filters each due to breakage problems during sawing.

While the improved filter design has a proven potential of achieving transmission values above 70%, the first set of filters to be produced by MIBL were disappointing. After all processing and sawing of the filters was complete the best filters demonstrated peak transmissions of 63% while the majority of the filters were about 57% transmittance. Figure 30a shows the number of fabricated filters that achieved a particular peak transmittance and Figure 30b shows the number of fabricated filter verses the wavelength of peak transmission. Our target for the wavelength of peak transmittance was 1420 to 1460 nm based on spectral response of the PV cells.

To populate the advanced design testbed unit 48 filters were required. The filters were arranged in two rows, upper and lower, of twenty-four each around the cylinder. Each filter was ranked and matched to the PV cell arrays so as to maximize the performance of each filter-cell array combination. Figure 31 is a schematic diagram of how the filters were laid-out in the advanced design outer sleeve. Each color represents filters that were cut from the same original

substrate and gives the filter number, the process name, and the maximum transmittance. Figure 32 shows the performance of the filters for the upper and lower row of the cylinder. After testing both soldering techniques and gluing techniques as means of bonding the filters to the metal sleeve, it was concluded that using a two part, high temperature epoxy was the most repeatable, benign, and repairable option. Our final choice for the epoxy was found to not allow vacuum leaks down to 10^{-9} range and to maintain this hermitic seal up to 200°C. After all the filters were bonded, the vacuum integrity of the sleeve was tested using a helium spectrographic leak detector to ensure a vacuum tight seal. These filters and construction techniques performed well during the Army demonstration, however, further development was needed. It was determined that improvements were needed in two area: 1) the number of filter windows should be reduced to reduce the number of seals that were required to the outer metal sleeve, and 2) an inorganic high temperature adhesive is required to seal the filters to the metal sleeve to minimize out-gassing and subsequent vacuum leaks.

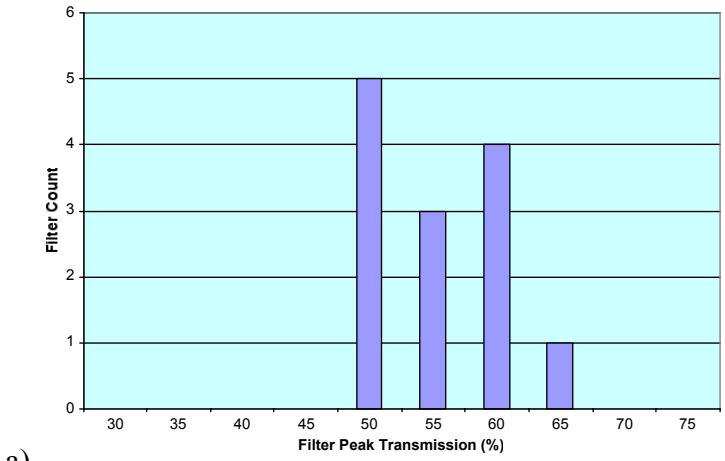

a)

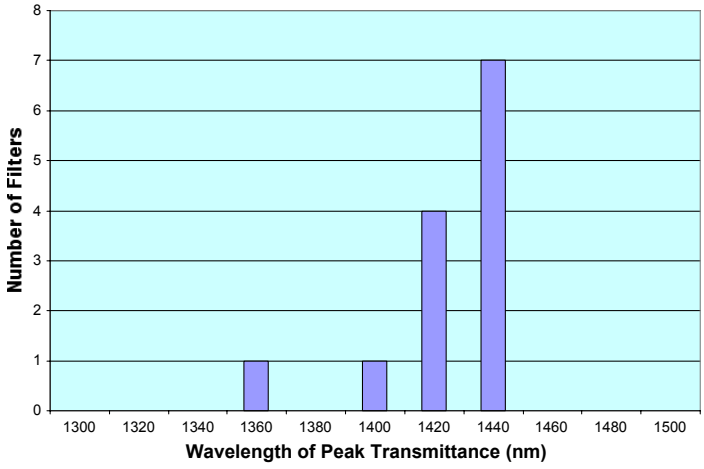

b)

Figure 30. Peak Transmittance Value versus Number of Filters Fabricated (a), Wavelength of Peak Transmission versus Number of Filters Fabricated (b)

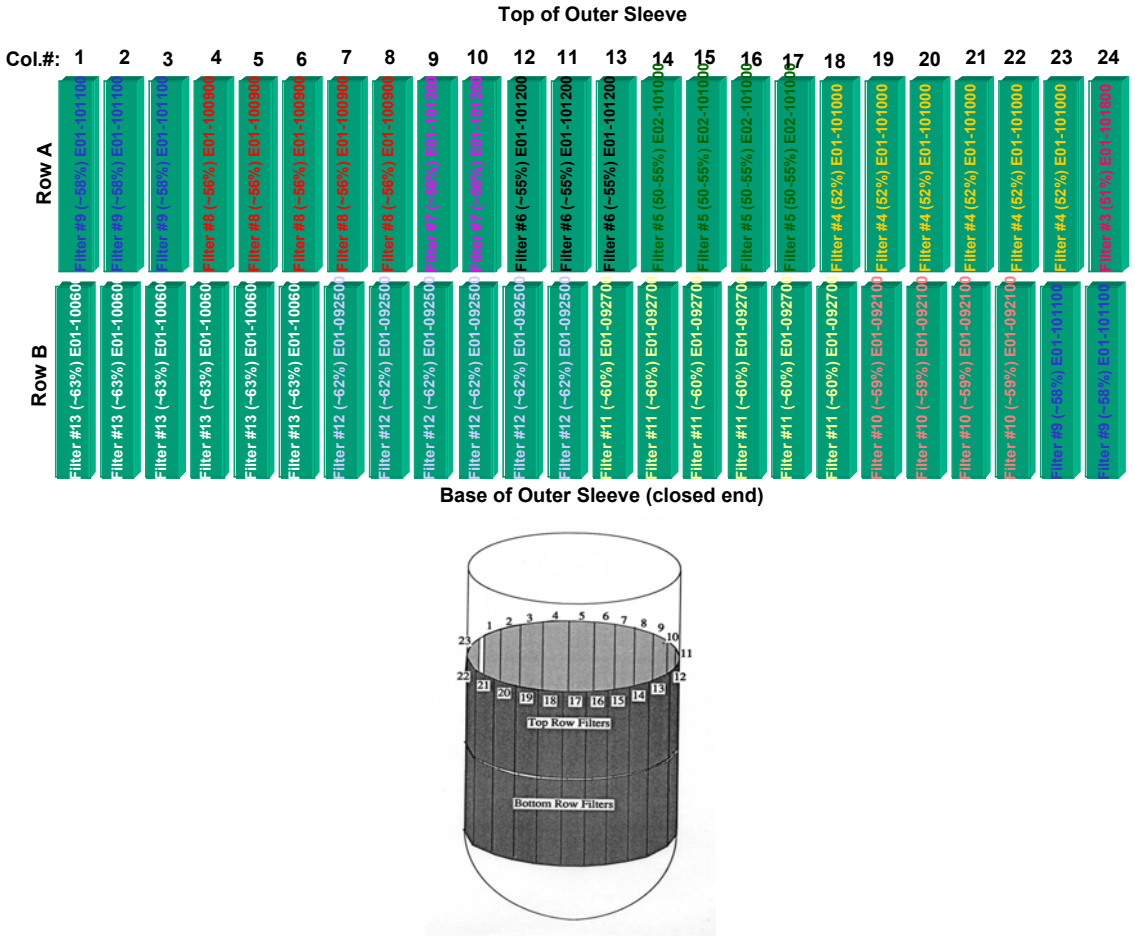

Figure 31. Schematic of Filter Layout in Advance Design Outer Sleeve Showing Relation Between Column Number and Position in Sleeve (Top Row = A, Bottom Row = B)

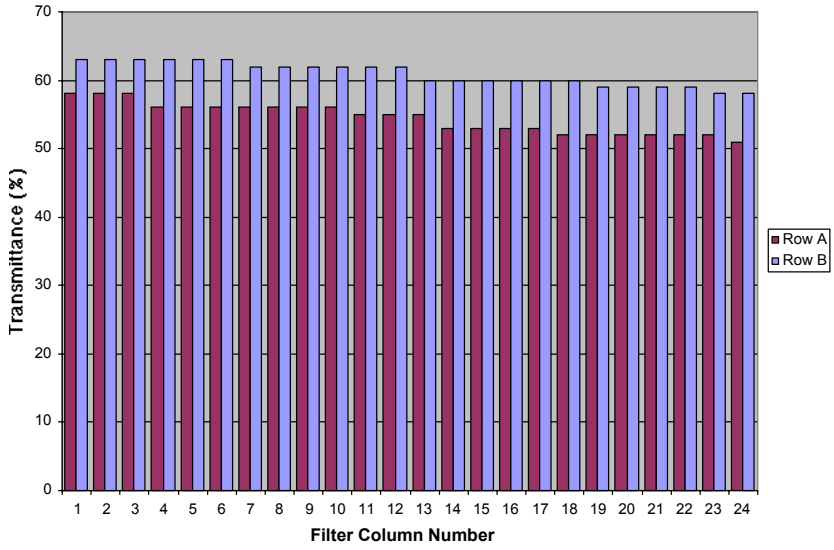

Figure 32. Filter Performance Top Row (A) and Bottom Row (B) of the Assembled Advanced Design Sleeve

4.2. Optical Coupler Development

The TPV electrical converter consists of an array of optical elements that couple the blackbody radiation onto the PV cells. The details of the development of the optical elements have been presented in an earlier deliverable report to the CEC. The development of the PV cells will be presented in 4.3 of this report. An array of couplers employed during an earlier program for the US Army is illustrated in Figure 33. This array contains one optical element for each PV cell in the TPV electrical converter. The couplers are located on the outer wall of the thermal and spectral control subassembly opposite the emitter and bonded to the spectral control filters. The inner faces of these elements are bonded to the outer wall with an optically clear adhesive. They intercept the omni-directional blackbody radiation, which is somewhat forward directed and transmitted by the filters, and couple the energy into PV cells located at the bases of the prisms. This design utilized 216 individual elements. The fabrication, alignment and final bonding of these couplers to the outer sleeve was a time consuming and exacting process. It was determined that improvements to the prism array were required and these improvements were to address the problem of fabrication and installation.

The design for the outer sleeve of the PIER SGTPV converter called for twelve spectral control filters to be bonded to the outer metal sleeve of the converter. This configuration yielded twelve flats onto which the optical couplers were now to be adhered so that each flat would contain eighteen elements (two columns of nine elements each). A configuration amenable to glass molding was finalized, and outside glass forming vendors were contacted to get fabrication quotes. Two vendors were chosen for preliminary fabrication testing with the results sent to our lab for final evaluation. The results of testing and evaluation of the prisms are presented in an earlier deliverable report. The coupler arrays were then ordered from the best supplier.

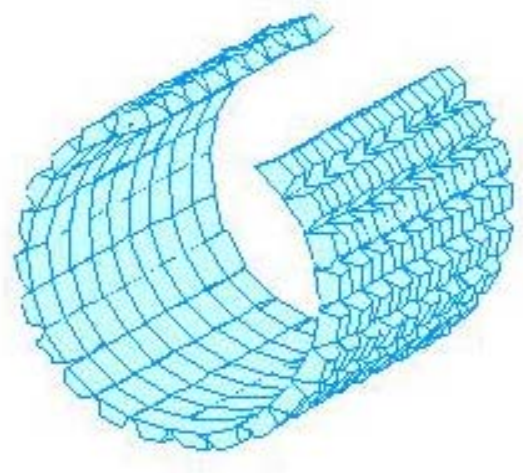

Figure 33. Coupler Array for a 500 Watt TPV Electrical Converter Developed for the US Army

4.3. GaSb PV Cell Development

GaSb is a relatively new photovoltaic material for making low-bandgap cell that can respond to mid-infrared wavelength photons to 1.7 microns. This makes them very useful for converting the blackbody spectra in TPV systems. EDTEK, Inc. holds a license from the Boeing Company for the production and sale of these cells. The details of our developmental effort to optimize

their performance and fabrication processes for the SGTPV are presented in the following sections.

4.3.1. Photovoltaic Cell Fabrication and Process Development

Photovoltaic cell geometry is principally dictated by the application: in TPV applications, the geometry of the heat source dictates that the cell active area be either rectangular or square. The TPV testbed system designed by EDTEK requires 1 cm x 1 cm square cells. In this design, the TPV panel wiring dictated that the square cells shall have busbars on all four sides. Therefore, in our cell design optimization we stipulated that the cells have square active area with four busbars.

The grid pattern on the front side of the cell was optimized such that the total power loss due to: 1) the emitter sheet resistance, 2) the ohmic contact resistance of the grids and 3) the geometrical grid shading loss is minimized for a cell of width 1 cm. An optimized grid shape for such a cell was established such that the total power loss under these conditions is about 7%. A three level photolithography mask that incorporates this grid pattern was designed and procured from Photo Science Inc.

The key process steps in the fabrication of GaSb TPV cells are shown in Figure 34. First we define the device size and active area. For this we deposit silicon nitride using Plasma Enhanced Chemical Vapor Deposition (PECVD) technique and use the first level mask and photolithography to define and then etch off silicon nitride in the active area. This is followed by a low temperature zinc diffusion step. Next we deposit silicon nitride; this silicon nitride serves both as a zinc diffusion barrier and as an antireflection coating. Using the second level photolithographic mask, the grid pattern is defined, the next step etches off the nitride in the grid region. A second zinc diffusion step is then carried out at a higher temperature. This high temperature diffusion serves both to increase the junction depth and to create a highly doped, degenerate region under the grids. This p+ region facilitates making the grids a low resistant ohmic contact to the emitter. The backside of the wafer is then etched, cleaned and metallized by evaporating specific metal layers sequentially. The last step, namely front side metallization, is carried out using the third level photolithographic mask followed by evaporation of the top metal layers. At each mask level various alignment marks are provided to ensure alignment between the three lithography steps.

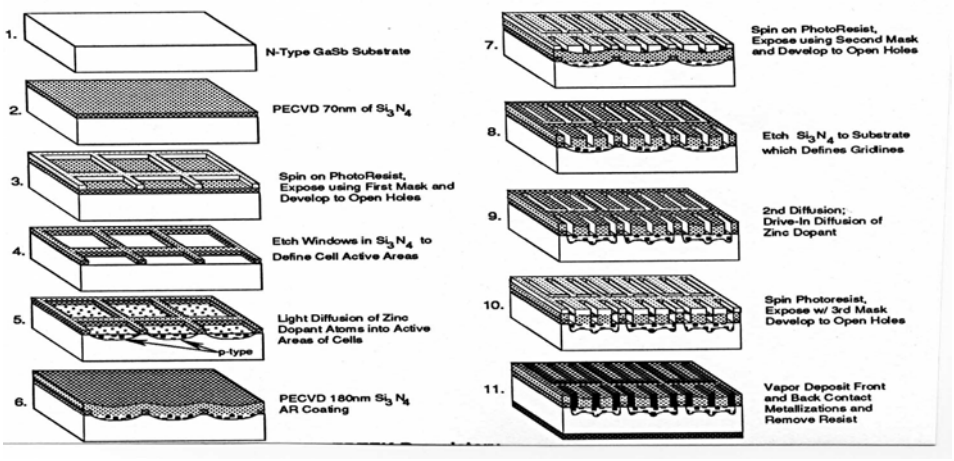

Figure 34. Schematic of TPV PV Cell Fabrication Process

GaSb wafers processed using the above recipe did not consistently yield good devices. Some batches produced excellent devices (with Voc>0.4V and FF > 70%) while others yielded devices with average electrical characteristics (Voc~0.3V and FF ~60%) though all were processed using the same recipe. Considerable effort was therefore spent to (a) identify the factors that cause such performance variability and then (b) develop methods to eliminate such variability and thus arrive at a robust process.

A detailed consideration of the diffused junction based PV diode fabrication process used here led us to focus (1) on the diffusion technique and (2) on the GaSb passivation process.

GaSb TPV cell fabrication process, as outlined in Figure 34, involves zinc diffusion step. Temperature induced morphology changes led us to alter the diffusion process to reduce these changes. The diffusion process parameters were then modified in terms of diffusion temperature and time to yield good quality devices. This new process, besides improving the electrical characteristics of the cell also improved the batch to batch yield.

Another important aspect relating to the performance of these GaSb devices pertains to quantum efficiency. Quantum efficiency, or spectral response of the photocells, indicates the efficiency of the cell to convert the incident photon energy into a useful electron-hole pair. For p-on-n devices, similar to the GaSb device studied here, if the device is not passivated properly, the quantum efficiency would be low because of high recombination of the carriers. GaSb devices were originally fabricated using liquid etching (acid etching) based passivation techniques. However, these techniques were not robust enough to yield high quality devices. In order to achieve a dependable process, other passivation techniques were investigated. As a result of these efforts we have developed a proprietary passivation process that consistently yield devices with excellent spectral response. In Figure 35 we show the spectral response of a cell using this new passivation technique along with that using the old passivation method. The new passivation technique increased the quantum efficiency by over 10% when compared to that of the previously processed devices. As a result of incorporating both the modified diffusion process and passivation method the yield per batch increased to over 80%.

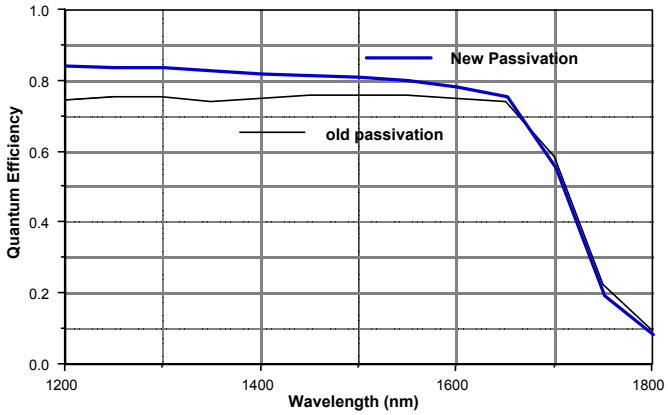

Figure 35. Quantum Efficiency Variation as a Function of Wavelength for GaSb Devices Using Old and New Passivation Techniques

4.3.2. Device Electrical Performance

Tellurium doped wafers procured for the fabrication of EDTEK's TPV cells were n-type (n ~3 to 5e17/cc) (100) GaSb wafers of 25 mils nominal thickness. The sheet resistance of the wafers were measured and documented. These wafers were subsequently processed into GaSb TPV devices using the modified process scheme outlined above. As mentioned earlier a series of device process optimization experiments were carried out first. Temperature and duration of both first and second "drive-in" diffusions were varied to arrive at optimum conditions that correspond to maximum device performance. The key process monitors in these optimization experiments are shown in Table 3.

The electrical characteristics of a typical device processed at EDTEK using optimized procedure are shown in Figure 36. Here the various current versus voltage curves correspond to exposure to different light intensities. The variation of short circuit current, I_{SC}, with open circuit voltage, V_{OC} is given by the diode I-V relation,

$$I = I_0(\exp(nqV/kT)-1) - I_{SC}$$

Where:
I_O is the diode saturation current,
n is the diode ideality factor,
q is the electronic charge,
k is the Boltzman factor and
T is the temperature.

Table 3. Key Process Monitors Used In Tpv Cell Optimization

1.0 Diffusion Process Monitors
- a. Forming Gas Flow and Pressure
- b. Diffusion Temperature
- c. Diffusion Time
- d. Sheet Resistance After Diffusion

2.0 PV Cell Process Monitors
- a. Back Contact Metallization Adhesion Test
- b AR Coating Spectral Reflectance
- c. Front Contact Metallization Adhesion Test

3.0 PV Cell Qualification
- a. I-V Characteristics
- b. Quantum Efficiency Measurements

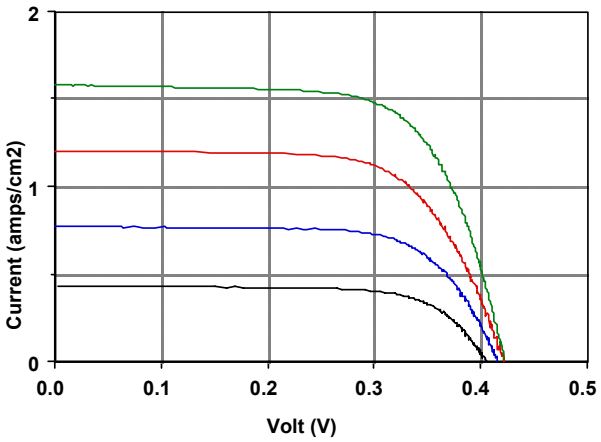

Figure 36. I-V Curves Under Different Light Intensities

The dependence of open circuit voltage and fill factor on cell temperature is shown in Figure 37 and Figure 38. V_{OC} changes by about 1.5 mV per degree while the fill factor changes by 0.09% per every degree change in cell operating temperature. The decrease in open circuit voltage with increasing temperature is due to decreasing bandgap with temperature and the attendant increase in dark current. The decrease in fill factor with increasing temperature is due in part to the decrease in open circuit voltage and in part to the increasing roundness in the knee of the I-V curve as the temperature increases. Our measurements of maximum power point values (P_{max}) shown in Figure 39 indicate a net power gain of 2 mW/cm^2 for each degree decrease in cell operating temperature.

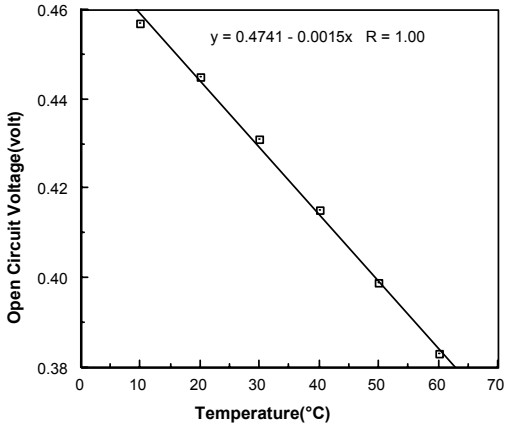

Figure 37. Variation of Open Circuit Voltage with Temperature

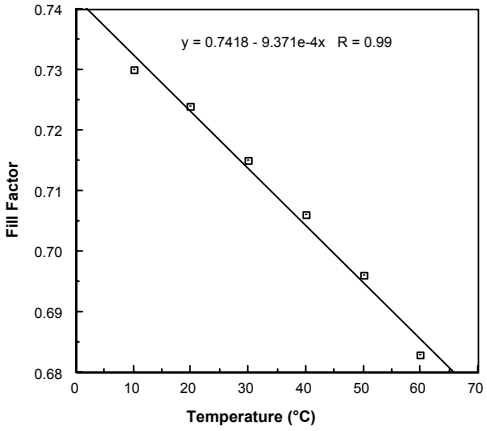

Figure 38. Variation of Fill Factor with Temperature

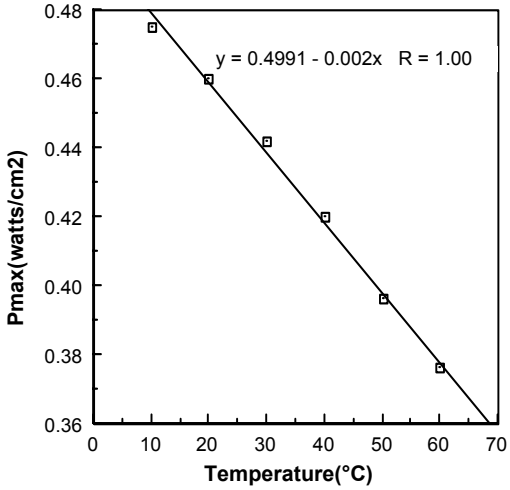

Figure 39. Dependence of Power at the Maximum Power Point on Temperature

4.3.3. Cell Manufacturing Cost Evaluation

Since the GaSb PV cells are the major cost element in the SGTPV system, we have performed an evaluation of the manufacturing costs. The first element in the cell manufacturing cost is the starting wafer. To evaluate large volume manufacturability of TPV cells designed several batches of GaSb wafers were processed into cells. Incorporation of process improvements mentioned in the above section resulted in fabrication of high quality GaSb devices with a high yield in a given batch and also good batch to batch reproducibility. However, even with a yield of over 80%, the unit cost of a GaSb cell is rather high (see Table 4). This is primarily due to the cost of a GaSb wafer. The cost of a 2" diameter wafer was over $300 when this program was initiated in 1998. With increase in wafer suppliers and overall wafer demand this unit cost has come down to $100 range.

Table 4. Data For Wafer And Processed Unit Cell Cost

Year	Batch Size	Unit Wafer Cost	Unit Cell Cost
1994	four 2"-wafers	$450	$160
1999	eight 2"-wafers	$225	$60
2000	six D-shaped wafers	$100	$30
2000+	100 D-shaped wafers	$50	$5

The GaSb crystal is grown by Czkorski technique using a (211) oriented seed crystal. The (100) oriented wafer cut from the as grown original ingot is not circular but rather "D" shaped. A circular wafer is cut out of this D shaped crystal through additional mounting and grinding and thus adding to the cost of the final product. The GaSb device processing technique adapted by EDTEK does not necessarily require circular wafers. However, one issue we should be concerned with relates to edge beads formation during the spinning of photo-resist on non-circular substrates. This can be overcome through several edge bead removal techniques that are well established. Also the devices we are making (1cm x 1cm) are rather large by semiconductor device standards and hence losing some edge areas in the wafer may not result in the reduction of number devices obtainable per wafer. This aspect is illustrated in Figure 40 where we show a 1) "D"-shaped wafer and 2) a circular wafer processed with the cells clearly delineated. We were able to get 16 devices from this "D" shaped wafer where as the 2" circular wafer yielded only 8 cells. However, all "D" shaped wafers are not of uniform size and on an average we get about 14 devices per wafer. Thus just by switching to "D" shaped wafers we were able to decrease the cost by a factor of nearly 2.

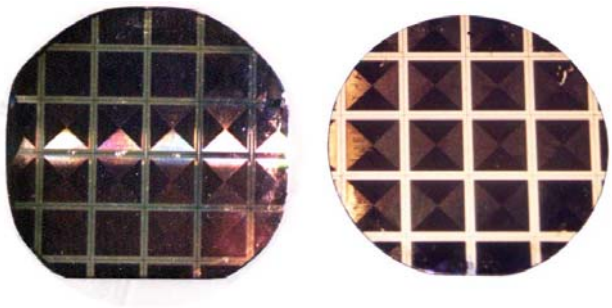

Figure 40. Photographs of Processed D Shaped and Circular Wafers

The second element in the cell manufacturing cost is the processing of the wafers into individual PV cells. The innovations introduced in GaSb device processing scheme to improve device quality and yield resulted in very little increase in processing costs. Unlike conventional photovoltaic cells these TPV cells have to be designed to carry high currents, up to 10A/cm^2, as the illumination intensities are high. Therefore the front grids in TPV cells should be thick to carry such high currents. The front grids are incorporated by a photolithography lift-off process and so in our original design, the grid lines were thin for easy lift-off. Subsequently the grid thickness was increased by a gold electroplating process. This electroplating process involved another photolithography process and these steps added to the overall processing costs. More recently, we have been successful in eliminating this plating process by developing a lift-off process where thick metal could be vapor deposited. Incorporation of this lift-off scheme reduced the overall wafer processing cost by over 25%.

4.3.4. Process Reproducibility

To evaluate and document yield and electrical characteristics of the cells and thus confirm the stability of the fabrication process, one hundred (100) oriented "D" shaped GaSb wafers with specified dopant uniformity, etch pit density, thickness and surface finish were procured from a national vendor. Measurements such as sheet resistance, spectral transmittance, and surface finish were carried out on select wafers. Four batches of wafers were processed using the optimized processing scheme. Five wafers were used for each batch. Figure 41 shows the open circuit voltage (V_{OC}) and fill factor (FF) obtained for the dies from a typical wafer. The V_{OC} and FF values are uniformly very high for most of the dies on this wafer. Our tests show excellent uniformity in the electrical characteristics of various cells from a single wafer.

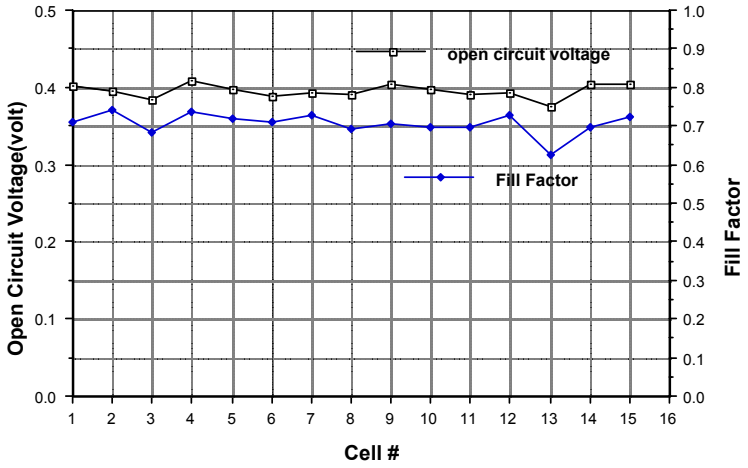

Figure 41. Open Circuit Voltage (Voc) and Fill Factor (FF) Values for Devices from a D Shaped Wafer

In Figure 42, Figure 43, Figure 44, and Figure 45 we show the frequency values of short circuit current; I_{SC}; open circuit voltage; V_{OC}, fill factor; FF and power at the maximum power point, P_{max} for devices from wafers that were processed in several separate batches. Over 80% of the devices exhibit P_{max} values greater than $0.1 watt/cm^2$. In summary these results confirm the establishment of a fabrication process for manufacturing high quality GaSb devices. Device quality uniformity in a given batch and batch to batch repeatability of GaSb TPV cell fabrication at EDTEK is also established.

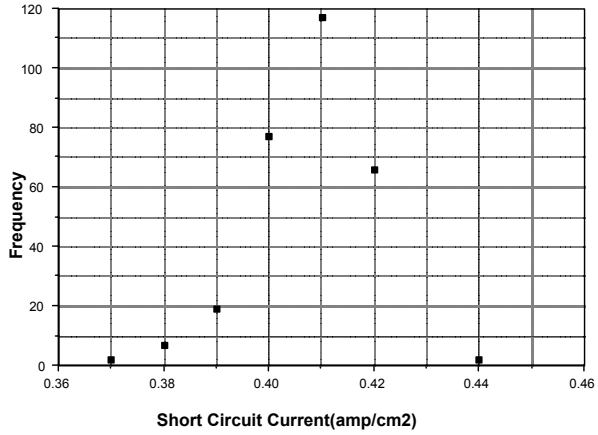

Figure 42. Frequency Distribution of Short Circuit Current of Devices Fabricated in Several Batches

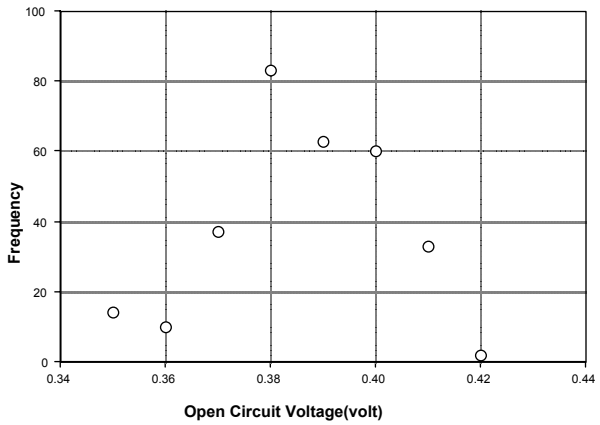

Figure 43. Frequency Distribution of Open Circuit Voltage of Devices Fabricated in Several Batches

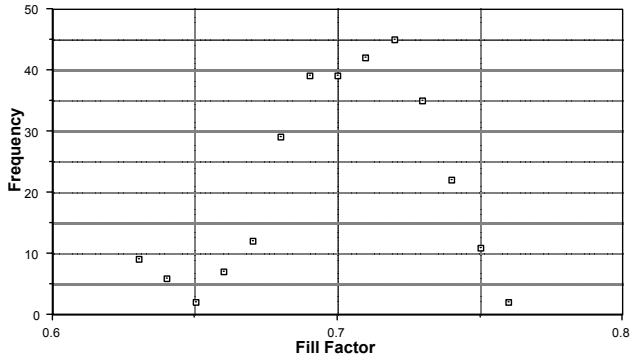

Figure 44. Frequency Distribution of Fill Factor of Devices Fabricated in Several Batches

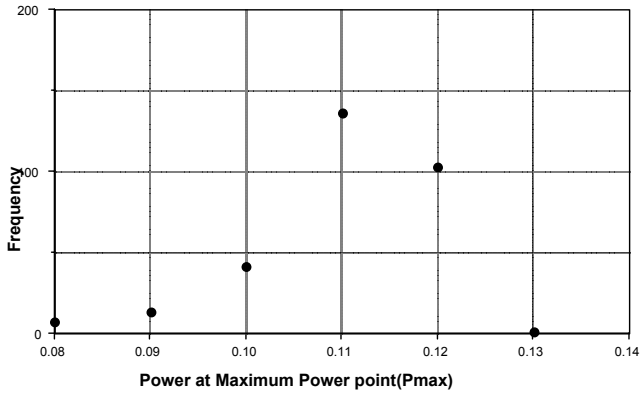

Figure 45. Frequency of P_{max} for Devices Fabricated in Several Batches

4.4. Photovoltaic Array Development

Figure 46a shows the configuration of the PV cell arrays as configured for the previous conducted program sponsored by the US Army[6]. In this program, the PV cell arrays were built in four flexible arrays that could be wrapped around the diesel TPV heat source assembly. One

of the PV cell arrays is shown in the photograph of Figure 46b. The cells are connected in series strings of six cells each that are wrapped radially around the converter. This connection scheme was chosen because it was felt that the radial energy flux uniformity would be better than the longitudinal uniformity. Each array has nine six-cell-strings, as shown in the photograph. Figure 47 shows a typical current-voltage characteristic for the six cell strings. These strings are stacked to cover the full face of the emitter. The six cell strings are connected together from quadrant to quadrant to yield 24 cells in series around the converter. Three of these 24 cell strings are then connected in series to form 72 cell strings that yield the desired 28 volts. The configuration of the PIER converter precluded the use of this previous design since the filters and prism arrangement was not in a continuous circular form. The new design calls for twelve filters to encircle the emitter each of which having a 1.25" x 5.1" area where the prisms and cells must be bonded flat. Photovoltaic arrays for the PIER project now mirror the prism array as introduced in the previous section; each of the twelve arrays consist of 18 cells arranged in two rows of 9 cells each, Figure 48. The key development for this array was the interconnect system used to arrange the cells into series connected arrays. Previous cell-to-cell interconnects was accomplished using a electrically conductive epoxy to bond a silver mesh from the cell bus-bars to the metallization of the substrate boards. This epoxy was found to degrade over time and thereby reduce array electrical performance. Arrays for the PIER project employed low temperature solder for both bonding the PV cells to the ceramic substrates and for interconnecting the cell into series strings. This resulted in improved electrical performance of the arrays. A measure of array performance is the fill factor of the series connected cells. Individual cells fill factors average approximately 0.72 with a theoretically ideal fill factor being about 0.75. Series connected fill factors of the arrays were 0.70 demonstrating excellent PV array performance.

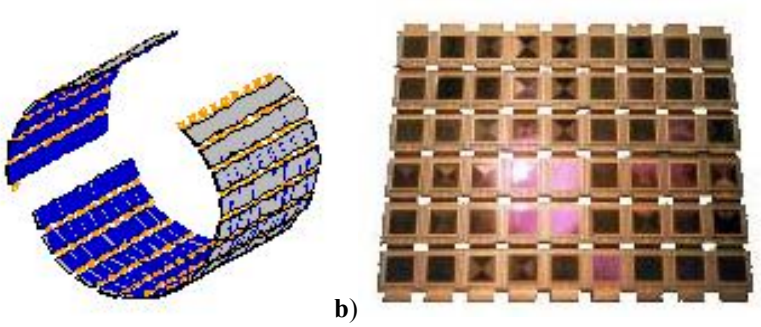

Figure 46. Schematic of TPV Converter Photovoltaic Cell Arrays (a) and Photograph of a single TPV Cell Array from a Previous Study[6] (b)

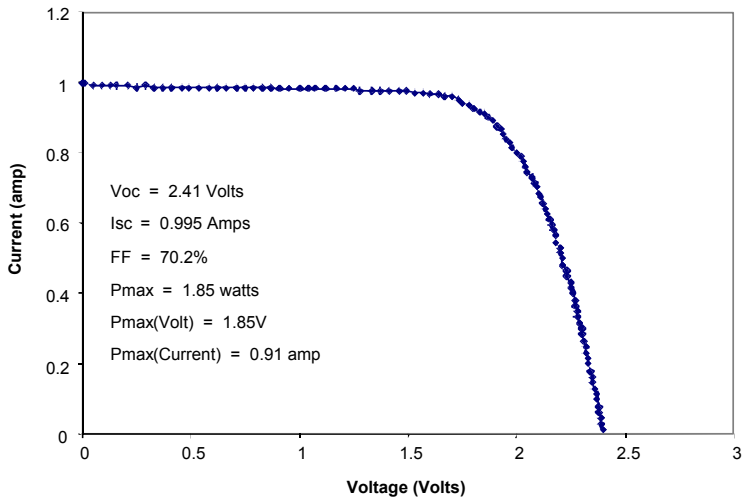

Figure 47. Typical Current Voltage Characteristic Measured for a Six Series-Connected PV Cell String in the Testbed TPV

1)

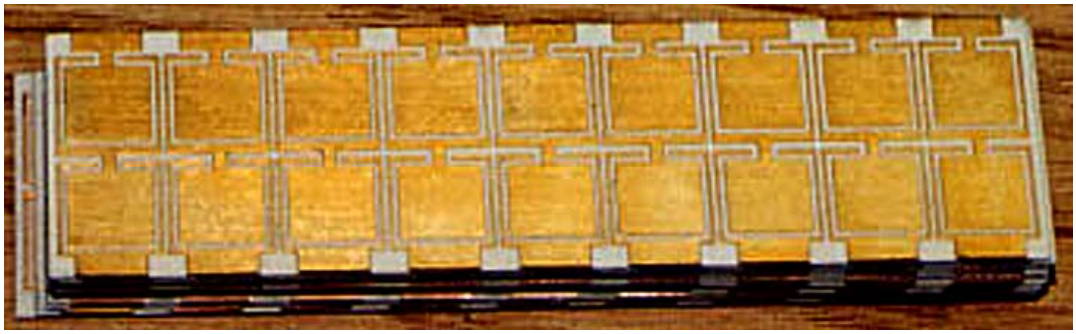

2)

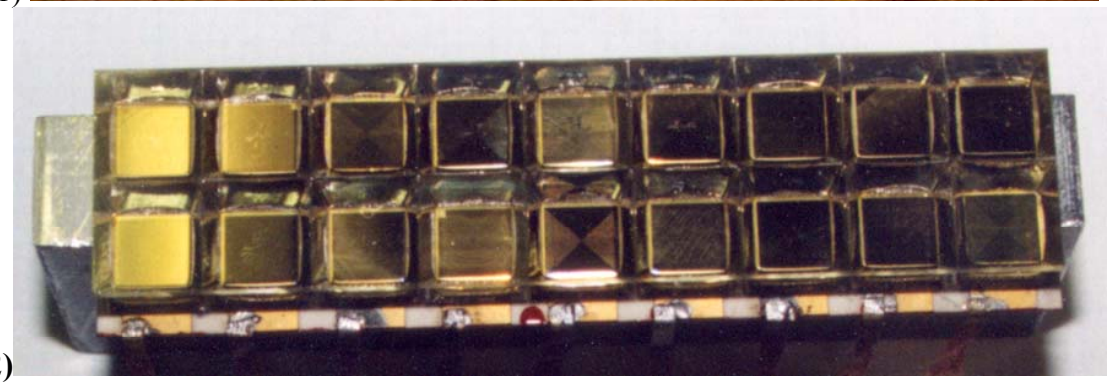

Figure 48. Photographs of the SGTPV 2x9 Array Showing 1) the Ceramic Board Before Cells are Bonded in place and 2) Complete Array with Board and Cells.

4.5. Solar Concentrator Dish Development

Figure 49 illustrates the concentrator dishes that we have developed for use with the CEC Pier Project as well as our future product lines. EDTEK has developed an integrated manufacturing process for producing durable, economical, precisely formed, and optically superior point focus concentrators. The vertically integrated process combines six essential manufacturing steps to be performed in three production machines. The six essential steps are listed below and the

work performed to implement them in pilot production equipment is detailed in subsequent paragraphs.

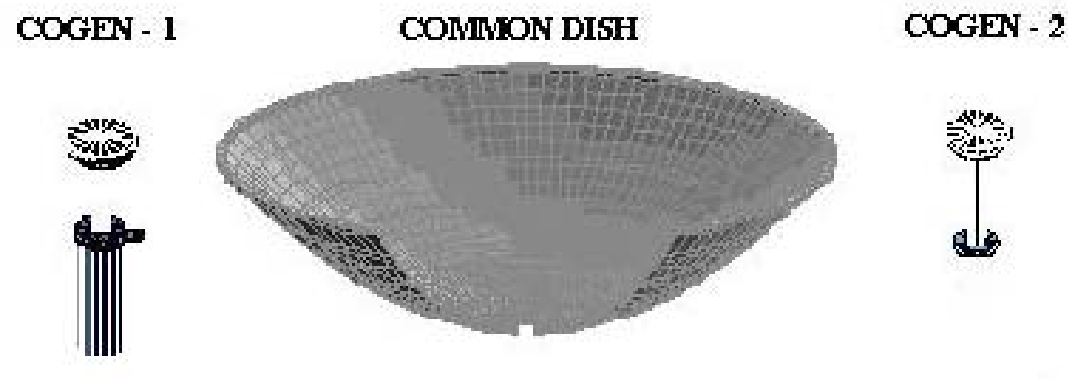

Figure 49. EDTEK Plans to Manufacture a 56-inch Diameter Concentrator Dish to Support Two Solar-to-Electric Converters, COGEN-1 and COGEN-2

Forming of the Reflector Substrate: A metal sheet substrate is formed onto a die by. An insulated, temperature controlled die is used to permit rapid heating and forming over a temperature range between the annealing point and the solution temperature of the metal. Aluminum is the preferred substrate metal for this process although it could also be applied to steel and other metals. This step requires about 20 minutes including the heat up cycle.

Tempering the Formed Substrate: While still pressurized on the die to prevent warpage and to maintain thermal contact, the aluminum sheet is rapidly cooled to freeze the impurities in a solid solution. After removal from the chamber these impurities subsequently precipitate in clusters to age harden and temper the substrate during a two-week storage period at room temperature. This step requires about 10 minutes.

Forming a Specular Surface: After the substrate is formed and tempered a proprietary coating process has been developed to smooth the surface of the substrate to make it a specular surface onto which a reflective coating can be deposited to form the concentrator's mirror surface. The details of this proprietary process have been presented in an earlier proprietary report delivered to the CEC.

Depositing Reflective Coating: A reflective silver film is vapor deposited from a thermal evaporation source onto the seamless, pinhole-free cured polymer substrate. This step requires about 10 minutes of deposition time.

Depositing Protective Coating: Maintaining an uninterrupted vacuum, a high density SiO_X coating is deposited over the silver reflective surface. The thermal evaporation deposition of the SiO_X coating is assisted by simultaneous bombardment of the surface with energetic argon atoms (ion assisted deposition). Ion assisted deposition enhances the bonding and density of the SiO_X film as well as reducing pinhole formation. This step requires about 20 minutes.

Removal and Storage: The part is then carefully removed from the chamber and stored to allow the age hardening to proceed. The age hardening requires from two hours to two weeks depending on the storage temperature.

Thus, a manufacturing process is described which can produce high quality formed reflector parts at about one third of the cost of the same parts fabricated by a sequence of discrete parts using materials purchased from vendors.

These steps yield precisely formed metal substrates with highly specular, reflective surfaces protected by state-of-the-art optical coatings. Forming at elevated temperature virtually eliminates springback and produces precision contoured metal substrates. Concentrator durability and economy are enhanced by an integral, baked-on, inert substrate specularizing and bonding layer that eliminates adhesives and edge taping. It is estimated that the integration of the production process which eliminates the profit, sales costs, and assembly labor required by current manufacturing practices using discrete subassembly parts obtained from multiple vendors will reduce primary reflector costs by a factor of 3. We estimate that the complete formed, coated, and hardened, high quality reflectors will have a manufacturer's sales price of about $2.36/sq ft in modest production. When compared to the $2.50 to $3.50/sq ft costs of adhesive backed reflective films (which cannot be formed into compound curved dishes) which are currently in popular use this vertically integrated process is truly enabling for cost competitive electricity generated from renewable energy production.

All of the steps of this manufacturing process except the surface smoothing step (step no. 3 above) had been demonstrated on prior programs. During this task we have developed and demonstrated the substrate smoothing process. As a cost share effort, we have also designed and fabricated the equipment to implement the entire process. These designs, the fabricated hardware, and the developmental efforts performed to demonstrate the substrate smoothing process are described in the following paragraphs.

4.5.1. Substrate Forming Process & Tempering (Process Steps 1 & 2)

In order to be able to use off-the-shelf rolled aluminum sheet for substrate stock, it is necessary to use a process that minimizes spring back and is not subject to variations in different batches of materials or in materials from different vendors. EDTEK forming is such a process. In this process the aluminum stock is heated to a temperature which lowers its tensile strength minimizing internal stresses. The hot sheet material is then forced into a die. The material is left very precisely conformed to the die; however, it is also left in its dead soft (T-0) annealed condition which is not desirable in light of future handling and use. The fact that the material is annealed to its dead soft condition can be overcome by selecting a suitable alloy and during the forming process, setting up the conditions for tempering to occur after the part is cooled down.

For our parts we have chosen the aluminum alloy that is corrosion resistant and it is amenable to the age hardening. As discussed above, without age hardening, the concentrator reflectors are left in the annealed condition. It would be much more advantageous to have a tempered part that was less sensitive to handling. The age hardened final condition makes the part less sensitive to handling. The hardened material is about five times stiffer than untempered material, thus, a durable and accurate concentrator will be the result. In our screening of materials we found two likely aluminum alloy candidates that can be age hardened.

The forming process begins by inserting an aluminum blank into the machine and close the lid. The machine then cuts and strengthens the outer edge of the part in preparation for forming. The aluminum blank is isolated and then heated to forming temperature.

Once the aluminum sheet is properly heated, it is forced into the die and held to facilitate its cooling to the die temperature. With the part still held in the die, a second forming step further strengthens the part so that it can also be used as attach points and frame-work for making arrays of the dishes.

At this point, the part is released from the chamber and lifted the formed part out of the die. The chamber is then opened and the formed dish is removed from the chamber and stored for hardening before the substrate smoothing and reflective coatings are applied Figure 50 illustrates the overall forming machine.

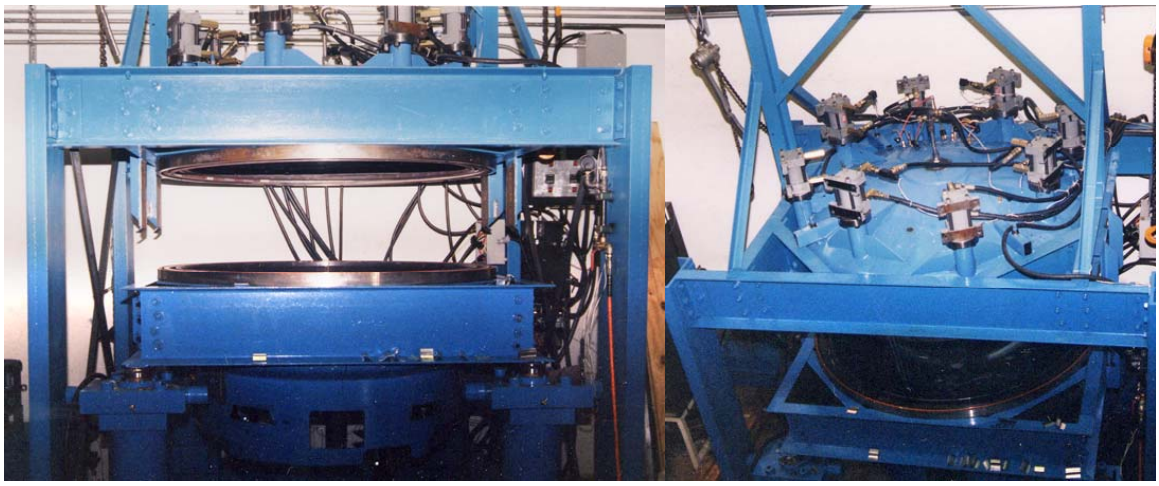

Side View Top View

Figure 50. Side and Top View Photos of Forming Machine Design

4.5.2. Substrate Smoothing (Process Step 3)

The substrate smoothing process has been described in a prior document submitted as a proprietary deliverable to the CEC.

4.5.3. Vacuum Deposition of Reflective Coating (Step 4 of Process)

After we have a precisely formed substrate with a specular surface it is necessary to apply a reflective coating. In the past, most users have employed adhesive backed polyester films with vapor deposited reflective films protected by dielectric (glass) coatings on their surface. These discrete films are expensive and labor intensive to apply to formed substrates and cannot be formed into compound curved surfaces such as dishes. As an alternative we have developed the capability to vapor deposit the reflective and dielectric coatings directly onto the compound surface of our concentrator dish. For the reflective coating we have the option of using aluminum or silver. The trade off between the two has to do with total solar reflectance versus corrosion resistance. Silver has the best overall solar reflectance; however, it is more subject to corrosion if there are pinholes in the protective coating layers. Thus, the ultimate choice depends on the application and environment that the part will be subjected to. For most

applications we will use silver because of the greater efficiency that it affords in the overall system. A cross sectional drawing of the system designed and under construction for this application is shown in Figure 51. This system consists of a 5-foot diameter, 5-foot high deposition chamber pumped by a cold trapped 10-in diffusion pump with flanges for adding two additional 10-inch diffusion pumps as required to increase production throughput. The crucible for the metal evaporant charge is mounted on a flange that is automatically raised and lowered by an actuator to provide access by an operator for re-supplying the source. The dish is loaded into the top of the chamber facing downward toward the source. During deposition a portion of the evaporant is ionized and accelerated toward the source to assist in densifiying the coating which improves its resistivity and, hence, reflectance. Deposition rate is monitored by a conventional quartz oscillator rate-monitor.

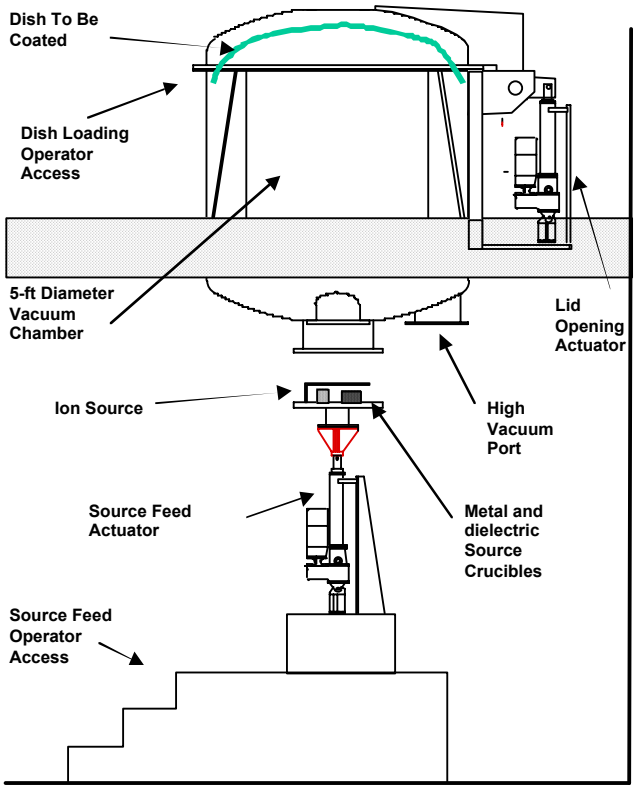

Figure 51. Cross Sectional Drawing of Reflective Metal and Dielectric Coating Machine

4.5.4. Vacuum Deposition of Dielectric (glass) Protective Coating (Step 5 of Process)

The dielectric used as a protective coating is an SiOx material evaporated from a resistance heated source located on the same flange as the metal source shown in Figure 51 and discussed in the previous section. Again, ion assisted deposition is used to produce a more dense and pinhole free coating for maximum protection of the reflective layer.

4.5.5. Removal and Storage of Completed Dish Reflector

The sixth and final step of the process is to remove the coated dish from the chamber and to store it in a suitable place for the hardening process to go forward to completion. This process can require several weeks at room temperature or it can be accelerated to a few minutes by storage at an elevated temperature.

4.6. Fossil Fueled Tpv Generator Development

For purposes of developing the hybrid solar/fossil fueled TPV generator system it is convenient to first discuss the fossil-fueled and solar-fueled systems separately and then using the experience gained to combine the two technologies into the hybrid system. For this reason we first discuss our efforts to develop the fossil-fueled TPV followed by the development of the solar-fueled system. Finally, the Hybrid SGTPV system development will be discussed.

4.6.1. Fossil Fueled TPV Radiant Energy Source Development

The TPV operates by utilizing a local heat source to heat an emitter to incandescence. Low and gap photovoltaic cells then convert the radiant infrared energy from the emitter to electricity. One of the major subsystems of the TPV, therefore, is the radiant infrared energy source.

4.6.1.1. Emitter/Combustion Chamber

We have developed and tested a silicon carbide emitter and tested it extensively with a fossil-fueled TPV system. The configuration of the emitter tested is shown in Figure 52. It consists of a silicon carbide cup. The open end of the emitter cup seals to the combustion chamber bulkhead to form a combustion chamber. A silicon carbide cylinder is inserted inside the emitter cup from the combustion chamber bulkhead to act as a flame baffle. The flame baffle forces exhaust gases from the combustion inside the chamber to exit through the annular channel formed between the flame baffle tube and the inside of the emitter cup. Thus, the emitter side walls receive heat by convection from the exhaust gases and by radiation from the flame tube walls. The primary energy loss mechanism from the emitter is radiation from its outer walls. This configuration results in maximum heat being transferred to the emitter in a radially uniform manner. Further, although there may exist a temperature gradient in the exhaust gases between the entrance and exit of the annular space, the gradient in temperature longitudinally along the emitter surface will be small. The analysis that supports this assertion is summarized Figure 53. This small variation in surface temperature is due to the low thermal resistance of the silicon carbide cup walls (.00064 W/C). The resistance of the radiation transfer from the cup wall surface to the converter (.037 W/C).tends to equalize the temperature over the surface of the emitter cup. The uniformity of the emitter surface temperature has been verified experimentally. The results of the experimental measurements and photos of the emitter during operation and after operation are shown in Figure 54. As can be seen from the photograph of the emitter glowing through a perforated screen, the illumination is quite uniform over the surface of the emitter. A more objective verification was made by optical pyrometer measurements shown in the inset graph of Figure 54. The longitudinal variation was about 20°C out of 1060°C. Also shown in the figure is the inside of the combustion chamber (flame tube) after a one-hour burn. The inside remains absolutely clean throughout the burn.

Figure 52. TPV Combustion Chamber and Emitter Configuration

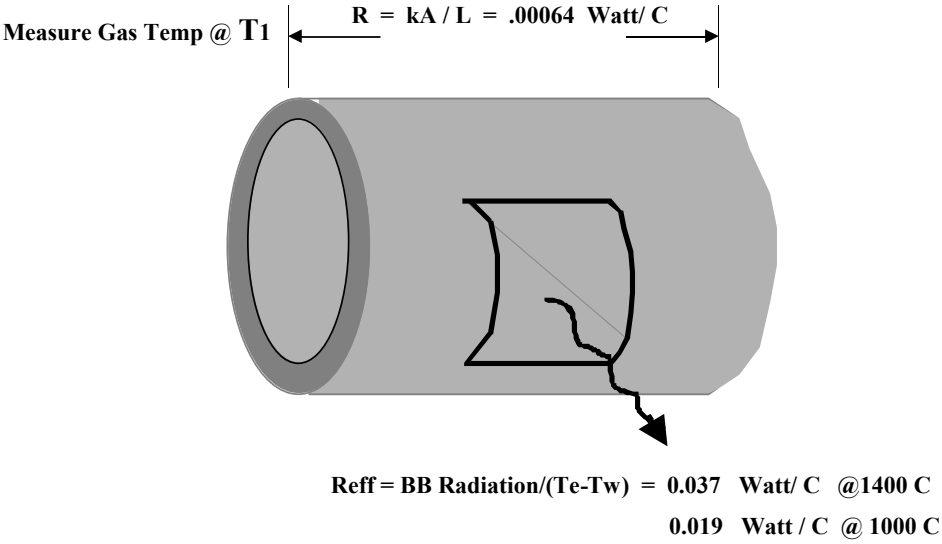

Emitter cannot sustain a large temperature gradient at operating conditions

Figure 53. Analysis of Thermal Profile on Emitter Surface

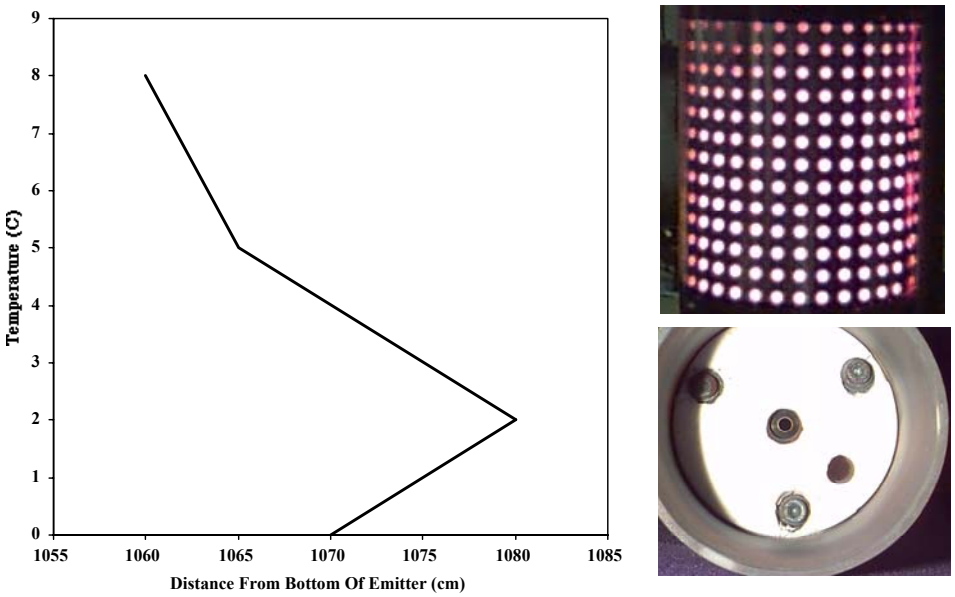

Figure 54. Measured Emitter Temperature and Photographs of Emitter Glowing Through a Screen and of the Inside of Combustion Chamber After One-Hour Burn

4.6.1.2. Burner/Recuperator

The recuperator design consists of a heat exchanger. This heat exchanger is located at the exit of the emitter cup so that it intercepts the exhaust gases from the cup. An insulating plug fills the inner region of the heat exchanger. Adjacent to this insulator is a metal shell forming a plenum between it and the inside wall of the exhaust plenum. Cold combustion air enters this chamber and travels toward the combustion chamber picking up heat from the exhaust plenum wall. A second stream of cold combustion air enters a plenum defined by the exhaust plenum and the evacuated quartz sleeve. This stream of air also picks up heat from the exhaust. This heat transferred to the combustion air is returned to the combustion chamber.

The importance of the return of heat energy to the combustion chamber by the recuperator is illustrated by the data in Table 5. By reducing the parasitic losses, the recuperator significantly influences the efficiency of the TPV system.

Table 5. Dependence Of Tpv System Efficiency On Recuperator Performance

Recuperator Efficiency (%)	System Electrical Efficiency (%)
69	15.2
70	16.5
80	17.8
90	19.1
95	19.8
100	20.7

The recuperator design was tested and the measured performance parameters are presented in Figure 55. These measurements show the recuperator efficiency to be approximately 70%. After an approximately one-hour burn the recuperator remained absolutely clean as shown in Figure 56.

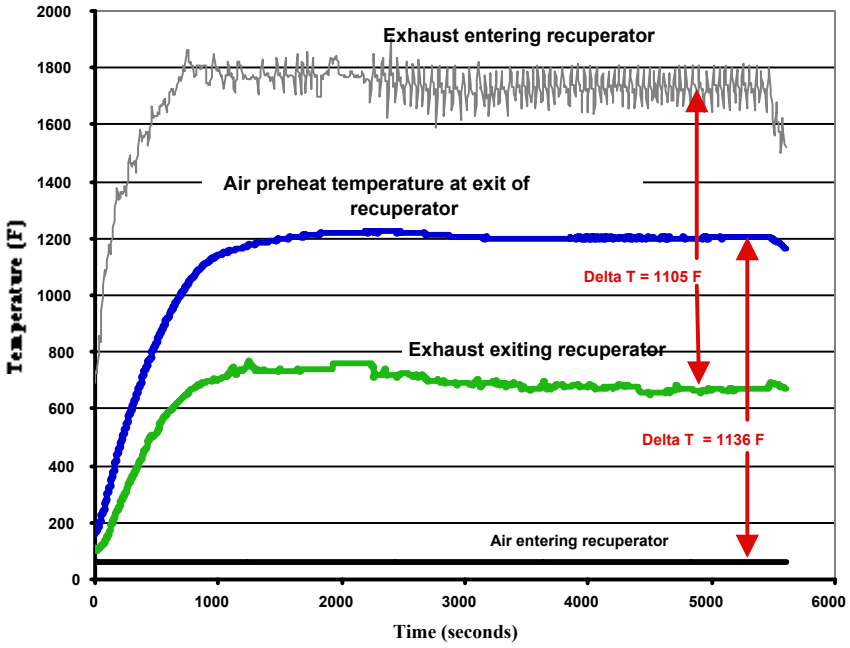

Figure 55. Measured Recuperator Performance Parameters

Figure 56. Recuperator Performance Parameters

4.6.1.3. Evacuated Thermal Control Package

In order to minimize parasitic losses of thermal energy out of the TPV system, the emitter, burner, and recuperator must be contained in a thermally isolating package. During the course of our developmental program we designed, fabricated and evaluated several configurations. The first configuration evaluated is illustrated in Figure 57. It consists of two concentric quartz tubes with an evacuated gap between their concentric walls. The emitter, burner, and recuperator are inserted into the inner tube forming a "thermos bottle" enclosure to prevent thermal energy loss from the walls of the system. With the exception of the section of the wall adjacent to the emitter, the inside of the outer wall is coated with vapor deposited gold which reflects infrared energy with about 98% efficiency. The section of the wall adjacent to the emitter is coated with a resonant-mesh infrared band-pass filter instead of a vapor deposited gold coating. The transmittance characteristics of this filter relative to the blackbody spectrum emitted by the emitter walls are shown in the inset in Figure 57. Also shown in the inset of Figure 57 is the spectrum of energy transmitted from the emitter through the walls and out of the package to a converter which will be discussed later. The resonant mesh IR band pass filters are the linchpin to high efficiency TPV performance. Therefore much effort has been expended in developing and optimizing both the filters and the manufacturing process for the filters. The details of this effort were presented in 4.1 of this report.

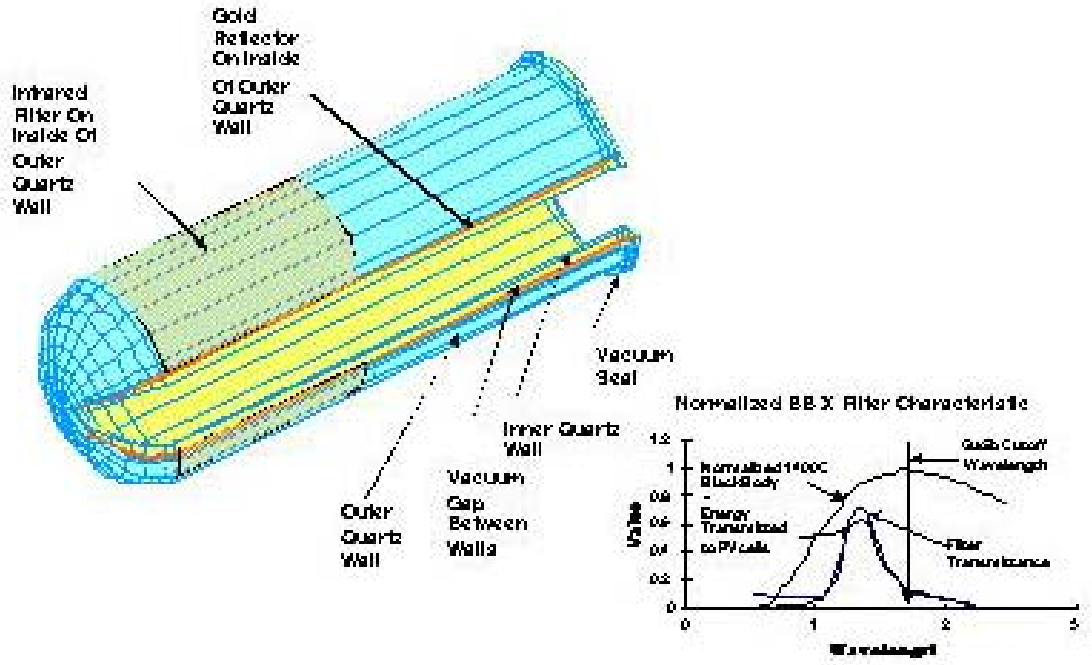

Figure 57. Thermal Isolation Package Version 1

4.6.1.4. Evaluation of Evacuated Sleeve Thermal Control Package

The evacuated sleeve thermal control system equipped with resonant micromesh IR band pass filters was tested and found that sufficient vacuum could not be maintained between the walls as the emitter heated to operating temperatures. The filters were fabricated on thin glass substrates and glued to the inner wall of the outer quartz sleeve with a low volatiles silicone adhesive. In spite of its low volatiles rating, it was the adhesive that limited the system. As it warmed up it outgassed and limited the emitter temperature that could be achieved to less than 1050°C. In order to achieve the design specifications for the TPV we need an operating emitter temperature of 1400°C. Because of this deficiency, a new metal outer sleeve was designed.

4.6.1.5. Advanced Evacuated Sleeve Thermal Control Package

The series of tests, analyses, and evaluations discussed above revealed a wealth of knowledge about the TPV system and suggested several improvements that can be made in its design in order to improve both its performance and reliability. The first major improvement is in the converter design. In order to achieve the full potential of the TPV generator we must be able to operate at temperatures on the order of 1400°C. In order to accomplish this, we must eliminate materials that can outgas and or migrate onto adjacent surfaces in the vacuum gap. At the same time, we need to address the fragility of quartz and eliminate it as a structural member in the generator. The new design used a metal cylinder for the outer sleeve. Two rings of 24 windows each were formed into the cylinder so that they would be located adjacent to the emitter when it is in position inside the quartz sleeve. The filters are then formed on glass substrates that are bonded into the windows in the metal cylinder. In this design, the bonds between the metal

and glass are shadowed from the blackbody spectrum by the metal frame into which the substrates are bonded. This configuration was intended to eliminate the heating and subsequent outgassing of the bonding adhesives.

The new metal sleeve package design was fabricated and tested in the EDTEK TPV test bed. Figure 58 shows the sleeve and filters (without converter array) under test. The glow of the emitter can be seen through the filters in the figure. The tests indicated that the new design was survivable to emitter operating temperatures up to 1500°C; normal operating temperatures are 400°C. Figure 59 shows thermal data from one of these calorimetric TPV thermal tests. Peak emitter operating temperature shown in the figure is 1500°C.

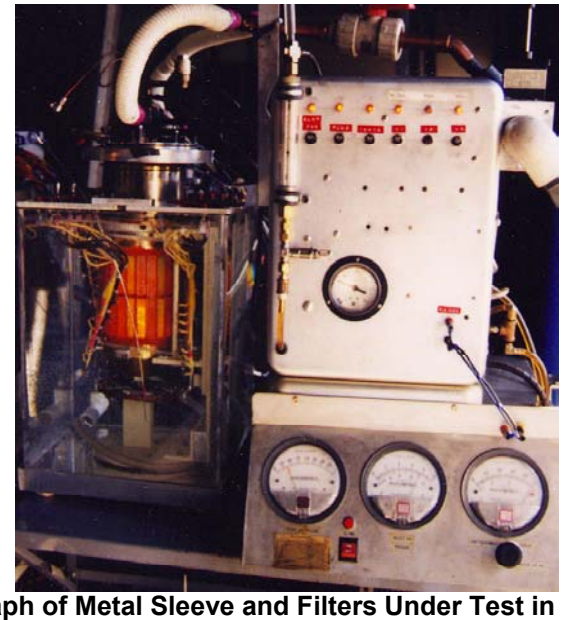

Figure 58. Photograph of Metal Sleeve and Filters Under Test in EDTEK TPV Testbed

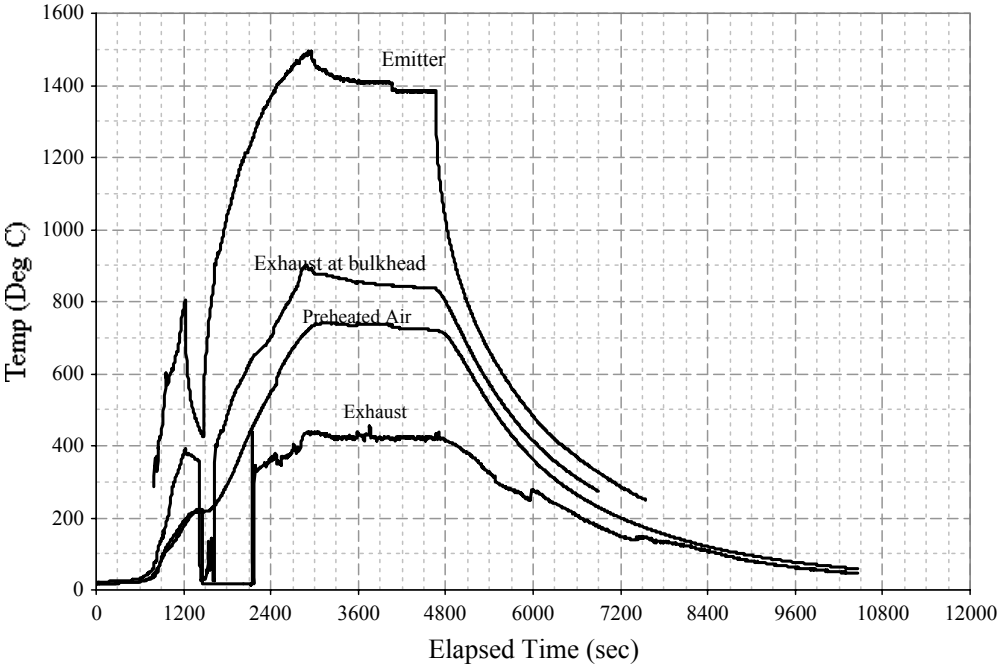

Figure 59. Emitter and Recuperator Operating Temperature Versus Time for the Improved Evacuated Thermal Control Sleeve.

4.6.2. TPV Electrical Converter Development

The radiant energy source provides an intense source of narrow band infrared energy that is transmitted through the walls of the evacuated thermal control sleeve. The narrow band of energy is tuned to match to the most efficient wavelength regime for electrical conversion by the GaSb PV cells. The electrical converter consists of the prism array described in 4.3 bonded to the outside surface of the IR filter substrates described in 4.1. The PV cell arrays, described in 4.2, are bonded to the bases of the prisms so that the prisms collect the radiant energy and concentrate it onto the PV cells. This concentration allows an unilluminated space around the PV cells for making electrical interconnections without incurring parasitic losses by absorption of the radiant energy. Thus, the electrical converter surrounds the emitter section of the radiant heat source. Figure 42 illustrates how the full burner, recuperator, thermal and spectral control, prism, and PV cell arrays are assembled together in the previously studied[6] diesel-fired TPV system.

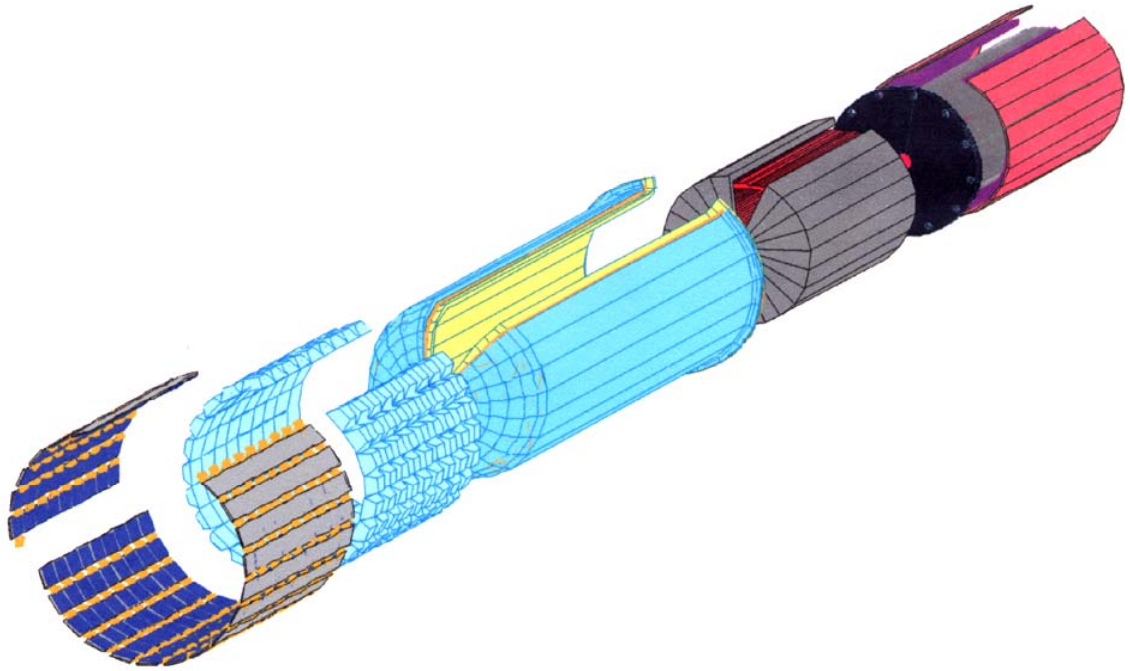

Figure 60. Full TPV Heat Source, Thermal and Spectral Control, and Converter Assembly

A test unit based on the technology developed in the preceding sections was fabricated for evaluation testing. The main differences between the unit fabricated for the PIER project and units fabricated for previous studies occur in areas of IR filter sealing, PV cell array build-up, cell cooling design, and vacuum gap management. During preliminary testing of the filter vacuum-sealing process, our goal was to improve the method that the filters were bonded to the outer housing of the TPV converter. A technique was developed to use an inorganic adhesive to secure the filters in place. This adhesive had the promise of being able to withstand high temperatures without out-gassing into the vacuum gap; something the previous adhesives did not accomplish. To further back up the inorganic adhesive seal, an organic material was placed over the inorganic adhesive. Figure 61 is a photograph of the filters after bonding into the outer TPV housing. The organic high temperature adhesive is seen as the red glue-line in the figure. The photo shows the filters before the prism arrays are bonded in place. The comb-like projections are passive heat sinks intended to cool the organic glue-line between filters. These heat sinks will be attached to the water-cooled jackets bonded to the back of the ceramic boards supporting the PV cell arrays.

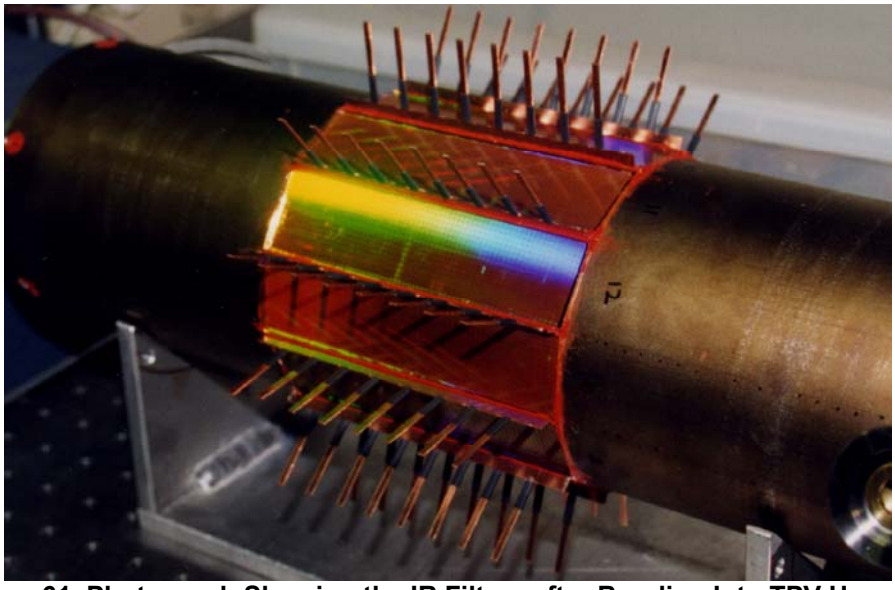

Figure 61. Photograph Showing the IR Filters after Bonding Into TPV Housing.

The next step in the converter fabrication is the build-up the cell arrays. This begins with bonding the PV cells to the ceramic boards followed by the interconnection of the cells to the conductive lines on the ceramic boards. A prism array is then bonded to Each 2x9 cell sub-assembly. Figure 62 is a photograph showing this cell-board sub-assembly. Figure 63 is a photograph of TPV converter outer housing with the cell-board sub-assemblies recently bonded in place. The wires protruding from sub-assemblies will be interconnected to form the series connected cell strings. Twelve water-cooled jackets are bonded to the back of the ceramic boards to cool the cells, prisms, and filters. Figure 64 shows the twelve water-cooled jackets prior to bonding to the boards.

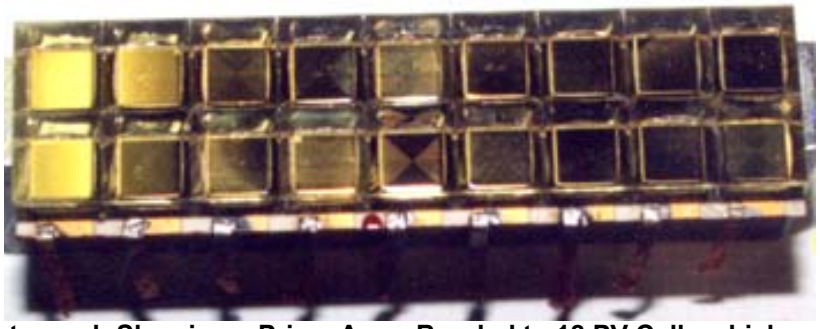

Figure 62. Photograph Showing a Prism Array Bonded to 18 PV Cells which were Previously Bonded to the Ceramic Board

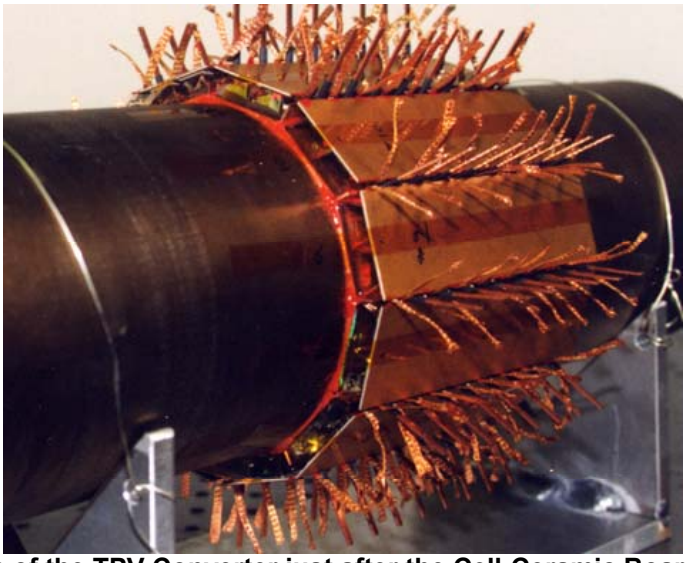

Figure 63. Photograph of the TPV Converter just after the Cell-Ceramic Board Sub-Assemblies are Bonded in Place

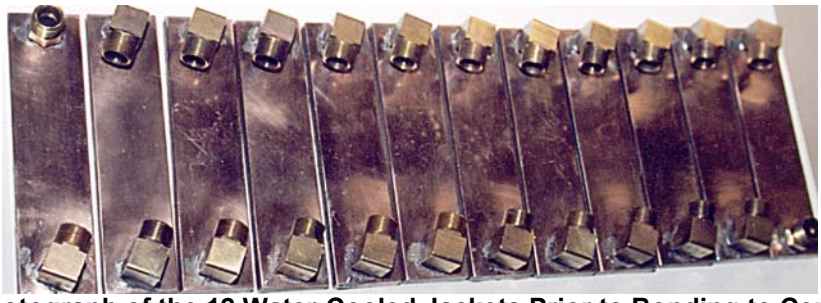

Figure 64. Photograph of the 12 Water-Cooled Jackets Prior to Bonding to Ceramic Boards

The Figure 65 of this section shows the completed converter module. The water-cooled jackets are bonded in place and interconnected to allow water circulation. The PC cell leads have been soldered to form nine series-connected strings. Additional copper cooling lines have been bonded to the outer housing to further pick-up waste heat from the system. This heat will be brought out to a heat-exchanger allowing the SGTPV unit to generate hot water as well as electrical power. Figure 66 is a view into the center of the converter unit. This view allows observation of the IR filters from the inside of the converter.

4.6.2.1.

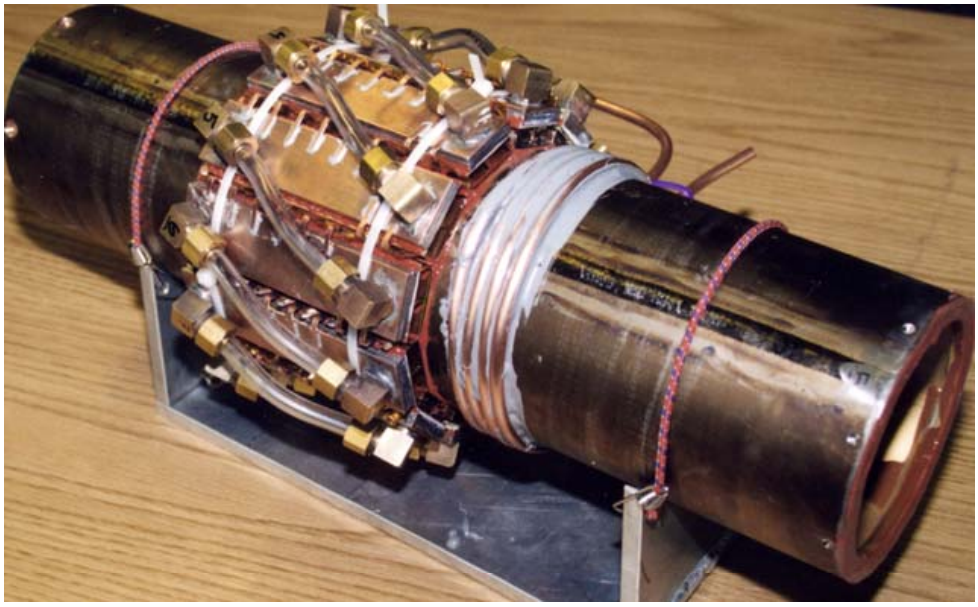

Figure 65. Full TPV Heat Source, Thermal and Spectral Control, and Converter Assembly for PIER SGTPV Project

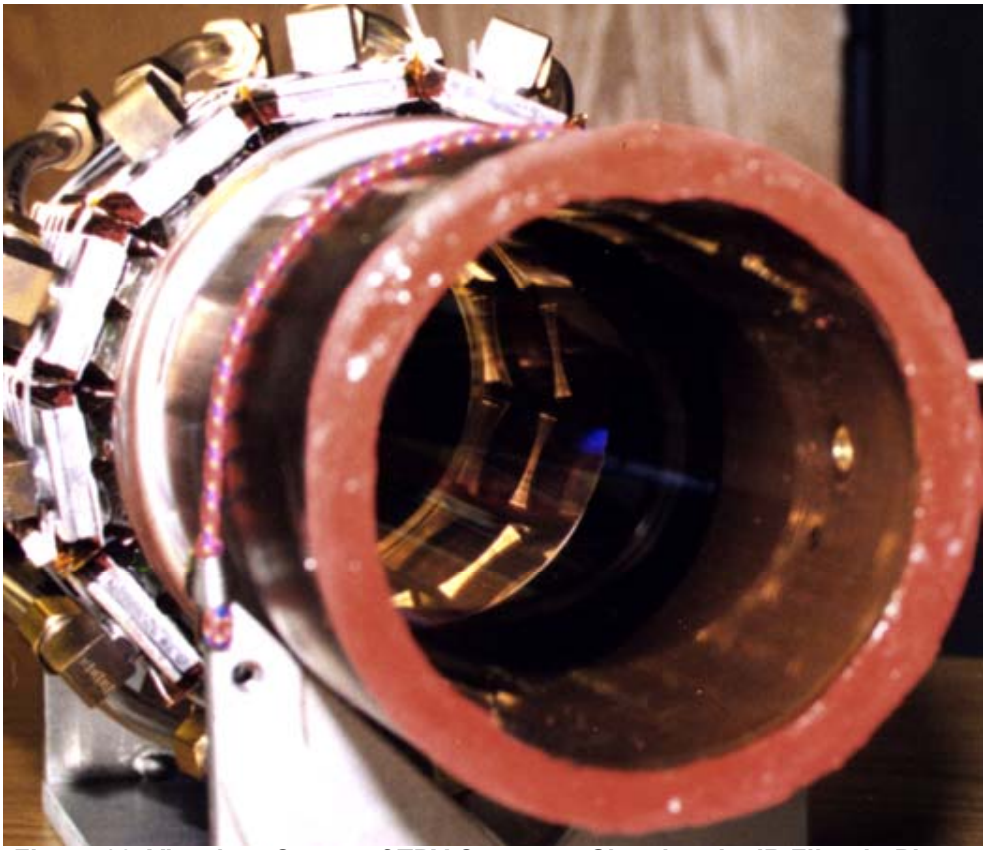

Figure 66. View into Center of TPV Converter Showing the IR Filter in Place.

5.0 System level Test and Evaluation of Fossil Fueled TPV

In order to assess the performance of the TPV heat source and electrical converter as a system a testbed was fabricated. The test-bed enabled us to immerse the TPV unit in a water bath calorimeter so that we could measure and evaluate thermal energy transmitted out through the walls and PV cells of the TPV unit. The unit was also instrumented throughout with thermocouples to monitor key gas temperatures throughout the system as well as emitter temperature. Instrumentation was also provided for monitoring gas pressures and air flows throughout the unit. A digital scale was used to monitor fuel consumption continuously throughout the test. A curve tracer was employed with a multiplexor to allow monitoring the I-V characteristics throughout the tests. All the data were recorded on a computer and stored for analysis. These tests and their results are described in detail in the following sections.

5.1. Test-Bed Unit Description

In order to evaluate the performance of the TPV system as well as its various subsystems, a testbed unit was fabricated. Figure 67 and Figure 69 show photographs of key subsystems of the testbed converter during fabrication and assembly. Figure 67 shows the evacuated sleeve with the resonant mesh IR filters installed. The system is illuminated from below and the strong colors present are due to the diffraction grating effects of the filters in the visible spectrum. Figure 68 shows the TPV converter during assembly with one quadrant of PV cell/prism arrays removed for viewing. It should also be noted that one half of the IR filters had not yet been installed. This configuration permits the viewing of each of the major components in the TPV converter. Looking straight into the center, one can see the cells. To the bottom center, the installed filters are visible. A finned heat sink assembly surrounds the assembly. The copper colored bands are conductors brought out from each series string of six cells. During the test, it was possible to monitor the output of each of the 36 strings of six series-connected cells.

Figure 67. Photograph of Filters Installed in Evacuated Quartz Sleeve

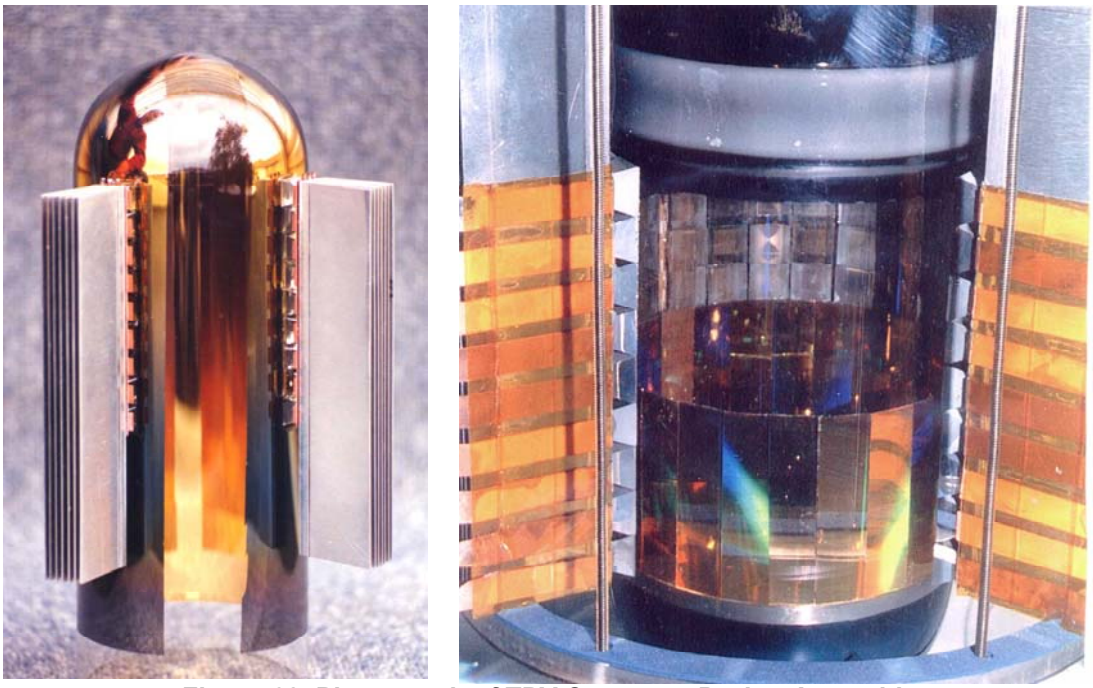

Figure 68. Photograph of TPV Converter During Assembly

For thermal evaluation of the system the test unit was thoroughly instrumented with thermocouples. Seventeen thermocouples were installed in the test bed generator unit to monitor temperatures occurring during testing. Other instrumentation gather data on PV cell performance, fuel flow and consumption, intake fan vacuum, nozzle air pressure, combustion chamber pressure, fuel pump pressure, and oxygen content of exhaust. The instrumentation allows full evaluation of the performance of the system and its subsystems.

5.2. TPV system Tests and measurements

There are several physical mechanisms operating simultaneously in the TPV system. First, there are the thermal mechanisms associated with the burner, heat source, and parasitic thermal losses. Second, there are the electrical conversion issues and PV cell performance. All of these mechanisms must be understood and measured to fully evaluate the performance of the TPV system and to determine ways to improve the performance. Figure 69 presents the important thermo-optical and electrical features that need to be considered in the evaluation. In the remainder of this section we will discuss the results of measuring and evaluating each of the physical mechanisms along with the thermal-to-electrical performance of the TPV generator.

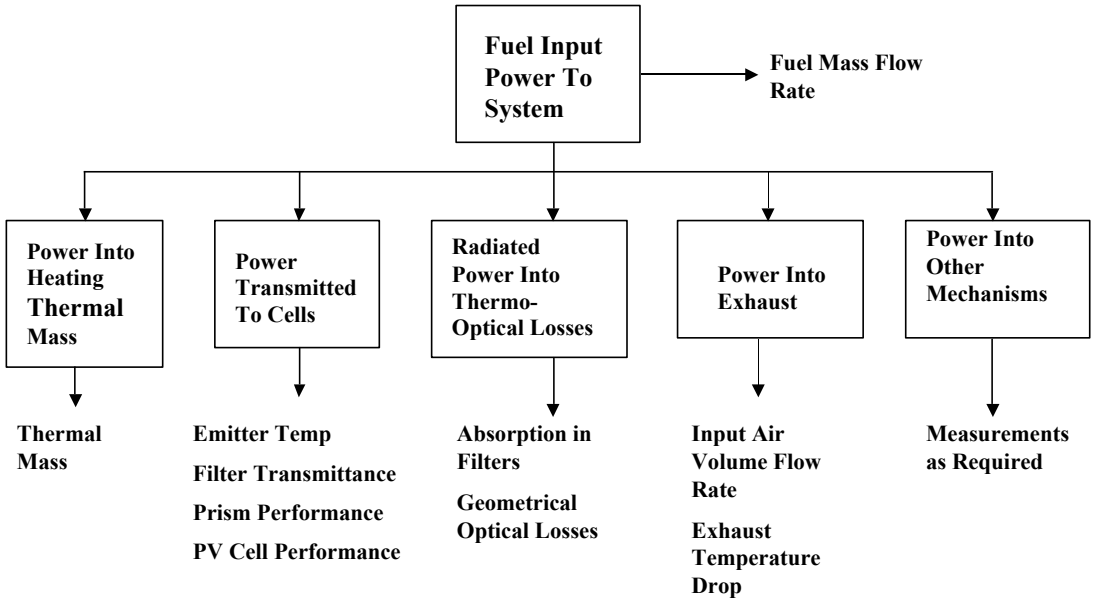

Figure 69. Illustration of Important Physical Mechanisms That Must be Evaluated in the TPV System

First, it is important to know the actual total amount of fuel energy being delivered to the system. We measured the fuel-input rate in two ways. A flow meter was inserted into the fuel line and provided a visual indication of the fuel-input rate through out the tests. The second and most accurate measurement employed a scale that measured the mass of fuel in the fuel tank at 15-second intervals. From these data, the fuel rate could be adjusted during the test and the fuel input rate accurately calculated. A typical fuel input-rate data calculated from the weight measurements is presented in Figure 70.

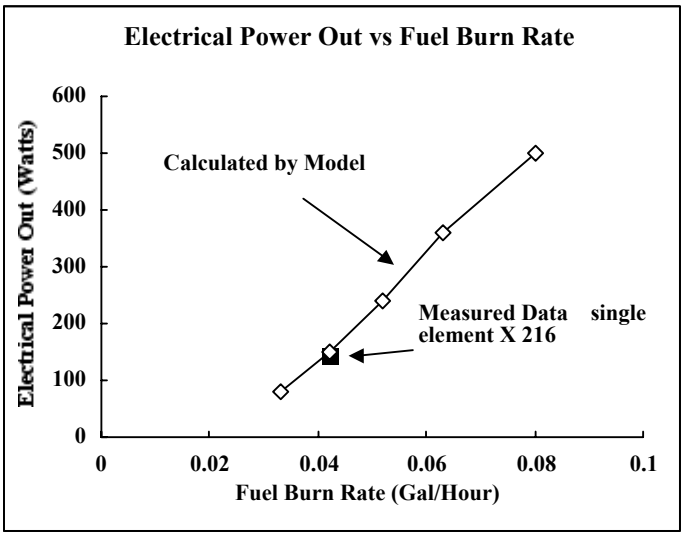

Figure 70. Typical Fuel Burn Rate During System Level Tests

Initially, the system must warm up internally before the steady state operating condition is established. We measured the thermal mass of the system indirectly by measuring the rate of temperature rise at the exhaust bulkhead (center of the system) under different firing rates. We first calculated the overall thermal mass by considering the measured weights of the various components within the generator and the quartz sleeve and then using published specific-heat data for the materials involved. This calculation yielded an average thermal mass of 51.64 watts/°C/min. For a given heat input into the generator, the specific heat can be calculated by measuring system temperature change per unit time. For example, at the early heat up stage of a burner run, before radiant heat losses become substantial, the thermal mass is the dominant heat sink except for the burner exhaust. By measuring the rate of temperature rise and subtracting the exhaust gas energy from the total energy delivered to the system, it was possible to experimentally determine the effective thermal mass of the generator. These measurements yielded numbers between 50 and 55 watts/°C/min, in good agreement with the mass and specific heat calculation. To further confirm this number we constructed a spreadsheet model to simulate the system during cool-down with a known flow rate of air passing through the generator. The modeled cool-down data, using the 51.64 watts/°C/min specific heat number, is compared with the system measured data in Figure 71. The agreement is quite good between the modeled and experimental results. The thermal mass value of 51.64 watts/°C/min was adopted for this evaluation.

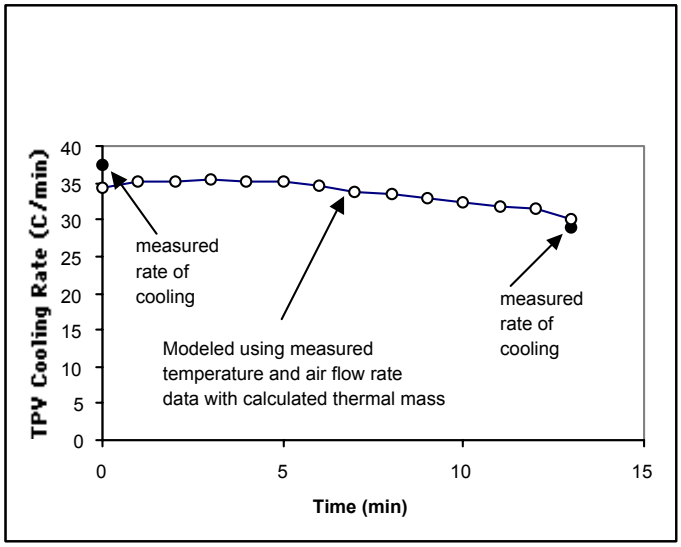

Figure 71. Comparison of Measured Generator Cooldown Data and Model Calculations

The next two important factors to be measured were the power delivered to the PV cells and the thermo-optical losses in the system. Under no-load conditions, these two factors encompass the electrical power converted by the PV cells, the waste heat in the PV cells, the energy absorbed in the filters, and the parasitic thermal losses in the gold-film reflectors throughout the evacuated quartz sleeve. There was no practical way to measure all these parameters discretely, however, we measured their aggregate sum by immersing the completely assembled TPV testbed system in the water bath calorimeter. Water was circulated in the bath by a pump that circulated one gallon per minute of water (measured by a flow meter) through an external air heat exchanger. By measuring the temperature rise of the known mass of the water bath surrounding the generator as well as the temperature drop in the heat exchanger at constant flow rate, it was possible to calculate the energy deposited by the generator. This energy, when no electrical load was applied to the PV cells, represented the aggregate sum of energy transmitted into the PV cells, into the gold-film reflectors, through cracks between filters, and all the other parasitic thermal losses in the system.

The blackbody spectrum at a given emitter temperature can be calculated. The resultant spectrum can then be multiplied by the measured spectral transmittance of the filter to determine the amount of energy transmitted from the blackbody spectrum through the filter as illustrated in Figure 72. The energy transmitted through the filter was calculated for different emitter temperatures as shown in Figure 73. The data were used to construct the curves shown in Figure 74. This energy transmitted by the filter is proportional to the current generated by the PV cells. The resultant in-band transmitted energy was then integrated with the measured cell spectral quantum efficiency and current-voltage performance data presented in 4.3 to yield theoretical power values for the cells as a function of blackbody, i. e., emitter, temperature.

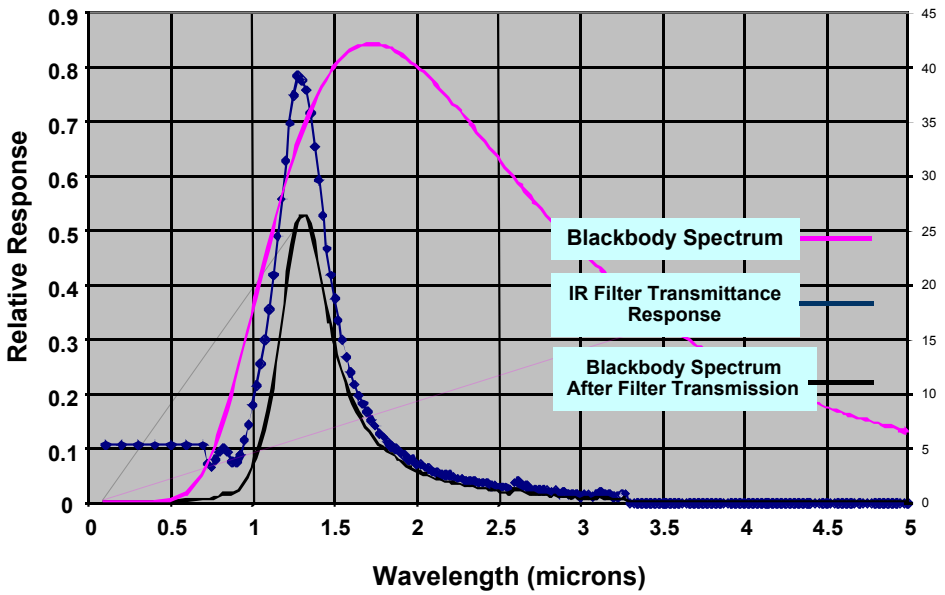

Figure 72. Illustration of Resultant Blackbody Spectrum After Being Transmitted Through the IR Filter

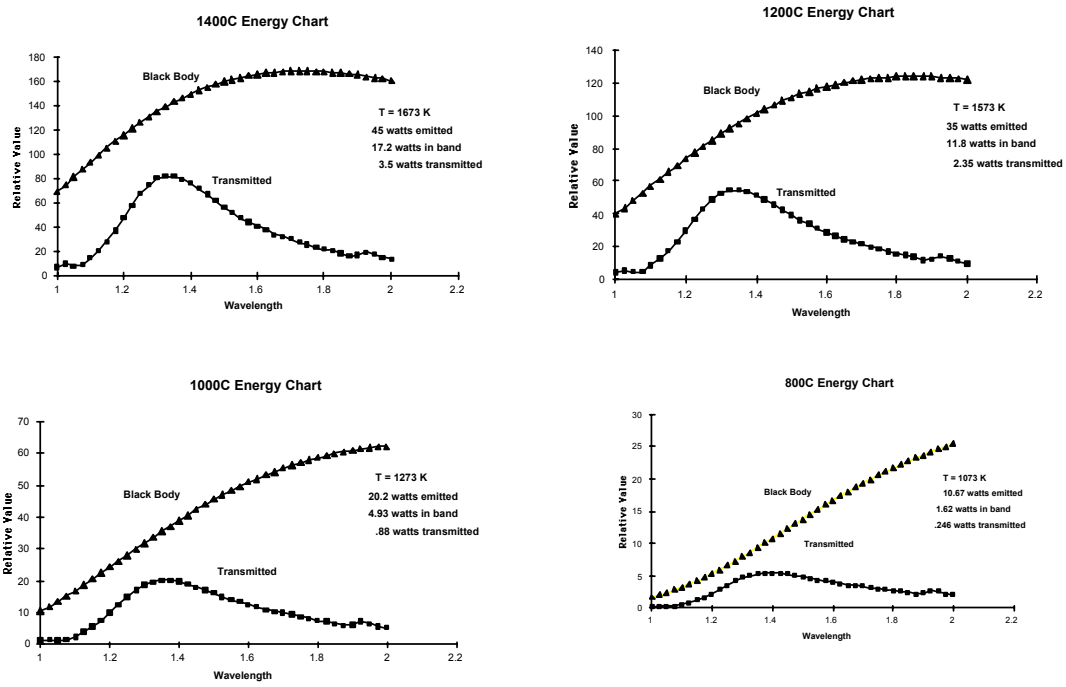

Figure 73. Summary of Energy Transmitted Through Filters From Blackbody Spectra at Various Emitter Temperatures

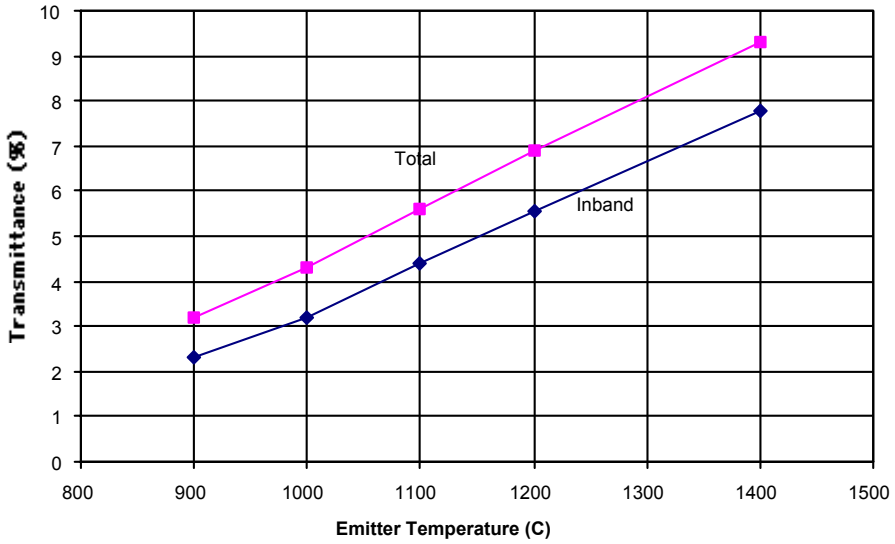

Figure 74. Summary of Transmitted Power Results Obtained From Integrating the Spectral Transmittance with the Blackbody Spectrum

The PV cells were arranged in 36 arrays or strings of six series-connected cells. During the testbed evaluation tests, leads were brought out from each of the 36 strings so that they could be measured individually Figure 75 presents a typical I-V characteristic for one of the six cell strings. The cells were monitored as a function of emitter temperature as the system warmed up to operating temperature. The power from the strings was then summed to obtain the total system power produced. Being able to monitor each string allowed us to evaluate the uniformity of the power produced over the surface of the emitter. This information will serve as a guide for determining the optimal pattern for connecting the strings into full arrays thereby obtaining maximum power in future tests. Figure 76 shows the power produced versus operating emitter temperature.

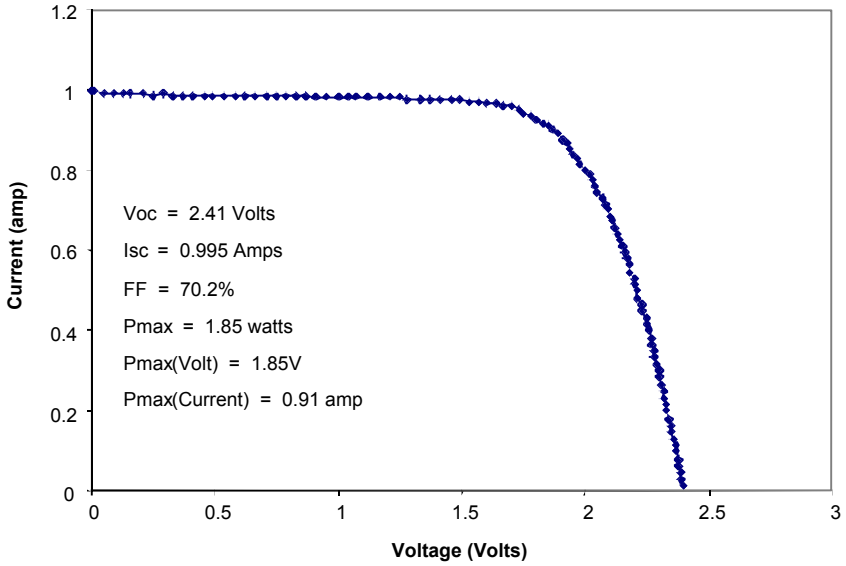

Figure 75. Typical Current Voltage Characteristic Measured for a Six Series-Connected PV Cell String in the Testbed TPV

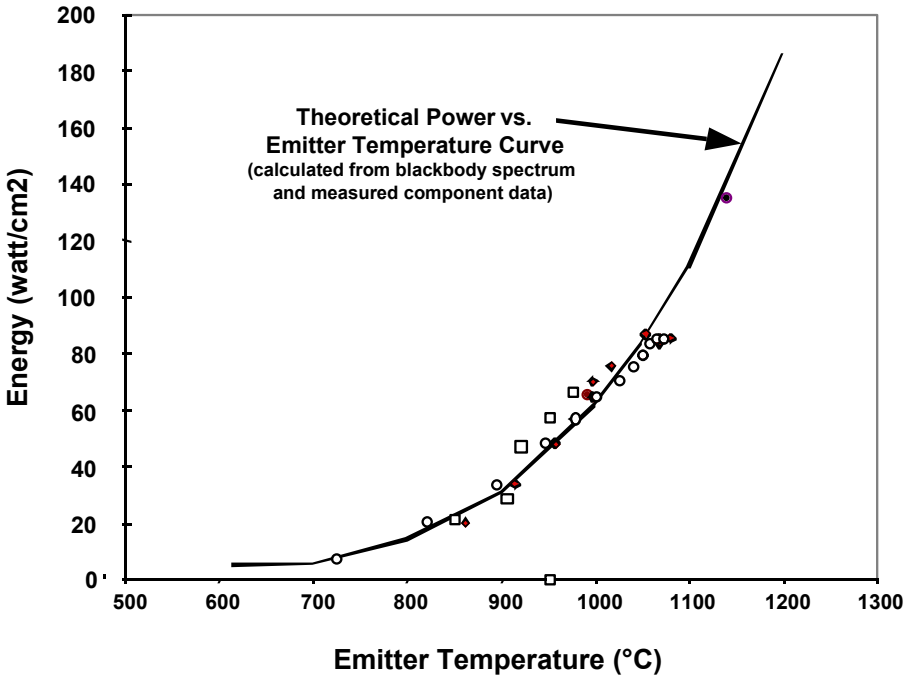

Figure 76. Comparison of Experimental Versus Theoretical TPV Power Performance

The remaining parameter needed to calculate the energy balance, and hence system efficiency for the testbed TPV system, is the energy expelled in the exhaust gas stream to the atmosphere. To determine the exhaust gas energy, three parameters are needed; the gas mass flow rate, the exit exhaust temperature, and the ambient air temperature. Thermocouples were used to measure the temperature of the exit exhaust and the ambient air. The gas mass flow rate was determined in two ways. In the first way, the percentage of oxygen in the gas stream was measured and correlated with the excess air above that needed for full combustion of the fuel, see Figure 77a. The amount of air needed to combust the fuel was a known quantity. With the percentage of excess air known, then the gas mass flow rate in the exhaust stream could be calculated. The second method of determining the exhaust mass flow rate was by measuring the vacuum created at the intake orifice to the combustion air fan. We used an air velocity meter in a plenum of known cross section to correlate the fan intake vacuum to the air flow volume as shown in Figure 77b. The airflow volume and density were then used to calculate the mass flow rate. These two methods yielded values that closely agreed; therefore, we conclude that we have sufficient accuracy in our measurement of the exhaust energy for purposes of our evaluation of the TPV testbed. In summary, we have two methods of determining the airflow volume in order to calculate the exhaust losses. These two methods are listed below:

A: Set excess air by measuring O2 percentage in exhaust

B: Determine air flow volume from empirical calibration chart

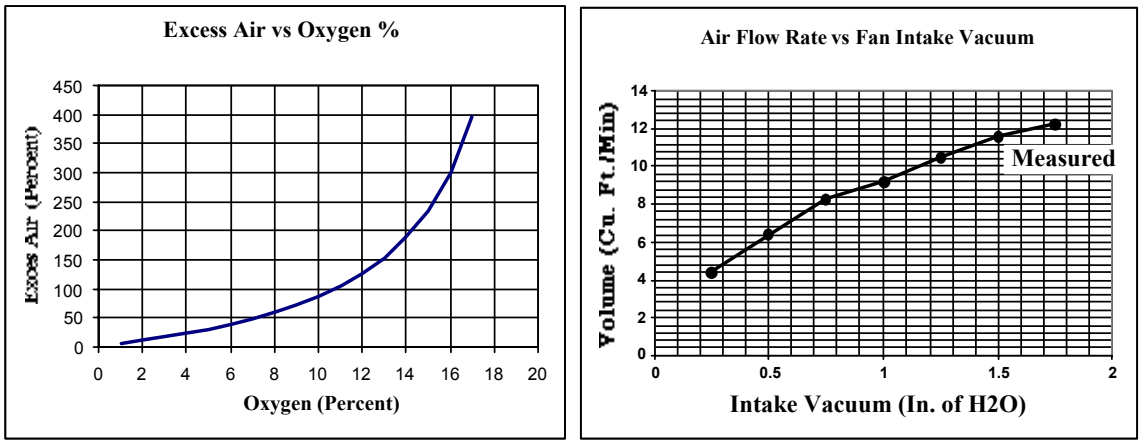

a) Excess Air versus Oxygen in Exhaust b) Combustion Air versus Intake Vacuum

Figure 77. Calibration Curves for Exhaust Gas Mass Flow Rate Determination

Finally, we have a category for unexpected losses in the system. These are losses that cannot be explained by the model parameters discussed above. When these unexpected losses occur, they must be identified on a case-by-case basis.

5.3. System Level Test Evaluation

Using the above model we began system level tests on the TPV testbed. The first problem that we encountered was that we were unable to operate the system at the 1400°C-design temperature. The limitation was that the glue that we had used to bond the filters to the inside of the outer quartz sleeve wall began outgassing at operating temperatures above about 1100°C. The subsequent loss in vacuum between the walls of the quartz sleeve resulted in thermal conduction across the gap giving unacceptable losses in the system. However, within the constraint of lower-than-expected operating temperature we conducted a test and evaluation program on the testbed.

The results of the electrical power measurements compared to expected values as a function of emitter temperature were presented in Figure 76. The power production over the temperature range was exactly as predicted from analysis of the performance data of the components. However, we had large unexpected losses that were not predicted by the model, see energy balance data in Table 6. In the case labeled run no. 3 in the table, the unexpected loss amounted to almost half the total input power. During the run radiant energy could be seen escaping from the domed region at the end of the quartz sleeve and from the recuperator. The gold reflector on the inside surface of the outer wall of the quartz sleeve had not adhered well. During the installation of the filters a large portion of the gold film that should have been around the recuperator section was rubbed off. Further, during the acetone rinse required to remove protective plastic coatings from the filters, a large fraction of the gold film in the domed end was removed. It was postulated that replacing the gold film would eliminate the extraneous parasitic losses. Unfortunately, we could not re-deposit gold into the domed end region with the filters in place. We did re-deposit the gold in the recuperator end. A subsequent run, labeled run no. 1 in the table, was made and the extraneous losses were reduced by about 350 watts. We then glued aluminum foil into the domed end to replace the missing gold film. While the aluminum foil was not as good a reflector as the gold film, it did reduce the extraneous losses by about 500 watts. Further inspection after the run revealed that the aluminum foil had curled at one point and was touching the inner quartz sleeve creating a conductive thermal shunt across the vacuum gap. We then proceeded to remove the thermal shunt and to take several other steps such as vacuum baking the system to outgas the adhesive used to bond the aluminum foil in place and remove any opportunity for thermal conduction across the vacuum gap. Figure 78 summarizes the results of these efforts.

Table 6. Energy Balance For Three Tpv Testbed Run Conditions

Run No.	Energy into thermal mass	Energy exhausted to air	energy into coolant	Total energy into system	Energy in fuel burned	Energy expected into coolant	Discrepancy	Comment
3	300	849	2461	3610	3760	876	1585*	Poor Gold Reflector
1	0	1351	2100	3451	3364	876	1224	New gold around recuperator end
2	341	1714	1583	3638	3760	876	707	Aluminum foil glued into domed end**

* Discrepancy far exceeds tolerance of design errors

* Suspect that there is a shunt between inner and outer sleeve created by aluminum foil

Conclusion: We believe that the descrepancy can be eliminated by refurbishing gold coating

Efficiency at 876 watts into coolant would be 10.5% at 1150 C

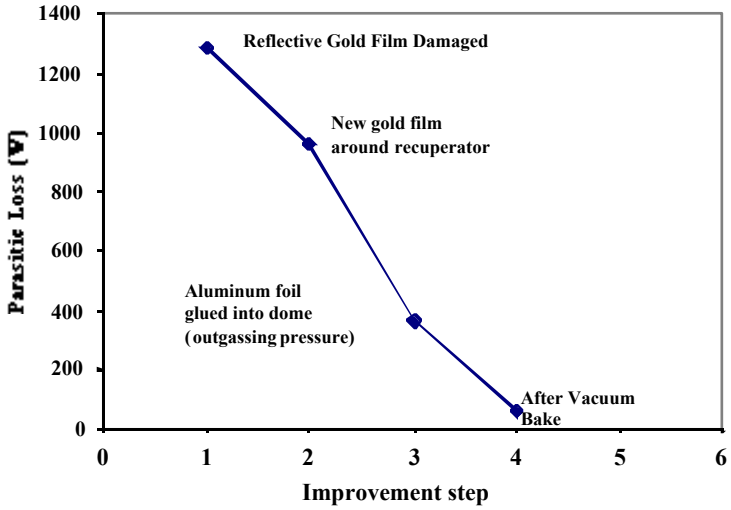

Figure 78. Unexpected Non-Cavity Related Parasitic Losses Versus Improvement Steps

Based on the results from run no. 2, shown in Table 6, the fuel-to-electric efficiency was projected to be approximately 10.5% at 1150°C. This result is in agreement with our model projections. The model further projects that at 1400°C the efficiency will be approximately 15%.

At this point in the evaluation program, Brookhaven National Laboratory (BNL) personnel came to EDTEK to instrument the burner and evaluate the performance of the nozzle and recuperator. Table 7 presents typical thermal balance data from one of the thermal evaluation runs performed by BNL.

Table 7. Typical Thermal Balance Results

TEST INFORMATION	
Test Date	4/13/00
Start Time	3:30 PM
End Time	4:50 PM
Duration	80 Minutes
ENERGY INPUT	
Average	2775 watts
Last 15 minutes	2419
BURNER DATA	
Air preheat	704 C
Chamber discharge	983 C
Top Exhaust	355 C
Excess air	81.8%
Exhaust energy	682 watts
ENERGY INTO CALORIMETER	
From external heat exchanger	1606 watts
From overall heat balance	1737 watts
From chamber heat balance	1708 watts
RECUPERATOR EFFECTIVENESS	69.4%

BNL performed may test runs on the unit at temperatures up to 1150°C. From these tests they made the following conclusions:

1. Temperature around the circumference of the unit is good.
2. Gas temperature leaving the chamber/emitter area is lower than expected.
3. Longer run times than previously made are required to complete good heat balance.
4. Recuperator effectiveness is lower than expected, i.e., 69% versus 80%. The top end exhaust divider doesn't contribute to effectiveness.
5. The next set of performance tests should wait for completion of the improved design.
6. The energy loss to the cooling fuel is low, on the order of 50 watts, as predicted.

As mentioned earlier, BNL made many thermal runs to ~1150°C emitter temperature during their evaluation. As these runs progressed it was noticed that the parasitic losses into the

coolant were increasing above those expected from the model and the power out of the cells at a given emitter temperature was dropping. Every surface was inspected and found to be in good condition except that evidence of glue migration from the cracks between the filter substrates onto the surface of the filters was observed. It was postulated that the glue, having a refractive index greater than vacuum (i.e. >1), might have shifted the resonant frequency of the filters to longer wavelengths. This shift would result in more energy being transmitted from the blackbody spectrum with a drop of power in the cells because the energy would be out of band to the cells.

A fixture was prepared that allowed us to measure the spectral transmittance of the filters through the quartz sleeve wall. We found that the resonant frequency had indeed shifted as illustrated in Figure 79. Thirty-six of the filters were measured and found to have shifted a comparable amount. Figure 80 shows the effect of the shift of the resonant frequency to longer wavelength on the energy transmission from a blackbody spectrum. Figure 81 shows the effect of the frequency shift on the cell response.

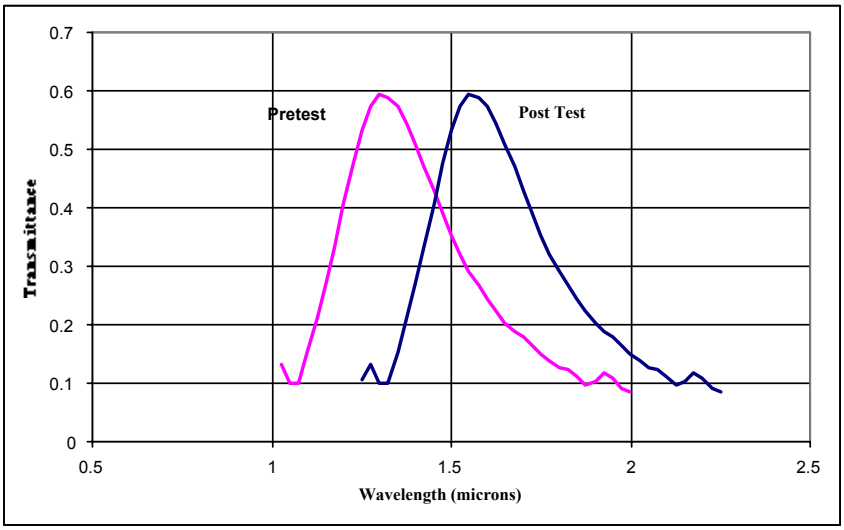

Figure 79. Spectral Characteristics of Filters Before and After Burner Tests

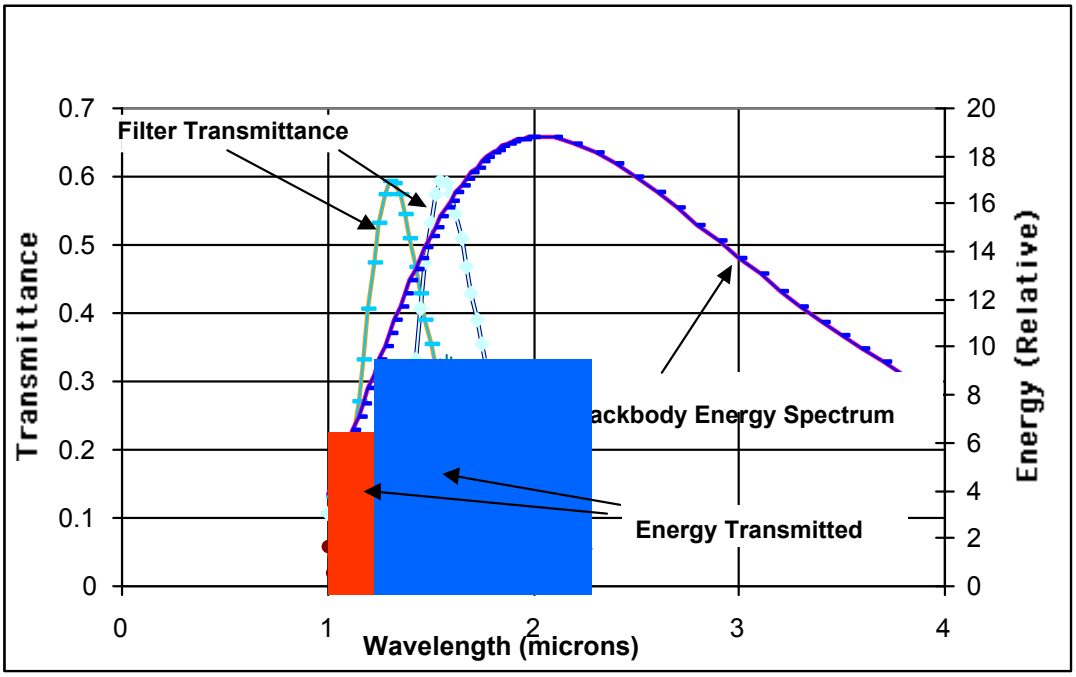

Figure 80. Illustration of the Effect of Resonant Frequency Shift on Thermal Energy Transmitted

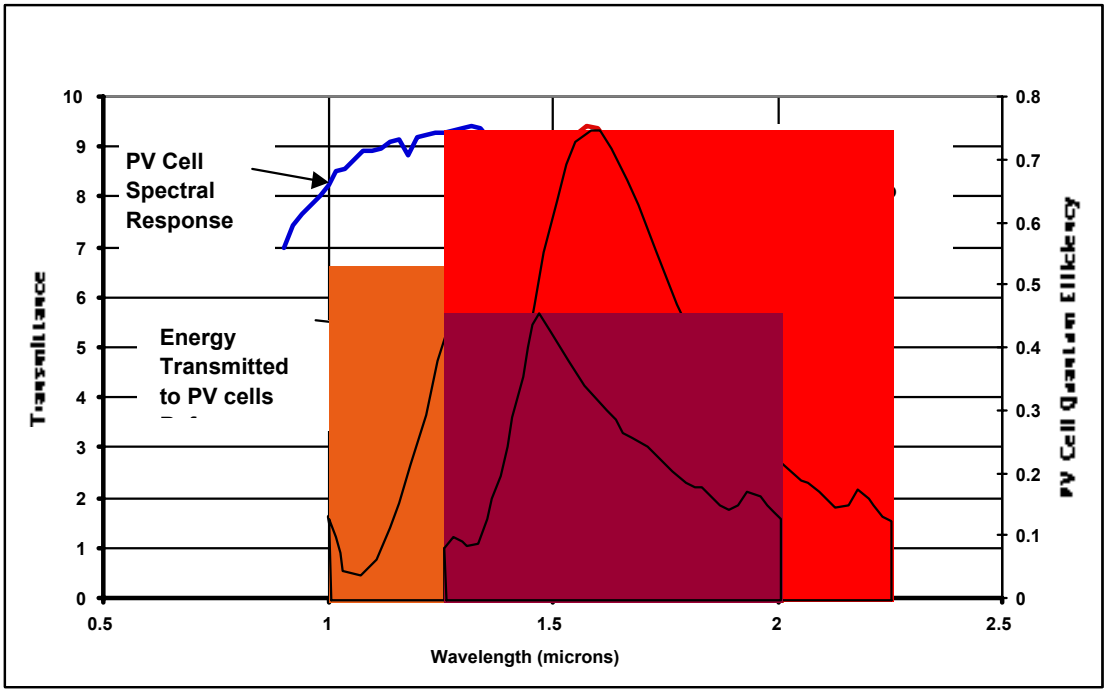

Figure 81. Illustration of the Effect of Resonant Frequency Shift on PV Cell

It was confirmed that the adhesive contamination on the surface of the filters had shifted their resonant frequency. This, for practical purposes, ended the usefulness of this testbed unit.

Never the less, many useful lessons have been learned and conclusions can be drawn from the experience with the TPV testbed unit. A typical energy balance from one of the last test runs was presented in Table 6. A summary of the electrical performance during one of the test runs with contaminated filters is presented in Table 8. In addition this table has performance projections that would be expected for a refurbished unit with gold coatings instead of aluminum foil in the dome and uncontaminated filters. The model prediction for the performance of both the current unit and a refurbished unit at 1150°C and 1400°C emitter temperature is also presented. The measured efficiency at 1150°C with the frequency-shifted filter is 6.1%; however; based on our experimentally confirmed model, the efficiency is projected to reach 14.1% with a refurbished unit at 1400°C.

The preceding set of testbed evaluation tests have suggested several design improvements for the next generation advanced testbed unit which will allow it to reach the 1400°C operating temperature. Lessons learned during the filter development phase have suggested improvements in the filter that should permit our exceeding 16% efficiency. The advanced-design, which incorporates these design improvements, will be discussed in 5.0.

Table 8. Summary Of The Demonstration Testbed Performance And Analysis

Summary of Demonstration Testbed Performance and Analysis					
	FREQUENCY SHIFTED FILTER	ORIGINAL FILTER			
				(Aluminum foil replaced)	
	(1150°C)	(1150°C)	(1400°C)	(1150°C)	(1400°C)
EMITTER/FILTER/PV CELL ZONE					
Absorption in gold film	292 Watts	292 Watts	558 Watts	292 Watts	558 Watts
In-Band transmittance	295 Watts	515 Watts	1249 Watts	415 Watts	1249 Watts
Out-of-band transmittance	454 Watts	109 Watts	244 Watts	109 Watts	244 Watts
Leakage per cracks between substrates	106 Watts	106 Watts	202 Watts	106 Watts	202 Watts
DOMED END ZONE					
Absorption in uncoated end around evacuation port	129 Watts	120 Watts	243 Watts	2.3 Watts	4.1 Watts
Absorption in aluminum foil	201 Watts	201 Watts	304 Watts	50 Watts	152 Watts
RECUPERATOR ZONE					
Absorption in aluminum foil	53 Watts	53 Watts	106 Watts	27 Watts	53 Watts
Absorption in gold film	103 Watts	103 Watts	206 Watts	103 Watts	206 Watts
Total energy transmitted to coolant	1633 Watts	1408 Watts	3112 Watts	1104 Watts	2668 Watts
Total energy transmitted to coolant as measured by calorimeter	1606 Watts				
ENERGY IN EXHAUST*	198 Watts	182 Watts	402 Watts	182 Watts	345 Watts
TOTAL ENERGY INTO SYSTEM	1805 Watts	1590 Watts	3514 Watts	1286 Watts	3013 Watts
ELECTRICAL					
Power out	110.3 Watts	141 Watts	425 Watts	141 Watts	425 Watts
SYSTEM PERFORMANCE					
Oil-to-electric efficiency	6.1 %	8.86 %	12.09 %	10.96 %	14.1 %

5.4. Advanced Test-Bed Fabrication, Test, and Evaluation

Building on the experience gained in the first series of system level tests, an improved design for an evacuated thermal control sleeve was designed and fabricated. This unit has been described in 3.4. Additionally, the dipole filters were replaced by the higher throughput tripole filters discussed in 4.1. New PV cell arrays were fabricated using more optimized cells discussed in 4.3 which yielded about 10% more power out for a given light intensity. The 54-cell arrays used in the former unit were replaced with single column 9-cell arrays as was illustrated in figure 3-14. This change allowed the removal and repair of single columns of cells if necessary and facilitated better alignment of the arrays with the emitter.

This unit was assembled and tested both with and without the electrical converter subsystem. The test without the electrical subsystem was discussed in 4.6. It showed that if the filter substrates were kept cool, the new sleeve design could operate at emitter temperatures as high as 1500°C. Having completed these tests and confirmed the adequacy of the new evacuated thermal control sleeve, we assemble the electrical converter subassembly onto the test unit and proceeded with testing it Figure 82 shows a photograph of this test unit. Note that it has wiring harness for monitoring each of the 36 six-cell strings just as the first converter did.

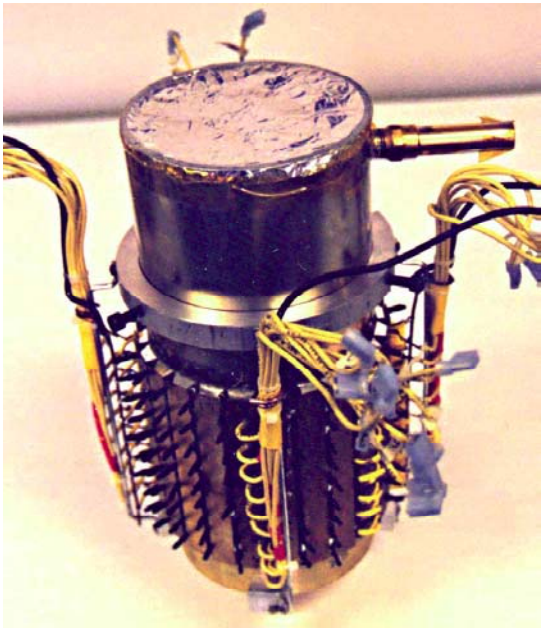

Figure 82. Advanced TPV Testbed Unit Assembled for Calorimeter Testbed Testing

The results of the testing were analyzed in a manner similar to that discussed for the preceding unit in 5.2. Figure 83 presents the output power results compared to emitter temperature. As can be seen, the output of the generator is following the theoretical curve calculated from the filter, blackbody, and PV cell characteristics very closely. At the highest temperature, the electrical efficiency is approximately 10.85% compared to about 5% at 1000°C. The efficiency increases with increasing emitter temperature because the amount of in-band energy increases relative to the parasitic losses in the system. Thus, we can project from the relative amount of in-band energy transmitted at 1400°C versus parasitic losses that the efficiency will be about 15% at 1400°C.

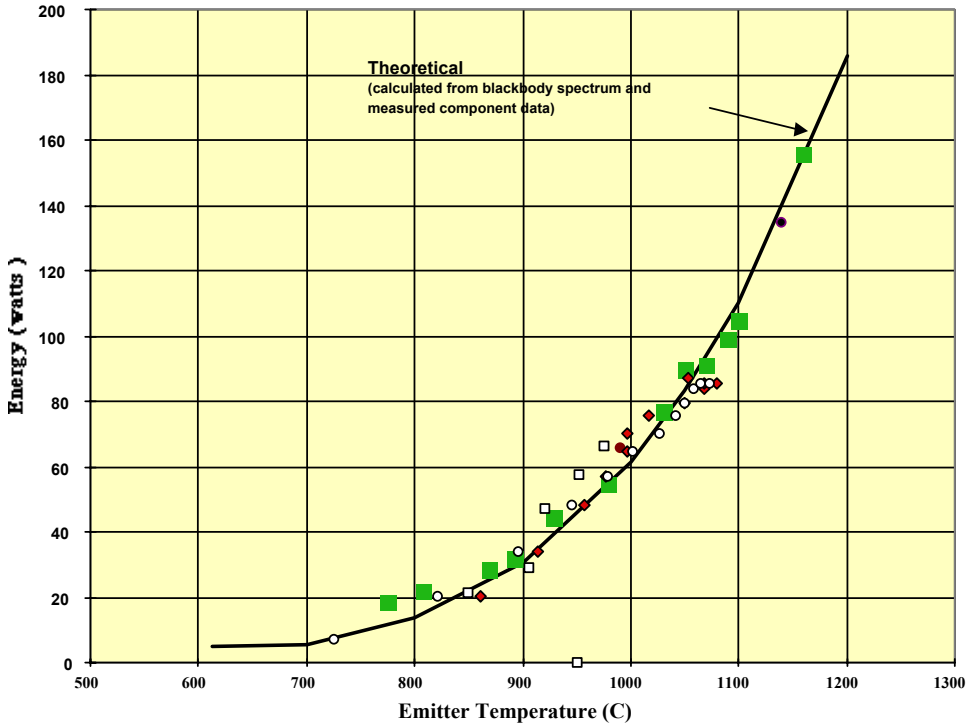

Figure 83. Electrical Power Out of Advanced TPV Versus Emitter Temperature

Unfortunately, at this point in the test program, an operator error, i.e., failure to open the vacuum valve to the evacuated sleeve allowed the system to overheat and the test device was damaged beyond further meaningful testing.

6.0 Solar Tpv Generator Development

6.1. Solar TPV Proof-of-Concept Experiment

The basic concept to be used for the proof of concept solar TPV evaluation uses a small, 10-inch diameter cassegrainian type solar concentrator to direct sunlight into an elliptical optical imaging TPV cavity. Neither the concentrator nor the cavity design are optimized designs but simply are used as a testbed vehicle to evaluate and experimentally verify the functional performance of the newly developed TPV filter/cell technology for solar energy conversion applications. The remainder of this section describes each element of the testbed, presents experimentally measured performance data for each critical element, and incorporates physical modeling and analysis of the experimental data.

6.1.1. Solar Concentrator

The solar concentrator to be used in the evaluation is a small, cassegrainian system having a 10-inch primary parabolic dish and a 1.5-inch secondary hyperbolic reflecting lens. The concentrator is illustrated in the photograph of Figure 84. It has a 2-axis tracking system based on a two-stage sensor system mounted on the sun side of the secondary reflector suspension system. The first stage of the solar tracking detector consists of four small 5mm x 5mm GaAs photovoltaic cells located every 90 degrees around the periphery of the sensor. These cells provide coarse tracking and are used primarily to acquire the sun. Once the concentrator is pointed nominally at the sun, the second sensor stage takes over. The second stage consists of a four-quadrant silicon detector mounted at the base of a collimator tube. The collimator tube defines the solar tracking accuracy. The current unit has an accuracy of ±0.1 degree about the solar axis.

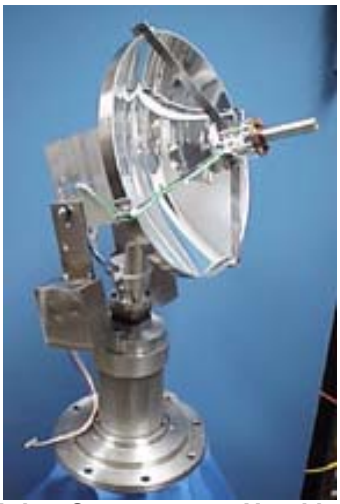

Figure 84. Photograph of Cassegrainian Concentrator Used in STPV Proof-of-Concept Evaluation

Calibration of the testbed solar concentrator consisted of two steps, 1) a calorimetric measurement of the absolute solar power directed to the focal point of the cassegrainian system, and 2) establishing the relationship between this absolute energy measurement and the short circuit current of one of the GaAs cells used in the first stage of the solar tracking sensor system discussed above. In order to make the absolute power measurement a small calorimeter was designed and fabricated so that it could be fitted into the focal region of the concentrator instead

of the testbed solar TPV receiver. The calorimeter consisted of a copper block of known weight and specific heat, a deep, high aspect ratio hole was drilled in the block to intercept and capture the concentrated solar power. The inside of the hole was also painted black in order to enhance its trapping capability. A type "E" thermocouple was attached to the base of the copper block and the entire unit was then encased in a Styrofoam insulating jacket. Figure 85 shows the measured results of a typical calibration run with the testbed system. Using the average rate of heating of the copper block (the energy loss through the Styrofoam insulation is negligible over the measurement period), the copper's measured weight, and published data for its specific heat, the absolute energy into the unit could be calculated. A typical value for these measurements was 16.6 watts. This energy input value of 16.6 watts corresponded to a short circuit current value of 2.75 mA on one of the GaAs detector cells. The short circuit current of this detector cell, so calibrated was then used as monitor of input power level during the testbed evaluation tests.

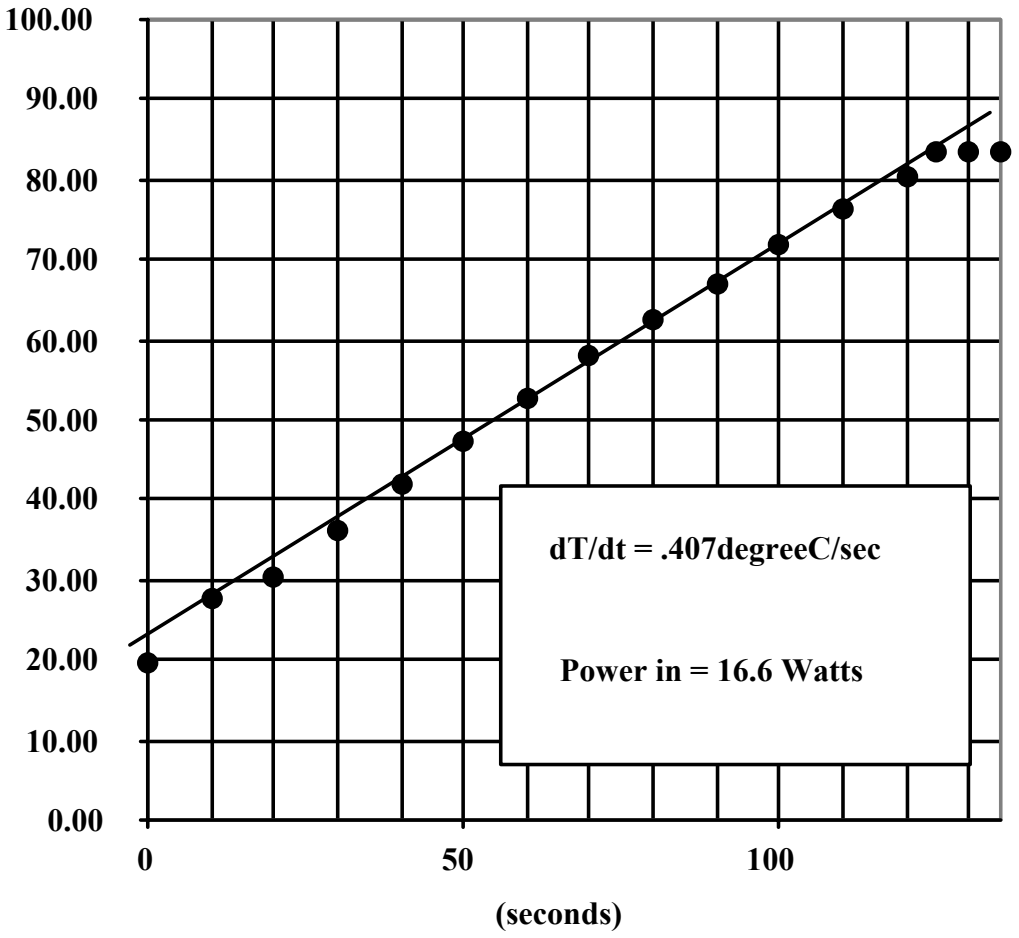

Figure 85. Calorimeter Measurement of Solar Energy Input to the TPV Cavity

6.1.2. TPV Proof-of-Concept Receiver

The proof-of-concept solar TPV receiver consists of an absorber/emitter, an optically imaging cavity, and an array of filtered PV cells. The absorber emitter is so called because it first must absorb the incoming solar energy and then emit it as infrared energy having a lower temperature gray body spectrum (longer wavelength) than the sun. The cavity is considered to be optically imaging because it has an elliptical shape with the absorber/emitter located at one of the focal points of the ellipse. The filter forms a planar surface at the midpoint between the two foci of the ellipse so that the absorber emitter always "sees" an image of itself being reflected by the filter plane. Radiation emitted from either side of the absorber emitter is directed either directly onto the filter plane or is reflected onto it after a single reflection from the elliptical cavity wall. Radiation striking the filter plane is either transmitted through the filter or is reflected back to the absorber emitter. The optical elements collect the radiation transmitted through the filter and direct them onto PV cell. Each element of the proof-of-concept receiver is described and its physical properties and/or performance evaluated in the following sections.

The proof-of-concept TPV cavity consists of an elliptical cavity having an absorber/emitter located at a focal point of the ellipse and a filtered PV array located on a plane at the midpoint between the two foci of the ellipse. The configuration used for modeling is illustrated in Figure 86. In order to evaluate the thermo-optical performance of the cavity a three-dimensional ray tracing model was developed using the measured parameters for each element within the system as presented in the preceding sections. The model allows rays to be emitted from a user-defined grid of points covering the surface area of both sides of the absorber/ emitter disk. The rays angles of emission with respect to the normal to the absorber/emitter surface is determined by a cosQdΩ probability distribution. Figure 87 shows a three-dimensional view of a group of rays emitted from various locations on the emitter surface and traced throughout the cavity. The blackbody distribution is used to determine the energy, or frequency, of the emitted rays. For example, a group of rays is released corresponding to each of a series of pre-selected intervals of energy, or wavelength covering the entire spectrum of interest. The relative number of rays in each interval is determined by the blackbody distribution. The rays for each energy interval are then allowed to interact with the surfaces they encounter according to the spectral absorptance, transmittance, or reflectance of that surface. Each surface has its characteristic absorption, transmittance, and reflectance properties supplied as input parameters to the model. Absorbed energy is accumulated for each interactive surface. Thus, energy is traced through the system until it is either transmitted into the cells, absorbed in the cavity walls, lost through the cavity aperture, or is reabsorbed in the emitter. This completes the thermo-optical model of the system. In addition to tracking the energy deposition, or absorption in the cell-filter surface, the spatial absorption in the filter and transmission of energy to the PV cells, over the surface of the cell-filter area is also determined. Figure 87 shows the spatial distribution of these rays as they strike the filter-cell area at the base of the elliptical cavity. The spatial distribution of energy is determined as a function of X and Y coordinates and is stored in spreadsheet form to assist in the electro-optical optimization of the system. This information assists in the design and optimization of the PV cell layout in the converter array. The electrical performance of the TPV cavity is calculated by entering the energy transmitted into the cells as a function of frequency, or wavelength, into a model of the cell which integrates over the measured spectral response of the cells to determine short circuit current. The short circuit

current is then multiplied by measured open circuit voltage and fill factor parameters measured for the cells to calculate maximum power out for the cells. Cavity efficiency is then defined as maximum power out of the cells divided by the total solar energy absorbed by the absorber emitter and radiated into the cavity as infrared energy.

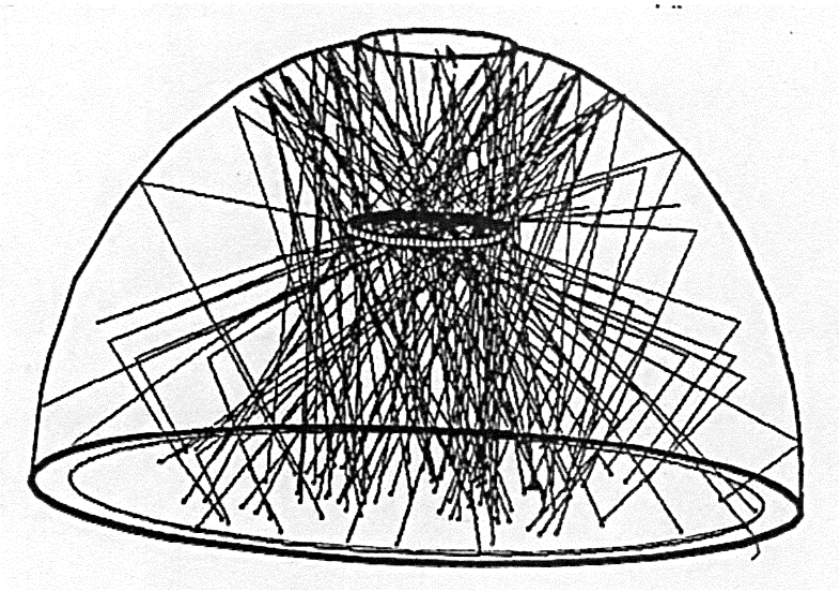

Figure 86. TPV Cavity Geometry Used in Three-Dimensional Modeling

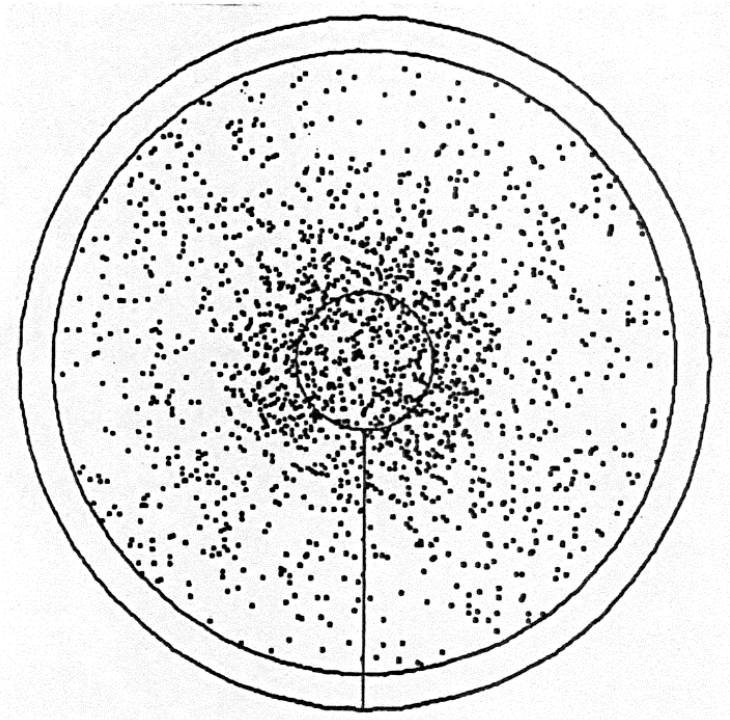

Figure 87. Spatial Distribution of Rays Striking Surface of the TPV Filter

To limit conductive and convection losses from the absorber emitter and to prevent oxidation of the emitter, the test bed TPV cavity must be evacuated. In order to evacuate the test bed TPV

cavity, a window must be placed over the entrance port through which the solar energy is directed to the absorber/emitter. Therefore, a sapphire window was placed over the port with an "O" ring seal. The spectral transmittance of the sapphire window was measured to be about 86% over a wavelength range encompassing the solar spectrum. The two interfaces between the sapphire window and the air on one side and the vacuum on the other give rise to a total of about 14% attenuation of the solar energy. The attenuation is the result of reflections at the interfaces because of the mismatch between the optical indices of air, sapphire, and vacuum respectively. Thus, the energy actually directed onto the absorber emitter is typically about 16.6 watts x 0.86 or 14.3 watts.

The absorber emitter must be made of a material that is highly absorbing to sunlight as well as having good emittance in the infrared. The material must also be able to withstand high temperatures with low outgassing under vacuum. The material selected was tungsten. The measured spectral characteristics of the tungsten surfaces are presented in Figure 88 as function of angle of incidence. As can be seen from the normally incident data, the solar energy, which is very nearly normally incident is absorbed with an efficiency of about 90%. At the same time, the emittance of the surface to omnidirectional graybody radiation of ~1400 K is about 0.5 corresponding to an angle of incidence of 45 degrees where most of the graybody energy is emitted on average. Thus, the values used for evaluation of the system was solar absorption of 90% and thermal emittance of 0.5

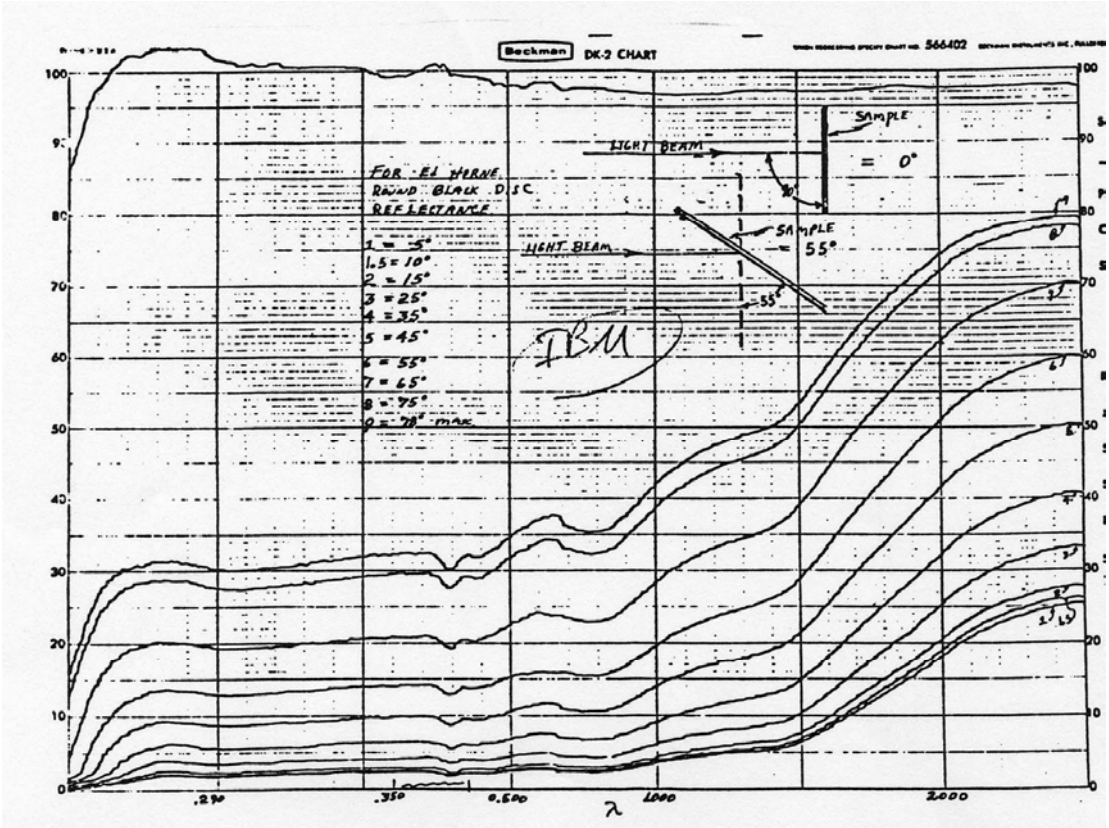

Figure 88. Spectral Reflectance of Dendritic Tungsten Surface as a Function of Angle

A GaSb optimized resonant mesh infrared bandpass filter, low-bandgap GaSb PV cells, and coupling elements have been developed on other programs at EDTEK. The goal of this effort is to design a solar TPV experiment using these components. A basic cell-filter array layout was designed. The second design consists of four 15.7 mm x 15.7 mm optical elements coupled with four 11.5 mm x 11.5 mm PV cells. The PV cells have 10 mm x 10 mm active areas surrounded by 1.5 mm side busbars on all sides. Each of the cells will see the same flux by symmetry so that we can again use a series string of four cells. Unfortunately, the light intensity across each cell will vary so that the same equalizing of voltage that occurred at the array level in the first design will occur at the cell level in this design. The array does offer considerable simplification of design. The optical elements also concentrate the light onto the cells by as shown by the measured data presented in Figure 89 which increases the voltage and hence the conversion efficiency of the cells by about 10% overall. The unilluminated areas between cells offer convenient space for cell interconnections without parasitic losses. Based on these considerations, the second array design was chosen for use in our experiment.

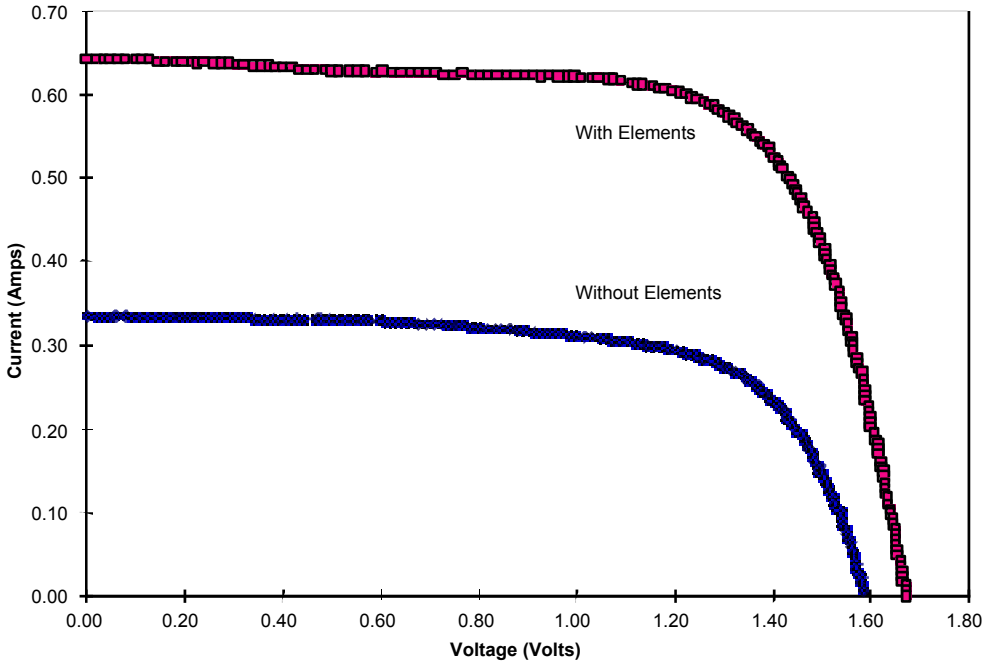

Figure 89. Measured Performance of GaSb PV Cells With and Without Concentrating Elements

6.2. Fabrication and Assembly of Test-Bed Solar TPV

The elliptical cavity was machined from brass. The inside wall of the cavity is coated with vapor deposited silver for maximum reflectance of incident infrared rays. Figure 90 and Figure 91show photographs of the front solar entrance window and the inside of the elliptical cavity. The absorber emitter is suspended at the focal point of the ellipse by four small (3-mil) diameter wires emanating radially from the cavity wall. A tungsten/rhenium thermocouple is spot welded to the underside of the dendritic tungsten absorber/emitter. The thermocouple is attached to the side of the absorber emitter facing away from the sun to avoid erroneous readings for the absorber/emitter temperature. The tungsten absorber being located at the focal point of the elliptical cavity results in emitted energy being reflected from the walls of the cavity to the base of the cavity onto a resonant mesh infrared band pass filter.

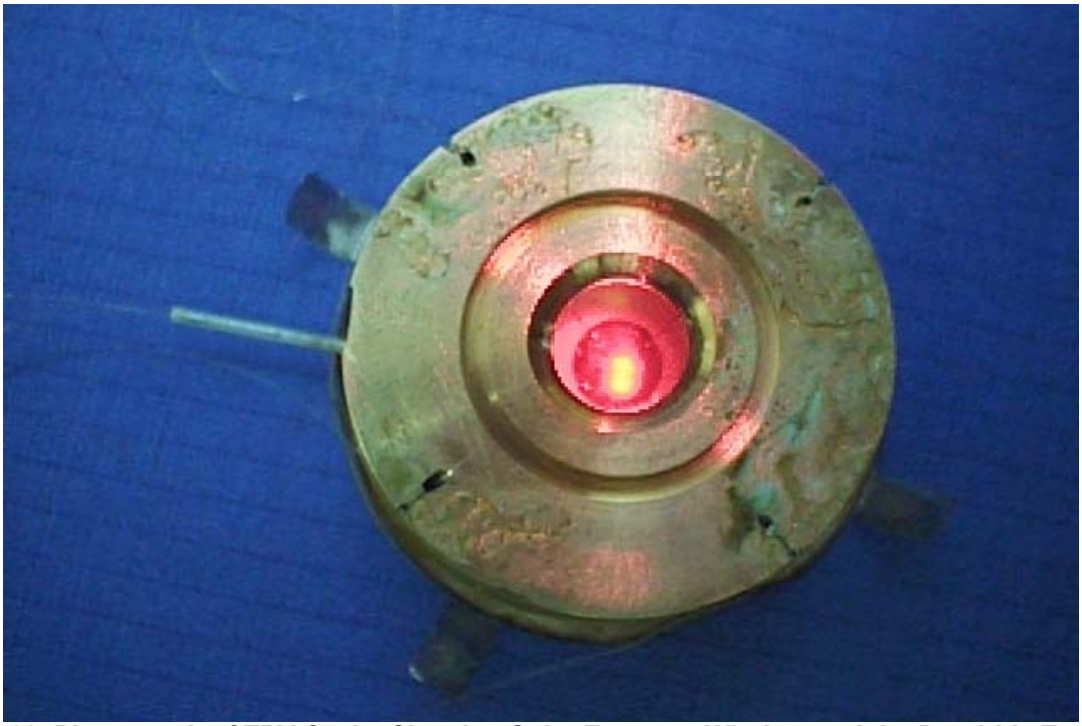

Figure 90. Photograph of TPV Cavity Showing Solar Entrance Window and the Dendritic Tungsten Emitter Illuminated by a HeNe Laser Beam

Figure 91. Photograph of TPV Cavity Showing the Dendritic Tungsten Emitter/Absorber, Tungsten Suspension Wires, Tungsten/Rhenium Thermocouple, and the Reflective Walls of the Elliptical Cavity

A resonant mesh infrared band pass filter was placed at the midpoint between the two foci of the ellipse. The band of energy transmitted by the filter is directed into an array of concentrating elements to which the filter substrate was glued. The performance of the elements was measured by testing the current-voltage characteristics of the PV cells before and after their application. By comparison of wavelengths of the transmitted rays to the spectral response of the GaSb PV cells, the transmitted energy is optimum for conversion to electricity by the cells. Further, the filter reflects the incident out-of-band energy which the cells cannot convert to electricity away with broadband reflectance of >98%. Since the filter plane is located at the midpoint between the foci of the elliptical cavity, the out-of-band energy reflected by the filter is directed immediately back to the tungsten absorber where it is reabsorbed to maintain the equilibrium temperature of the absorber/emitter. The cells are laid up on a printed circuit formed by etching copper film that is laminated onto a ceramic substrate as can be seen in the photograph of Figure 92. Finally, the TPV cavity is sealed by "O" rings and evacuated for testing.

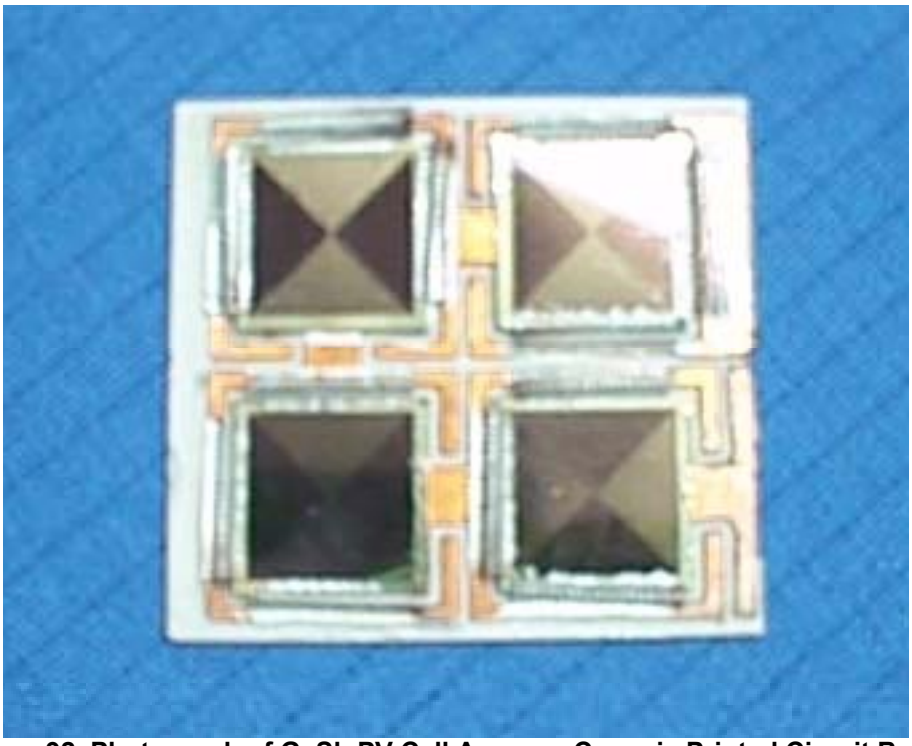

Figure 92. Photograph of GaSb PV Cell Array on Ceramic Printed Circuit Board

Cooling for the PV cells is provided by a heat sink and blower fan that is bonded to the back of the cell array with thermally conductive epoxy.

The fully assembled TPV cavity is mounted to the back-side of the primary reflector in a cassegrainian type solar concentrator which was shown in Figure 84. The primary concentrator dish is 10 inches in diameter while the elliptical TPV cavity is 1.4 inches in diameter. The dish has a 2-axis tracking drive with the tracking sensor mounted on the sun side of the secondary lens in the cassegrainian system.

6.3. Experimental Testing of GaSb Based Solar TPV System

The primary objective of these experiments was to confirm the modeled performance of the filter/cell converter module and, thus, verify the model as a design tool. The cavity used to provide the radiant energy input for this evaluation was far from optimal. The cavity had originally been constructed for use in a space vacuum chamber without a solar entrance port window. For this test it was necessary to add a window to seal the cavity; however, the geometry of the cavity did not allow for a high conductance vacuum line to the vacuum pump so that a high vacuum could not be attained in the cavity. It was beyond the scope of this effort to fabricate a new cavity. Thus, the cavity was evacuated several times and purged with nitrogen to eliminate oxygen effects on the tungsten emitter and the pressure allowed to remain relatively high in the cavity. The vacuum attained was on the order of 0.01 Torr which was not sufficient to eliminate gas convection/conduction from the emitter to the cavity walls. The purpose of the initial tests was to determine and differentiate the optical and thermal performance of the cavity. The optical performance of the elliptical TPV cavity and its effectiveness at transferring radiant energy to the cavity base has been modeled as discussed earlier. The thermal performance of the cavity is determined by two factors, the conduction from the emitter to the cavity walls due to the suspension wires that hold the emitter at the focal point of the ellipse and the convection/conduction transfer of energy from the emitter to the cavity walls due to the imperfect vacuum pressure inside the cavity. Thus, the evaluation of the cavity is complicated by several factors. Equation 6-1 expresses the energy balance inside the cavity.

(6-1)

$$Q_{solar}[T_{win}] = E_{rad}[1-R_w] + E_{rad}[T_f] + kA[T_e-T_w]/L + h_{(Te)}[T_e-T_w]$$

Where:

Q_{solar}	=	Solar energy delivered to cavity entrance window by the concentrator
T_{win}	=	Cavity entrance window transmittance
E_{rad}	=	Energy radiated by the emitter
R_w	=	Cavity wall reflectance
T_f	=	Filter transmittance
k	=	Thermal conductivity of tungsten emitter suspension wires
A	=	Cross sectional area of tungsten emitter suspension wires
L	=	Length of tungsten emitter suspension wires
$h_{(Te)}$	=	Convection/conductance coefficient of gas partial pressure in cavity
T_e	=	Emitter temperature
T_w	=	Cavity wall temperature

Since all of these factors tend to complicate the evaluation of the filter/PV cell converter, a series of simple experiments were performed which eliminated all the non-radiation

components from the measurement. The cavity performance was first measured with a vapor deposited gold reflector at the base instead of the filter/PV cell converter. A second measurement was then made with the filter/PV cell converter in place. The difference in emitter temperature observed between these measurements is due to the energy transmitted into the PV cell converter by the filter.

The emitter temperature was the primary parameter of interest in these tests. Figure 93 shows data for two typical runs, one with the reflective base only and one with the filter and PV cell array in place.

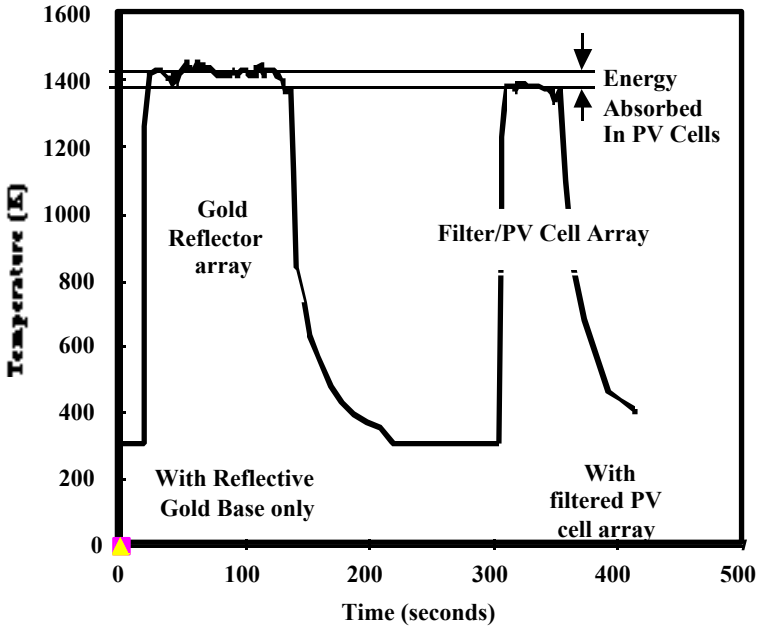

Figure 93. Measured Emitter Temperature as a Function of Time and Solar Input Energy With Gold Reflective Base Only and With Filter/PV Cell in Place

Other pertinent parameters measured either prior to or during these tests are listed below:

Incident solar intensity
Concentrator efficiency
Cavity entrance window transmittance
Solar absorption of dendritic tungsten absorber
Thermal emittance of dendritic tungsten absorber
Temperature of dendritic tungsten absorber
Cavity wall reflectance
Cavity base reflectance
Cavity vacuum pressure
PV cell short circuit current, I_{sc}
PV cell open circuit voltage, V_{oc}
PV cell fill factor
PV cell temperature

Figure 94 shows a comparison of measured electrical power out versus emitter temperature for the solar TPV cavity as well as data collected from a diesel fueled TPV system developed on a DoD program. The measured data from these tests are superimposed on a theoretical curve constructed by multiplying the theoretical graybody emittance curve by the specular transmittance of the TPV filter and the PV cell electrical efficiency at the resonant wavelength of the filter transition band. This model is expressed mathematically by:

$$P_{out} = E \times A \times [BB[T^4_e - T^4_w] \times [T_f(\square W)] \times I_{sc} \times V_{oc}/V_{bg} \times FF$$

Where:

E = Graybody thermal emittance
BB = Boltzmann's constant
W = Wavelength

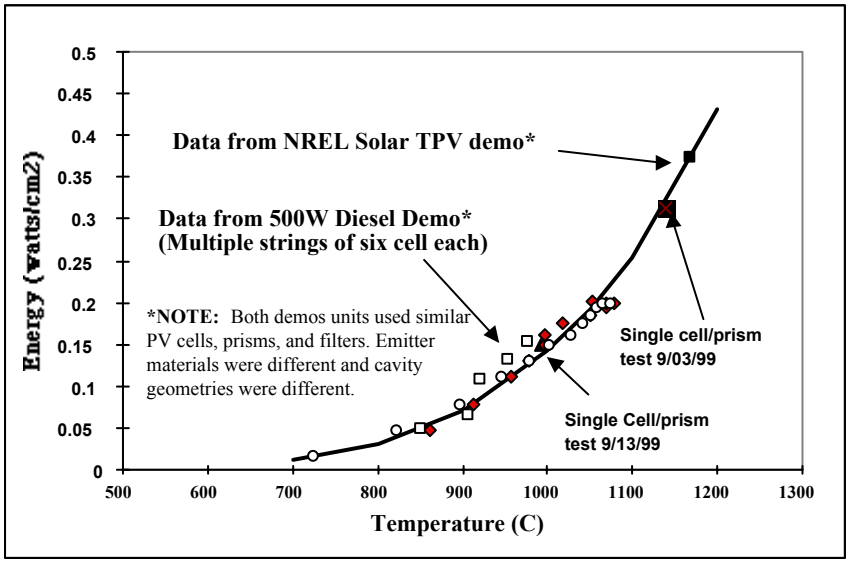

Figure 94. Comparison of Measured and Theoretical TPV Power Out Versus Emitter Temperature

6.4. ANALYSIS OF GaSb TPV RESULTS

From the data in Figure 93, the emitter temperatures reached with the gold reflector only and with the filter/cell converter were 1136°C and 1084°C, respectively. From the measured surface area and emittance of the emitter, calculations show that the amount of power being radiated by the emitter in each case is 11.2 watts and 9.63 watts, respectively. The difference in the two radiated power values of 1.56 watts represents the amount of energy transmitted into the PC cell assembly by the filter. The measured power out of the cells was 0.382 watts. Therefore, the filter/converter efficiency was :

Filter/PV Cell Converter Eff. = 0.382 watts/1.56 watts = 0.245

This experimental value compares well with the value obtained by averaging the PV cell quantum efficiency over the peak transmittance band of the filter, V_{OC}, and fill factor data which are shown in Figure 95.

Filter PV Cell Converter Eff. = QEave x (V_{OC}/Vbg) x FF

= 0.64 x (.4/.7) x 0.7 = 0.256

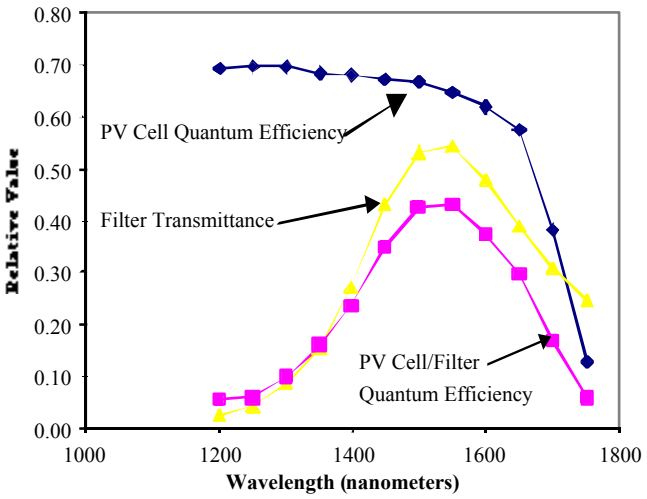

Figure 95. PV Cell QE Filter Transmittance Data

From the above data, the cavity efficiency or emitter -to-cell efficiency can be calculated by reducing the filter/PV cell efficiency by the cavity window loss and wall reflectance values

Cavity Efficiency = Filter/PC Cell Eff. x Window Loss x Wall Reflectances = 0.245 x .92 x .97 x .97 = 0.212

The above value agrees well with the value of 19.6 obtained by the more rigorous three-dimensional ray tracing model discussed earlier which accounted fully for multiple reflections in the cavity due to the non-unity emittance of the tungsten emitter.

From the data presented in Figure 94 it can be seen that the electrical power out agrees well with the expected value obtained by modeling the graybody emitter and the measured spectral transmittance of the filters combined with the measured PV cell parameters. Thus, from the preceding analyses of experimental results it is concluded that the filter/PV cell converter works as expected and verifies the analytical model which can now be used to design and optimize a converter for use with a hybrid solar/natural gas TPV system.

6.5. Solar TPV Receiver Development

Having successfully completed the proof-of-concept experiment described in 6.1 we began developing a configuration of solar receiver. The first issue that was addressed was a solar aperture design. The aperture must admit concentrated beam of solar energy into the TPV cavity while limiting the escape of infrared energy back out of cavity. The system was to be tested at the National Renewable Energy Laboratory (NREL) Solar Furnace so an aperture was designed to accommodate the beam received at the furnace. The beam diameter is approximately 4-inch diameter and has a ray cone angle of ±30 degrees. A water-cooled front window limits the portion of the solar furnace beam that impinges on a smaller quartz window into the TPV cavity. On the cavity side of the aperture a gold-coated spherical surface reflects infrared radiation energy back into the cavity. The relatively small area of the entrance window limits the radiation loss back out of the cavity.

Figure 96 shows a photograph of the aperture ready for installation in the solar receiver test unit at NREL.

Figure 96. Solar Aperture Ready for Installation in the Solar Receiver Test Unit

In order to test the preliminary SGTPV receiver design, an emitter and an evacuated thermal control sleeve based on the advanced fossil fueled receiver design discussed in sections 3.4 and 3.5 was fabricated and fitted with four 9-cell PV modules. One module was installed in each quadrant of the receiver. The windows between the modules were filled with gold reflectors deposited on metal substrates. Figure 97 shows the configuration of the receiver test article.

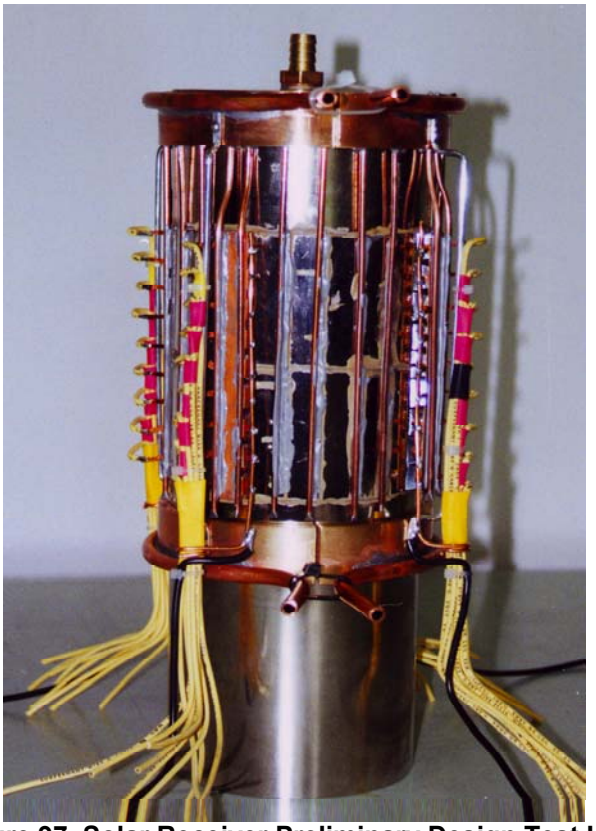

Figure 97. Solar Receiver Preliminary Design Test Unit

The solar aperture was then installed in the TPV receiver as shown in Figure 98. The system was then inserted into the water bath calorimeter testbed and instrumented for test as shown in Figure 99.

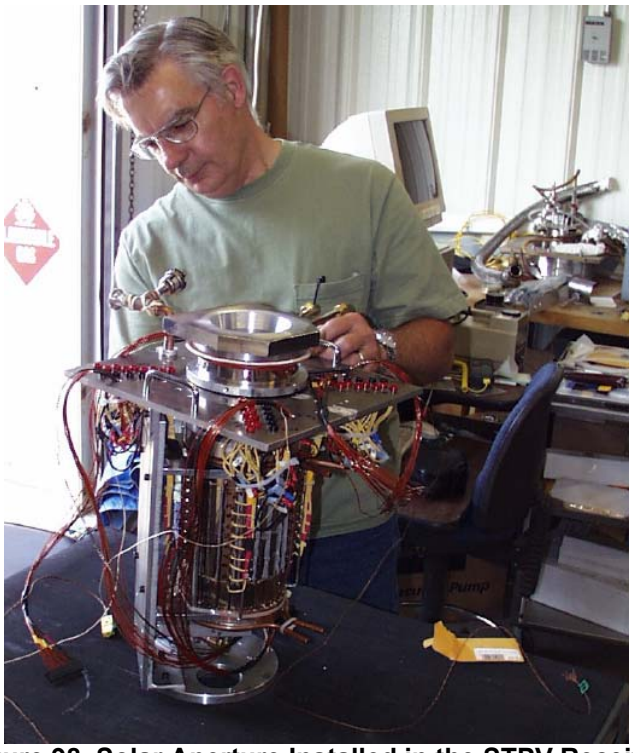

Figure 98. Solar Aperture Installed in the STPV Receiver

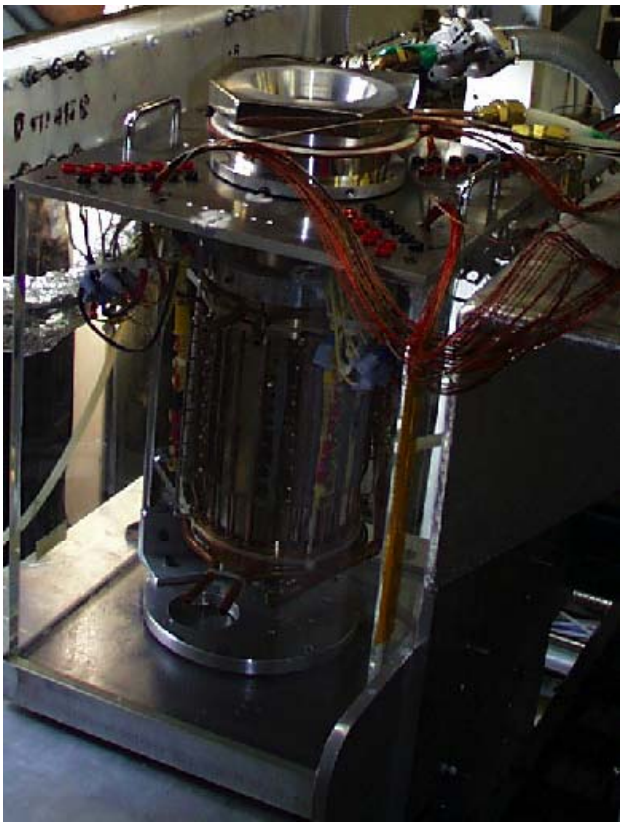

Figure 99. Complete STPV Receiver and Solar Aperture Installed in Calorimeter Bath

During the testing it was found that the TPV emitter could not be heated above about 850°C in the STPV test unit. This was determined to be due to two features. First, the aperture window was too small due to a miscommunication between EDTEK and NREL. The window admitted only 10% of the furnace beam (800 watts) instead of the 1500 watts desired. Secondly, Because the aperture was not insulated and the cavity was air filled, the thermal gradients in the cavity resulted in large convection losses out of the cavity. Thus, we learned some valuable lessons about STPV design even though the operating temperatures reached by the system were not as high as desired. The PV cell currents observed were typical of the fossil fueled converter tests at the equivalent temperature.

6.6. Advanced Solar Aperture and STPV Receiver

A new second aperture design was generated to overcome the short comings of the first test aperture discussed in 6.5. The new design has a larger aperture and a conical reflector to direct approximately 20% of the solar furnace beam into the TPV cavity. A second improvement is that the entire aperture area is evacuated to prevent convection losses out of the TPV cavity. This aperture has been tested at the NREL furnace and found to admit sufficient energy into the TPV cavity. Figure 100 shows the energy admitted into the TPV cavity as a function of incident solar furnace energy. As can be seen, the efficiency is about 30% when the solar furnace beam is stopped down so that it has a tighter angular distribution. When the solar furnace beam is unshuttered the aperture efficiency approaches the expected 20% yielding about 2000 watts into the cavity. This aperture appears to be adequate. We will test it with a TPV converter module that has a full complement of 24 each of 9-cell modules and will give a good indication of the expected power from a solar TPV. Figure 101 shows the full STPV converter ready for test with the advanced aperture when time is available on the NREL solar furnace.

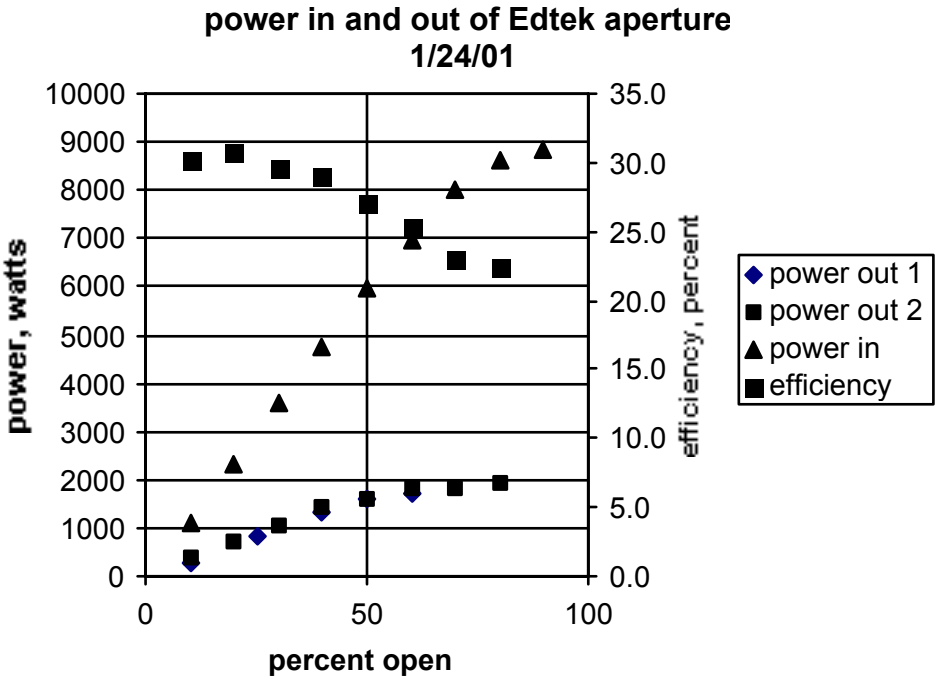

Figure 100. Experimental Measurement of Solar Aperture Efficiency

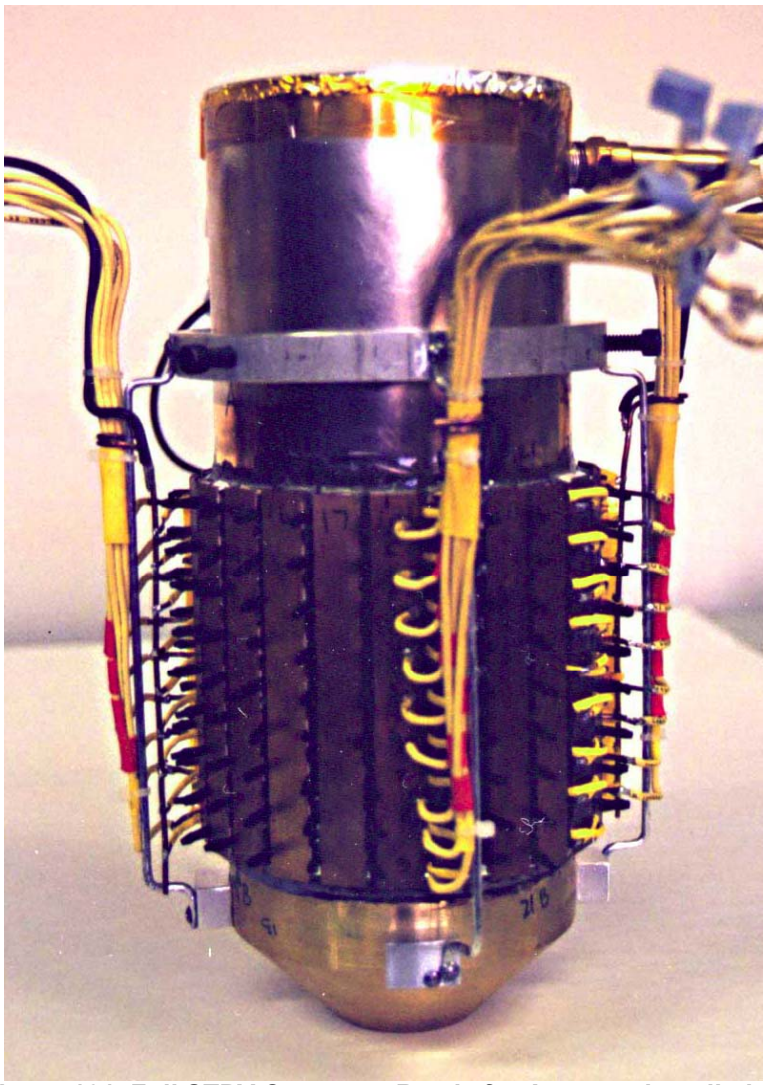

Figure 101. Full STPV Converter Ready for Aperture installation

Unfortunately, the NREL Solar Furnace Facility became engaged in long-term test on another project. The schedule and priority of these long-term tests precluded further testing of this solar TPV testbed unit.

7.0 Hybrid SGTPV System Development And Fabrication

For the hybrid solar/gas thermophotovoltaic (SGTPV) system we drew on experience from both the fossil fueled TPV and the solar TPV to develop the design discussed in 3.0. Basically, these two technologies are merged into a single unit that can run on natural gas (or other fossil fuels) and when the sun is available it utilizes the solar energy to reduce the gas consumption rate proportionately. The system that was fabricated to accomplish these functions is described in the following sections.

7.1. Solar Concentrator Fabrication

The design of the solar concentrator dish was discussed in 3.1. The development of the dish and the equipment for fabricating it was discussed in 4.5. On a cost share effort, EDTEK has developed and fabricated a pilot production capability for fabricating the concentrator dishes. Figure 102 shows a photograph of the dish-forming machine we deployed. Figure 103 shows the vacuum coating machine for applying reflective coatings. Figure 104 shows a finished dish from the pilot production line.

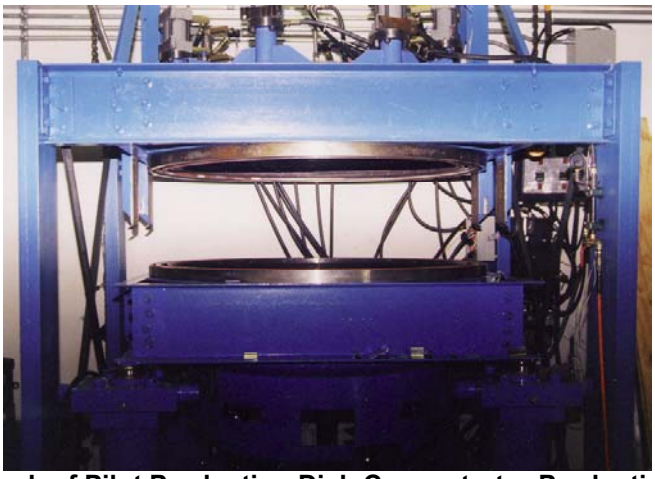

Figure 102. Photograph of Pilot Production Dish Concentrator Production Forming Machine

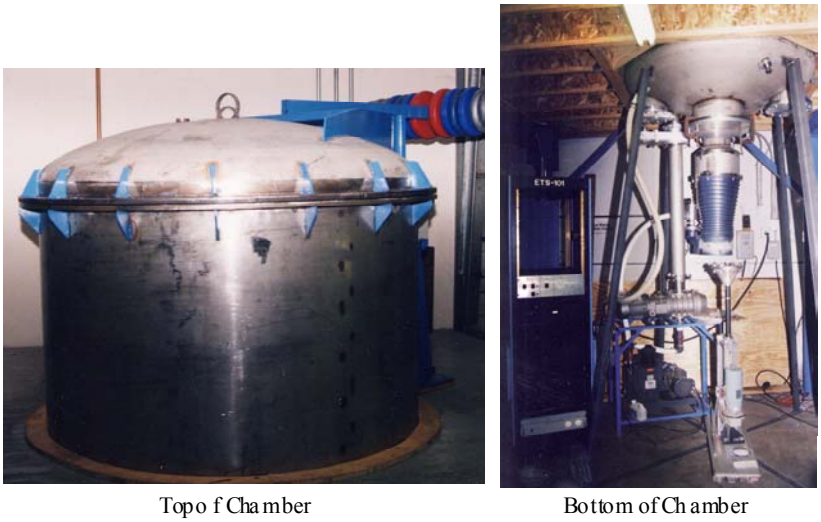

Figure 103. Photograph of Pilot Production Dish Concentrator Coating Machine

Figure 104. Photograph of Finished Pilot Production Concentrator Dish

7.2. Tracking Sensor and Drive System

Our objective for the tracking and drive system is to develop a system that uses, to the degree possible, off-the-shelf mass produced products to keep costs low and that required a minimum of power from the system to drive the tracking subsystem.

7.2.1. Tracking Drive System Development and Fabrication

Technical requirements for the system are that a) it be able to acquire the sun from positions far off the sun, b) having acquired the sun, it would be able to track the sun to better than 0.1 degree of offset error, c)) at the end of the day the system should return to its "home" position and rotate the dish to face the ground during the night, d) in the event of high winds that the system be allowed to "weather vane" or turn edge-on to the wind. Further, the system should minimize power usage to reduce parasitic power drain. During the course of developing the tracking drive system to meet these requirements we explored several options.

Prior to fabricating the prototype drive system, a breadboard test set up was made to determine if sufficiently small motion steps could be obtained to facilitate tracking to ±0.1 degree accuracy. It was found that we could control to steps on the order of 0.002 inches per step which give plenty of control for the tracking function.

7.2.2. Tracking Sensor and Control System

EDTEK uses a proprietary sensor system developed on cost share programs to provide the signal for locating and locking on to the sun for tracking purposes. Control is provided by single board microcomputer that is discussed in the 7.2.3.) In order to provide control for solar concentrator the microcomputer must, in addition to receiving the suns sensor signals and sending solar tracking commands to the drive system, provide such "housekeeping" functions such as; 1) return to home position at night, 2) ground facing stowage, and 3) release of the tracker in high winds. Figure 105 shows a photograph of the tracking drive, base mount, and sensor system mounted with a small dish for testing the tracking functions.

Figure 105. Photograph of Mounting, Tracking, and Sensor Assembly

7.2.3. Micro-Computer Control System and Software Development

The micro-computer control system is a vital part of the SGTPV system. The computer must sense the transducer signals from the various subsystems of the SGTPV, i. e., the solar position sensors, the burner status sensors, and the electrical voltage status sensor. The computer must then act upon the sensor signals to:

Provide 2-axis tracking control functions.

Provide burner control functions as discussed above.

Provide switching voltage regulator control functions.

A microcomputer that can meet all these requirements has been selected. Figure 106 shows a photograph of the single board computer. EDTEK has developed the software for the computer to govern the various control functions identified in earlier sections.

Figure 106. Photograph of the Single Board Micro Computer Selected to Control the SGTP System

7.2.4. Concentrator Base and Mechanical Drive Assembly

Figure 107 illustrates our mechanical drive and concentrator base assembly. A special gear translates the linear motion from the actuator to horizontal rotation and a conventional

connecting rod accomplishes this function for the vertical rotation. All of the parts are selected from off-the-shelf mass-produced inventories in order to keep costs at a minimum.

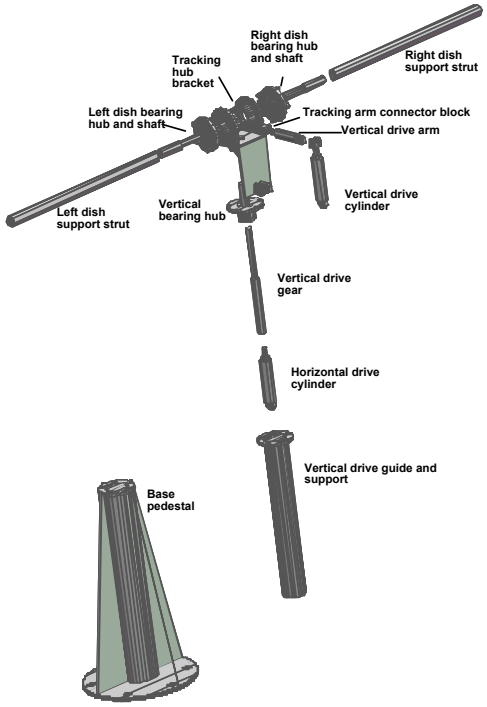

Figure 107. Tracking Drive System Mechanical Assembly

7.3. SGTPV Converter Development and Fabrication

7.3.1. SGTPV Solar Aperture Development

Based on the experience with the apertures designed for the solar furnace beam, we have developed a design for the beam generated by the EDTEK concentrator dish. The design is compatible with the thermal control jacket design for the TPV. Instead of using an evacuated cavity which is not practical for the SGTPV, we couple the incident energy downward into the TPV cavity. A thick insulating ceramic foam plug prevents convection losses. A reflective spherical surface at the end of the TPV cavity directs infrared energy back into the SGTPV cavity and minimizes parasitic losses back out of the cavity.

7.3.2. SGTPV Emitter Development

The emitter for the SGTPV is similar to the fossil fuel burner emitter except that it has the absorption chamber for solar energy on the end of it. Figure 108 shows a photograph of the fabricated silicon carbide emitter part. Thus, the SGTPV emitter is a double chambered silicon carbide cup. The solar energy is absorbed in the silicon carbide cavity. Heat from the natural gas combustion is absorbed in the larger chamber that is sealed to the combustion chamber bulkhead. Due the high degree of insulation on both ends of the emitter, the primary means of energy escaping from the emitter is by radiation from its side walls through the IR band pass filters and into the PV cells for conversion to electricity. As discussed in the 4.6.1.1), the

radiation transfer of energy is equivalent to a very high thermal resistance. Since the conductance of the silicon carbide walls is very low relative to the effective radiation resistance, the temperature of the emitter tends to equalize at an approximately uniform temperature. When no solar energy is present, the fossil fuel burn rate is increased to maintain constant emitter temperature.

Figure 108. Photograph of Fabricated Silicon Carbide Emitter Parts

7.3.3. Burner/recuperator Development

The SGTPV burner recuperator is based on experience with the recuperator developed for the fossil fuel burner described in Sections 3.0 and 4.0. The SGTPV burner recuperator is almost identical in design to the fossil fuel burner system except for modifications in the fuel nozzle to accommodate gaseous fuel.

Because of the high degree of preheating of the combustion air via the recuperator, the gas and air cannot be mixed before they enter the combustion zone. In our design the fuel is injected through a fuel nozzle at the center of the bulkhead and the preheated air is fed through a swirl nozzle that imparts a spiral motion to the air fuel mixture and hence the flame as it enters and traverses the combustion chamber. The air fuel mixture is ignited initially by means of a hot surface igniter inserted through the bulkhead and a ceramic quarl which serves the functions of insulating the igniter and bulkhead from the combustion zone temperature and it also helps shape the burn pattern in the combustion chamber. Figure 109 presents a photograph of the fabricated burner recuperator parts.

Figure 109. Photograph of Fabricated Burner/Recuperator Parts

7.3.4. Evacuated Thermal Control Sleeve

For the SGTPV we have chosen a twelve faceted geometry for the filter windows. This is the best compromise to reduce parts count and still maintain radial flux symmetry on the TPV Cell. The windows will accommodate two vertical columns of 9 cells each or 18 cells per window. Thus, even though the emitter is a curved surface and the windows are flat, the two adjacent cells in the two columns will receive the same total radiation flux from the emitter. The glass filter substrates are bonded to the metal frames to form the vacuum tight seal. Experiments have been performed to confirm that windows can be successfully bonded to the body of the metal sleeve. It was found during the testing of the completely assembled test-unit that the filter bond was not robust. At operating temperatures the filter seal was very brittle and failed after a short time. This failure prevented us from gathering data on the SGTPV systems at its full operating temperature. Figure 110 shows a photograph of the evacuated thermal control sleeve during fabrication.

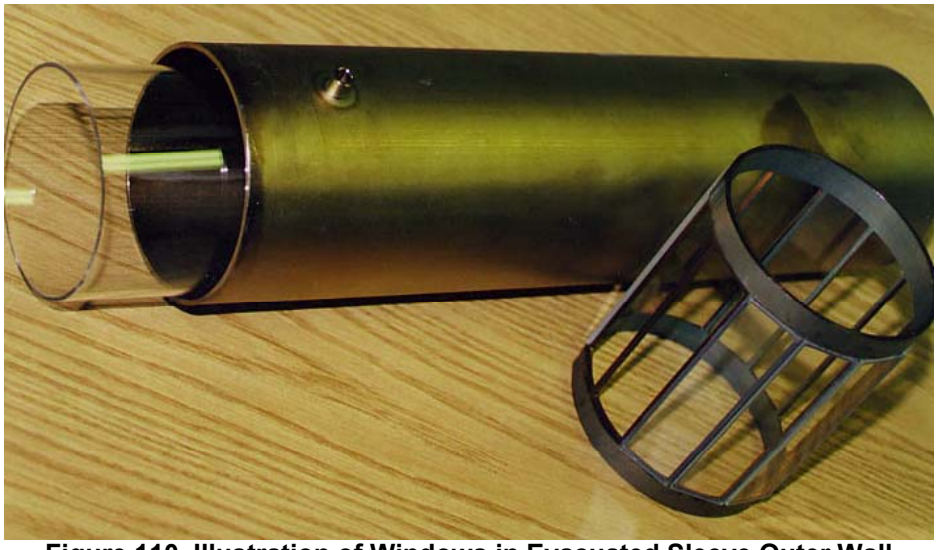

Figure 110. Illustration of Windows in Evacuated Sleeve Outer Wall

7.3.5. SGTPV Filter Development and Fabrication

The tripole filter design developed for use in the SGTPV was discussed in detail in 4.1. EDTEK has deployed a pilot production line for fabricating these filters. Figure 111 shows the pilot production masked ion beam lithography system that is central to the production of the EDTEK patented resonant mesh IR band pass TPV filters. The filter production process has been matured to the point that is has a greater than 80% yield. The pilot production line has a capacity to produce up to 250 kW of SGTPV modules per year. Figure 112 shows the production for the current SGTPV prototype.

Ion Source and Beam-Line

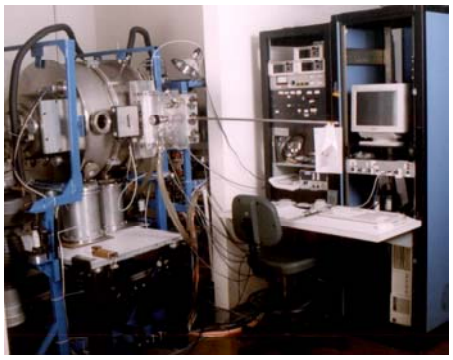

Exposure Chamber and Control Console

Figure 111. Pilot Production Masked Ion Beam Lithography Equipment for Resonant Mesh IR Band Pass Filters

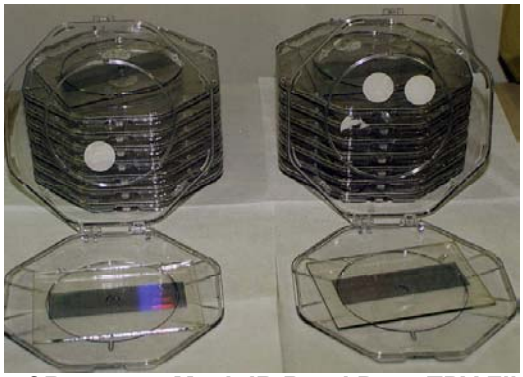

Figure 112. Production Run of Resonant Mesh IR Band Pass TPV Filters fabricated for The PIER Project Prototype Generator Demonstration

7.3.6. SGTPV Photovoltaic Cell Development and Fabrication

The development of the GaSb TPV cells for this PIER project was discussed in 4.2. The pilot line production equipment EDTEK has deployed is shown in Figure 113. The process for producing the cells has been matured so that the product yield is about 95%. A production batch of TPV cells fabricated for the PIEAR prototype TPV generator is shown in Figure 114.

Nitride Deposition

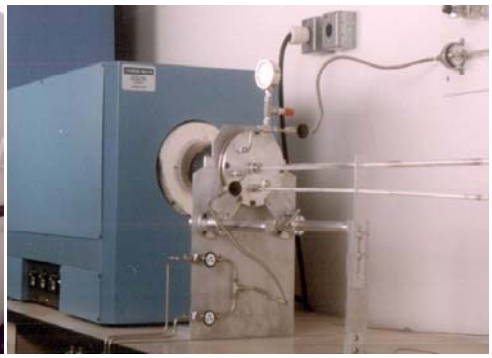

Junction Diffusion

Photolithography

Figure 113. Pilot Line Production Equipment for GaSb TPV Cells

Figure 114. Production Batch of TPV Cells Fabricated for the PIER Prototype SGTPV

7.3.7. Electrical Converter

The SGTPV converter design has been improved. The electrical converter will consist of twelve arrays of 18 PV cells each. The cells will be arranged in two side by side columns with 9 cells per column as shown in Figure 115, a completed 2x9 cell array. Each two adjacent cells will be connected in series. In this way the two cells can be connected to their counterparts in the adjacent modules and so around the converter to form radial strings of series connected cells just as we tested in the fossil-fueled converter. Figure 116 shows the converter parts fabricated for the PIER prototype SGTPV generator.

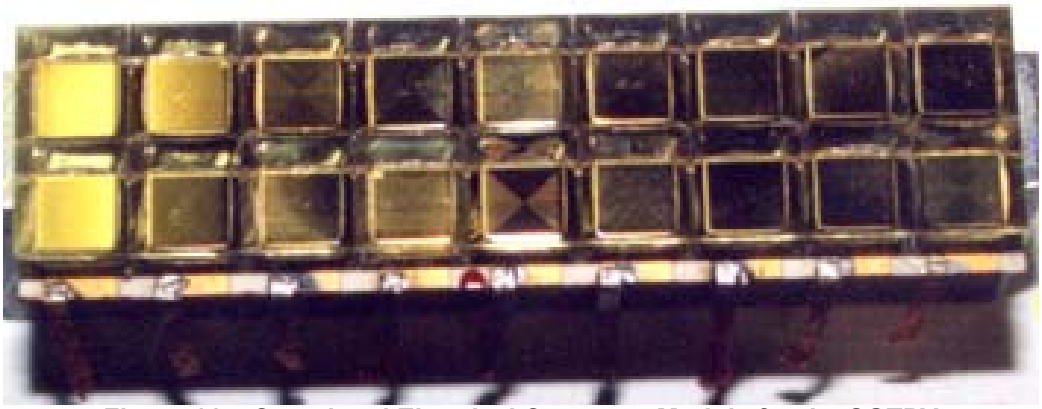

Figure 115. Completed Electrical Converter Module for the SGTPV

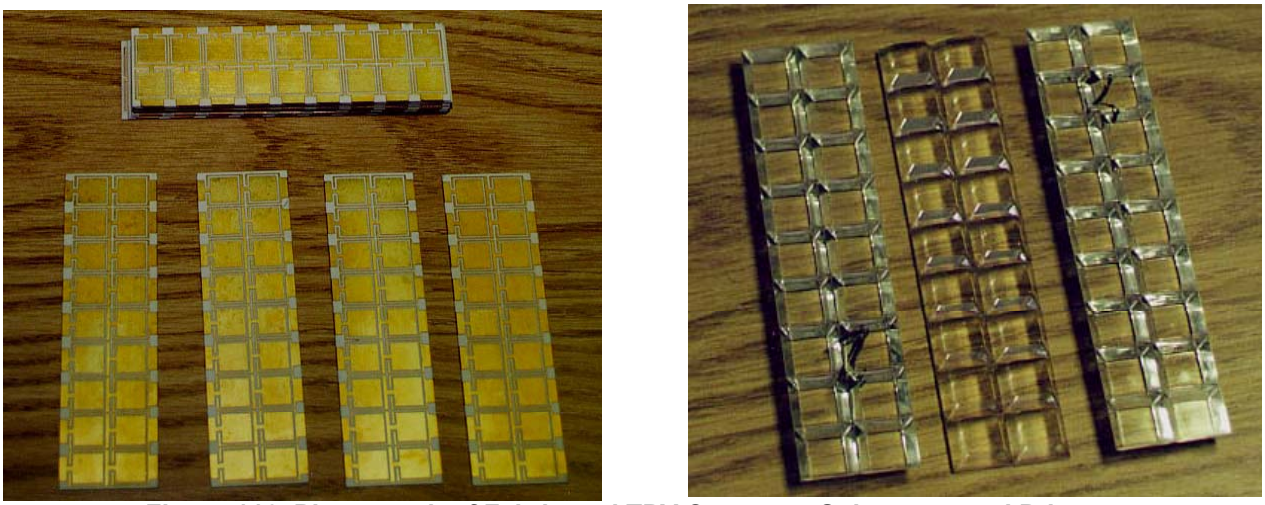

Figure 116. Photograph of Fabricated TPV Converter Substrates and Prisms

7.3.8. Converter Thermal Control System

In order for the converter to operate efficiently the PV cells must be kept as cool as possible. We adopted the goal of keeping the PV cells at 14°C or less above ambient temperature. First, the cells were bonded to alumina substrates, which has thermal conductivity similar to aluminum. The substrates are in turn bonded to a water-cooled jacket. This jacket is a hollow rectangular shaped copper substrate through which a coolant is circulated. A single water-cooled back plate is bonded to each 2x9 PV cell array at the back of the ceramic board. Figure 117 is a photograph of the twelve copper jackets prior to bonding them to the PV arrays. Figure 118 shows the destination of the cooling plates. This is a photo of the cell/alumina board after installation onto the outer sleeve of the converter. The cooling plates of Figure 117 will be bonded to the back of the ceramic boards using high thermal conductive adhesive. After bonding, the water cooled back plates are serially plumbed using plastic tubing and then leak checked. Figure 119 is a photograph of the installed water-cooled jackets showing the water line connections from one back plate to the next. Notice in this photo the passive cooling finger attached to the back side of the cooling plates. These fingers draw heat from the adhesive line between the IR filters and sink that heat to the water cooled back plates. This passive cooling was installed to minimize thermal shock to the critical vacuum seal of the outer converter housing.

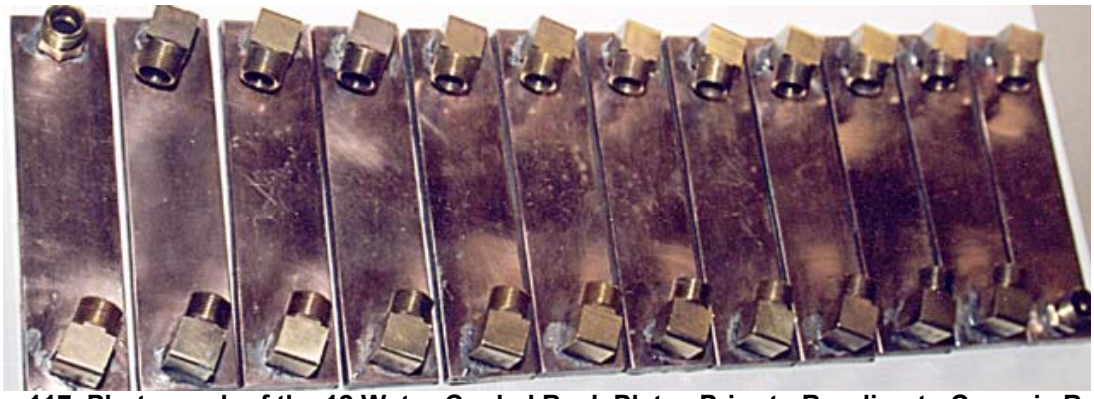

Figure 117. Photograph of the 12 Water-Cooled Back Plates Prior to Bonding to Ceramic Boards

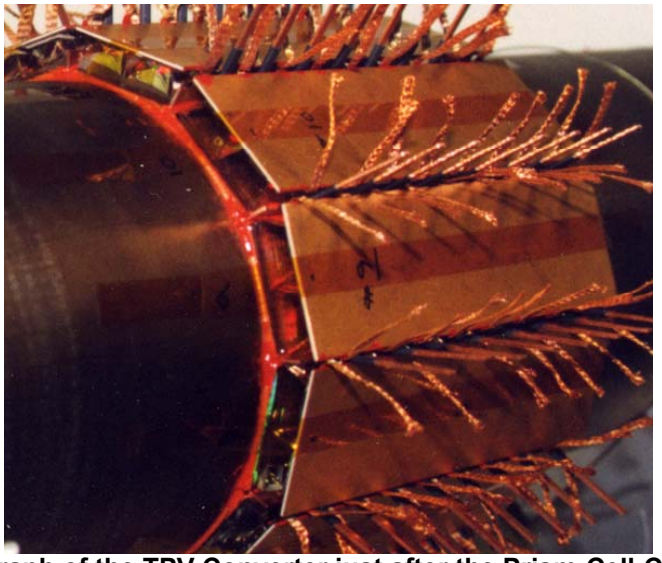

Figure 118. Photograph of the TPV Converter just after the Prism-Cell-Ceramic Board Sub-Assemblies Prior to Bonding of Water-Cooled Back Plates

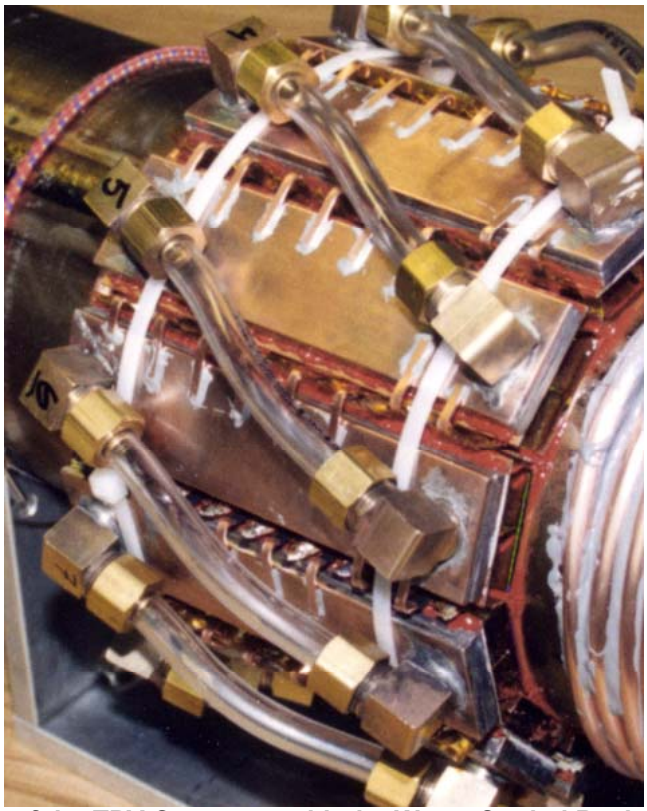

Figure 119. Photograph of the TPV Converter with the Water-Cooled Back Plates Bonded in Place and Interconnected.

This water-cooled heat exchanger will be used for the demonstration SGTPV module. For the PIER demonstration, city water will be used to as coolant through the primary cooling loop, i.e. the copper back-plates shown in Figure 119. A secondary coolant loop may be attached to the end of the heat exchanger to extract thermal energy in hot water to allow the co-generation function of the unit.

7.3.9. SGTPV Control System

In order to make the system autonomous and user friendly, a sophisticated electronic control system is required. The TPV electronics are composed of burner control electronics, TPV array voltage switching regulator, and starting battery charging electronics. The TPV mechanical assembly consists of the structure that houses the electronics, burner/recuperator, burner mechanical controls, and the TPV array converter. The requirements for the electronics assembly subsystems are described below. These requirements were used as a guide in designing these subassemblies for the SGTPV demonstration unit.

7.3.9.1. Burner Control Electronics Requirements

The burner control requires a few basic functions to monitor it and maintain control. These function are listed and defined below:

BATTERY ON: The burner controls shall connect the starting battery to the electronic controls by operation of a BATTERY ON switch.

START: The burner controls shall initiate a START sequence by starting a coolant circulation pump, cooling fan and combustion blower which pressurizes the combustion chamber. Following this timing event, two fuel solenoids for the fuel nozzle and one fuel solenoid for the igniter and the ignition device are operated. After this event when a satisfactory combustion temperature has been reached, one fuel solenoid to the nozzle is shut down.

ALARM: The burner controls shall provide a control signal verifying flame operation from a flame sensor. Presence of flame shall allow continuation of the combustion process and a display indication of NORMAL operation. The fuel ignition device and fuel ignition solenoid shall then be turned off. Lack of flame shall initiate a restart of fuel hot surface igniter and fuel solenoid. If a second failure of flame is sensed, the burner controls shall initiate a STOP sequence and provide an ALARM signal.

FUEL BURN RATE: As solar energy is added or subtracted form the system, the gas burn rate will be increased or reduced accordingly.

STOP: The burner controls shall provide a shutdown control sequence stopping the fuel pump, and fuel flow through solenoids, and then purging combustion chamber with cooling air by continued operation of the combustion blower and cooling fan until a safe temperature is reached.

DISPLAY: The burner controls shall display BATTERY, ARRAY, LOW BATTERY, and ALARM conditions.

MANUAL CONTROLS: The burner controls shall have a BATTERY ON switch, a START switch, and a STOP switch.

MAINTENANCE: The burner controls shall have internal test points to measure temperatures in combustion chamber, PV array voltage, battery voltage, and other useful maintenance parameters.

7.3.9.2. TPV Array Switching Regulator Requirements

The PV array can be converted to the desired output form such as 120 or 240 volts ac when the output dc voltage from the converter is maintained within reasonable limits. The requirements for a regulator or listed below.

SWITCHING: The regulator shall switch the TPV array output within one tenth of a millisecond of detection of out of range voltage parameter.

DISCONNECT: The switching regulator shall disconnect the TPV array output from the LOAD by means of a control signal from the control electronics. This shall occur whenever the TPV array voltage falls below a minimum specification, or when it has not reached the minimum in the starting mode. A microcomputer (which was discussed in a 7.2.3) will control the switching of the converter.

7.3.10. Summary and Status of SGTPV Development

EDTEK has developed a unique co-generating solar-gas thermophotovoltaic system that is based on a modular solar concentrator. The COGEN-2 hybrid solar/fossil TPV/thermal receiver can replace the use of expensive natural gas or electricity to supply both electricity and hot water simultaneously. In addition the unit operates continuously 24 hours per day, using solar energy to displace natural gas when the sun is out and switching to natural gas when the sun goes down. A single EDTEK dish can deliver 500 watts electricity and 6 to 8 gallons of water at 150°F per hour. In a typical solar location the dish will deliver approximately 12 kW-hr electric and 144 to 192 gallons of 150°F hot water per day. The system is also able to operate with air cooling, if the total hot water capacity is not needed the unit automatically switches to air cooling to maintain thermal control. The system makes an economical choice for meeting both electric and on-site hot water needs.

COGEN-2 HYBRID SOLAR/FOSSIL TPV/THERMAL SPECIFICATIONS

Dish diameter	56 inches
Dish collection aperture	17.1 sq. ft.
Maximum thermal power intercepted	1700 watts
Electric production	500 watts
Hot water production	144 to 192 gallons per day
Air cooling	when hot water demand drops
Gas-to-electric efficiency	15%
Solar-to-electric efficiency	30%
Reflector	glass protected silver
Collection efficiency	91%
Primary concentration ratio	800:1
Tracking	2-axis
Tracking accuracy	+/- 0.2 degrees
Control	Autonomous
Night and weather protection	ground facing stowage
Wind protection	releases to turn edge-on

All the receivers are modular and can be interchanged or retrofitted in the host concentrator without modification. Clusters of up to six basic concentrator modules can be arrayed on each tracking system. This clustering and module interchangeability provides maximum flexibility for fitting and maintaining each individual customer's needs. Photographs of the prototype SGTPV generator module and the complete modular prototype SGTPV system consisting of the generator mounted in the 2-axis tracking solar concentrator module fabricated for testing and demonstration in this PIER program is shown in Figure 120 and Figure 121, respectively. Figure 122 is a photograph of the back side of the SGTPV system showing the TPV converter installed in the solar concentrator dish.

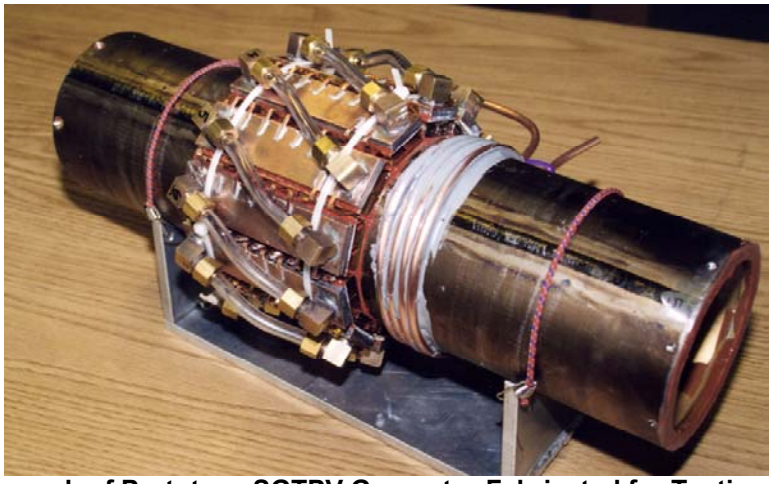

Figure 120. Photograph of Prototype SGTPV Generator Fabricated for Testing and PIER Project Demonstration

Figure 121. Photograph of Complete SGTPV Module

Figure 122. Photograph of Back Side of SGTPV Module Showing Mounted TPV Converter

The concentrator's "fast optics" focus the concentrated sunlight *inside* the rim of the dish. In this way it insures personal safety and no fire hazards because no hot spots can occur *outside* the dish. The system is also durable and weather resistant. The dish substrate is fabricated from fully tempered aluminum alloy for maximum weather resistance. The substrate is coated with an inert smoothing layer to create a mirror surface. The mirror surface is coated with silver. A glass over coating protects the silver. The conformal nature of the coatings offers maximum weather sealing to avoid moisture penetration, being the primary failure of past concentrator coatings. The EDTEK dishes have been soaked for weeks under water without damage.

The concentrator dishes are mounted on a stable platform with a strong, simple 2-axis tracking system driven by ultra reliable actuators. An onboard computer wakes he system in the morning, tracks the sun throughout the day, and then returns it to the ground facing "home" position at night. Throughout the day the weather is monitored and the dish allowed to weather-vane if the wind speed exceeds safe levels. When the weather becomes too severe, the computer returns the dish to the ground facing "home" position for its protection.

The hybrid thermophotovoltaic generator units are based on technologies developed over several years for fossil fuel only units and for solar fuel only. These technologies have been fused together in the COGEN 2 to yield the hybrid solar-gas TPV unit. The COGEN 2 SGTPV systems are designed to be cost competitive. Off-the-shelf mass-produced components and design simplicity have been emphasized throughout the systems for maximum reliability and economy. Thus, the EDTEK COGEN 2 SGTPV system provides a highly reliable and economical energy for our customers.

The performance testing and evaluation of the PIER SGTPV prototype is discussed in 7.0.

8.0 Test And Evaluation Of SGTPV

The SGTPV prototype fabrication and assembly was completed and testing of it was performed at EDTEK prior to its transport to Roseville, California for demonstration to the California Energy Commission. Initially, all subsystems of the prototype functioned as expected. First, the gas burner, recuperator, microcomputer controller, and a solenoid gas flow control valve were tested and calibrated. For these tests the burner/recuperator/emitter assembly was inserted into the quartz tube with the light pipe and insulation in the opposite end. This assembly was then inserted into a metal sleeve and the retaining flanges clamped onto its ends. In this way the heat source subassemblies could be tested without risk of damaging the TPV converter. The fuel burn rate was measured first by placing a small bottle of gas on a mass scale and measuring the use of fuel in grams per minute as the burner was tested at different burn levels. Second, a rotameter was placed in the fuel line and calibrated against the mass scale. The rotameter was then used to monitor fuel burn rate from a larger bottle of gas used as the supply during the remainder of the test program. The control voltage supplied by the microcomputer to a gas control solenoid valve was also recorded at a series of computer control settings programmed into the microcomputer. Table 9 shows the results of one of these calibration test runs. The burn rate, in watts, were calculated from the grams per minute data and the known fuel content per unit mass. Figure 123 shows the rotameter calibration used to determine the fuel burn rate during subsequent SGTPV evaluation tests. Figure 124 is a photograph of the test setup employed to make these gas burner calibration runs.

Table 9. Summary of Gas Burner Fuel Supply System

Setting	Computer Control Volts	Rotameter	Fuel gms/min	watts
0	1.82	1.30	1.8	1881
1	2.01	1.27	2.6	2171
2	2.19	1.67	3.2	2447
3	2.46	2.37	4.3	3590
4	2.93	3.40	6.2	5176
5	3.44	4.60	8.9	7430

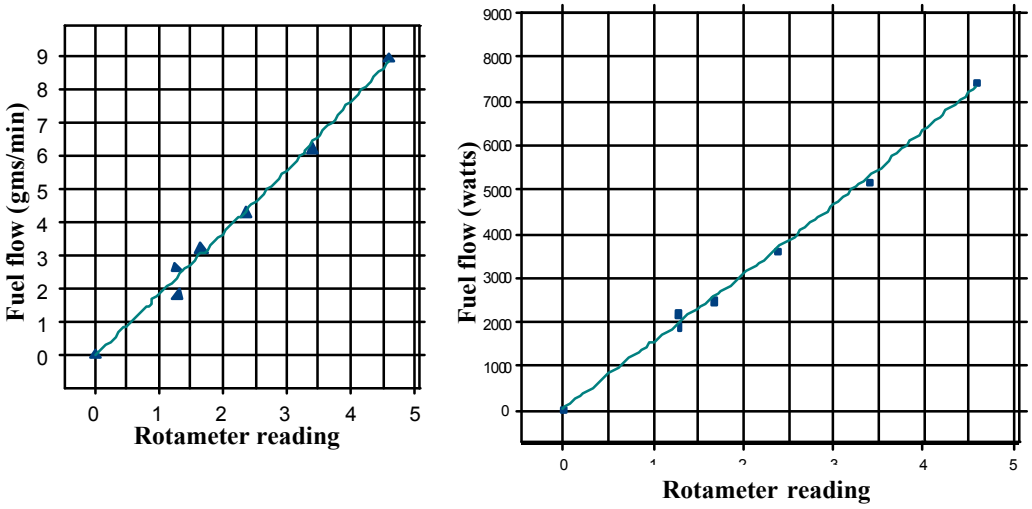

Figure 123. Rotameter Calibration Versus a) Mass flow Rate and b) Watts

Figure 124. Photograph of the TPV Burner Test Set-up

The airflow to the burner was supplied by a fan driven by a brushless dc motor controlled by voltages applied to a pulse width modulator by the microcomputer. For each computer control setting, the oxygen content of the exhaust gases was measured to determine the excess air being supplied to the burner. For each burn rate computer control setting, an optimal air control setting was established and programmed into the microcomputer. The results of these calibrations are presented in Table 10. A type B thermocouple was embedded into the SiC emitter to monitor emitter temperature. The signal from this thermocouple was supplied to the

computer where it was compared to a programmed constant temperature value. If the measured emitter temperature was above or below the preset value then the microcomputer would switch the burner fuel and air to the next lower or higher setting as appropriate. The successful demonstration of these functions verified the computer control of the burner. The control was necessary for the hybrid system so that when the sun supplied energy to the emitter the burner would reduce its burn rate thereby maintaining a constant operating temperature. The microcomputer was also programmed to control start up and shut down of the burner.

Table 10. Summary of Gas Supply versus Air Supply Calibration Results

Fuel Setting	Air Setting
0	0
1	0
2	2
3	6
4	7

During these tests the burner/recuperator was also instrumented to measure air and gas pressures at various points throughout the system. During an earlier series of tests on a cost share program[6], the recuperator had been observed to have serious air leaks at seals at the top cap of the burner and at temperature sensitive air leaks in spot welded seams in the recuperator heat exchanger shells. A new recuperator and end cap seal design was incorporated into the SGTPV design to eliminate these air leaks. The increased nozzle pressure and decreased intake vacuum indicate that the air leaks have been eliminated and more air is being delivered to the nozzle for less total air taken into the system. The decreased combustion chamber pressure also indicates that leaks in the recuperator shells are no longer supplying air through the exhaust plenum and all the air is traveling through the nozzle to get into the combustion chamber. The pressure measurements of Table 11 indicate that the new design is a dramatic improvement over the previous design[6].

Table 11. Pressure Measurement Comparisons Between Previous[6] and New SGTPV Recuperator Design

Measurement Point	Pressure in Previous design (inches H_2O)	Initial Pressure in New SGTPV design (inches H_2O)	Post Burn Pressure in New SGTPV design (inches H_2O)
Air inlet orifice pressure (Total air supply)	1.25	0.33	0.33
Air supply (nozzle) pressure	4.70	7.30	7.30
Combustion Chamber Pressure	0.60	0.25	0.25

The temperature of the air-side of the ceramic insulating plug on the light pipe (solar entrance) end of the burner was also monitored and found to rise only slightly above ambient

temperature. This in spite of the emitter being extremely hot and the sides of the metal tube adjacent to the emitter glowing orange. This verified the improved insulator subsystem of the new design.

The above tests concluded the evaluation of the heat source subsystems. All the heat source subsystems were observed to operate according to the design.

The heat source components discussed above were then inserted into the vacuum thermal control jacket onto which were mounted the TPV converter components. One of the critical design changes to the TPV converter was a new method for the sealing of the IR band pass filters to the outer metal sleeve of the vacuum thermal control jacket. Unfortunately, during one of the initial testing runs with the gas burner as the heat source, a vacuum leak developed in the seals between the filter substrates and the vacuum thermal control jacket. The new design had worked well when tested in an oven environment where everything came up to temperature simultaneously. However, in the actual application, thermal gradients produced across the materials interfaces proved to be a weak point in the overall system. The resultant vacuum leak prevented our testing the unit to full power. Proceeding to full power testing would have permanently damaged the SGTPV prototype and eliminated any chance of repair of the unit at a later date. Testing was continued to confirm the performance of all the SGTPV subsystems within the limitations imposed by the vacuum leak. A typical plot of the TPV cell short circuit current as a function of emitter temperature is shown in Figure 125. At 780C emitter temperature, the unit developed about 55 milli-amp of current at an open circuit voltage of 0.4 volts per cell. With 216 cells and fill factors of 0.7, the unit was producing about 3.3 watts of electric power. Design emitter temperature is 1400 C producing 500 watts electric power, so it is evident that the achieved temperature of 780C is just at the threshold for turn-on of TPV conversion. We were then unable to get direct measurements of SGTPV operating efficiency, however, it is constructive to consider the test results from a previous diesel fueled TPV prototype designed and built on a cost share program funded by the U. S. Department of Defense[6]. The TPV converter technology in this unit was similar to the SGTPV converter except for the filter vacuum seals. The results from the oil fired TPV testbed unit are shown in Figure 126 and they confirm that the SGTPV had only reached the threshold for TPV turn-on at 780C emitter temperature.

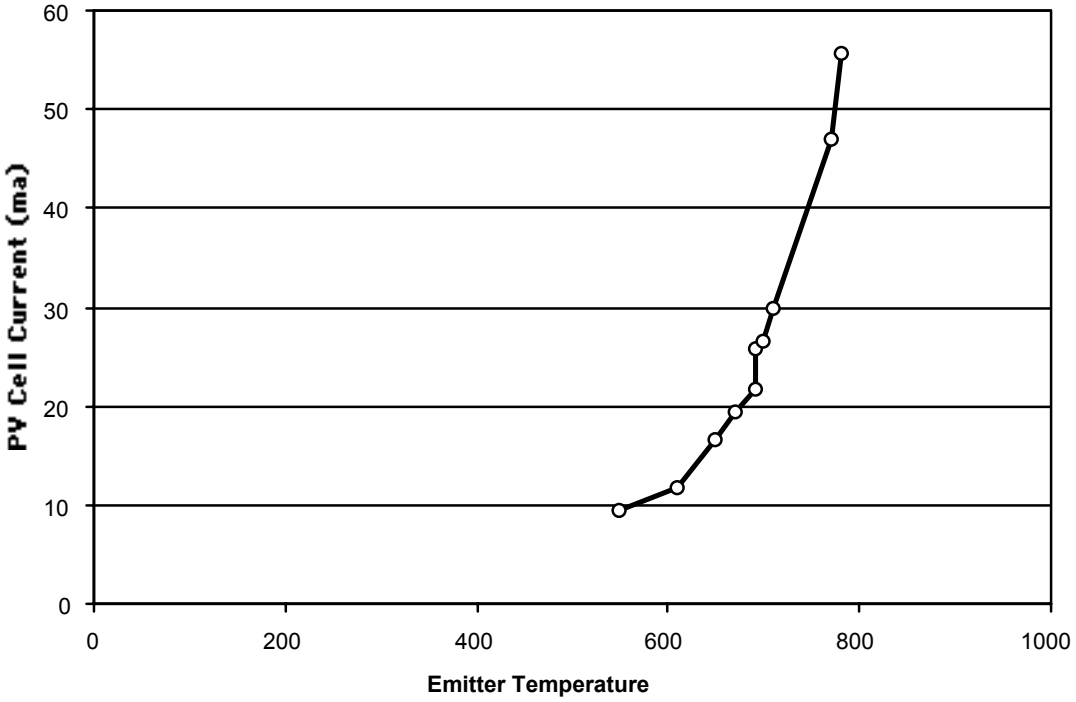

Figure 125. TPV Cell Short Circuit Current Versus Emitter Temperature During Gas Burner Test Run

Although we did not get operational data at the design operating temperature for the SGTPV, we can infer the gas-to-electric efficiency that would have been reached based on the fuel burn-rate data obtained during a twenty minute run with emitter temperature of 780 C. During this run, the fuel burn rate was observed to be 750 watts with 14.4% oxygen in the exhaust. From Figure 127 it is seen that 14.4% oxygen equates to 220% excess air. The fuel burn rate adjusted to 0% excess air is calculated as follows:

$$\textbf{Fuel burn rate} = E_{system} + E_{exhaust} = 750 \text{ watts (measured)}$$

Where:

E_{system} is the energy in the system

$E_{exhaust}$ is energy lost to the exhaust.

For a recuperator effectiveness of 70% at 0% excess air:

$$\mathbf{E_{exhaust}\ is \sim (0.3 \times E_{system})}$$

If there is 220% excess air in the exhaust then

$$\mathbf{Fuel\ burn\ rate = E_{system} + 0.3(1 + 2.2)\ E_{system}}$$

and the actual fuel burn rate adjusted for 0% excess air is

$$\mathbf{Adjusted\ fuel\ burn\ rate = 750\ watts \times (E_{system} + E_{exhaust}) / (E_{system} + 0.96)}$$

$$\mathbf{= 497\ watts}$$

Then, if we extrapolate this fuel burn rate to that required for 1400 C operation by the blackbody equation we get the full operational fuel burn rate as

$$\mathbf{Fuel\ burn\ rate\ at\ 1400\ C = 497\ watts \times (1400 + 273)^4 / (780 + 273)^4}$$

$$\mathbf{= 3167\ watts}$$

Assuming the design power output of 500 watts, then the approximate efficiency would be:

$$\mathbf{SGTPV\ gas\text{-}to\text{-}electric\ efficiency \sim 100 \times (500\ watts / 3167\ watts)}$$

$$\mathbf{= 15.8\%}$$

Thus, it was concluded that, as far as could be determined by the limited measurements available from the SGTPV prototype, its electrical conversion was behaving roughly as designed.

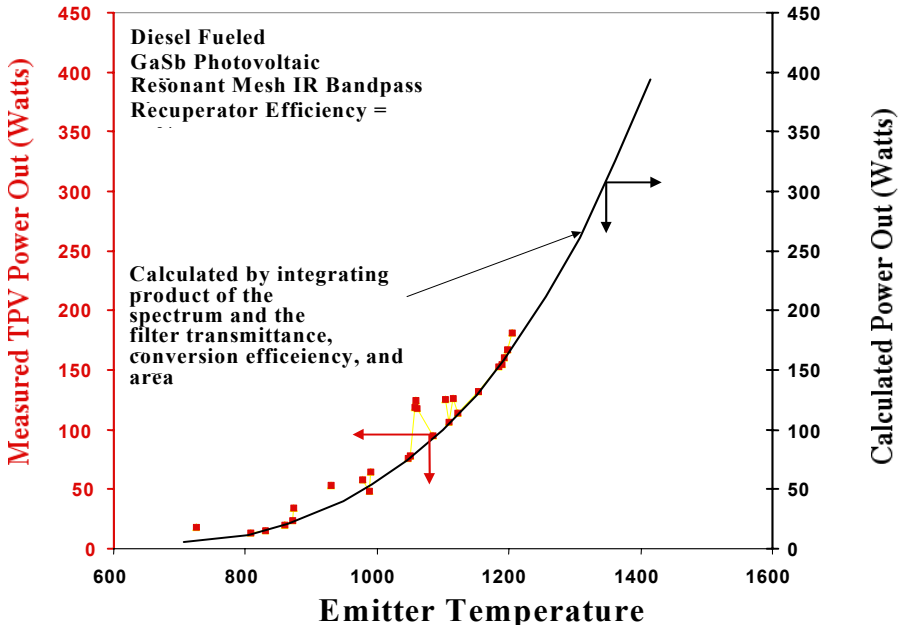

Figure 126. Power out versus Emitter Temperature for Previous Oil Fired TPV Testbed

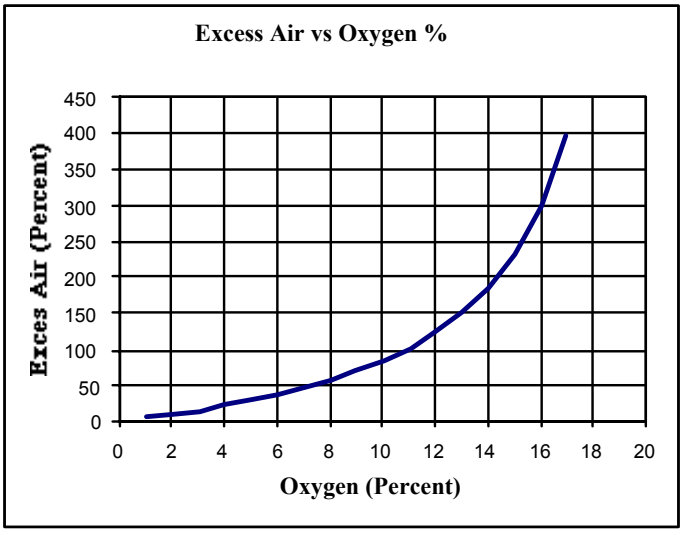

Figure 127. Percentage Excess Air versus Percentage Oxygen In Exhaust

With the gas burner testing concluded the prototype was transported to Roseville, California for solar testing and demonstration to the California Energy Commission. The SGTPV power generation system was transported disassembled. The major components to be assembled on-site were two solar concentrators, the concentrators support base and tracking hardware, the TPV converter housing with its coolant plumbing, air and gas plumbing, and the electrical output interface. The assembly of these components into the complete SGTPV system was an uneventful operation owing to EDTEK's excellent design, engineering, workmanship, and attention to detail. The operation began with the solar concentrator dish to their

support/mechanical/tracking hardware. Figure 128 show some of the details of this assembly. In this figure the support arm is shown just prior to attachment of the solar dish. One of the dish mounting flanges is clearly visible on the cross arm; the second flange is yet to be attached. The dish is lying reflector face down showing its backside support struts. Portions of the dish tracking hardware can also be seen attached to the vertical support pier. The support hardware was attached to the transport trailer that had been blocked to provide a firm support.

Figure 128. Assembly of a Solar Dish Mounting and Tracking Hardware

The solar dish was mounted to the support crossbeam via the mating of two accurately machined flanges. The flange on the cross-member of the support/tracking assembly served the dual purpose of supporting the solar dish and the TPV converter module. This flange is shown in Figure 129 without the converter module in place.

Figure 129. Assembly of a Solar Concentrator Dish and the Dish Mounting and Tracking Hardware

Figure 130 is a photograph of the TPV converter module prior to attaching it to the cross arm flange of the dish support. The photo also shows the two mounted dishes and the central support pier and tracking hardware. The TPV converter module in this photo still requires the insertion of the propane burner/recuperator subassembly and the solar collecter subassembly into the center cylinder of the TPV converter. The TPV converter module is shown assembled and mounted to the support crossbeam in Figure 131. The photo shows the portion of the module that contains the propane burner assembly, located outboard from the dish attachment, and the PV arrays and their thermal control hardware, located just adjacent to the dish-mounting flange. The portion of the converter module not seen in this figure is the solar collecting end. This part penetrates through the dish to reside at the focal point of the secondary mirror of the solar concentrator dish. A good view of the solar collecting end of the module is found in Figure 132 and Figure 133.

Figure 130. TPV Converter Module Shown Prior to Insertion of Burner and Solar Collector Subassemblies

Figure 131. Evacuation of the SGTPV Converter Subsystem after Mounting on Solar Concentrator Flange

The fully assembled SGTPV system is photographed in Figure 132. The far dish of the photo is complete with TPV converter subassembly and from this view the solar collecting hardware is apparent. The near dish is included to properly balance the two-dish system and is without a TPV subassembly. Centered between the two concentrator dishes is the sun-sensor. This unit feeds solar tracking information to the on-board computer that, in turn, drives the tracking mechanism to keep the dishes aim at the sun to within ±0.1 degree accuracy.

Figure 132. Photograph of Complete SGTPV System as Demonstrated to the CEC on 3/28/02

After the assembly of all subsystems, a preliminary system check revealed that the vacuum leak in the filter seals previously discussed had worsened considerably. It was determined that the converter could not be operated for very long either on-sun or using the gas burner without risking thermal damage to the converter components. Never the less, we were able to align the system to the sun and test out the operation of the microcomputer-controlled sun tracker. It was found that the computer control worked as intended and the tracking sensor could be aligned to the sun by programming biases into the software to account for differences in response between the photocells within the sensor.

The primary parabolic reflector was then aligned to the sensor by adjusting screws designed into its mounting structure. Although proper tooling to achieve perfect alignment of the secondary mirror to the primary was not on-site, we were able to achieve reasonably good alignment visually. During this visual alignment, the bright focal point could be seen reflecting from the side of the light pipe as the system came into alignment. When the focal point coincided with the end of the light pipe, the bright reflection disappeared indicating that the light pipe was working as expected and transmitting the solar energy into the TPV emitter cavity. Figure 133 is a photograph of the SGTPV module aligned on-sun. The photograph shows the quartz rod trapping solar radiation and guiding to into the emitter cavity. Measurements of the emitter temperature during short burns with the gas burner compared with short exposures on-sun showed that the emitter heating was roughly equivalent from the two sources. The solar input was on the order of 700 to 800 watts while the expected design input was on the order of 1050 to 1100 watts for a 900 watt/m^2 peak solar intensity (with a silvered primary and aluminized secondary reflectors). Given that the tests were performed between 3:30PM and 4:30PM, crude visual alignment in the field, and the lack of instrumentation to quantitatively measure the incident solar intensity at the demonstration site, it is concluded that the solar system is performing roughly as expected. We intend to make a detailed, instrumented evaluation of the solar subsystems in the future at the EDTEK site using calorimetry to measure the dish's energy concentration-ratio.

Figure 133. Photograph of Solar Concentrator Aligned On-Sun

We also intend to explore the possibility of repairing the SGTPV converter to allow more thorough testing at or near the design operating temperature.

Based on the above observations and discussion, it is concluded that the following accomplishments have been achieved:

1. A complete solar/gas TPV prototype has been designed, developed, fabricated, and tested.
2. Heating of the emitter by a gas burner has been demonstrated.
3. Production of electricity by gas burner heating has been demonstrated.
4. Heating of the emitter by concentrated solar energy has been demonstrated.
5. Heating of the emitter by a gas burner and concentrated solar energy simultaneously has been demonstrated.
6. With the above accomplishments, the feasibility of the hybrid solar/gas TPV concept has been demonstrated.
7. Computer control of the air and fuel mixture to the gas burner has been demonstrated.
8. The computer controlled sun tracking system has been demonstrated.
9. Control of local "house keeping" functions such as night time stowage has been demonstrated.
10. Solar concentration by the EDTEK fabricated parabolic dishes has been demonstrated.
11. A commercialization plan for the SGTPV has been compiled.
12. A production readiness plan for the SGTPV has been compiled.

As discussed above, the entire prototype unit was transported and set up on a property in Roseville, California for demonstration of the above functions to CEC personnel. This demonstration also generated considerable interest among the local Roseville citizenry. About 22 interested persons visited the site and interest in purchasing our solar concentrator system was expressed by several of the visitors.

9.0 Conclusions and Recommendations

9.1. Conclusions

9.1.1. Project Objectives and Achievements

The overall objective of this PIER project is to develop, fabricate, test, and demonstrate both the technical and economical viability of an SGTPV module that can run alternately, or simultaneously, on solar heat input and/or natural gas. In order to achieve this overall goal, a set of specific goals were established for both technical and economical performance. These goals and the degree to which they were achieved are described in the paragraphs below. Also described are the technical achievements realized as a result of the developmental program.

Technical Goals

The technical performance goals for the project are:

1. To demonstrate a pre-production prototype hybrid solar/natural gas TPV system that can convert sunlight to electricity with ~25% overall efficiency and natural gas to electricity at an overall efficiency of 20% while producing process grade hot water at a recovery efficiency of ~83%.
2. To develop an absorber/emitter for the TPV system that can operate at 1600°C to increase energy densities on the PV array by a factor of 2.6:1 over the current design operating at 1400°C in order to lower materials and PV cell costs.

Technical Achievements

1. In response to stated goal number 1 above, a pre-production prototype hybrid solar/natural gas commercial SGTPV system was designed, fabricated, tested, and demonstrated to the California Energy Commission in Sacramento. The system features 1) a unique modular design such that customer power needs can be easily accommodated by adjusting the number of modules to be delivered, 2) a solar aperture for admitting sunlight into the SGTPV and an emitter design for running simultaneously on sunlight and gas, 3) an improved high throughput IR band-pass filter for increased power density, 4) a high concentration prism for reducing PV cell requirements, and 5) a modular, low-cost, high-performance parabolic concentrator system. The tested SGTPV system met most of our technical objectives. Each component of system functioned to design with the exception of the vacuum seal in the converter thermal control package. The failure of this vacuum seal precluded performance evaluation at full operating power. However, reduced power testing was successful and extrapolation from these lower power levels indicated that at full operating power a gas-to-electric efficiency of 15.6% and a solar-to-electric efficiency of 22.3% would be achieved. Further, our laboratory has measured 83% thermal residue recovery in similar TPV systems.

A summary of the successful technical developments is outlined below.

1. A pre-production prototype hybrid solar/natural gas commercial TPV system that meets most of our technical objectives.

2. A unique modular design that can operate either from concentrated solar energy or a natural gas burner or operates from both of these power sources simultaneously.
3. A solar aperture for admitting sunlight into the SGTPV system.
4. An emitter design for running simultaneously on sunlight and gas.
5. A gas burner/recuperator subsystem.
6. An improved vacuum thermal control package for the SGTPV converter.
7. An improved high throughput IR bandpass filter for the SGTPV.
8. An improved vacuum tight seal for bonding filter substrates to the thermal control package.
9. A eighteen faceted prism array design for concentrating the transmitted thermal energy onto the PV cells.
10. Thermal control and heat recovery system for PV cell arrays and recuperator exhaust system.
11. Developed a low-cost, high performance concentrator for supplying the solar energy to the TPV system.
12. A conformal reflective coating process for a 1.6 square meter aperture parabolic concentrator dish.
13. A unique solar tracking system that is integrated with the mounting pedestal for the concentrator.
14. Microcomputer based electronic/software control system for the entire SGTPV system.

During the test and evaluation program, the following functions were demonstrated:

1. A complete solar/gas TPV prototype has been designed, developed, fabricated, and tested.
2. Heating of the emitter by a gas burner has been demonstrated.
3. Production of electricity by gas burner heating has been demonstrated.
4. Heating of the emitter by concentrated solar energy has been demonstrated.
5. Heating of the emitter by a gas burner and concentrated solar energy simultaneously has been demonstrated.
6. With the above accomplishments, the feasibility of the hybrid solar/gas TPV concept has been demonstrated.
7. Computer control of the air and fuel mixture to the gas burner has been demonstrated.
8. The computer controlled sun tracking system has been demonstrated.

9. Control of local "housekeeping" functions, such as night-time stowage, has been demonstrated.

10. Solar concentration by the EDTEK fabricated parabolic dishes has been demonstrated.

11. A commercialization plan for the SGTPV has been compiled.

12. A production readiness plan for the SGTPV has been compiled.

2. In response to stated technical goal number 2., materials screening and testing was performed in an attempt to design a burner/recuperator/converter unit that would accommodate an emitter temperature of 1600°C. It was found that the 1600°C emitter temperature objective must be abandoned due to materials compatibility considerations. However, the goal of achieving a 2.6:1 reduction in PV cell usage was achieved by two different approaches. First we increased the energy density on the PV cells by a factor of 1.36:1 by increasing the transmittance of the IR band-pass filters. Secondly, we improved the yield of our cell production process from 60% to 95% in addition to working with GaSb wafer vendors to lower the cost of wafers from $240 to $110 each. These two approaches lowered the PV cell cost by a factor 4.6 thereby exceeding our original goal.

Economic Goals and Achievements

In addition to achieving the technical goals for the system, it is recognized that several cost and economic goals must be achieved in order for the system to be commercial viable. In the final analysis, the hybrid, co-generation techniques used in this project will only constitute a true breakthrough for distributed photovoltaic power if the entire system can be manufactured within market driven cost goals. The formula for determining this can be stated simply: The cost of the system (including debt service) plus the cost of its operation and maintenance must be less than the after-tax income it accumulates over its operational life. To address these issues a commercialization plan and a manufacturing/production plan has been developed as part of this project. These plans address the following questions:

- What are the projected costs of the system in large-scale manufacturing?
- What are the projected maintenance and operation costs?
- What is the value of the energy the system delivers over its life?

Three additional considerations significantly impact this issue:

- What is the competing rate of interest available to potential investors; i.e., the U.S. 30-year bond?
- What tax regulations apply; i.e., what are the applicable depreciation rates; what investment credits are available; and what rate of income and property taxes apply to the income flow and the installation itself?
- What is the projected increase in the value of the energy produced over the life of the system (i.e., what is the likely increase in the cost of the fuel source being displaced)?

The overall intent of this project was to provide valid input data for determining the answers to the above questions through design, fabrication, and demonstration of a prototype system. To this end, the following identified economical/cost goals were put forth in the beginning of this program:

1. To develop an infrared concentrating prism with a concentration ratio of 7:1 that can reduce overall cell active area requirements and, hence, reduce system cell cost, being the dominant obstacle to commercialization, by a factor of 7 compared to current systems operating with little or no concentration.

   Achievement: We achieved 4:1 concentration with a secondary prism. The remaining cost reduction was achieved by increasing GaSb TPV cell production yields from 60% to 95% and by working with the semiconductor wafer vendor to lower GaSb material costs. This effort reduced our starting wafer costs from $240. each to $110. each. These achievements with the filter work, discussed in the technical portion, reduced our PV cell costs by a factor of 12 thereby exceeding our goal.

2. To develop and demonstrate a vertically integrated manufacturing process for producing low-cost high performance concentrator dishes (CR>1000:1) at low cost ($3.40/sq. ft.) which is comparable to the adhesive backed, reflective coated films currently used by most systems before substrate and film application labor costs are considered.

   Achievement: We have developed a pilot production process that can produce field ready concentrator dishes in small volume at a price of $6.96/sq. ft. With further automation enabled by large volume, the price drops to $4.06/sq. ft with the conformal reflecting finish coating costing about $1.74 and $1.01 respectively in low and high volume production.

3. To develop a business plan and financial strategy for the commercialization of the SGTPV.

   Achievement: We have developed both a commercialization plan and a manufacturing/production readiness plan that shows the SGTPV to be a very competitive product for point of use power generation.

In addition to the above achievements directed toward promoting economic viability for the SGTPV system we have also accomplished the following items:

An improved high yield process (~95%) for producing lower cost and higher performance GaSb PV cells with pilot production equipment that can produce cells capable of ~ 0.25 Mw/yr in SGTPV modules.

An improved pilot filter production process and equipment that can produce filters capable of ~ 0.25Mw/yr in SGTPV modules.

Deployed pilot production equipment for fabricating 1.6 square meter parabolic concentrator dishes capable of producing ~ 2Mw/yr in SGTPV modules.

Developed an alliance with a GaSb PV cell vendor that promises to reduce the cost of GaSb wafers by about a factor of 5 below current best prices.

9.2. Commercialization Potential

EDTEK intends to manufacture, market, install and service a hybrid solar/fossil fueled thermophotovoltaic (TPV) generator based on a low-cost, high performance modular solar

concentrator. The SGTPV system can use concentrated sunlight or fossil fuels either individually or simultaneously. This products overcomes the cost-obstacles historically associated with photovoltaics. Most of the desired technical goals were achieved during this PIER development program and the SGTPV technology and its commercial potential remain very strong. This is because there is a clear path leading to the successful achievement of the unrealized technical goals. The reason for not achieving these goals was the failure of a vacuum seal in the converter thermal control package. Without this seal, thermal control was lost resulting in overheating of various components of the TPV converter. The overheating caused low efficiency conversion of thermal energy to electrical energy resulting in our inability to demonstrate desired overall operating efficiency numbers. It will be necessary to resolve this faulty vacuum seal before development can continue.

EDTEK is now developing a solution to the vacuum-seal problem that has been a weak point our TPV design. The best solution would be to completely do-away with the requirement for this seal. This is the approach that we are taking. Preliminary computer modeling and testing indicate that our proposed solution is the correct one. The development and testing of this new converter concept must be completed before moving forward to commercialization.

All of the economical objectives were achieved during this PIER program. The development resulted in an approximate 12x reduction in PV cells costs to the system. This exceeded our goal by a factor of three. Additionally, during the program, EDTEK developed a pilot production process that can produce field ready concentrator dishes in small volume at a price of approximately $4.06/sq.ft. At this point, no other pre-commercialization steps are required except as noted above.

Market Potential

The following discussion outlines the great market potential of the developed SGTPV power generation system. The primary market is for users with concurrent needs for electricity and hot water. These users include individual, commercial, light industrial, and institutional users. We have segmented the market based on three factors: sunlight, electric rates, and population density. The analysis indicates that the most favorable states for initial product entry are California, Arizona, New Mexico, and Hawaii. The potential market is summarized in Table 12.

Table 12. Summary of Potential Market

Customer Type	Number of Users	Total kW-hr/yr	Total Annual Revenue For Market Sector (At $0.07/kWh)
Supermarkets	47,040	20,603M	$1,442,246,400
Mini markets	70,364	9,245M	$647,208,072
Hospitals	8,036	10,559M	$739,151,280
Hotels & Resorts	55,468	17,006M	$1,190,454,216
Athletic Clubs	13,132	2,876M	$201,313,560

Food Processors	15,876	2,781M	$194,703,264
Restaurants	228,340	70,000M	$4,900,633,080
Total Available Market			$9,315,709,872
Available Served Market			$931,570,987
Projected Annual Sales			$93,157,099

The needs of all of these users are currently being filled by local utilities generating electricity primarily from natural gas and/or oil and/or propane or natural gas for heat. However, there are three current factors that tend to favor our product. First, our product can produce power at significantly lower cost at the user's site with a reliability equal to the utility's grid. Our cost analyses indicate that we can produce power at the customer's site at a cost equal to the central utility's bus bar production cost before distribution. Second, the current trend is towards deregulation of the utilities and a more competitive market which favors our type of products. Third, our product utilizes clean, renewable energy during the day and at night operates as a topping cycle on the customer's existing local natural gas use so that there is a large environmental benefit to using our product.

The primary market for our products includes users of electric power with a concurrent need for process grade hot water. These users include individual, commercial, light industrial, and institutional users. Secondary markets for our thermophotovoltaic products are self-powered appliances, and lightweight portable generators. Self-powered appliances and topping cycle applications constitutes a very broad market touching potentially on almost every household and industry. Light-weight portable generators find applications in remote applications, recreation vehicles and boats, as well as for conventional construction use.

Historical trends point to a very bright future for economically competitive renewable energy resources. Figure 134 taken from the California Energy Commission's Historical Energy Information, Energy Watch, Volume 16[8] shows the trend in recent years for electrical power production. As can be seen, the fastest growing industry within the energy production industry is the category of self or co-generation. The renewable resources (geothermal, organic waste, wind and solar) segment of the market has grown from almost 0% to 11% of the total production in California. At the national level, out of a total production of nearly 300 billion kWh, renewables have grown from almost zero to a market of about 33 billion kWh/year in just 10 years. At an average cost of 10 cents/kWh this represents a $3.3 billion market. As quoted in the Energy Watch, "A notable trend over the last 10 years has been the emergence of non-utility generation of electricity. With the exception of hydroelectric and geothermal facilities, virtually all renewables are independently owned, as are many gas-fired co-generation units." Thus, in an era when renewable energy was only marginally cost effective and generally required government subsidies, the *national* market grew at a rate of about 3.3 billion dollars per year. Indeed, if one considers the graph in Figure 134, it can be seen that for California most of the real growth was in the renewables which were displacing the conventional, incumbent utilities

production. The growth rate of power generated from renewable resources has been about $330 M/yr, or a rate of 10%/yr over the past 10 years. With the emergence of more cost effective technologies we can expect this growth to continue.

With the recent escalation in energy prices, rolling blackouts, trend towards deregulation of the energy market and use of incentives to encourage the use of renewable energy resources, It is not unreasonable to project that our technology could capture 10% of the growing demand for renewables. At this rate, the available market would begin at $33 M/yr in California alone and grow by an additional $33 M/yr thereafter into the foreseeable future. At this point the data indicate that in California, only about 10% of the available market is served by renewable power generation. All of the southwestern states are pursuing similarly aggressive approaches to renewable energy resources so that it is not hard to extrapolate to a market of greater than $100 M/yr in the year 2005 with an increasing growth rate thereafter.

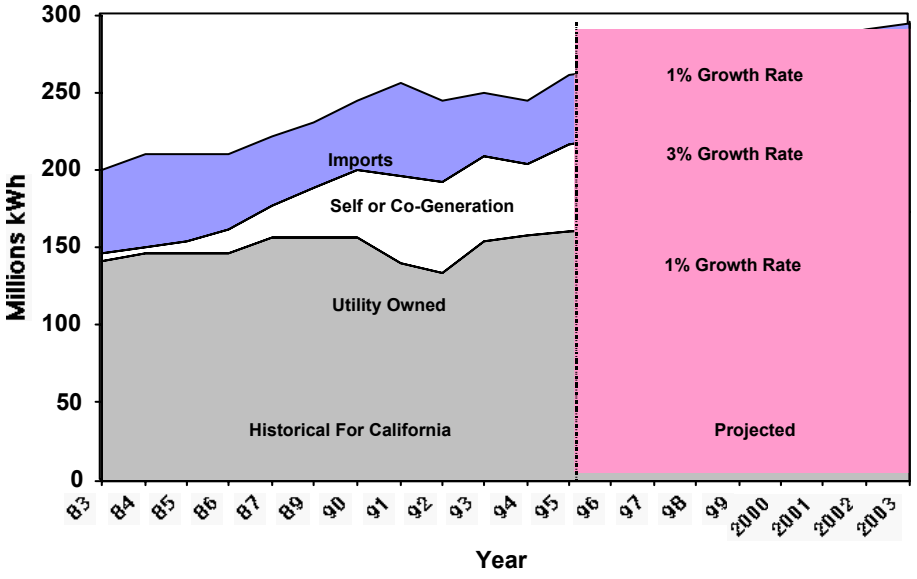

Figure 134. Historical Trends For Energy Production In State Of California

Having established the existence of a significant market for independent, distributed power production, we now look more specifically at potential customers for our product in order to segment the market to those customers who are actual potential buyers. This segmentation will give a more realistic insight into the actual size of our potential market. To accomplish this segmentation, and market size determination we need to consider three basic factors; sunlight, electric rates, and population density. We will now consider these three factors in order.

Sunlight: By the nature of our products our customers are confined to those areas that have significant amounts of annual direct normal sunlight. Direct normal sunlight is that light that reaches the Earth's surface without being scattered by the atmosphere so that it can be concentrated by reflector optics. These areas have been identified by the National Renewable Energy Laboratory, (NREL)[9] and are shown in the chart of Figure 135.

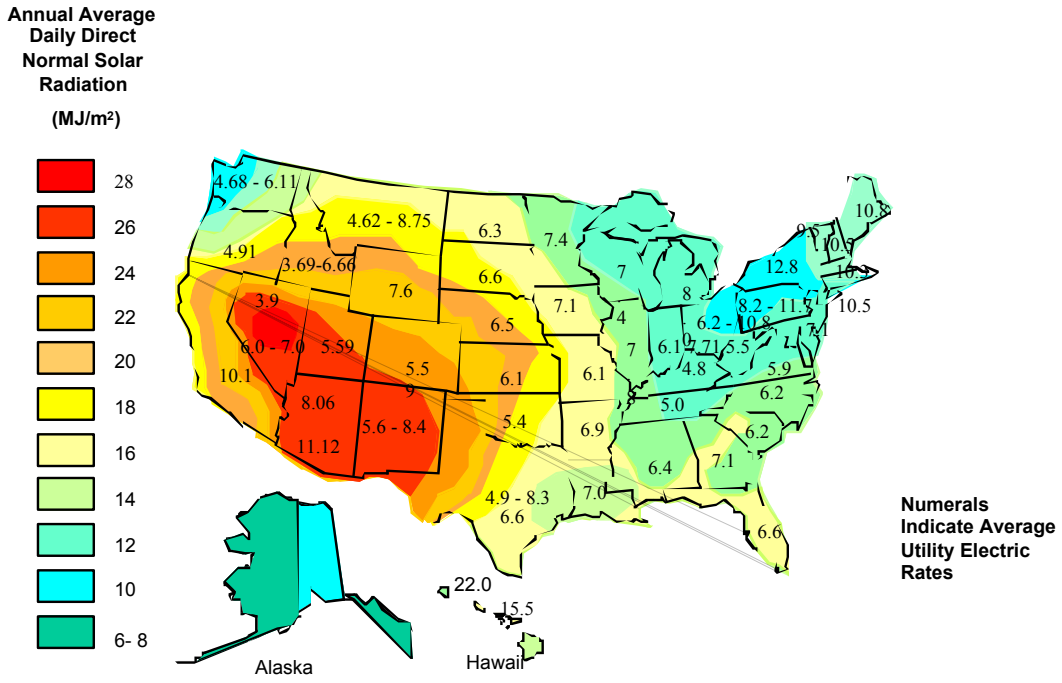

Figure 135. Regional Solar Radiation And Electric Rate Data For The United States

Electric Rates: The size of the market can be further refined by considering local retail rates for electricity and natural gas. While natural gas rates tend to be less localized, electric rates can vary widely depending on the method of generation , distribution, and local politics or regulations. For example, the northwest has access to hydroelectric generation and the retail user's rates are generally less than 6 cents per kWh while in the southwest, fossil fuels are used and the rates can go as high 13 to 14 cents per kWh. Currently, energy prices are highly volatile and much higher than has been the norm for the last several years; however, we expect prices to stabilize within a couple of years as new generating capacity is brought on line and the stable prices will probably be closer to the past norms than the current high prices. therefore, we are basing our business on the conservative assumption and using the lower historical prices. The Edison Electric Institute Typical Bills and Average Rates Report[10] publishes annual data on national, regional, and local electric power rates. Data from the winter 1997-98 report rates have been compiled and presented for each state by superposition on the solar radiation data in Figure 135. Regions where high rates and high solar radiation intersect make economically favorable locations for the first targeted market applications of our product. From our projections of life cycle costs for our system, which is detailed in appendix III, we have determined areas that have annual average daily direct normal solar radiation and electric rates sufficient to make them candidates for the application of our hybrid systems. Figure 136 shows the geographic distribution of these economically favorable areas within the continental United States. Within this broad overall market area, we have further segmented the market to those regions with both the highest solar intensities and the highest electric rates. These selected areas are targeted for our first marketing efforts. These most favorable target regions are also indicated in the chart of Figure 136.

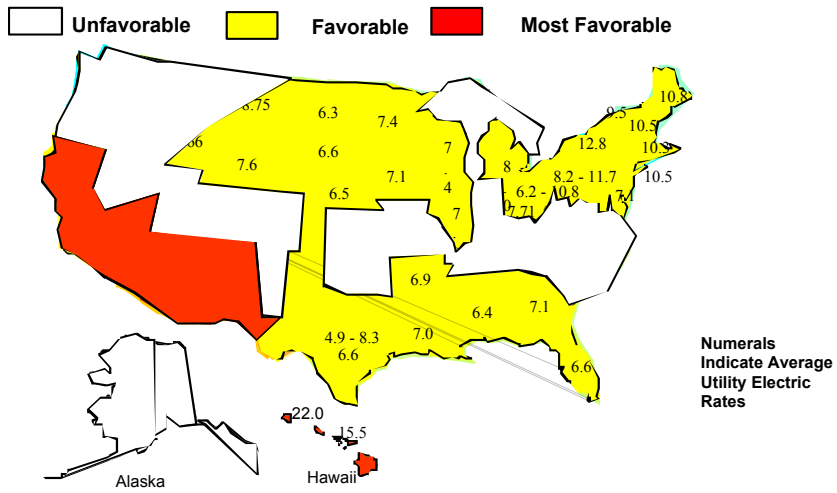

Figure 136. Favorable Regions For EDTEK Systems In The United States Population Density:

By considering the population of the identified economically favorable areas we can begin to get a realistic estimate of the total potential U. S. market and of the available served market. The types of potential users we have targeted, supermarkets, hotels, restaurants, and hospitals generally tend to be proportional to population. Thus, by knowing the population of a targeted region one can fairly accurately estimate the potential customers in the targeted area. By consulting the telephone yellow pages for areas of known population and counting the number of listings for each customer type, we have developed factors for the number of each type of user per capita. Using these factors and the population density for the areas, we can then establish the number of potential customers of each type in the economically favorable areas shown in Figure 136. From the data in Figure 136, and the factors for each customer type determined from the yellow page listings of centers of known population, we have estimated the size of the market for our product. The analysis for the total available market is summarized in table 9.2 for supermarkets, mini-markets, hospitals, resorts and hotels, athletic clubs, food processors, restaurants, prisons, and heavy agricultural users of irrigation are targeted as prime potential customers.

Table 13. Summary of Total Market Size Analysis

Customer Type	Population	Number of Users	Average Peak kW Per Customer	Total kW·hr/yr	Total Initial Equipment Cost	Total Annual **Revenue For Market Sector** (At $0.07/kWh)
Supermarkets	196M	47,040	50	20,603M	3,057.6M	$1,442,246,400
Mini markets	196M	70,364	15	9,245M	1,372M	$647,208,072
Hospitals	196M	8,036	150	10,559M	1,567M	$739,151,280
Hotels & Resorts	196M	55,468	35	17,006M	2,523.8M	$1,190,454,216
Athletic Clubs	196M	13,132	25	2,876M	$426.8M	$201,313,560
Food Processors	196M	15,876	20	2,781M	$412.8M	$194,703,264
Restaurants	196M	228,340	35	70,000M	$10,389M	$4,900,633,080
Total Available Market			330		$19,749M	$9,315,709,872
Available Served Market					$1,974M	$931,570,987
Projected Annual Sales						$93,157,099

The analysis is based on the assumption of on-site generation displacing retail electric utility rates at the local site. The cost of initial equipment illustrates the capital investment required by the user while the total dollars column indicates the "annual revenue" accrued from the displacement of utility electric and gas bills. By considering the summary in Table 13 it can be seen that the total market is very broad. If we now look at the available served market which EDTEK has targeted for the first penetration, the population it represents is about 10 percent of the total available market population. Our ultimate goal is to capture 10% of the served available market which will result in approximately $100,000,000 per year in sales. Our strategy to achieve this is a modest ramp up from five test customers in 2002 to 1,000 customers per year in 2006. At this stage sufficient product maturity and marketing infrastructure will have been achieved to warrant the significant investment required to deploy the production equipment and promotional programs to rapidly expand the market to our goal of 10% of the available served market.

9.3. Recommendations

The developed SGTPV components are fully functional with the exception of the aforementioned vacuum seal problem in the TPV converter unit. The recommendations for further development center around this problematic seal. The focus should be on methods to either strengthen this seal so that it will survive its operational environment or develop an alternative design that would completely do-away with the need for this seal. It is recommended that the latter development path be followed and EDTEK is currently investigating TPV converter design changes that would accomplish the removal of this seal while still maintaining high thermal to electric conversion efficiency. Preliminary computer modeling indicate that our proposed design changes will be successful. Upon completion of modeling and component testing, the new converter design must be fabricated and its operational parameter confirmed.

It is further recommended that the SGTPV system fabricated under this PIER program be refurbished with the new converter design and tested. The testing will be carried out to confirm the performance of the converter and, subsequently, the entire SGTPV system. Ultimately, the goal will be to demonstrate and confirm the overall system efficiency with the desired sunlight-to-electric efficiency of 25% and gas-to-electric conversion at 20%.

9.4. Benefits to California

The potential benefits of the SGTPV to the State of California are summarized below. The on-site distributed power can save money for individual, light-industrial, and commercial users in California. The local on-site power generation using cost effective sun-power can substantially reduce the peak demands on central power generation stations and provide stability for the using customers. EDTEK has calculated that the SGTPV can generate electricity at a cost of about $0.035 per kilowatt hour at the point of use. With current point of use (retail) rates running around $0.16 per kilowatt hour in California, this represents a substantial cost savings to the California users. These distributed power systems can also reduce the peak power demands and hence reduce capital investments in "over capacity" equipment by central power generators. It is estimated that by the year 2004 SGTPV systems will generate 17.5 million kW-hrs/year and by 2006 the numbers will be approximately 175 million kW-hrs/year. In addition to the benefits to immediate users and the power industry, the establishment of an infra structure for selling, installing, and servicing these new power systems will create many high quality jobs throughout the State of California. For example, our pilot production equipment can produce about 2 Mw of product per year. Our estimate is that for each 2 Mw installed would employ 20 workers in high quality jobs. Our commercialization plan calls for production to expand tenfold in the fifth year so that 200 new workers would be added per year thereafter.

Environmentally, each co-generating SGTPV unit will displace natural gas consumption when the sun is available. When we combine the solar contribution with the natural gas generation and consider that the thermal residue also displaces natural gas, our net efficiency (defined as useful energy produced/natural gas burned) 72.8% which is about a factor of two higher than that of central power generating stations which have higher electrical conversion efficiencies but cannot use the solar heat nor can they retrieve and use the thermal residue. Thus, each Mw of SGTPV production reduces pollutant emissions by one-half what they would be for the central

generation plant. Another benefit that is hard to quantify is satisfaction and the piece of mind of users being insulated from price fluctuations and brown outs that are beyond their control.

10.0 References

1. Horne, W.E., and Thompson, M. A., "Thermophotovoltaic Space Power System", Final Report, Contract NAS8-33436, NASA MSFC, Huntsville, AL, 1986.
2. Horne, W. E. et al, "Thermophotovoltaic Thermal-to-Electric Conversion Systems Report", Final Report for Jet Propulsion Laboratory, Contract 959595, Dec. 1993.
3. Horne, W.E., Morgan, M.D., and Sundaram, V., "Radioisotope TPV Power System Phase I, Component Optimization", EG&G Mound Contract 245915-5854, 1995.
4. Horne, W.E., Morgan, M.D., and Sundaram, V., "IR Bandpass Filter Production Process", DOE SBIR Contract: DE FG03 94ER81742-A002, (1995).
5. Horne, W.E. et al, "Hybrid Solar/Fossil Thermophotovoltaic Power System: Phase-II." National Renewable Energy Laboratory Contract No. YAF-7-17623-02, 1999 to present.
6. Horne, W.E., Morgan, M.D., Sundaram, V., Butcher, T, and Charters, R., "Development of 500 Watt Diesel Fueled TPV Power Supply", DARPA/CECOM Contract: NO. DAAB07-97-C-6025, 1997 to present.
7. Horne, W. E. et al, Point Focus Solar Concentrator Manufacturing Process, Final Report, Sandia Contract No. AL-6011B, November 1996.
8. Historical Energy Information Energy Watch, Volume 16, Published April 1997 by the California Energy Commission.
9. Insolation Data Manual and Direct Normal Solar Radiation Data Manual, SERI/TP-220-3880 DE90000353, July 1990, UC Categories: 234,270.
10. Typical Bills and Average Rates Report, Winter 1998, Published by Edison Electric Institute, 701 Pennsylvania Ave., N. W., Washington DC 20004-2696.

11.0 GLOSSARY

Acronyms Definitions:

PIER	Public Interest Energy Research
TPV	Thermophotovoltaics
IR	Infrared
PV	Photovoltaic
CEC	California Energy Commission
SGTPV	Solar/Gas Thermophotovoltaic
W	Watts
DARPA	Defense Advanced Research Projects Agency
CECOM	U.S. Army Communications And Electronics Command
nm	Nanometer (10^{-9} Meters)
MIBL	Masked Ion Beam Lithography
EBL	Electron Beam Lithography
RIE	Reactive Ion Etch
SEM	Scanning Electron Microscope
PECVD	Plasma Enhanced Chemical Vapor Deposition
FF	Fill Factor
BNL	Brookhaven National Laboratory
CVD	Chemical Vapor Deposition
NREL	National Renewable Energy Laboratory
STPV	Solar Thermophotovoltaic